



ΠΟΛΥΤΕΧΝΕΙΟ ΚΡΗΤΗΣ

ΓΕΝΙΚΟ ΤΜΗΜΑ

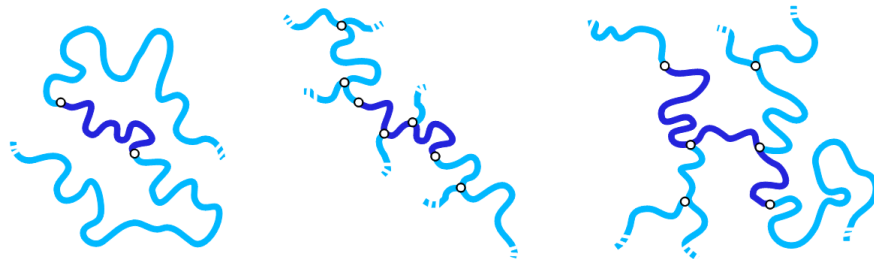
**ΠΡΟΓΡΑΜΜΑ ΜΕΤΑΠΤΥΧΙΑΚΩΝ ΣΠΟΥΔΩΝ:
ΕΦΑΡΜΟΣΜΕΝΕΣ ΕΠΙΣΤΗΜΕΣ ΚΑΙ ΤΕΧΝΟΛΟΓΙΑ**

Rheology of commercial polyolefins: Relating the viscoelastic behaviour to microstructure

Ρεολογία εμπορικών τηγμάτων πολυμερών:
Συσχετίζοντας την ιξωδοελαστική συμπεριφορά
με την μοριακή δομή

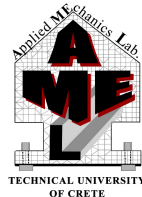
Ιωάννης Σ. Στρατηγάκης

Επιβλέπων: Αλέξανδρος Δ. Γκότσης



ΠΟΛΥΤΕΧΝΕΙΟ ΚΡΗΤΗΣ, ΓΕΝΙΚΟ ΤΜΗΜΑ

ΕΡΓΑΣΤΗΡΙΟ ΜΗΧΑΝΙΚΗΣ ΤΩΝ ΥΛΙΚΩΝ



RHEOLOGY OF COMMERCIAL POLYOLEFINS: RELATING THE VISCOELASTIC BEHAVIOUR TO MICROSTRUCTURE

Ρεολογία εμπορικών τηγμάτων πολυμερών:
Συσχετίζοντας την ιξωδοελαστική συμπεριφορά με την
μοριακή δομή

Ιωάννης Σ. Στρατηγάκης

Διπλωματική διατριβή υποβληθήσα στα πλαίσια των απαιτήσεων για
την απόκτηση του Μεταπτυχιακού Διπλώματος Ειδίκευσης
στο πρόγραμμα

«ΜΗΧΑΝΙΚΗ ΚΑΙ ΤΕΧΝΟΛΟΓΙΑ ΥΛΙΚΩΝ ΚΑΙ ΚΑΤΑΣΚΕΥΩΝ»

του Γενικού Τμήματος του Πολυτεχνείου Κρήτης

2 Φεβρουαρίου, 2015

ΔΙΠΛΩΜΑΤΙΚΗ ΔΙΑΤΡΙΒΗ ΜΕΤΑΠΤΥΧΙΑΚΟΥ ΔΙΠΛΩΜΑΤΟΣ ΕΙΔΙΚΕΥΣΗΣ

Ιωάννης Σ. Στρατηγάκης ,
αρ. μητρώου: 2012040336

e-mail: istratigakis@isc.tuc.gr

Τριμελής Συμβουλευτική Επιτροπή:

1. Αλέξανδρος Δ. Γκότσης, καθηγητής Πολυτεχνείου Κρήτης, επιβλέπων
2. Κωνσταντίνος Προβιδάκης, καθηγητής Πολυτεχνείου Κρήτης
3. Ιωάννης Τσομπανάκης, αναπλ. καθηγητής Πολυτεχνείου Κρήτης.

Παρουσιάστηκε στην επιτροπή στις 29 Ιανουαρίου, 2015

Εικόνα εξωφύλλου:

From left to right: A model HDPE of linear architecture, a LLDPE with some sparse short-chain branching and a commercial LDPE with long-chain branches on the backbone and on its branches.

Από αριστερά προς τα δεξιά: Γραμμικό Πολυαιθυλένιο Υψηλής Πυκνότητας (HDPE), γραμμικό Πολυαιθυλένιο Χαμηλής Πυκνότητας με κοντές διακλαδώσεις (LLDPE) και Πολυαιθυλένιο Χαμηλής Πυκνότητας με μακριές διακλαδώσεις στον κορμό και στους κλάδους (LDPE).

ΔΙΕΥΘΥΝΣΗ ΕΡΓΑΣΤΗΡΙΟΥ:

ΠΟΛΥΤΕΧΝΕΙΟ ΚΡΗΤΗΣ, ΓΕΝΙΚΟ ΤΜΗΜΑ
Εργαστήριο Μηχανικής των Υλικών

Κτήριο Επιστημών, Πανεπιστημιούπολη, Κουνουπιδιανά, 73100 Χανιά

τηλ. 2821037259
fax. 2821037672
e-mail: gotsis@science.tuc.gr

Contents

Acknowledgements	3
Abstract	5
Σύνοψη	7
Nomenclature	29
1 Introduction	37
1.1 The Molecular Structure of Polymers	38
1.2 Polyolefins : Examples of Branched Polymers	39
1.3 The Scope of the Thesis	41
2 Structure and Fluid Mechanics of Polymers	43
2.1 The Random Coil Model	43
2.1.1 Random Walks	43
2.1.2 Conformational Distributions	45
2.1.3 The Hookean Spring	45
2.1.4 GPC Characterization of LCB in Polymers	46
2.2 The Stress Tensor	47
2.2.1 The Polymer Stress Tensor	47
2.3 Finite Deformation Tensors	48
2.4 The Rate of Deformation Tensor	49
2.5 The Newtonian Fluid	50
2.6 The Generalised Newtonian Fluid	51
2.6.1 Power Law	52
2.6.2 Cross Model	52
2.6.3 Extensional Thickening Models	52
2.6.4 Temperature and Pressure Dependence of Viscosity	53
2.7 Characterisation of Viscoelasticity	53
2.7.1 Linear Dynamic Measurements	53
2.7.2 Non-linear strain dependence	55
2.7.3 Simple shear flow	55
2.8 Balance Equations in Newtonian Flow Fields	56
2.8.1 Mass Balance	56

2.8.2	Momentum Balance	57
2.8.3	Energy Balance	58
3	Constitutive Equations for Polymer Melts	59
3.1	Linear Viscoelasticity	59
3.2	The General Linear Viscoelastic Model	60
3.3	The Lodge Equation for a Rubber-Like Liquid	62
3.4	Non-Linear Viscoelasticity	68
3.5	The Modified Rubber-Like Liquid Model	70
3.5.1	The Wagner-I Equation	70
3.5.2	The PSM Damping Function	78
3.5.3	The Power-Law Damping Function	78
3.6	Reptative Dynamics for Entangled Polymer Melts	86
3.7	The Doi-Edwards Constitutive Equation	87
3.7.1	The Independent Alignment Approximation (IAA)	91
3.7.2	The History Integral	92
3.7.3	Predictions of Reptation Theories	93
3.7.4	The Effect of Polydispersity on the Rheology of Entangled Melts	93
3.7.5	The Effect of Long-Chain Branching on the Rheology of Entangled Melts	94
3.7.6	The Effect of Strain-Induced Crystallisation on the Rheology of Entangled Melts	97
3.8	Maxwell-Type Differential Constitutive Equations	103
3.8.1	The Upper-Convected Maxwell Differential Equation	103
3.8.2	The eXtended Pom-Pom Model	104
3.8.3	The Rolie-Poly Constitutive Equation for Linear Polymer Melts	106
4	Experimental	107
4.1	Introduction	107
4.2	Shear Flows	107
4.2.1	Cone and plate geometry	108
4.2.2	Parallel disk geometry	108
4.3	Extensional Flow	109
5	Results	117
5.1	Dynamic Measurements	117
5.2	Step-Strain Tests	126
5.3	Uniaxial Elongation	126
6	Discussion	137
6.1	The Relaxation Spectrum	137
6.2	Thermorheological Complexity of Commercial PEs	138
6.3	The Damping Function	142
6.3.1	Damping Function from Shear Flow Measurements	142
6.3.2	Damping Function from Extensional Flow Measurements	143
6.4	LCB and Rheology	148

6.4.1	Estimating B_n from Rheological Data	148
6.4.2	Correlation between B_n and x_n	149
6.4.3	Correlation Between x_n and the Branching Structure	152
6.4.4	Correlation Between the Values of x_n Determined from Shear and Uniaxial Extensional Measurements	155
7	Conclusions and Recommendations	161
7.1	Conclusions	161
7.2	Recommendations	164
	Bibliography	172
A	Fourier Transform Integrals	173
B	The Doi-Edwards Universal Orientation Tensor	175
C	Tables	179
D	Graphs from the Theoretical Section	185
	Βιογραφικό	207

DECLARATION

I hereby declare that the work presented here has been my independent work and has been performed during the course of my M.Sc. studies at the Department of Applied Sciences, Technical University of Crete, Chania.

All contributions drawn from external sources have been acknowledged with due reference to the literature.

ΔΗΛΩΣΗ

Δηλώνω υπεύθυνα ότι η παρούσα διατριβή είναι προϊόν ανεξάρτητης εργασίας μου που διεξήχθη κατά τις μεταπτυχιακές μου σπουδές στο Γενικό τμήμα του Πολυτεχνείου Κρήτης, στα Χανιά.

Για ό,τι δεδομένα ή πληροφορίες χρησιμοποίησα που προέρχονται από εξωτερικές πηγές έχουν δοθεί οι αρμόζουσες αναγνωρίσεις και αναφορές.

Ιωάννης Σ. Στρατηγάκης

Acknowledgements

I would like to thank my supervisor Prof. Alexandros D. Gotsis as well as Dr. Chris Tsenoglou for their invaluable help and patience that added to the accomplishment of the present Thesis. I would also like to thank Prof. Dimitris Vlassopoulos and his colleagues for their help and encouragement during my experimental work in the research facilities of FORTH. I would finally like to thank my parents for their patience during those years and my sister for making studying easier.

This project was supported by the programme COVISCO-THALES of the Operational Programme Education and Lifelong Learning, co-financed by Greece and the European Union (NSRF, 2007-2013, European Social Fund).



Co-financed by Greece and the European Union

Abstract

The rheological response of commercial polydisperse polyolefins under various types of deformation has been investigated in detail. A wealth of experimental data that has been available in the literature was gathered and is presented in this work. These data include several types of commercial polymer melts of varying microstructural architecture that have been tested under various types of rheological deformation. In addition, experimental data on two commercial polyethylenes provided by Eni S.p.A., the LDPE Riblene FF20 and the HDPE Eraclene FA506, provide a direct insight into the similarities and differences of the rheological response of commercial polyolefin melts under different types of deformation. Finally, a number of molecular constitutive theories are suggested in order to explain the results on a physical basis. This research aims at gaining understanding in the relation between the molecular structure of polymers and their rheological behaviour.

The modified rubber-like liquid theory, which is based on the permanent network hypothesis, Boltzmann's superposition principle, the concept of a fading memory and the idea of the separation of time and strain effects, is used as the starting point of this study. This simple phenomenological model that was initially proposed by Lodge and was later modified by Wagner is then compared to recently suggested molecular constitutive theories that are based on direct physical criteria in order to explain the experimental observations. The goal of this study is to prove that a representative physical basis can be the starting point of a successful rheological theory. In this context, a damping function in the form of a simple power law is used to predict the rheological response of commercial polypropylene blends tested under uniaxial extensional flow. Analysis of the experimental results leads to the conclusion that a finest description of the molecular structure of these melts is necessary in order to predict the complex behaviour of polyolefin melts. The results are also compared against the predictions of the same model for commercial polydisperse PE, PP and PS melts.

A modified version of the Doi and Edwards theory has been proposed by Tsenoglou et al. and presented in this work for the first time. A nonlinear viscoelastic parameter is introduced into the constitutive equation. This extended model provides a physical explanation of the strain softening of commercial LDPE melts, which is observed under large magnitudes of step-strain in shear deformation, as well as the appropriate strain hardening, which is observed when polymer melts are tested against uniaxial extensional deformation. The detailed research then follows aims at the way that this parameter correlates with the branching content of the melts under consideration.

Mathematical methods that are commonly used to investigate the thermorheolog-

ical complexity of commercial PE's are proposed and applied into the rheology of the commercial Riblene and Eraclene melts. The efficiency of these methods to provide an insight into the microstructural architecture of polymer melts is thoroughly examined. In addition, molecular constitutive theories that are provided in differential form, such as the eXtended Pom-Pom model, are also employed in order to make exact predictions of the rheological behaviour of melts under various types of deformation. These models are finally used in order to infer the molecular characteristics of commercial polyolefins from rheological data.

Σύνοψη

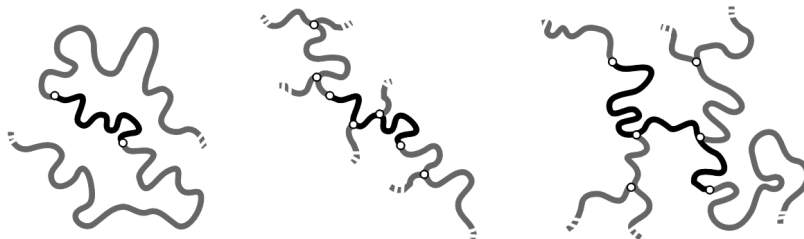
Εισαγωγή

Σκοπός της παρούσας μεταπτυχιακής διατριβής είναι η μελέτη της ρεολογίας εμπορικών πολυμερών, και συγκεκριμένα όσων ανήκουν στην κατηγορία των πολυολεφινών και η σύνδεση μέσω θεωρητικών μοντέλων της μακροσκοπικής τους μηχανικής απόκρισης με την μικροσκοπική δομή του υλικού. Οι πολυολεφίνες όπως π.χ. το πολυαιθυλένιο ανήκουν σε μια ευρύτερη κατηγορία υλικών που ονομάζονται *θερμοπλαστικά* ακριβώς επειδή όταν θερμανθούν μετατρέπονται σε υγρά και όταν κρυώσουν ανακτούν και πάλι τις αρχικές τους ιδιότητες. Αυτή η τελευταία ιδιότητα των θερμοπλαστικών υλικών όπως και άλλες που σχετίζονται άμεσα με την μικροδομή του υλικού είναι που καθιστά τα υλικά αυτά προτιμητέα σε ένα μεγάλο εύρος διεργασιών μορφοποίησης και παραγωγής εμπορικών προϊόντων από πλαστικό, καθώς και το γεγονός ότι μπορούν να ανακυκλωθούν σε μεγάλο βαθμό έτσι ώστε να περιοριστεί η επιπλέον παραγωγή πλαστικού το οποίο δεν είναι βιοαποικοδομήσιμο οπότε και επιζήμιο για το περιβάλλον.

Μοριακή Δομή

Ο τεχνικός όρος *μακρομόριο* ή *μακρομοριακή αλυσίδα* ή *πολυ-μερές* καθιερώθηκε μόλις την πρώτη δεκαετία του 20 αιώνα από τον χημικό Hermann Staudinger για την περιγραφή την μικροδομής των υλικών αυτών. Τα υλικά αυτά αποτελούνται από μικρές αυτόνομες χημικές μονάδες όλες όμοιες μεταξύ τους που όταν συνδέονται χημικά σχηματίζουν μεγαλύτερες δομές, τα μακρομόρια. Στην κατηγορία των *εύκαμπτων μακρομορίων* ανήκουν οι πολυολεφίνες όπως το πολυαιθυλένιο και το πολυπροπυλένιο που χρησιμοποιούνται ευρέως στην βιομηχανία για την παρασκευή προϊόντων καθημερινής χρήσης όπως π.χ. συσκευασίες τροφίμων, χημικών κτλ., πλαστικές σακούλες διαφόρων χρήσεων, εξαρτήματα αυτοκινήτων, σκαφών και πολλά άλλα.

Ένα πολυμερικό υλικό αποτελείται από ένα μεγάλο σε αριθμό σύνολο μακρομοριακών αλυσίδων οι οποίες μπορούν όταν η παραγωγή γίνεται σε μικρές ποσότητες και κάτω από αυστηρά ελεγχόμενες εργαστηριακές συνθήκες να έχουν όλες το ίδιο μήκος, να αποτελούνται δηλαδή από μακρομόρια τα οποία φέρουν τον ίδιο σχεδόν αριθμό μονομερών. Ωστόσο σε βιομηχανική κλίμακα η ιδιότητα αυτή περιορίζεται δραματικά και έτσι όλα τα εμπορικά πολυμερή καταλήγουν τελικά να αποτελούνται από μια κατανομή μηκών ή όπως λέγεται συνήθως *μακρομοριακών βαρών*. Το μέσο



Σχήμα 1: Από αριστερά προς τα δεξιά : Γραμμικό Πολυαιθυλένιο Υψηλής Πυκνότητας (HDPE), γραμμικό Πολυαιθυλένιο Χαμηλής Πυκνότητας με κοντές διακλαδώσεις (LLDPE) και Πολυαιθυλένιο Χαμηλής Πυκνότητας με μακριές διακλαδώσεις στον κορμό και στους κλάδους (LDPE).

κατά αριθμό μοριακό βάρος, M_n αφορά στην κατανομή με βάση τον αριθμό των αλυσίδων με συγκεκριμένο μήκος, ενώ το μέσο κατά βάρος μοριακό βάρος, M_w αφορά στην κατανομή με βάση το βάρος ανά μονάδα όγκου. Ο αριθμητικός λόγος αυτών των δύο κατανομών, M_w/M_n αναφέρεται συχνά ως *πολυδιασπορά* και είναι ένας δείκτης της ευρύτητας της κατανομής των μηκών των μακροαλυσίδων του υλικού.

Κατηγορίες Πολυμερών

Τα πλαστικά κατηγοριοποιούνται με βάση τη χημική σύσταση της επαναλαμβανόμενης μονάδας, την πυκνότητα, την διαδικασία παραγωγής και άλλες ιδιότητες που αφορούν στην αρχιτεκτονική δομή των μακροαλυσών. Οι πολυολεφίνες είναι μια κατηγορία θερμοπλαστικών υλικών, οι επαναλαμβανόμενες μονάδες των οποίων είναι υδρογονάνθρακες. Με βάση την διαφορά στην πυκνότητα τα πιο ευρέως χρησιμοποιούμενα πολυμερή είναι τα *Χαμηλής Πυκνότητας Πολυαιθυλένια*, LDPE, *Χαμηλής Πυκνότητας Γραμμικά Πολυαιθυλένια*, LLDPE και τα *Υψηλής Πυκνότητας Πολυαιθυλένια*, HDPE. Η διαφορά μεταξύ αυτών αφορά στην πυκνότητα και στην αρχιτεκτονική των μακροαλυσίδων. Τα HDPE αποτελούνται κατά κύριο λόγο από *γραμμικές αλυσίδες* σε αντίθεση με τα LLDPE στα οποία υπάρχουν συνήθως κοντοί κλάδοι χημικά συνδεδεμένοι στον κύριο κορμό ή τα LDPE στα οποία υπάρχουν μακριές αλυσίδες χημικά συνδεδεμένες στον κύριο κορμό, ενώ πάνω σε αυτές υπάρχουν επιπλέον μακριές ή κοντές αλυσίδες επίσης χημικά συνδεδεμένες (βλ. Σχ.1) έτσι ώστε να δημιουργούνται δομές διακλαδισμένων μακρομορίων.

Τανυστές Παραμόρφωσης και Τάσης

Για την μαθηματική περιγραφή της απόκρισης ενός τήγματος πολυμερούς σε εξωτερικές διαταραχές χρησιμοποιείται ευρέως η *τανυστική άλγεβρα* σε μορφή *καταστατικής εξίσωσης*. Συγκεκριμένα όσον αφορά την ρεολογία πολυμερικών τμημάτων ενδιαφέ-

ρουν πρωτίστως οι τανυστές πεπερασμένης παραμόρφωσης

$$\text{κατα Lagrange} \quad E_{ij} = \frac{\partial x_i}{\partial x'_j}, \quad i, j = 1, 2, 3 \quad (1)$$

$$\text{κατα Euler} \quad F_{ij} = \frac{\partial x'_i}{\partial x_j}, \quad i, j = 1, 2, 3 \quad (2)$$

όπου $\delta x / \delta x'$ χαρακτηρίζει τον λόγο τελικής προς αρχικής διάστασης. Από αυτούς προκύπτουν αντίστοιχα και οι τανυστές Finger και Cauchy μέσω των σχέσεων

$$C_{ij}^{-1} = \sum_{k=1}^3 \frac{\partial x_i}{\partial x'_k} \cdot \frac{\partial x_j}{\partial x'_k}, \quad i, j = 1, 2, 3 \quad (3)$$

$$C_{ij} = \sum_{k=1}^3 \frac{\partial x'_k}{\partial x_i} \cdot \frac{\partial x'_k}{\partial x_j}, \quad i, j = 1, 2, 3 \quad (4)$$

οι οποίοι διαφέρουν από τους αντίστοιχους της πεπερασμένης παραμόρφωσης καθώς δεν περιέχουν πληροφορία που να αφορά σε στροφή αλλά μονάχα σε καθαρή παραμόρφωση. Ορίζονται επίσης και οι τανυστές κλίσης ταχύτητας

$$L_{ij} = \frac{\partial v_i}{\partial x_j}, \quad i, j = 1, 2, 3 \quad (5)$$

όπου \underline{v} είναι το διάνυσμα της ταχύτητας όπως αντίστοιχα και του ρυθμού παραμόρφωσης

$$2\underline{\underline{D}} = (\nabla \underline{v})^T + \nabla \underline{v} \quad (6)$$

Τέλος, ο τανυστής τάσης δίνεται από την σχέση

$$\underline{\underline{T}} = -p\underline{\underline{I}} + \underline{\underline{\sigma}} \quad (7)$$

όπου p είναι η υδροστατική πίεση, $\underline{\underline{T}}$ είναι ο ολικός τανυστής τάσης, $\underline{\underline{\sigma}}$ είναι ο ιξώδης τανυστής τάσης και $\underline{\underline{I}}$ είναι ο μοναδιαίος τανυστής.

Καταστατικές Εξισώσεις

Η απλούστερη μορφή καταστατικής εξισώσεως που βασίζεται στην αρχή της υπέρθεσης του Boltzmann είναι το γραμμικό ιξωδοελαστικό μοντέλο το οποίο στην πιο γενική του μορφή στις τρεις διαστάσεις δίνεται από την σχέση:

$$\underline{\underline{\sigma}} = \int_{-\infty}^t G(t-t') 2\underline{\underline{D}} dt', \quad (8)$$

όπου $G(t-t')$ είναι το διατμητικό μέτρο χαλάρωσης και δίνεται από την σχέση:

$$G(t) = G_0 \exp\left(\frac{-t}{\tau}\right), \quad (9)$$

αν χρησιμοποιηθεί μόνο ένας χρόνος χαλάρωσης, τ ή από την σχέση:

$$G(t) = \sum_{i=1}^N G_i \exp\left(\frac{-t}{\tau_i}\right) \quad (10)$$

αν χρησιμοποιηθεί ένα άθροισμα από διαφορετικούς χρόνους χαλάρωσης.

Η *συνάρτηση μνήμης* που εισήχθη από τον Boltzmann για να περιγράψει την *χρονοεξαρτώμενη* απόκριση των ιξωδοελαστικών υλικών ή διαφορετικά των *υλικών με μνήμη* δίνεται από την σχέση

$$\mu(t) = -\frac{dG(t)}{dt} \quad (11)$$

και είναι συνάρτηση του διατμητικού μέτρου χαλάρωσης.

Η απλή αυτή περιγραφή είναι ακριβής όσον αφορά στη γραμμική ιξωδοελαστική συμπεριφορά των τηγμάτων πολυμερών, δηλαδή όταν η εξωτερική διαταραχή είναι πολύ μικρή σε ένταση ή πολύ αργή σε ρυθμό. Για μεγαλύτερες ή πιο γρήγορες παραμορφώσεις η ρεολογική συμπεριφορά των ιξωδοελαστικών υλικών παρουσιάζει σημαντικές αποκλίσεις από την γραμμική ιξωδοελαστικότητα. Ένας ακόμη λόγος για τον οποίο το γραμμικό ιξωδοελαστικό μοντέλο δεν χρησιμοποιείται στην ρεολογία τηγμάτων είναι και το γεγονός ότι δεν συμπεριλαμβάνει στο θεωρητικό του υπόβαθρο την μικροσκοπική δομή των πολυμερών, ο ρόλος της οποίας τελικά αποδεικνύεται πολύ σημαντικός όσον αφορά στην προβλεπτική ικανότητα μιας πλήρους θεωρίας για την ιξωδοελαστικότητα.

Ελαστικό Ρευστό του Lodge

Τα δύο αυτά μειονεκτήματα του γραμμικού μοντέλου επιλύθηκαν σταδιακά. Αρχικά εισήχθη από τον Lodge μια νέα καταστατική εξίσωση, το *ελαστικό ρευστό* ή *ρευστό του Lodge* το οποίο δίνεται από την σχέση:

$$\underline{\underline{\sigma}} = \int_{-\infty}^t \mu(t-t') \underline{\underline{C}}^{-1}(t', t) dt' . \quad (12)$$

Το μοντέλο βασίζεται σε μια παλιότερη ιδέα των Green και Tobolsky στην οποία το πολυμερικό ρευστό αποτελείται από μακρομοριακές αλυσίδες οι οποίες περιπλέκονται μεταξύ τους δημιουργώντας *προσωρινές διαπλοκές* οι οποίες τελικά ευθύνονται για την μακροσκοπική ρεολογική συμπεριφορά των πολυμερικών τηγμάτων, δηλ. προσδίδουν ελαστικό χαρακτήρα στο ρευστό, καθώς συγκρατούν τα μακρομόρια μεταξύ τους αλλά και ιξώδη χαρακτηριστικά καθώς δεν έχουν μόνιμη υπόσταση και μπορούν να καταστρέφονται και να επανασχηματίζονται. Η μη-γραμμική απόκριση του υλικού σε γρήγορες ή μεγάλες παραμορφώσεις υπολογίσθηκε χρησιμοποιώντας την *αρχή του διαχωρισμού μεταξύ των χρονοεξαρτωμένων γραμμικών αποκρίσεων και χρονοανεξάρτητων μη-γραμμικών αποκρίσεων* με την εισαγωγή μιας *συνάρτησης απόσβεσης* στην καταστατική εξίσωση του Lodge η οποία τελικά γράφεται σε πλήρη μορφή

$$\underline{\underline{\sigma}} = \int_{-\infty}^t \mu(t-t') h(I_{C^{-1}}, II_{C^{-1}}) \underline{\underline{C}}^{-1}(t', t) dt' , \quad (13)$$

όπου I_{C-1} και II_{C-1} είναι αντίστοιχα η πρώτη και δεύτερη αναλλοίωτη του τανυστή παραμόρφωσης του Finger.

Η καταστατική αυτή εξίσωση αναφέρεται συχνά ως το *τροποποιημένο ελαστικό ρευστό*. Η συνάρτηση απόσβεσης στην περίπτωση διατμητικής παραμόρφωσης δίνεται από την σχέση

$$h(\gamma) = \frac{G(t, \gamma)}{G(t)} \quad (14)$$

και αποτελεί ένδειξη *απώλειας μνήμης* στο υλικό. Περιγράφει ποσοτικά την απόκλιση που παρουσιάζει το διατμητικό μέτρο ελαστικότητας των πολυμερών από την γραμμική συμπεριφορά.

Συνάρτηση Απόσβεσης

Για την μορφή της συνάρτησης απόσβεσης έχουν προταθεί διάφορες αναλυτικές εκφράσεις. Ένα παράδειγμα είναι η εξίσωση του Wagner:

$$h(II_{C-1}) = e^{-n\sqrt{II_{C-1}-3}}, \quad (15)$$

ως συνάρτηση της δεύτερης αναλλοίωτης του τανυστή του Finger. Η συνάρτηση αυτή παίρνει την ανάλογη μαθηματική μορφή σε κάθε περίπτωση παραμόρφωσης. Για την ειδική περίπτωση της βηματικής αύξησης της διατμητικής παραμόρφωσης, η εξίσωση του Wagner γράφεται στην απλή μορφή:

$$h(\gamma_0) = e^{-n\gamma_0}, \quad (16)$$

όπου n είναι μια παράμετρος που χαρακτηρίζει την μη-γραμμική συμπεριφορά του τήγματος σε μεγάλες παραμορφώσεις. Τιμές της παραμέτρου n για τήγματα εμπορικών πολυαιθυλενίων που υποβλήθηκαν σε μετρήσεις χαλάρωσης τάσεων μετά από βηματική αύξηση της διατμητικής παραμόρφωσης από τον Τσενόγλου [9], δίνονται στον Πίνακα 1.

Μια ακόμη πρόταση για την συνάρτηση απόσβεσης είναι η εξίσωση PSM (Papanastasiou-Scriven-Macosko) που δίνεται στην περίπτωση βαθμωτής διατμητικής παραμόρφωσης από την σχέση

$$h(\gamma_0) = \frac{\alpha_{pap}}{\alpha_{pap} + \gamma_0^2}, \quad (17)$$

όπου α_{pap} μια σταθερά.

Και οι δύο συναρτήσεις απόσβεσης παρέχονται σε αναλυτική μορφή και απλοποιούν τους υπολογισμούς. Ωστόσο η περιγραφή αυτή, παρ' όλη την απλότητα που προσφέρει στους υπολογισμούς, τελικά θεωρείται εξαιρετικά απλοποιητική καθώς, όπως και το γραμμικό ιξωδοελαστικό μοντέλο, περιγράφει την φαινομενολογία της ρεολογίας των πολυμερών αγνοώντας οποιαδήποτε μικροσκοπική δομή του υλικού. Το γεγονός αυτό, αλλά και πρόσφατες πειραματικές ενδείξεις τις οποίες δεν συμπεριλαμβάνει, π.χ. η περιγραφή του Wagner, οδήγησαν σε μια διαφορετική μορφή της

Πίνακας 1: Τιμές της παραμέτρου n της απλής εκθετικής συνάρτησης απόσβεσης του Wagner για εμπορικά τυχαία διακλαδωμένα και γραμμικής αρχιτεκτονικής πολυαιθυλένια. Τα δείγματα χαρακτηρίζονται από ποικιλία μοριακών βαρών και πολυδιασποράς.

Sample	M_w (Kg/mol)	PI (M_w/M_n)	$T(^{\circ}C)$	n
LDPE.A2	451	27.5	150	0.134
LDPE.A4	305	30.3	150	0.11
LDPE.A7	268	24.6	110, 150	0.13
LDPE.B2	143	10.2	150	0.14
LDPE.C2	69	7.6	150	0.16
LDPE IUPAC A	231	10.0	130, 150	0.18
HDPE.A	181	13.7	140, 150, 170	0.34–0.38
HDPE.B	118	6.1	140,150	0.29
HDPE.C	113	11.2	150	0.28

συνάρτησης απόσβεσης που προτάθηκε από τον Τσενόγλου [6] και δίνεται από την σχέση

$$h(\lambda) = \lambda^{-\beta} \quad (18)$$

όπου $\lambda = \lambda(t', t)$ είναι η *σχετική παραμόρφωση* ως συνάρτηση του χρόνου και β είναι μια παράμετρος που χαρακτηρίζει την μη-γραμμική ιξωδοελαστική συμπεριφορά του υλικού και εξαρτάται μονάχα από το μέγεθος της παραμόρφωσης. Η εξίσωση Τσενόγλου μπορεί να γενικευτεί για όλες τις παραμορφώσεις εφελκυσμού μέσω της:

$$\beta \approx \beta_u \left(2 - \exp \left\{ -\sqrt{\frac{m_e + 0.5}{0.6}} \right\} \right), \quad (19)$$

όπου η παράμετρος m_e ($-0.5 \leq m_e \leq 1$) χαρακτηρίζει τον τύπο εφελκυστικής παραμόρφωσης.

Με βάση πειραματικά δεδομένα από την διεθνή βιβλιογραφία (βλ. Πίνακα 2) οι Tsenoglou et. al. [14] κατέληξαν στο συμπέρασμα ότι η παράμετρος $\beta \geq 1$ για γραμμικά πολυμερή και $\beta < 1$ για πολυμερή με μακριές διακλαδώσεις. Αποκλίσεις από αυτόν τον κανόνα για τα γραμμικά πολυμερή μπορεί να οφείλονται σε υψηλή πολυδιασπορά ή στην παρουσία μικρών ποσοτήτων μακριών διακλαδώσεων στο τήγμα κάτι που είναι λογικό για την περίπτωση εμπορικών γραμμικών πολυμερών. Πειραματικές μετρήσεις εφελκυσμού σε τήγματα γραμμικών και διακλαδωμένων PP (βλ. Πίνακα 3 και 4) από τους Gotsis et al. [5, 6] έδειξαν ότι οι προαναφερθείσες παραδοχές πράγματι ισχύουν. Από την εργασία των συγγραφέων προέκυψε μία αναλυτική σχέση που συνδέει την παράμετρο β με τον μέσο αριθμό μακριών διακλαδώσεων στο τήγμα, B_n

$$\beta_u \approx 2 \exp \left(-\alpha_u \sqrt[3]{B_n} \right) \quad (20)$$

Πίνακας 2: Τιμές της παραμέτρου β της συνάρτησης απόσβεσης Τσενόγλου για πολυολεφίνες διαφορετικής χημικής σύστασης, μοριακού βάρους και πολυδιασποράς που υποβλήθηκαν σε διαφορετικές πειραματικές μετρήσεις εφελκυσμού.

Ονομασία Δείγματος	M_w (Kg/mol)	(M_w/M_n)	Γεωμετρία Εφελκυσμού, m_e		
			$(m_e=-0.5)$	$(m_e=0)$	$(m_e=1)$
PS.50124	250	1.2	0.96		1.65
PS.606	180	2.5	0.66		1.21
IUPAC A	472	24.9	0.48	0.96	1.15
PS.I	398	2.9	0.80		1.16
LLDPE	158	12.5		1.04	1.17
HDPE.II	152	13	1.30		1.28
HDPE.S	104	5.5	0.85	0.92	0.92
PIB	120	2.2	1.17	1.49	1.33

οπου B_n είναι ο μέσος κατα βάρος αριθμός χημικών διασταυρώσεων ανα μακρομοριακή αλυσίδα και α_u μιά ελεύθερη παράμετρος. Απο την σχετική ανάλυση των πειραματικών αποτελεσμάτων (βλ. Σχ. 2 και 3) βρέθηκε ότι η παράμετρος α_u δεν παίρνει μιά μοναδική τιμή για το υλικό και φαίνεται να εξαρτάται εν γένει από το μέγεθος του B_n . Η γενίκευση τουλάχιστον για τα εμπορικά πολυμερή άμεσου ενδιαφέροντος είναι πολύ δύσκολη καθώς πολυμερή με τον ίδιο αριθμό χημικών διασταυρώσεων παρουσιάζουν σημαντικές διαφορές στον βαθμό εφελκυστικής εργοσκληρυνσης (βλέπε Σχ. 4). Το συμπέρασμα είναι πως πρέπει να συμπεριληφθούν και άλλες ιδιότητες του υλικού όπως, π.χ., η κατανομή των χημικών διασταυρώσεων και το σχετικό μέγεθος τους ως προς το μέγεθος της κύριας αλυσίδας κ.ά., ώστε να καταστεί δυνατή μια ενοποιημένη περιγραφή.

Μοριακή Θεωρία Doi-Edwards

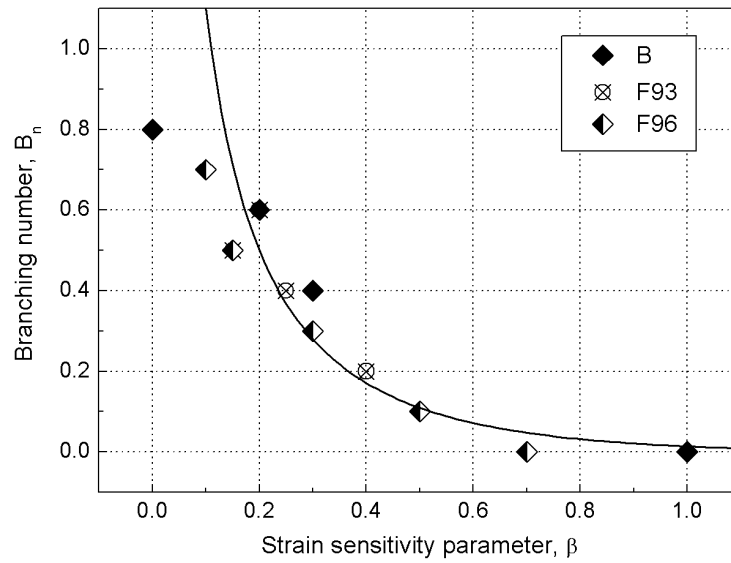
Πειραματικές μετρήσεις της ρεολογίας τήγμάτων πολυμερών σε δυναμική διάτμηση που πραγματοποιήθηκαν από τον Onogi [63] έδειξαν ότι το δυναμικό μέτρο ελαστικότητας των πολυμερών μεταβάλλεται με το μοριακό βάρος. Συγκεκριμένα έδειξαν ότι αυξάνοντας το μοριακό βάρος ενός τήγματος πολυμερούς, που περιλαμβάνει γραμμικές αλυσίδες και χαρακτηρίζεται από μικρή πολυδιασπορά, πάνω από ένα κατώτατο όριο, M_C , εμφανίζεται ένα πλατό στο ελαστικό τμήμα του δυναμικού μέτρου ελαστικότητας ή, αντίστοιχα, στο διατμητικό μέτρο χαλάρωσης, του οποίου το μέγεθος αυξάνει με το μοριακό βάρος. Η εξήγηση δόθηκε αρχικά από τον de Gennes και αργότερα από τους Doi και Edwards σε μορφή μαθηματικής θεωρίας με ελέγχιμες προβλέψεις. Μακριές αλυσίδες μεγάλου μοριακού βάρους περιπλέκονται μεταξύ τους δημιουργώντας έτσι ένα είδος φυσικών διαπλοκών μεταξύ των αλυσίδων στο τήγμα, οι οποίες, τελικά, ευθύνονται για τους αργούς χρόνους μετάβασης του τήγματος στην ισορροπία μετά από εξωτερική παραμόρφωση. Η τάση και, κατ' επέκταση, το μέτρο χαλάρωσης του τήγματος εξαρτώνται εν γένει από το μέγεθος της παραμόρφωσης.

Πίνακας 3: Μοριακά χαρακτηριστικά εμπορικών πολυπροπυλενίων με τυχαία κατανομή μακρών διακλαδώσεων που παρασκευάστηκαν από το αντίστοιχο γραμμικό πολυμερές προσθέτοντας στο τελευταίο διαφορετικά ποσοστά διασταυρωτή, P-26 και τιμές της παραμέτρου β και του δείκτη εργοσκήρυνσης, SHI, όπως προσδιορίστηκαν από μετρήσεις μονοαξονικού εφέλκυσμού σε θερμοκρασία $T=190^{\circ}\text{C}$.

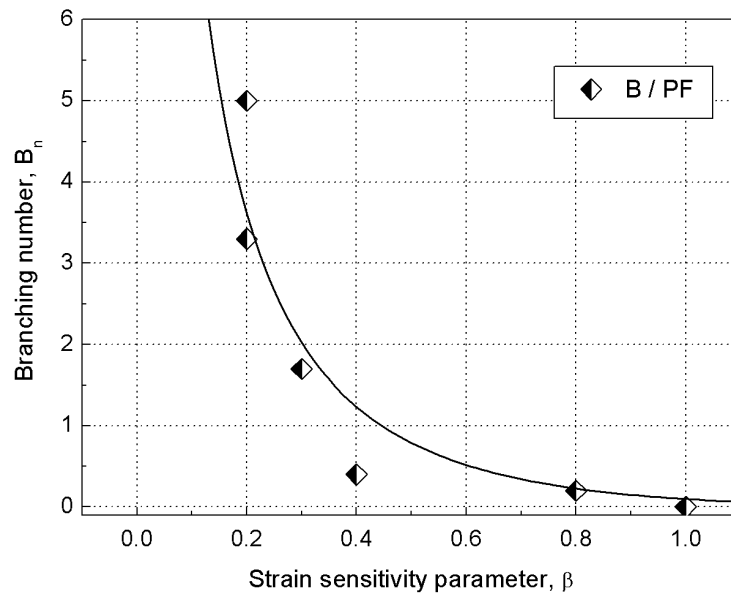
Sample	P-26 (mmol)	M_w (Kg/mol)	(M_w/M_n)	B_n	β	MFI (230/2.16)	SHI
B	0	422	6.2	0	1	2.3	2
	1	575	7.8	0.4	0.3	1.1	8
	2	574	7.6	0.6	0.2	0.6	10.5
	3	581	8.6	0.7	0.1	0.6	28
	5	571	8.9	0.8	0	0.6	-
F93	0	333	5.8	0	1.8	6	1.25
	1	381	7.1	0.2	0.4	3.4	6
	2	413	7.8	0.4	0.25	2.5	15
	3	456	7.9	0.5	0.15	2	16
	5	458	7.7	0.6	0.2	1.8	19
F96	0	314	7	0	0.7	12.2	2
	1	363	8.1	0.1	0.5	8	4.2
	2	389	9.3	0.3	0.3	5.8	6.5
	3	407	9.2	0.5	0.15	4.2	7.5
	5	414	8.6	0.7	0.1	3.1	10

Πίνακας 4: Μοριακά χαρακτηριστικά γραμμικού και μιγμάτων γραμμικού και εμπορικού διακλαδισμένου πολυπροπυλενίου σε διαφορετικές αναλογίες. Η παράμετρος β και ο δείκτης σκλήρυνσης, SHI, προσδιορίστηκαν για κάθε δείγμα από πειραματικές μετρήσεις ροής εφέλκυσμού σε θερμοκρασία $T = 190^{\circ}\text{C}$.

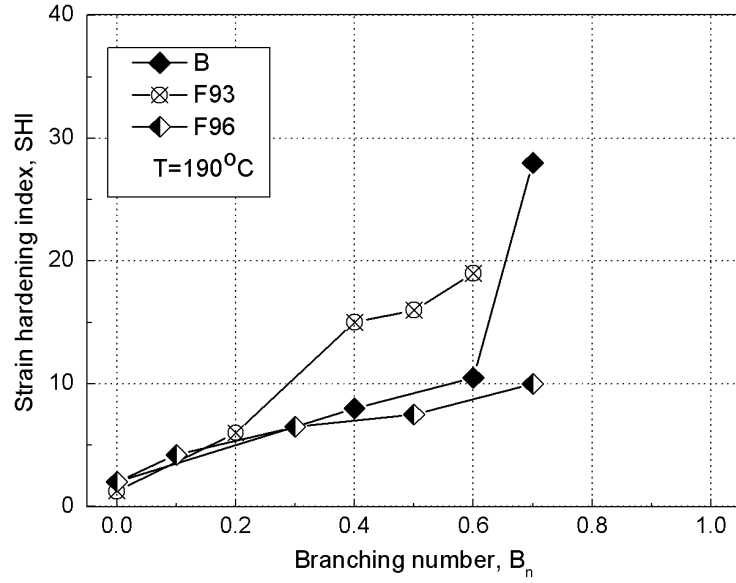
PF (%)	M_w (Kg/mol)	(M_w/M_n)	B_n	β	MFI (230/2.16)	SHI
0	422	6.2	0	1	2.3	2
12.5	388	6.3	0.2	0.8	3.2	2.7
25	400	6.4	0.4	0.4	3.0	3
50	485	8	1.7	0.3	2.7	6.4
75	569	7.9	3.3	0.2	3.2	9.6
100	629	9.5	5	0.2	4.6	14.7



Σχήμα 2: Ποσοστό διακλάδωσης, B_n , ως συνάρτηση της παραμέτρου β για τα δείγματα του Πίνακα 3



Σχήμα 3: Ποσοστό διακλάδωσης, B_n , ως συνάρτηση της παραμέτρου β για τα δείγματα του Πίνακα 4



Σχήμα 4: Μεταβολή του δείκτη σκλήρυνσης, SHI ως συνάρτηση του ποσοστού διακλαδώσεων, B_n για τα δείγματα του Πίνακα 3.

Οι προβλέψεις της θεωρίας δίνονται από την καταστατική εξίσωση:

$$\underline{\underline{\sigma}} = \int_{-\infty}^t \mu(t-t') \underline{\underline{\mathfrak{S}}}_{DE}(t, t') dt' \quad (21)$$

όπου $\mu(t-t')$ είναι το χρονοεξαρτώμενο μέρος (βλ. Εξ. 3.83 και 3.87) και $\underline{\underline{\mathfrak{S}}}_{DE}$ είναι ο τανυστής παραμόρφωσης δεύτερης τάξης του Larson και στην περίπτωση βαθμωτής διατμητικής παραμόρφωσης συνδέεται με την συνάρτηση απόσβεσης μέσω της σχέσης:

$$h_{DE}(\gamma_0) = \frac{\mathfrak{S}_{DE}}{\gamma_0} = \frac{15}{4} \frac{Q_{12}(\gamma_0)}{\gamma_0} \quad (22)$$

όπου $Q_{12}(\gamma_0)$ είναι ο τανυστής παραμόρφωσης των Doi-Edwards¹, σελ. 89. Οι προβλέψεις της θεωρίας για την περίπτωση ιδανικού τήγματος γραμμικού πολυμερούς που υφίσταται βηματική διατμητική παραμόρφωση δίδονται στο Παράρτημα Β.

Ωστόσο, παρόλο που η θεωρία δίνει τα σωστά αποτελέσματα για τήγματα που περιλαμβάνουν γραμμικές αλυσίδες, πειραματικές μετρήσεις σε εμπορικά τήγματα τυχαία διασταυρωμένων πολυμερών με μακριές αλυσίδες από τον Τσενόγλου (βλέπε Πίνακα 5) αποκλίνουν από τις προβλέψεις της θεωρίας. Ένας νέος μοριακός μηχανισμός προτάθηκε από τον Τσενόγλου για να εξηγήσει αυτή την συμπεριφορά και συνοψίζεται στην τροποποιημένη εξίσωση για την συνάρτηση απόσβεσης τήγματος

¹Ο ορισμός του Q_{12} για τυχούσα παραμόρφωση δίνεται από την Εξ. 3.82

Πίνακας 5: Φυσικές ιδιότητες των πολυαιθυλενίων του Τσενόγλου (βλ. και Πίν. 1).

Sample	M_b (kg/mol)	λ_b (10^4)	g_s	B_n	x_n	η_0 (150°C) (kPa · s)
LDPE.A2	2.83	1.77	0.117	80	0.76	234.4
LDPE.A4	2.35	2.40	0.136	73	0.83	19.95
LDPE.A7	1.92	2.61	0.128	70	0.77	7.24
LDPE.B2	4.17	1.20	0.296	17	0.74	69.2
LDPE.C2	3.68	0.78	0.427	5.4	0.75	19.06
LDPE IUPAC A	4.85	1.03	0.261	24	0.65	478.6

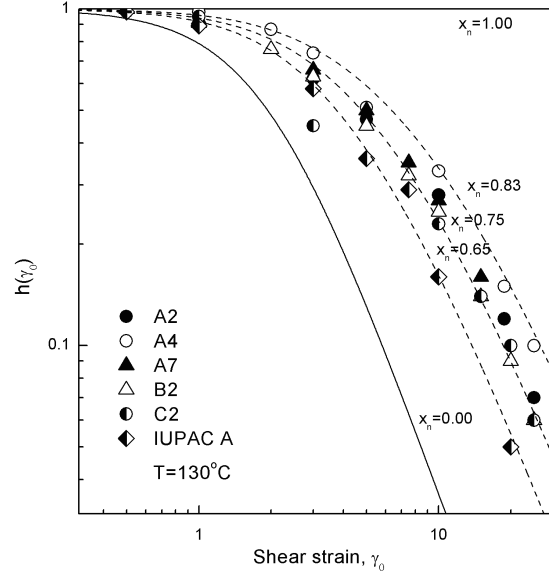
που υφίσταται βαθμωτή διατμητική παραμόρφωση και δίνεται από την σχέση:

$$h_{DE}(\gamma_0) = \left(\frac{15}{4} \frac{Q_{12}(\gamma_0)}{\gamma_0} \right) \left(\frac{1}{[(1-x_n) + \frac{x_n}{\langle |E \cdot u| \rangle}]^2} \right), \quad (23)$$

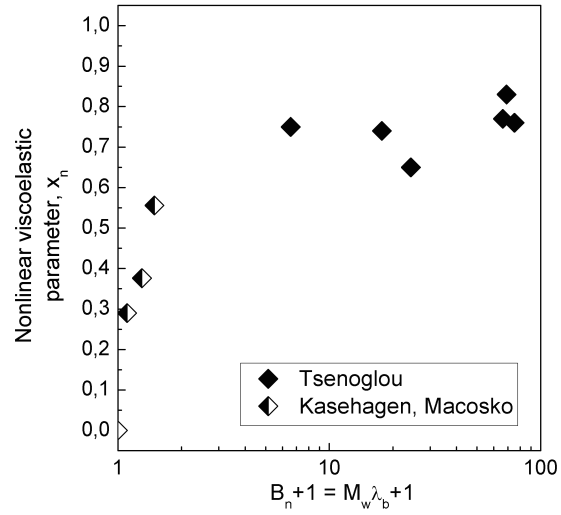
όπου x είναι η μη-γραμμική ιξωδοελαστική παράμετρος που χαρακτηρίζει την απόκλιση των πειραματικών μετρήσεων από την γραμμική συμπεριφορά και αντικατοπτρίζει το σχετικό μέγεθος του διακλαδωμένου μακρομορίου που συμπεριφέρεται ελαστικά. Με αυτόν τον τρόπο δίδεται μια φυσική εξήγηση για τις παρατηρούμενες αποκλίσεις από την καθιερωμένη φυσική περιγραφή της κλασικής θεωρίας των Doi και Edwards (βλ. Σχ. 5). Η εξάρτηση της παραμέτρου x_n από τον μέσο κατά βάρος αριθμό χημικών διακλαδώσεων στο τήγμα ανά μακρομόριο συνοψίζονται στο Σχ. 6 όπου παρουσιάζονται πειραματικά αποτελέσματα για τα εμπορικά πολυαιθυλένια του Τσενόγλου [9] αλλά και για μείγματα εμπορικών τυχαία διακλαδωμένων πολυβουταδιενίων με ένα γραμμικό πολυμερές ίδιας χημικής σύστασης σε διαφορετικές αναλογίες τα οποία παρασκευάστηκαν από τους Macosko και Kasehagen (βλ. Πίνακα 3.5 και 6.2).

Αποκλίσεις όμως από την περιγραφή αυτή παρατηρούνται με βάση πάντα τα πειραματικά αποτελέσματα του Τσενόγλου [9] και για εμπορικά γραμμικά πολυμερή (βλ. Πίνακα 3.10 και Σχ. 3.14, 3.15, 3.16 και 3.17) για τα οποία όμως οι αποκλίσεις από τις προβλέψεις της θεωρίας των Doi και Edwards σε μεγάλα μεγέθη παραμόρφωσης οφείλονται σε έναν διαφορετικό χημικό μηχανισμό που ονομάζεται κρυστάλλωση τήγματος και οφείλεται στην δυνατότητα που έχουν τα γραμμικής αρχιτεκτονικής πολυμερή να ευθυγραμμίζονται με το πεδίο ταχύτητας και να σχηματίζουν περιοχές υψηλού βαθμού τακτικότητας. Οι περιοχές αυτές αυξάνουν με την σειρά τους την ελαστικότητα του τήγματος και συχνά ευθύνονται για τις παρατηρούμενες αποκλίσεις από τις προβλέψεις της θεωρίας.

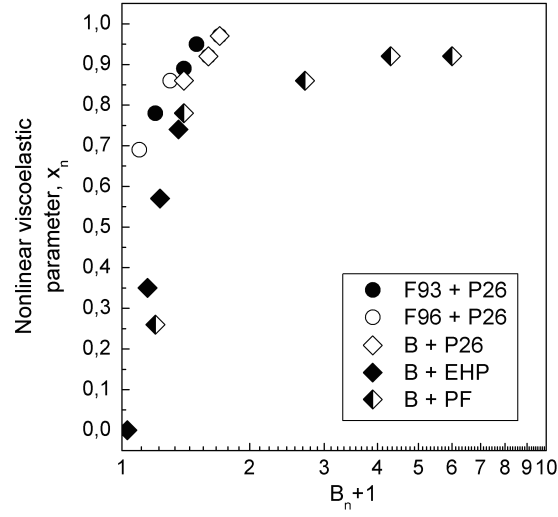
Η μετατροπή των πειραματικών δεδομένων των εμπορικών πολυπροπυλενίων των Gotsis et al. σε τιμές της παραμέτρου x_n σαν συνάρτηση του B_n δίνονται συγκεντρωτικά στο Σχ. 7 (βλ. και Πίνακα 6.3). Συνολικά όλα τα δείγματα των Σχ. 6 και 7 δίνονται συγκεντρωτικά στο Σχ. 8. Από αυτό το συγκεντρωτικό γράφημα φαίνεται πως οι τιμές x_n για τα πολυπροπυλένια (υπολογισμένες από δεδομένα εφελκυσμού) είναι



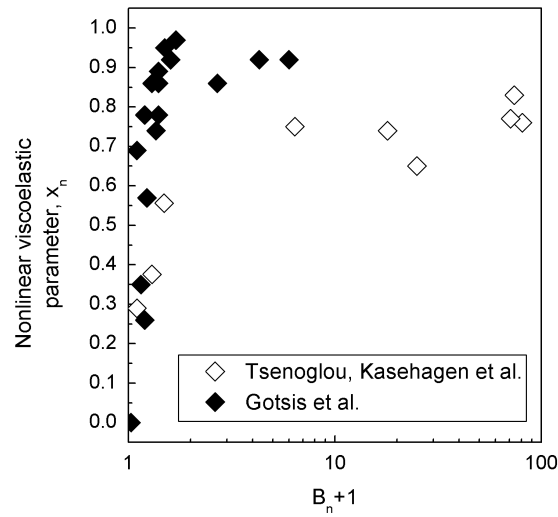
Σχήμα 5: Εξάρτηση της παραμέτρου x_n της τροποποιημένης συνάρτησης απόσβεσης των Doi-Edwards από το μέγεθος διατμητικής παραμόρφωσης για τα δείγματα του Πίνακα 5.



Σχήμα 6: Εξάρτηση της παραμέτρου x_n της τροποποιημένης συνάρτησης απόσβεσης των Doi-Edwards από το ποσοστό διακλαδώσεων, B_n για τα δείγματα του Πίνακα 5 και τα τροποποιημένα με τυχαία κατανομή μακρών διακλαδώσεων εμπορικά πολυβουταδιένια των Kasehagen και Macosko (βλ. Πίνακα 3.5 και 6.2).



Σχήμα 7: Εξάρτηση της παραμέτρου x_n της τροποποιημένης συνάρτησης απόσβεσης των Doi-Edwards από το ποσοστό διακλαδώσεων, B_n για τα δείγματα των Πινάκων 3, 4 και 6.1.



Σχήμα 8: Εξάρτηση της παραμέτρου x_n της τροποποιημένης συνάρτησης απόσβεσης των Doi-Edwards από το ποσοστό διακλαδώσεων, B_n για όλα τα δείγματα των Σχ. 6 και 7.

υψηλότερες από τις αντίστοιχες για τα πολυβουταδιένια και πολυαιθυλένια (υπολογισμένα από δεδομένα βαθμωτής διάτμησης). Ωστόσο δεν είναι ξεκάθαρο αν αυτή η διαφορά οφείλεται στον διαφορετικό τύπο πολυμερούς, διαφορές στην αρχιτεκτονική δομή των μακριών διακλαδώσεων μεταξύ των δειγμάτων, την πειραματική διαδικασία που ακολουθήθηκε στο εκάστοτε δείγμα για την δημιουργία μακριών διακλαδώσεων ή στον τύπο της παραμόρφωσης (εφελκυσμός ή διάτμηση) από τον οποίο προέκυψαν οι τιμές της παραμέτρου x_n . Είναι λογικό και αναμενόμενο ότι το x_n θα πρέπει να παίρνει την ίδια τιμή ανεξάρτητα του τύπου παραμόρφωσης που επιλέγεται για τον προσδιορισμό του (τουλάχιστον για πολυμερή ίδιας χημικής σύστασης).

Μοριακή Θεωρία ΧΡΡ

Καταστατικές εξισώσεις που περιγράφουν την ρεολογική συμπεριφορά των πολυμερικών τηγμάτων και ταυτόχρονα συνδέουν μακροσκοπικές παρατηρήσιμες ποσότητες με μοριακά χαρακτηριστικά και μικρομοριακούς μηχανισμούς μπορούν να αναπτυχθούν και σε διαφορική μορφή. Ένα παράδειγμα είναι το μοντέλο ΧΡΡ ή *εκτεταμένο μοντέλο rom-rom* και βασίζεται στην θεωρία Rom-Rom που ανέπτυξαν οι McLeish και Larson [72, 47]. Η προκύπτουσα τάση στα πλαίσια του μοντέλου αυτού δίνεται από την σχέση

$$\underline{\underline{\sigma}}_i + \tau(\underline{\underline{\sigma}}_i)^{-1} \underline{\underline{\sigma}}_i = 2G_i \underline{\underline{D}} \quad (24)$$

η οποία είναι τύπου Upper Convected Maxwell, όπου η παράμετρος που αντιστοιχεί στον χρόνο ή τους χρόνους χαλάρωσης έχει αντικατασταθεί από ένα συναρτησιοειδές, $\tau(\underline{\underline{\sigma}}_i)^{-1}$. Το συναρτησιοειδές $\tau(\underline{\underline{\sigma}}_i)^{-1}$ περιλαμβάνει παραμέτρους που αντιστοιχούν σε μοριακούς μηχανισμούς και ευθύνονται για την μακροσκοπική ρεολογική συμπεριφορά του υλικού. Το μοντέλο ΧΡΡ χρησιμοποιεί βασικά στοιχεία της θεωρίας των Doi και Edwards, αναπτύχθηκε ωστόσο εξ' αρχής σε δική του θεωρητική βάση. Από την ανάλυση των πειραματικών δεδομένων σε δείγματα εμπορικών πολυαιθυλενίων με χρήση του μοντέλου ΧΡΡ διαφαίνεται η ικανότητά του να περιγράφει επακριβώς τη ρεολογία των τηγμάτων σε ομοαξονικό εφελκυσμό (βλέπε Σχ. 5.17, 5.18, 5.19 και 5.20). Επίσης εξετάζεται η δυνατότητα που μπορεί να προσφέρει η θεωρητική δομή του μοντέλου στην ανάκτηση χρήσιμων πληροφοριών για την μοριακή δομή του εκάστοτε τήγματος, όπως π.χ. ο προσδιορισμός του μέσου αριθμού χημικών διασταυρώσεων στο τήγμα μόνο από δεδομένα ρεολογίας, κάτι το οποίο είναι πολύ δύσκολο να επιτευχθεί με μεθόδους άλλες εκτός από αυτήν του ρεολογικού χαρακτηρισμού.

Μοριακή Θεωρία Rolie-Poly

Μια ακόμη καταστατική εξίσωση (σε διαφορική μορφή) χρησιμοποιήθηκε για να περιγράψει την ρεολογική συμπεριφορά γραμμικών πολυολεφινών. Το μοντέλο Rolie-Poly αφορά μονάχα σε γραμμικά πολυμερή και αποτελεί μια απλοποιητική εκδοχή ενός πιο ολοκληρωμένου μοντέλου που αναπτύχθηκε από τους Likhtman και Graham [7, 62].

Πίνακας 6: Μοριακά χαρακτηριστικά των εμπορικών δειγμάτων Riblene και Eraclene που εξετάστηκαν πειραματικά σε διάτμηση και εφελκυσμό.

	LDPE Riblene® FF20	HDPE Eraclene® FA506
MFI (2.16/190) (gr/10 min)	0.8	-
MFI (5/190) (gr/10 min)	-	0.6
MFI (21.6/190) (gr/10 min)	-	15
Density (25°C)(gr/cm ³)	0.921	0.939
Melting Point (°C)	112	129
M_n (kg/mol)	13.4	12.3
M_w (kg/mol)	160.3	196.6
M_z (kg/mol)	841.1	1536.0
M_w/M_n	12.0	16.0
g'_s	0.612	-
g_s	0.612	-
B_n	8.8	-

Πειραματικό Μέρος

Στο πειραματικό μέρος χρησιμοποιήθηκαν δύο εμπορικά δείγματα πολυαιθυλενίου, ένα χαμηλής πυκνότητας πολυαιθυλένιο με τυχαία κατανομή μακρών διακλαδώσεων και εμπορική ονομασία Riblene® FF20 και ένα γραμμικό υψηλής πυκνότητας πολυαιθυλένιο με εμπορική ονομασία Eraclene® FA506. Τα μοριακά χαρακτηριστικά και των δύο δειγμάτων δίνονται στον Πίνακα 6.

Και τα δύο δείγματα υποβλήθηκαν σε μετρήσεις διάτμησης και εφελκυσμού. Συγκεκριμένα το δείγμα Riblene® υποβλήθηκε σε βαθμωτή διάτμηση, δυναμική διάτμηση και μονοαξονικό εφελκυσμό ενώ το Eraclene® σε δυναμική διάτμηση και μονοαξονικό εφελκυσμό.

Τα δείγματα παρασκευάστηκαν με συμπίεση των πελλετών σε θερμαινόμενη πρέσα σε μορφή παραλληλεπίπεδης πλάκας. Για τις μετρήσεις διάτμησης κόπηκαν από την πλάκα κυκλικά δείγματα διαμέτρου $2R_p \approx 25$ mm και πάχους 0.5 - 1.0 mm. Για τις μετρήσεις εφελκυσμού κόπηκαν ορθογώνια δείγματα διαστάσεων 60 x 10 x 15 mm³. Οι μετρήσεις σε δυναμική διατμητική ροή και για τα δύο δείγματα έγιναν σε διαφορετικές θερμοκρασίες ενώ οι μετρήσεις εφελκυσμού πραγματοποιήθηκαν σε θερμοκρασία 150°C για το Riblene® και 170°C για το Eraclene®. Για τις μετρήσεις βηματικής διάτμησης χρησιμοποιήθηκε μόνο ένα δείγμα ενώ για τις μετρήσεις δυναμικής διάτμησης χρησιμοποιήθηκε ένα δείγμα για κάθε θερμοκρασία μέτρησης.

Πριν την έναρξη των μετρήσεων πραγματοποιήθηκε μέτρηση για τον προσδιορισμό του γραμμικού ορίου απόκρισης και των δύο υλικών. Μετρήθηκαν τα μέτρα ελαστικότητας G' και G'' των δύο δειγμάτων σε συχνότητα 1 rad/s και προσδιορίστηκε το μέγιστο πλάτος ταλάντωσης στο οποίο τα δύο δείγματα συμπεριφέρονται γραμμικά. Το μέγιστο πλάτος ταλάντωσης για γραμμική συμπεριφορά καθορίζεται ως το μέγιστο πλάτος στο οποίο τα G' και G'' μεταβάλλονται με τον ίδιο ρυθμό. Και

για τα δύο δείγματα ορίσθηκε πειραματικά το γραμμικό όριο σε $\approx 0.05 - 0.1$ μονάδες διατμητικής παραμόρφωσης.

Για τις μετρήσεις βηματικής αύξησης της διάτμησης χρησιμοποιήθηκε το ρεόμετρο ARES-II[®] της Rheometric Scientific με ανάλυση 2-2000 mNm σε διάταξη κώνου-επίπεδης πλάκας. Πραγματοποιήθηκαν μετρήσεις σε ένα εύρος διατμητικών παραμορφώσεων 0.01 - 2.0 όπου η παραμόρφωση ορίζεται μέσω της σχέσης:

$$\gamma_0 = \frac{\phi}{\beta_c}, \quad (25)$$

όπου ϕ , είναι η γωνία στρέψης μεταξύ κώνου και σταθερής πλάκας και β_c είναι η γωνία που σχηματίζει ο κώνος με την πλάκα. Στην συγκεκριμένη περίπτωση $\beta_c \approx 0.1$ rad. Κρατώντας σταθερή την παραμόρφωση, μετράται η τάση ως συνάρτηση του χρόνου μέσω της

$$\sigma_{12} = \frac{3M_t}{2\pi R_p^3}, \quad (26)$$

όπου M_t ροπή στρέψης μετρούμενη μέσω της δύναμης που ασκείται στο άκρο της πλάκας και R_p η ακτίνα της κυκλικής πλάκας.

Για τις μετρήσεις δυναμικής διάτμησης χρησιμοποιήθηκε το ίδιο ρεόμετρο σε διάταξη πλάκας-πλάκας και απόσταση μεταξύ πλακών 1.0 - 1.5 mm. Οι μετρήσεις έγιναν σε εύρος συχνοτήτων 0.1 - 100 rad/s και σε διαφορετικές θερμοκρασίες, 120 °C - 190 °C για το Riblene[®] και 150 °C - 200 °C για το Eraclene[®]. Η συχνότητα διατμητικής παραμόρφωσης δίνεται από την σχέση:

$$\dot{\gamma} = \frac{\omega R_p}{h_p}, \quad (27)$$

όπου h_p η απόσταση μεταξύ των πλακών. Η προκύπτουσα τάση υπολογίζεται από την σχέση:

$$\sigma_{12} = \frac{M_t}{2\pi R_p^3} \left[3 + \frac{d \ln M_t}{d \ln \dot{\gamma}} \right], \quad (28)$$

όπου M_t η προκύπτουσα ροπή στρέψης μετρούμενη πάντα μέσω της δύναμης που ασκείται στο υλικό στο άκρο της πλάκας.

Για τις μετρήσεις εφελκυσμού χρησιμοποιήθηκε το ρεόμετρο RME[®] της Rheometrics Scientific με ανάλυση 0.1 - 200 mN. Πραγματοποιήθηκαν μετρήσεις μονοαξονικού εφελκυσμού σε εύρος ρυθμών εφελκυσμού 0.01 - 2.0 s⁻¹ και για τα δύο δείγματα. Κρατήθηκαν μονάχα οι μετρήσεις οι οποίες ήταν έγκυρες. Τέλος έγιναν οι απαραίτητες σύμφωνα με τα πρότυπα διορθώσεις όσον αφορά τον πραγματικό ρυθμό εφελκυσμού καθώς αυτός διαφέρει εν γένει από τον προκαθορισμένο από τον χρήστη ανάλογα με τον τύπο δείγματος και τον ρυθμό εφελκυσμού. Η διόρθωση έγινε μετρώντας την ελάττωση του πλάτους του δοκιμίου ανά τακτά χρονικά διαστήματα υπολογίζοντας έτσι τον πραγματικό ρυθμό εφελκυσμού. Η τάση υπολογίζεται από την σχέση:

$$\sigma(t) = \frac{F(t)}{A(0)} = \frac{F(t)}{A_0 e^{-\epsilon t}}, \quad (29)$$

όπου $F(t)$ η μετρούμενη δύναμη εφελκυσμού και $A_0 e^{-\epsilon t}$ χαρακτηρίζει την ελάττωση του κάθετου στον άξονα εφελκυσμού εμβαδού του δοκιμίου με τον χρόνο για τον

εκάστοτε ρυθμό εφελκυσμού, $\dot{\epsilon}$. Το ιξώδες εφελκυσμού ως συνάρτηση του χρόνου υπολογίζεται από την σχέση:

$$\eta_E(t) = \frac{\sigma(t)}{\dot{\epsilon}} \quad (30)$$

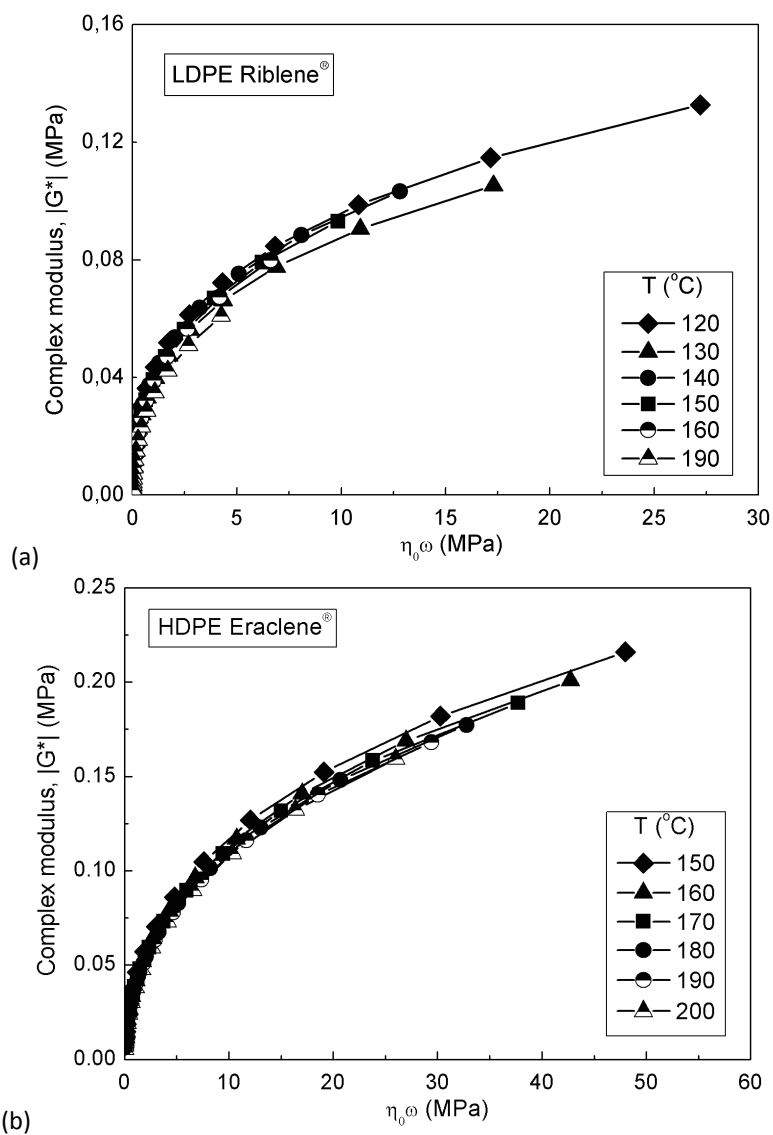
Μικρές διορθώσεις έγιναν και για τα δύο δείγματα, υπολογίζοντας τις πραγματικές αρχικές διαστάσεις των δοκιμίων μέτρησης αφού τα τελευταία υπέστησαν διόγκωση λόγω των υψηλών θερμοκρασιών των μετρήσεων.

Αποτελέσματα

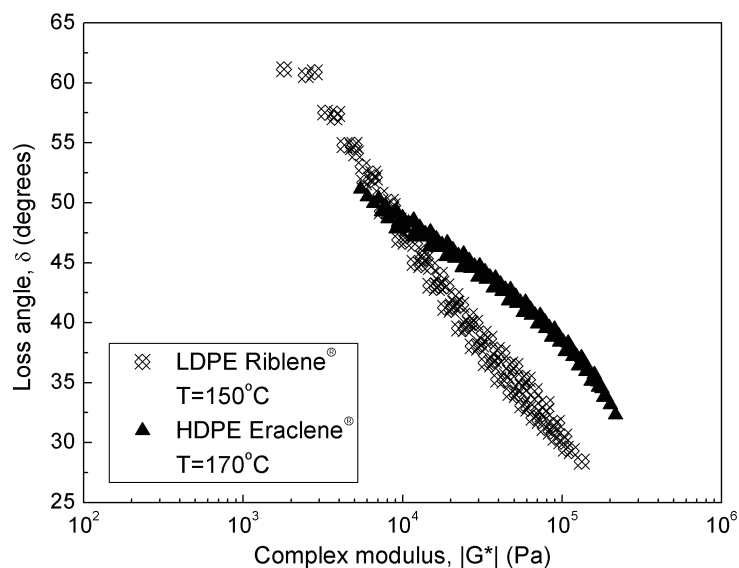
Τα αποτελέσματα και η θεωρητική ανάλυση όλων των πειραματικών μετρήσεων δίνονται ξεχωριστά για κάθε δείγμα στους Πίνακες και τα αντίστοιχα Σχήματα του Κεφαλαίου 5. Συγκεκριμένα στον Πίνακα 5.3 δίδονται οι παράμετροι του φάσματος χαλάρωσης των δύο δειγμάτων. Στον Πίνακα 5.1 δίδονται οι παράμετροι του μοντέλου του Cross για το ιξώδες ως συνάρτηση της συχνότητας διάτμησης για διαφορετικές θερμοκρασίες. Στον Πίνακα 5.4 δίνονται οι κρίσιμοι χρόνοι, t_{cr} , για κάθε θερμοκρασία μέτρησης και για τα δύο δείγματα που αντιστοιχούν στους χρόνους ή αντίστοιχα στις συχνότητες στις οποίες τα δυναμικά μέτρα ελαστικότητας G' και G'' εξισώνονται. Στον Πίνακα 5.2 (και γραφικά στο Σχ. 5.9) δίδονται οι σταθερές α_T σε κάθε θερμοκρασία και για τα δύο δείγματα που προκύπτουν από την υπέρθεση των δυναμικών μέτρων ελαστικότητας των δύο πολυμερών. Από τις τιμές αυτές και με χρήση γραμμικής παρεμβολής προκύπτει μια μέση ενέργεια ενεργοποίησης για κάθε δείγμα, ≈ 50.4 kJ για το Riblene® και ≈ 32.5 kJ για το Eraclene®. Οι παράμετροι του τροποποιημένου μοντέλου του Lodge βρέθηκαν να είναι $n = 0.25$ για το Riblene® και $n = 0.28$ για το Eraclene® όπως προκύπτουν από την προσαρμογή του μοντέλου στα αποτελέσματα ιξώδους σαν συνάρτηση της θερμοκρασίας. Αντίθετα βρέθηκε ότι $n = 0.23$ από τα πειράματα βαθμωτής διάτμησης για το Riblene. Οι τιμές της συνάρτησης απόσβεσης για το Riblene® δίνονται στον Πίνακα 5.5 και γραφικά στο Σχ. 5.9. Από τις μετρήσεις εφελκυσμού υπολογίστηκε η εκθετική παράμετρος του μοντέλου Τσενόγλου και βρέθηκε $\beta = 0.25$ για το Riblene® και $\beta = 0.40$ για το Eraclene®. Οι τιμές της συνάρτησης απόσβεσης δίνονται στους Πίνακες C.3 και C.4 του Παραρτήματος C και γραφικά στο Σχ. 5.16 και για τα δύο δείγματα. Ο δείκτης εργοσκήρυνσης, SHI, υπολογίστηκε για το Riblene από την πειραματική καμπύλη εφελκυστικού ιξώδους σε ρυθμό εφελκυσμού $\dot{\epsilon} \approx 0.081$ (sec^{-1}) και βρέθηκε ≈ 10.2 . Στους Πίνακες 5.6 και 5.7 δίνονται οι παράμετροι της προσαρμογής του μοντέλου XPP στα δεδομένα εφελκυσμού για το Riblene® και το Eraclene® αντίστοιχα. Οι προβλέψεις του μοντέλου Rolie-Poly δίνονται στα Σχ. 5.21 και 5.22. Τέλος οι προβλέψεις του τροποποιημένου μοντέλου των Doi και Edwards και για τα δύο δείγματα δίνονται στα Σχ. 6.4, 6.5, 6.6, 6.7 και 6.8.

Συζήτηση / Συμπεράσματα

Η παράμετρος n της απλής εκθετικής συνάρτησης του Wagner, παίρνει την τιμή $n = 0.23$ για το δείγμα Riblene® από τα πειράματα βηματικής διατμητικής παραμόρφωσης. Όταν χρησιμοποιηθεί η θεωρία του τροποποιημένου μοντέλου του Lodge, τότε



Σχήμα 9: Θερμορρολογική πολυπλοκότητα στα δείγματα (a) Riblene® και (b) Eraclene® με βάση την τεχνική των Wood-Adams και Costeux.



Σχήμα 10: Θερμο-ρεολογική πολυπλοκότητα στα δείγματα Riblene® και Eraclene® με βάση την τεχνική των VanGurp και Palmen.

τα πειραματικά δεδομένα ιξώδους σταθερού ρυθμού διάτμησης ως προς συχνότητα δίνουν $n = 0.25$. Η μικρή αυτή διαφορά αυτή εκτιμάται πως δεν οφείλεται σε πειραματικό λάθος ούτε σε λανθασμένη χρήση της θεωρίας. Αντίθετα, αν συγκρίνουμε τα πειραματικά δεδομένα βαθμωτής διάτμησης για το Riblene® με τα αντίστοιχα για τα πολυαιθυλένια του Τσενόγλου, παρατηρούμε ότι για τα τελευταία η μέγιστη παραμόρφωση ξεπερνά πάντα τις 20 μονάδες διάτμησης ενώ για το Riblene® η μέγιστη διάτμηση ήταν μόνο 2. Για να υπολογιστεί σωστά η εκθετική παράμετρος του Wagner χρειάζονται βηματικές παραμορφώσεις τουλάχιστον έως 10 μονάδες διάτμησης, που είναι περίπου και το ανώτατο όριο στο οποίο η εκθετική συνάρτηση απόσβεσης περιγράφει με ικανοποιητική ακρίβεια τα πειραματικά αποτελέσματα. Από τα πειραματικά δεδομένα διαπιστώθηκε ότι τα εμπορικά πολυαιθυλένια χαμηλής πυκνότητας έχουν μικρότερες εκθετικές παραμέτρους σε διάτμηση απ' ότι τα αντίστοιχα γραμμικά πολυαιθυλένια. Αυτή η παρατήρηση ισχύει γενικά για τις πολυολεφίνες και σε πειράματα εφελκυσμού, όπου ο προσδιορισμός της παραμέτρου β της συνάρτησης απόσβεσης του Τσενόγλου για πολυμερή διαφορετικής χημικής σύστασης και μοριακής αρχιτεκτονικής δείχνει ότι $\beta \geq 1$ για γραμμικά πολυμερή ενώ $\beta < 1$ για πολυμερή με διακλαδώσεις.

Η θερμορεολογική πολυπλοκότητα, χαρακτηριστικό των εμπορικών πολυμερών, απεικονίστηκε με την βοήθεια μιας μαθηματικής τεχνικής που προτάθηκε από τους Wood-Adams και Costeux (βλ. Σχ. 9). Χρησιμοποιώντας τα πειραματικά δεδομένα από τις μετρήσεις δυναμικής διάτμησης και για τα δύο δείγματα, υπολογίστηκαν πρώτα τα μιγαδικά μέτρα ελαστικότητας για κάθε θερμοκρασία και στην συνέχεια απεικονίστηκαν ως συνάρτηση του γινομένου της συχνότητας διάτμησης με το ιξώδες μη-

δενικού ρυθμού διάτμησης. Για ένα γραμμικό πολυμερές οι προκύπτουσες καμπύλες υπερτίθενται πλήρως ενώ για τα δύο δείγματα της παρούσας εργασίας αυτό δεν ήταν εφικτό. Για το διακλαδωμένο πολυαιθυλένιο Riblene® η μη-υπέρθυση των προκύπτουσών καμπυλών είναι αναμενόμενη. Αντίθετα για το γραμμικό Eraglene® η μη-υπέρθυση αποτελεί ένδειξη ύπαρξης μακρών κλάδων στο πολυμερές. Το γεγονός αυτό δεν προκαλεί έκπληξη καθώς σε εμπορικά δείγματα γραμμικών πολυμερών η πολυδιασπορά στο δείγμα αλλά και ύπαρξη μικρών ποσοτήτων μακρών διακλαδώσεων είναι αναμενόμενη.

Μια ακόμη τεχνική που εφαρμόστηκε είναι αυτή που προτάθηκε από τους Van Gurp και Palmen (βλέπε Σχ. 10) και στοχεύει επίσης στην ανάδειξη της θερμορολογικής πολυπλοκότητας που συναντάται σε δείγματα εμπορικών πολυολεφινών. Ωστόσο η μέθοδος αυτή βασίζεται στην σύγκριση παρόμοιων πειραματικών καμπυλών από δείγματα πολυμερών με διαφορετική αρχιτεκτονική. Συγκριτικά με την μέθοδο που προτάθηκε από τους Wood-Adams και Costeux η τελευταία δεν απαιτεί σύγκριση με δεδομένα άλλων πειραμάτων και βασίζεται μονάχα στην παραδοχή ότι ο υπολογισμός του ιξώδους μηδενικού ρυθμού, η_0 που χρησιμοποιείται για την κατασκευή του γραφήματος είναι ακριβής.

Το μοντέλο XPP χρησιμοποιήθηκε για τον προσδιορισμό μοριακών χαρακτηριστικών, όπως, π.χ., τον αριθμό των χημικών διασταυρώσεων, στο δείγμα των δειγμάτων Riblene® και Eraglene® από δεδομένα ρεολογίας. Ένα δείγμα της προβλεπτικής ικανότητας του μοντέλου παρουσιάζεται μέσω των αποτελεσμάτων των Πινάκων 5.6 και 5.7 και των σχημάτων 5.17, 5.18, 5.19 και 5.20. Από τα δεδομένα των Πινάκων αυτών και συγκεκριμένα από τις παραμέτρους, q_i για κάθε δείγμα φαίνεται ότι και για τα δύο πολυμερή όλα τα $q_i \neq 1$, κάτι που δεν είναι αναμενόμενο για γραμμικά πολυμερή. Για το εμπορικό πολυμερές Eraglene® το αποτέλεσμα αυτό σηματοδοτεί την ύπαρξη μακρών κλάδων στο δείγμα, σε συμφωνία με τα αποτελέσματα των γραφημάτων Wood-Adams-Costeux και VanGurp-Palmen. Το ποσοστό διακλαδώσεων στο γραμμικό δείγμα δεν διαπιστώθηκε με καμία άλλη μέθοδο εκτός από αυτήν του ρεολογικού χαρακτηρισμού. Έτσι η εγκυρότητα των αποτελεσμάτων του μοντέλου XPP δεν μπορεί να επικυρωθεί περαιτέρω. Ωστόσο για το LDPE Riblene® ο μέσος αριθμός μακρών διακλαδώσεων προσδιορίστηκε με την μέθοδο GPC και βρέθηκε ≈ 8.8 ενώ οι προβλέψεις του μοντέλου XPP είναι $10 \leq B_n \leq 12$. Οι δύο πειραματικές τιμές για το B_n είναι αρκετά κοντά, ενισχύοντας έτσι την υπόθεση πως το ποσοστό μακρών διακλαδώσεων στο τήγμα μπορεί να προσδιορισθεί αρκετά ικανοποιητικά μονάχα από δεδομένα ρεολογίας.

Ιδιαίτερη έμφαση δόθηκε στις διαφορές μεταξύ της συνάρτησης απόσβεσης του Wagner και του μοντέλου Τσενόγλου για πειράματα μονοαξονικού εφελκυσμού. Η πρώτη είναι ένα φαινομενολογικό μοντέλο που στόχο του έχει την περιγραφή της ρεολογίας σε εφελκυσμό δειγμάτων πολυμερούς. Αντίθετα η πρόταση Τσενόγλου αφορά στην μικροδομή του δείγματος και συνδέει μικροσκοπικές ιδιότητες των πολυμερών με μακροσκοπικά παρατηρήσιμα ρεολογικά δεδομένα. Επίσης ένα ακόμη πλεονέκτημα της συνάρτησης απόσβεσης του Τσενόγλου είναι η γενίκευση που μπορεί να επιτευχθεί για όλους τους τύπους εφελκυστικής παραμόρφωσης προσφέροντας έτσι ένα ενιαίο πλαίσιο για την περιγραφή της ρεολογίας πολυμερικών τμημάτων σε συνθήκες εφελκυσμού.

Τέλος, όσον αφορά το τροποποιημένο μοντέλο των Doi και Edwards εξετάστηκε η

ικανότητά του να προβλέπει την τιμή της παραμέτρου x_n ανεξάρτητα από τον τύπο της παραμόρφωσης. Ωστόσο, για το δείγμα Riblene[®] $x_n \approx 0.38$ από δεδομένα βηματικής διατμητικής παραμόρφωσης, ενώ $x_n \approx 0.92$ από δεδομένα μονοαξονικού εφελκυσμού (βλ. Σχ. 6.4 και 6.5). Για το δείγμα Eraclene[®] $x_n \approx 0.26$ από δεδομένα διατμητικής παραμόρφωσης, ενώ $x_n \approx 0.79$ από δεδομένα μονοαξονικού εφελκυσμού (βλ. Σχ. 6.4 και 6.8). Μιά σύντομη θερμοδυναμική ανάλυση των πειραματικών αποτελεσμάτων και για τα δύο δείγματα οδήγησε στο συμπέρασμα ότι το μοντέλο των Doi και Edwards είναι αρκετά απλοποιητικό όσον αφορά την θερμοδυναμική περιγραφή της παραμόρφωσης στα τήγματα πολυμερών.

Δημοσιεύσεις και παρουσιάσεις σε συνέδρια που προήλθαν από την παρούσα εργασία

Μέχρι στιγμής (2 Φεβρουαρίου, 2015) από την παρούσα εργασία έχουν γίνει τρεις παρουσιάσεις σε διεθνή συνέδρια και είναι σε προετοιμασία μια δημοσίευση σε περιοδικό:

1. “Nonlinear Viscoelasticity of Commercial Low Density Polyethylenes : The Effect of Long Chain Branching in the Presence of Entanglements”, με τον Chris Tsenoglou και τον Alexandros D. Gotsis στο 9ο Ετήσιο Ευρωπαϊκό Συνέδριο Ρεολογίας, Απρίλιος 2014
2. “Rheology of Commercial Polyolefines : Relating the Viscoelastic Behaviour to Microstructure”, πόστερ με τον Chris Tsenoglou και τον Alexandros D. Gotsis στο 7ο Διεθνές Συνέδριο της Ελληνικής Εταιρίας Ρεολογίας, Ιούλιος, 2014
3. “Nonlinear Viscoelasticity of Commercial Low Density Polyethylenes : Relaxation Experiments and Constitutive Modeling of the Effect of Long Chain Branching in the Presence of Entanglements”, με τον Chris Tsenoglou και τον Alexandros D. Gotsis στο 7ο Διεθνές Συνέδριο της Ελληνικής Εταιρίας Ρεολογίας, Ιούλιος 2014
4. “Viscoelastic behaviour of branched polymers: Constitutive Modeling of the Effect of Long Chain Branching in the Presence of Entanglements”, σε προετοιμασία για να εκδοθεί στο Journal of Rheology, Μάρτιος 2015.

Nomenclature

Acronyms

DMA Dynamic Mechanical Analysis

GPC Gel Permeation Chromatography

HDPE High Density Poly-Ethylene

LCB Long Chain Branches

LDPE Low Density Poly-Ethylene

LLDPE Linear Low Density Poly-Ethylene

MFI Melt Flow Index

MWD Molecular Weight Distribution

PB Poly-Butadiene

PC Poly-Carbonate

PI Polydispersity Index

PIB Poly-Iso-Butylene

PP Poly-Propylene

PS Poly-Styrene

PTFE Poly-Tetra-Fluoro-Ethylene

SCB Short Chain Branches

SHI Strain Hardening Index

UCM Upper Convected Maxwell

UHMWPE Ultra High Molecular Weight Poly-Ethylene

XPP eXtended Pom-Pom

Greek Symbols

α	parameter of Wagner's damping function in uniaxial elongation
α_1	pressure dependent viscosity model parameter (Pa^{-1})
α_p	parameter of the PSM damping function
α_T	temperature dependent time shift factor
α_t	equilibrium length or tube diameter in the DE model (m)
α_u	parameter of Eq.3.66
α_x	parameter of the XPP model
$\bar{\eta}_{12}$	steady state shear viscosity ($Pa \cdot s$)
$\bar{\eta}_E$	steady state uniaxial extensional viscosity or Trouton viscosity ($Pa \cdot s$)
β	strain sensitivity parameter of the power law damping function
β_c	cone angle (rad)
β_T	temperature dependent modulus shift factor
β_u	parameter of Eq.3.66
δx	present infinitesimal vector notation (m)
$\delta x'$	past infinitesimal vector notation (m)
δ	loss angle (rad)
$\dot{\epsilon}$	uniaxial elongational strain rate (s^{-1})
$\dot{\gamma}$	shear rate (s^{-1})
ϵ	strain or ratio of change in length to undeformed length
ϵ_f	critical strain under the Considère criterion
ϵ_H	logarithmic or Hencky strain
η'	dynamic viscosity ($Pa \cdot s$)
η''	elastic part of the complex viscosity ($Pa \cdot s$)
η	viscosity ($Pa \cdot s$)
η^*	complex viscosity ($Pa \cdot s$)
η_{12}^+	time dependent growth of shear viscosity ($Pa \cdot s$)
η_1, η_2	scalar functions of the invariants of $\underline{\underline{2D}}$

η_E^+	time dependent growth of uniaxial elongational viscosity ($Pa \cdot s$)
γ_p	critical shear strain in the Doi-Edwards theory
Λ	backbone tube stretch in the XPP model
λ	extension or ratio of deformed to undeformed length
λ_b	ratio of the number of branch points per molecule to molecular mass (mol/Kg)
$\mu(t)$	Boltzmann's memory function (Pa/s)
ν	number of entropic springs or strands per unit volume
ν_x	parameter of the XPP model
Ω	number of internal configurations of the macromolecular chain
ω	angular or rotational frequency (rad/s)
ω_{cr}	critical relaxation frequency (rad/s)
ϕ	angle of rotation (rad)
π	constant ($\approx 3.14159 \dots$)
ψ_0	gaussian distribution function of the end-to-end distance
Ψ_1	first normal stress difference coefficient ($Pa \cdot s^2$)
Ψ_2	second normal stress difference coefficient ($Pa \cdot s^2$)
ρ	density (Kg/m^3)
τ	relaxation time (s)
τ_0	averaged relaxation time (s)
τ_1	longest relaxation time (s)
$\tau_{b,i}$	backbone orientation relaxation times in the XPP model (s)
τ_{cr}	critical relaxation time (s)
τ_d	disengagement time (s)
τ_e	time of path equilibration (s)
τ_i	characteristic relaxation time (s)
$\tau_{s,i}$	stretch relaxation times in the XPP model (s)
$\tau(\underline{\underline{\sigma}}_i)^{-1}$	relaxation time tensor in the XPP model
$\underline{\underline{\sigma}}$	extra or viscous stress tensor

v_s	specific volume (m^3/Kg)
η_0	zero shear rate viscosity ($Pa \cdot s$)
η_∞	high shear rate viscosity ($Pa \cdot s$)
σ^*	critical stress for the Cross viscosity model (Pa)

Roman Symbols

$\underline{\underline{2D}}$	rate of deformation tensor
$\underline{\underline{2W}}$	vorticity tensor
$\langle \underline{R^2} \rangle$	time averaged mean square end-to-end distance (m^2)
$\underline{\dot{Q}}$	total rate of heat (J/s)
$\underline{\dot{W}}$	total work done (J)
$\underline{\underline{\mathfrak{S}}}_{DE}$	Larson's second order orientation tensor
$\underline{\underline{\mathfrak{S}}}^{IAA}_{DE}$	Larson's second order orientation tensor in the IAA
$\underline{\underline{C}}$	Cauchy tensor
$\underline{\underline{C}}^{-1}$	Finger deformation tensor
$\underline{\underline{E}}$	inverse of the deformation gradient tensor
$\underline{\underline{F}}$	deformation gradient tensor
$\underline{\underline{I}}$	unitary tensor
$\underline{\underline{L}}$	velocity gradient tensor
$\underline{\underline{Q}}$	Doi-Edwards universal orientation tensor
$\underline{\underline{T}}$	total stress tensor
$\underline{\underline{U}}$	finite strain tensor
$\underline{\underline{F}}$	entropic spring force (N)
$\underline{\underline{F}}_b$	body forces (N)
$\underline{\underline{F}}_s$	surface forces (N)
\underline{g}	gravitational constant ($\approx 9.80m/s^2$)
\underline{q}	local heat flux ($J/s \cdot m^2$)
\underline{R}	end-to-end distance of the macromolecular chain (m)

\underline{r}	end-to-end distance of the primitive step (m)
\underline{r}_0	end-to-end distance of the initial step in the primitive chain (m)
\underline{u}	unit vector
\underline{v}	velocity vector (m/s)
A	parameter of Eq.3.48
$A(\lambda)$	function of the principal stretch ratio
$A(t)$	time dependent cross sectional area of sample during elongation (m^2)
b	average backbone bond length (m)
b_1	pressure dependent viscosity model parameter ($^{\circ}K^{-1}$)
b_K	length of the Kuhn segment (m)
B_n	weight averaged number of branches per molecule
c	constant of Eq.2.8
C_{∞}	Flory's characteristic ratio
cN	centi-Newton ($10^{-2}N$)
De	Deborah number
E	elongational modulus of elasticity (Pa)
e	total specific energy or energy per unit mass (J/Kg)
E_{α}	flow activation energy (J/mol)
f	branch point functionality
$f(\lambda)$	function of the principal stretch ratio
$F(t)$	time dependent force during elongation (N)
$F(t, M)$	relaxation function in Eq.3.98
$f(\underline{\sigma}_i)^{-1}$	extra function in the XPP model
G	shear modulus of elasticity (Pa)
G'	time-dependent elastic or storage modulus (Pa)
G''	time-dependent viscous or loss modulus (Pa)
g'_s	molecular size ratio defined in Eq.2.12
g_n	number of generations per tree-like polymer

G_N^0	plateau shear modulus of elasticity (Pa)
g_s	molecular size ratio defined in Eq.2.11
gfm	gram-force-meter ($\approx 0.02\ N$ with $g = 9.80m/s^2$)
h	damping function
$H(t)$	time dependent height of sample at elongation (m)
h_p	gap between plates in the plate-plate geometry (m)
I_D	first invariant of the rate of deformation tensor
$I_{C^{-1}}$	first invariant of the relative Finger strain tensor
II_σ	second invariant of the extra or viscous stress tensor ($Pa^2 \cdot s^2$)
II_D	second invariant of the rate of deformation tensor
$II_{C^{-1}}$	second invariant of the relative Finger strain tensor
III_D	third invariant of the rate of deformation tensor
$III_{C^{-1}}$	third invariant of the relative Finger strain tensor
J_e^0	steady state compliance (m^2/N)
K_1	pressure dependent viscosity model parameter ($Pa \cdot s$)
K_2	temperature dependent viscosity model parameter ($Pa \cdot s$)
k_B	Boltzmann's constant ($1.380 \cdot 10^{-23}\ J/^{\circ}K$)
L	contour length of the macromolecular chain (m)
$L(t)$	time dependent length of sample at elongation (m)
L_0	initial sample length (m)
L_f	final sample length (m)
m	parameter of Wagner's damping function in uniaxial elongation
M_0	molecular weight of monomer (Kg/mol)
M_b	average molecular weight of branch (Kg/mol)
M_C	critical molecular weight (Kg/mol)
M_e	molecular weight between entanglements (Kg/mol)
m_e	parameter of Eq.3.61
M_n	number averaged molecular weight (Kg/mol)

M_t	torque ($N \cdot m$)
M_w	weight averaged molecular weight (Kg/mol)
M_z	z-averaged molecular weight (Kg/mol)
N	number of independently directed steps in the primitive chain
n	parameter of Wagner's single exponential damping function in shear
N_0	degree of polymerization or number of backbone bonds
N_1	first normal stress difference (Pa)
N_2	second normal stress difference (Pa)
N_A	Avogadro's constant ($6.022 \cdot 10^{23} mol^{-1}$)
N_e	number of monomers in each step of the primitive chain
N_K	number of equivalent Kuhn segments
n_w	parameter of Eq. 2.15
p	hydrostatic pressure (Pa)
$P(t)$	time-dependent diffusion function in the Doi-Edwards theory
q_x	parameter of the XPP model
R	universal gas constant ($8.31441 JK^{-1}mol^{-1}$)
R_g	radius of gyration (m)
R_p	plate radius (m)
S	entropy ($J/^{\circ}K$)
sgm	number of segments per generation of a tree-like polymer
T	temperature ($^{\circ}C$ or $^{\circ}K$)
t	present time (s)
t'	past time (s)
T_{11}	first normal stress difference (Pa)
T_{22}	second normal stress difference (Pa)
$W(M)$	continuous molecular weight distribution
$W(t)$	time dependent width of sample at elongation (m)
x_n	non-linear viscoelastic parameter of the modified DE damping function

$\langle R_g^2 \rangle_b$ time averaged mean square radius of gyration for the branched polymer (m^2)

$\langle R_g^2 \rangle_l$ time averaged mean square radius of gyration for the linear polymer (m^2)

$\langle \underline{R}^2 \rangle^{1/2}$ root of the mean square end-to-end distance (m)

G^* complex shear modulus (Pa)

K_c cross viscosity model parameter (s)

m_p power law viscosity model parameter ($Pa \cdot s$)

n_c cross viscosity model parameter

n_p power law viscosity model parameter

Other Symbols

∇ del or nabla

Chapter 1

Introduction

Rheology is the science that deals with the way materials deform when forces are applied to them. The term is most commonly applied to the study of liquids and liquid-like materials, i.e. materials that flow, although rheology also includes the study of general deformation of (visco)elastic materials, even of those that cannot flow in regular time scales, as, for example, cross-linked elastomers.

The two key words in the above definition of rheology are *deformation* and *force*. In order to learn anything about the rheological properties of a material, we must either measure the deformation resulting from a given force or measure the force required to produce a given deformation.

There are two principal aspects of rheology [33]. One involves the development of quantitative relationships between deformation and force for the material. The information for the development of such a relationship is obtained from experimental measurements. For linear, elastic rubbers or Newtonian fluids, the simplest observations are sufficient to establish a general equation describing how the material will respond to any type of deformation. Such an equation is called a *constitutive equation* or a *rheological equation of state*. However, for more complex materials such as molten plastics, the development of a constitutive equation is a much more complex task that requires data from several types of experiment. The second aspect of rheology is the development of relationships that show how rheological behaviour is influenced by the structure and composition of the material as well as the temperature and pressure. Ideally, one would like to know how these parameters affect the constitutive equation.

Many materials of major commercial importance are examples of *soft matter*, a category of materials that includes molten polymers, colloids, foams and gels. When being deformed, these materials exhibit complex rheological behaviour. Their rheological properties are of central importance in their industrial processing behaviour and/or their end-use applications.

Polymers that become pliable or mouldable above a specific temperature and solidify upon cooling are called *thermoplastics*. These are nearly always converted to end-use products by means of melt forming operations, including profile extrusion, several moulding techniques, etc. In all these processes, the rheological properties of

the molten polymer are of crucial importance and must be taken into account in the design of processing equipment and selection of operating conditions.

Rheological data are also useful for polymer characterisation. This is because the viscoelastic behaviour of a melt is very sensitive to molecular weight distribution variations and branched structure details. Thus, melt rheology can often provide an accurate picture of molecular structure.

1.1 The Molecular Structure of Polymers

The widespread recognition of molecules as a class of materials only dates from about 1908, and the concept of very large molecules, or *macromolecules*, followed about 20 years later through the work of Hermann Staudinger. He was the first to test the hypothesis of a “long-chain-molecule” through his pioneering studies in novel synthetic paths for the chemical substance *isoprene*. His hypothesis proved to be correct in 1920's. Six years later he predicted that long molecules would be important in biology. The term *macro-molecular association* was first used in 1922 and later in 1924, the word *makromolekul* was finally established to describe the nature of these materials.

A *macromolecule (or polymer)* is a large molecule composed of many small simple chemical units, generally called *structural units*, connected together mostly by covalent bonds. In some polymers each structural unit is connected to precisely two other structural units and the resulting chain structure is called a *linear* macromolecule. In other polymers most structural units are connected to two other units, although some structural units connect three or more units, and we talk of *branched* molecules. Where the chains terminate, special units called *end groups* are found. For some macromolecular materials, all structural units are interconnected resulting in a three-dimensional *cross-linked* or *network structure* rather than in separate molecules. Such materials (e.g. cross-linked rubber), however, generally have no fluid phase.

Aside from minor corrections from end groups and branch points, the molecular weight of a macromolecule is the product of the molecular weight of a structural unit and the number of structural units in the molecule. Typical synthetic polymer macromolecules may have molecular weights between 10000 and 1000000 gr/mol. Even higher molecular weights have been achieved for some synthetic polymers of special importance. Typical examples of UHMWPE (Ultra High Molecular Weight Polyethylenes) include the Spectra® (Dyneema®) fibres used for marine ropes, industrial applications, ballistic armour, impact resistant panels and electronics, Gur® used for orthopedic implants, etc.

A polymer sample in which the molecular weight of all macromolecules is the same is called *monodisperse*. Synthetic monodisperse or “almost monodisperse” polymers may be prepared by special techniques, but are rarely used commercially. In contrast, most commercial polymers are *polydisperse*, that is, they contain molecules of many different molecular weights. Thus, one may talk of a distribution of molecular weights.

In order to describe molecular weight distributions in simple quantitative terms, various molecular weight averages have to be introduced. To calculate the *number-average molecular weight* of a given polymer sample each fraction of different molec-

ular weight is multiplied by the number of corresponding moles, the products are summed and the sum is divided by the total number of moles:

$$\bar{M}_n = \frac{\sum_i N_i M_i}{\sum_i N_i} . \quad (1.1)$$

The number-average molecular weight, \bar{M}_n , is particularly sensitive to additions of small amounts of low molecular weight fractions. An alternative form, is the *weight-average molecular weight*, for which the summation is done over all fractions of different molecular weights, each multiplied by the corresponding weight, and then the sum is divided by the total weight:

$$\bar{M}_w = \frac{\sum_i w_i M_i}{\sum_i w_i} = \frac{\sum_i N_i M_i^2}{\sum_i N_i M_i} . \quad (1.2)$$

In contrast to \bar{M}_n , the weight-average molecular weight, \bar{M}_w , is more sensitive to the high molecular weight fractions. One may further define molecular weight averages by taking ratios of higher moments of the molecular weight distribution,

$$\bar{M}_{z+j} = \frac{\sum_i N_i M_i^{3+j}}{\sum_i N_i M_i^{2+j}} \quad (1.3)$$

For $j = 0$, the *z-average molecular weight* is defined. For $j > 0$ ($j=1,2 \dots$), the *z+j-average molecular weight* is defined. For monodisperse samples, all these averages are equal, whereas for polydisperse samples, $\bar{M}_n < \bar{M}_w < \bar{M}_z < \bar{M}_{z+1} \dots$ etc.

The ratio \bar{M}_w/\bar{M}_n , known as the *dispersion ratio* or *polydispersity index*, is often taken as a simple measure of the polydispersity of a sample. Sometimes the *heterogeneity index*, $(\bar{M}_w/\bar{M}_n) - 1$, is used. The *variance* of the weight distribution, defined as the ratio $(\bar{M}_z - \bar{M}_w)/\bar{M}_w$, is also used, as well as the *rheological polydispersity*, $\bar{M}_z \bar{M}_{z+1}/\bar{M}_w^2$. These various measures of distribution breadth vary in their sensitivity to the different parts of the distribution. Thus, \bar{M}_w/\bar{M}_n depends more strongly on the low molecular weight tail, whereas \bar{M}_z/\bar{M}_w depends more strongly on the high molecular weight tail.

1.2 Polyolefins : Examples of Branched Polymers

Polyolefins are products of the polymerisation of olefins (alkenes). Polyethylenes (PE) and polypropylene (PP) are common polyolefins and they are the most widely used group of thermoplastic polymers today. Even though polyolefins are chemically simple macromolecules consisting of carbon and hydrogen atoms, they show a large diversity in mechanical properties in both the solid and the melt states. This is due to the variety in their molecular architecture as described by their molecular weight, their molecular weight distribution and the number, distribution and length of branches on their molecular chain backbone [4, 40].

Ethylene-based materials produced by the radical polymerisation of ethylene in reactors under low-pressure conditions with transition metal catalysts of various types

Table 1.1: Some synthetic olefinic polymers, their monomers and their structural units.

Monomer	Structural Unit	Common Name	Acronym
$ \begin{array}{c} \text{H} \quad \text{H} \\ \diagdown \quad \diagup \\ \text{C} = \text{C} \\ \diagup \quad \diagdown \\ \text{H} \quad \text{H} \end{array} $	$ \begin{array}{c} \text{H} \quad \text{H} \\ \quad \\ \text{---C---C---} \\ \quad \\ \text{H} \quad \text{H} \end{array} $	Polyethylene	PE
$ \begin{array}{c} \text{H} \quad \text{CH}_3 \\ \diagdown \quad \diagup \\ \text{C} = \text{C} \\ \diagup \quad \diagdown \\ \text{H} \quad \text{H} \end{array} $	$ \begin{array}{c} \text{H} \quad \text{CH}_3 \\ \quad \\ \text{---C---C---} \\ \quad \\ \text{H} \quad \text{H} \end{array} $	Polypropylene	PP

have predominantly linear chain structure. This subgroup includes high-density (HDPE), medium-density (MDPE) and linear low-density (LLDPE) polyethylenes. The use of higher α -olefins like butene, hexene and octene as comonomers results in the formation of short-chain branches (SCB) along their linear backbone chain. The use of catalysts, on the other hand, may result in long-chain branches (LCB). HDPE shows the typical rheology of a (mostly) linear chain polymer. The long linear chain of a typical LLDPE is composed of ethylene units with SCB. It has no LCB and a relatively narrow molecular weight distribution. The rheology of LLDPE is very similar to that of a linear chain polymer.

Polyethylenes produced under in reactors under high-pressure conditions with oxygen or peroxides as chain initiators have predominantly long-chain branched structure. This group includes the low-density poly-ethylenes (LDPE) which have many long-chain branches on the main chain and on the branches. Their highly branched molecular structure results in reduced crystallinity and increased melt elasticity when compared to their linear cousins, the HDPEs.

Propylene-based polymers are produced with transition metal heterogeneous catalysts (PP) and have linear chain structure with stereospecific arrangement of the propylene units (isotactic). Several commercial branched grades are also available, mostly produced by grafting long-chain branches on the linear PP chains either by electron beam irradiation or in the melt by using peroxides with relatively low decomposition temperature. These methods produce LCB-PP with broadened molecular weight distribution, complex branched structure and increased elasticity when compared to its linear cousin.

Long-chain branches in polymers are defined [4] as the branches of mostly the same chemical species as the long linear macromolecular chain on which they are

rooted. These branches are long enough to be able to form at least 2-3 entanglements each or they have lengths of at least 2.5 times the *molecular weight at the onset of entanglements*, M_C , of the polymer chain. This is in contrast to *short-chain branches* which have a length of the order of a few repeating units. Because of their length, the long branches act locally as individual molecules, are flexible and produce entanglements but are restrained in their motions by their roots on the backbone chain. The hydrodynamic volume of the branched chain, at least in theta conditions, is smaller than a linear chain with the same molecular weight. On the contrary, short chains cannot provide entanglements and can even reduce the main-chain flexibility protecting the individual backbone chain from its environment.

1.3 The Scope of the Thesis

The scope of the current thesis is to investigate the influence of the polymeric microstructure on the rheological response of the molten material. In order to achieve this goal, a wealth of experimental data on the rheology of commercial polymers of differing chemical composition and microstructural architecture had to be gathered for a comparison between the rheological properties of these materials. The criteria for the selection were the accuracy and integrity of the published data, as well as the variety of the types of rheological deformation. This led to a spherical view of the macroscopic rheological response of commercial polyolefin melts and insight in the way that the macroscopic behaviour is related to different aspects of the microstructural architecture. In addition, experimental investigation of some commercial PE melts under various types of deformation was deemed appropriate in order to have access to raw experimental data.

Mathematical modelling of the rheological behaviour of the melts had been conducted using constitutive equations of the integral and the differential forms. This was done in order to compare these two mathematical formalisms, as well as to make use of theoretical features that are only available in one of the two forms. Constitutive modelling had also been used in an attempt to make predictions about microstructural features of the melts under investigation, when the only means of characterisation was that of rheological testing.

The main goal of the thesis is to evaluate the damping function of the melts, which is appropriate for different flows. Thus, the damping function was evaluated using shear step-strain experiments and uniaxial extensional flow. The relaxation spectrum of the melts was evaluated by small angle oscillatory shear flow and used for the analysis of both shear and elongational flows. Attempts were made to relate the form of the damping function and the evaluated parameters of the constitutive equations with the molecular structure of the polymers.

Chapter 2

Structure and Fluid Mechanics of Polymers

2.1 The Random Coil Model

Common polymers such as the polyolefins consist of macromolecules. These are long chains of repeating groups of atoms connected together by covalent bonds. It is infrequent though that these chains (even those of linear architecture) assume long-stretched rod-like conformations. In the melt, these macromolecules have the form of random coils. Following the contour of such a macromolecule is similar to a walk that changes direction often in a random manner.

The picture of chain molecules as physical embodiments of *random walks* emerged in the early 1930's, during the period when Staudinger's macromolecular hypothesis was beginning to gain acceptance. Shortly thereafter, Guth and Mark and Kuhn were explicitly associating polymer conformations with random walks, thus leading to predictions relating molecular dimensions to chain length. The concept of the random walk evolved quickly from a tentative suggestion to the canonical model for flexible polymers. The random walk still remains the starting point for basic understanding of the polymeric liquid state.

2.1.1 Random Walks

Flexible molecules permit rotational motions of one bond about another so that a combinatorially huge number of configurations is accessible. On length scales much larger than that of a single monomeric unit, the details of distribution of allowed bond angles average out, producing a configuration distribution in the melt equivalent to that of a *random walk*. Because of their flexibility these macromolecules remain unoriented or isotropic at equilibrium in the densely packed melt state. Thus for long polymeric molecules the *time-averaged mean-square distance*, $\langle \underline{R}^2 \rangle$ separating one end of the molecule from the other obeys the random-walk formula

$$\langle \underline{R}^2 \rangle = N_0 b^2, \quad (2.1)$$

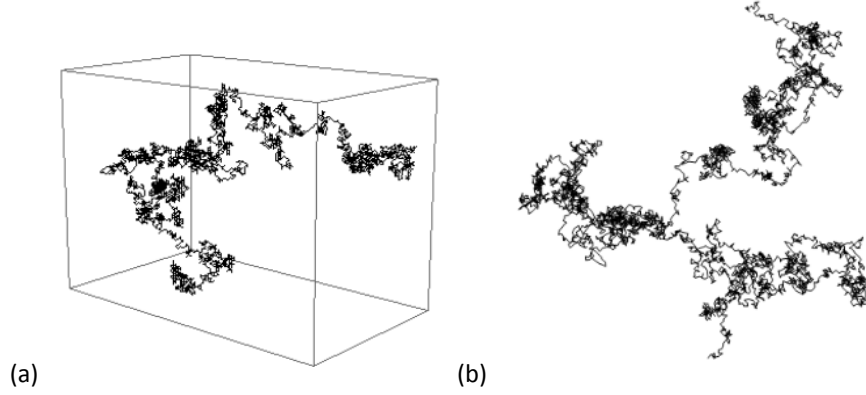


Figure 2.1: A *self-avoiding random walk* consisting of 10000 steps in (a) three dimensions and (b) its projection in two dimensions.

where N_0 is the number of backbone bonds composing the chain and b is an average bond length. This mathematical description of polymer chains is the simplest model of an *ideal polymer* and it is known as the *freely jointed chain model* with constant bond length and no correlations between the directions of neighbouring bond vectors. It resembles that of a random walk, where each vector corresponds to a step in the walk and each step direction is independent of the location and direction of all other steps. The contour length of the whole chain corresponds to a full path of a random walk (see Fig. 2.1).

The bonds in a real polymer chain, however, do not have complete rotational freedom. Because of bond angle restrictions there are correlations between the orientation of one bond and that of its near neighbours. Since bond angle restrictions make the average coil size $\langle R^2 \rangle$ more expanded than would otherwise be the case, a simple unified description is provided by the *equivalent freely jointed chain model*. The equivalent chain has N_K freely-jointed effective bonds of length b_K . This effective bond length b_K is called the *Kuhn length* or *Kuhn statistical segment*. These segments are considered to be made up by a number of monomer units. The mean-square end-to-end distance of the equivalent chain, is,

$$\langle R^2 \rangle = N_K b_K^2 = C_\infty N_0 b^2, \quad (2.2)$$

where C_∞ is called *Flory's characteristic ratio* and it is a relative measure of the flexibility of the chain. For a freely jointed chain, $C_\infty = 1$. For real chains, the bond angle restrictions lead to values of C_∞ in the range of 5 - 10. Therefore, the equivalent freely jointed chain has,

$$N_K = \frac{L^2}{C_\infty N_0 b^2} \quad (2.3)$$

equivalent bonds (Kuhn segments) of length,

$$b_K = \frac{C_\infty N_0 b^2}{L}, \quad (2.4)$$

where $L = N_K b_K$ is the *contour length* of the chain.

The root-mean-square end-to-end distance of a flexible polymeric macromolecule is $\langle \underline{R}^2 \rangle^{1/2} = N_K^{1/2} b_K$. A quantity related to $\langle \underline{R}^2 \rangle^{1/2}$ is the *radius of gyration*, \underline{R}_g , which is defined as the root-mean-square average distance separating a monomer from the centre of mass of the chain. For a flexible chain this is given by

$$\underline{R}_g = \frac{\langle \underline{R}^2 \rangle^{1/2}}{\sqrt{6}} . \quad (2.5)$$

2.1.2 Conformational Distributions

At equilibrium, the distribution of conformations of polymeric chains, in the melt, is given by a set of random walks, or equivalently, by the conformations of the freely jointed chain. If one end of the freely jointed chain with N_K links, each of length, b_K , lies at the origin, then the probability, $\psi_0 dR^3$, that the other end lies at a position between \underline{R} and $\underline{R} + d\underline{R}$ is given by a *Gaussian function*:

$$\psi_0(\underline{R}) = \left(\frac{3}{2\pi N_K b_K^2} \right)^{3/2} \exp \left\{ -\frac{3\underline{R} \cdot \underline{R}}{2N_K b_K^2} \right\} . \quad (2.6)$$

The second moment of this distribution function is the mean square end-to-end distance of the chain, that is,

$$\langle \underline{R}^2 \rangle \equiv \int R^2 \psi_0(\underline{R}) dR^3 = N_K b_K^2 , \quad (2.7)$$

where the integration is done over the whole space. The root-mean-square end-to-end separation distance of an undistorted coil scales with molecular weight according to a power-law, $\langle \underline{R}^2 \rangle^{1/2} \propto M^{0.5}$.

2.1.3 The Hookean Spring

The elasticity of flexible polymer molecules can be predicted from the configuration distribution function, $\psi_0(\underline{R})$. Suppose the ends of the polymer chain are held fixed so that the end-to-end vector of the chain is \underline{R} . The number of internal configurations, Ω , of the chain that satisfies this constraint is,

$$\Omega = c \psi_0(\underline{R}) , \quad (2.8)$$

with c a constant. The entropy of the chain, S , then is defined as,

$$S = k_B \ln \Omega , \quad (2.9)$$

where k_B is Boltzmann's constant. One can show [57] that in order to pull one end of the chain to increase the end-to-end distance, \underline{R} , the force we need to exert to overcome the *entropic spring force* of the chain, is

$$\underline{F} = 3k_B T \frac{\underline{R}}{(N_K b_K^2)} , \quad (2.10)$$

where T is the absolute temperature. An increase in the separation distance, \underline{R} , reduces the number of allowed configurations; the macromolecule resists this action with a force proportional to \underline{R} . A Gaussian chain therefore, acts like a *Hookean spring*.

2.1.4 GPC Characterization of LCB in Polymers

Gel Permeation Chromatography, (GPC) is a type of *Size Exclusion Chromatography, (SEC)* that separates analytes on the basis of size. Separation occurs via the use of porous beads packed in a column. The technique is often used for the analysis of polymers and allows for the determination of the polydispersity index (PDI) as well as the molecular weight averages (i.e. M_n , M_w and M_z).

A branched molecule has a smaller hydrodynamic volume than a linear molecule with the same molecular mass. Smaller molecules can enter the pores more easily and therefore spend more time in these pores, increasing their retention time. Conversely, larger molecules spend little if any time in these pores and are eluted quickly. The decrease in size is described by the *structure parameter* or *molecular size ratio*, g_s , defined as

$$g_s = \frac{\langle \underline{R}_g^2 \rangle_{br}}{\langle \underline{R}_g^2 \rangle_{lin}}, \quad (2.11)$$

where $\langle \underline{R}_g^2 \rangle_{br}$ is the *mean square radius of gyration* of the branched molecule and $\langle \underline{R}_g^2 \rangle_{lin}$ is the corresponding quantity for a linear molecule with the same molecular mass in the unperturbed state. This in turn is related to [69]

$$g'_s = \frac{[\eta]_{br}}{[\eta]_{lin}} \quad \text{and} \quad g'_s = g_s^{1.0 \pm 0.3}, \quad (2.12)$$

where $[\eta]_{br}$ is the *intrinsic viscosity* of the branched sample and $[\eta]_{lin}$ is the intrinsic viscosity of a linear sample of the same molecular mass distribution. Intrinsic viscosity measurements may be performed, e.g., by installing an *Ubbelohde viscometer* on-line with the SEC-equipment. Lecacheux et al. [16] has proposed an exponent of 1.2 in Eq. 2.12, while Kulin et al. [34] assumes that all possible values of the exponent should fall within the limits of 0.5 and 1.5.

The theory of Zimm and Stockmayer [8] is often used in order to translate the GPC data into a measure of branching content in the melt. The following analytical expressions are used in the case of (3-functional) random branching

$$g_s = \frac{3}{2} \left(\frac{\pi}{B_n} \right)^{1/2} - \frac{5}{2B_n} \quad (2.13)$$

$$g_s = \left[\left(1 + \frac{B_n}{7} \right)^{1/2} + \frac{4B_n}{9\pi} \right]^{-1/2}, \quad (2.14)$$

where B_n is the *branching number* or weight average number of branch points per molecule, in the melt and $\pi=3.14159$. One more analytical expression of this kind (3-functional random branching) is frequently encountered

$$g_s = \left(\frac{6}{B_n} \right) \left[\left(\frac{n_w}{2} \right) \ln \left(\frac{n_w + 1}{n_w - 1} \right) - 1 \right], \quad (2.15)$$

where $n_w = \sqrt{(2/B_n) + 1}$. The branching number, B_n may then be expressed as [34]

$$B_n = M_w \lambda_b . \quad (2.16)$$

The ratio of number of branch points per molecule to molecular mass is expressed by λ_b [34]. It corresponds to the number of branch points per unit molecular weight and can be used to evaluate the *average molecular weight of a branch* [9]

$$M_b = \frac{1}{2\lambda_b} . \quad (2.17)$$

Finally, the *branching frequency* [34] can be evaluated through

$$LCB/(1000C) = 1000M_0 \frac{B_n}{M_w} , \quad (2.18)$$

corresponding to the number of branch points per 1000 C atoms and M_0 is the *molar mass of the monomer*.

2.2 The Stress Tensor

The *total stress tensor*, \underline{T} in a flow field is written as the sum of the isotropic pressure, $p\underline{I}$ and the *extra or viscous stress tensor*, $\underline{\sigma}$,

$$\underline{T} = -p\underline{I} + \underline{\sigma} \quad (2.19)$$

It is very often the case that the principle of conservation of angular momentum for isotropic materials is invoked. This in turn implies that $\underline{\sigma}$ is symmetric, that is $\sigma_{ij} = \sigma_{ji}$. Polymeric melts are highly disordered liquids, thus they are considered isotropic at rest. It is also very frequent, when dealing with fluid mechanics, that the polymeric liquids be treated as incompressible fluids. Any deviation from the simple Hookean or Newtonian behaviour due to nonlinear dependence on deformation or deformation history are usually much greater than the influence of compressibility.

Constitutive equations are usually written in terms of $\underline{\sigma}$. However, experimentally we can measure only forces which when divided by the area give components of the total stress. This presents no problem for the shear stress components because $T_{ij} = \sigma_{ij}$ but the normal stress components will differ by p because $T_{ii} = -p + \sigma_{ii}$. Normal stress differences are used to eliminate p since

$$T_{11} - T_{22} = \sigma_{11} - \sigma_{22} \quad T_{22} - T_{33} = \sigma_{22} - \sigma_{33} \quad (2.20)$$

For the special case of *simple shear flow* we call $T_{11} - T_{22} = N_1$ and $T_{22} - T_{33} = N_2$ as the *first normal stress difference* and *second normal stress difference* respectively.

2.2.1 The Polymer Stress Tensor

In the special case of a polymeric liquid, the polymer contribution to the extra stress tensor (assuming the Gaussian chain assumption for the macromolecules in the fluid)

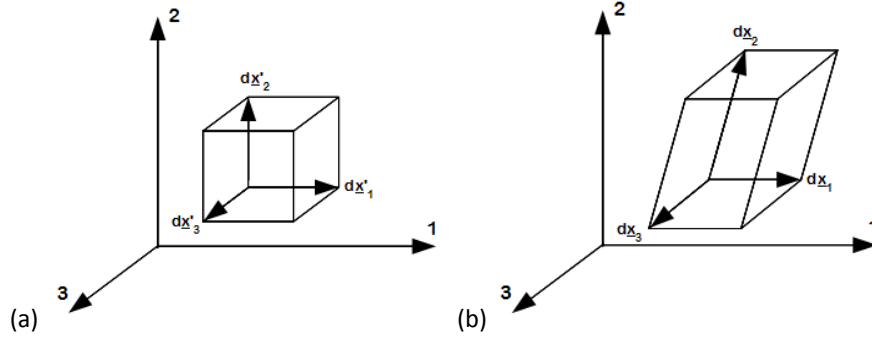


Figure 2.2: A fluid element (a) before and (b) after a general three-dimensional deformation seen from a Lagrangian point of view (see Eq.2.22).

results from the Hookean entropic spring force idea. To obtain the polymer contribution to the extra stress tensor, $\underline{\underline{\sigma}}$, for a fluid containing a large number of springs, a summation is carried out over the forces exerted on all different springs. For Gaussian chains, one may obtain [57]

$$\underline{\underline{\sigma}} = 3k_B T \nu \frac{\langle \underline{R} \underline{R} \rangle}{(N_K b_K^2)} , \quad (2.21)$$

where ν , is the number of springs per unit volume. Thus, *viscoelastic stresses* are produced by distortions of the distribution of polymer configurations. Mechanical stresses can therefore be attributed to anisotropies in molecular orientations, due to a finite macroscopic deformation. In simple shearing of polymer melts, for example, the primary normal stress difference, N_1 , is positive, implying that there is a higher degree of orientation in the direction of flow. The second normal stress difference, N_2 , in entangled melts of flexible polymer chains, is usually a factor of 3-10 times smaller in magnitude than N_1 and negative in sign, implying that the orientation in the velocity gradient direction is depleted of polymer orientations relative to the vorticity direction [57].

2.3 Finite Deformation Tensors

As mentioned in the previous section, the state of stress at any point in a material is determined by using the stress tensor. In an analogous way, a mathematical description of arbitrary deformations is needed in order to determine the deformation history of the material. The mathematical notation followed and the corresponding definitions are those recommended by IUPAC and can be found in Kaye et al. [1].

Considering a lump of fluid material, let a point in it at some past time t' occupy position \underline{x}' and let $\delta \underline{x}'$ be a vector embedded in the fluid element, with one end of the vector (the tail) at position \underline{x}' and the other end (the vector's head) at position $\underline{x}' + \delta \underline{x}'$. Between times t' and t , the vector is stretched and rotated along with the

fluid element in which it is embedded, and at time t the embedded vector is $\delta \underline{x}$. For a general three-dimensional deformation

$$E_{ij} = \frac{\partial x_i}{\partial x'_j}, i, j = 1, 2, 3 \quad (2.22)$$

and the ratio $\delta \underline{x} / \delta \underline{x}'$ is the *stretch ratio*. The tensor \underline{E} contains information not only on the stretching but also on the rotation of the fluid element in each of its three dimensions. This is the *Lagrangian description* in which the reference configuration is the configuration at $t' = 0$. The inverse tensor $\underline{F} \equiv \underline{E}^{-1}$ is usually called the *deformation gradient tensor*

$$F_{ij} = \frac{\partial x'_i}{\partial x_j}, i, j = 1, 2, 3 \quad (2.23)$$

This is the *Eulerian description* in which the current configuration is taken as the reference configuration. Since material response is determined only by stretching or rate of stretching and not by a solid body rotation, we would not expect the rotation to change our results. This principle is called *frame indifference*. In order to remove the rotation from the gradient deformation tensor, we introduce a new tensor, called the *Finger tensor*

$$C_{ij}^{-1} = \sum_{k=1}^3 \frac{\partial x_i}{\partial x'_k} \cdot \frac{\partial x_j}{\partial x'_k}, i, j = 1, 2, 3 \quad (2.24)$$

which is the inverse of the *Cauchy tensor*

$$C_{ij} = \sum_{k=1}^3 \frac{\partial x'_k}{\partial x_i} \cdot \frac{\partial x'_k}{\partial x_j}, i, j = 1, 2, 3 \quad (2.25)$$

In tensor notation $C_{ij}^{-1} = \underline{E} \cdot \underline{E}^T$. The Finger tensor describes the change in shape of a small material element between times t' and t , not whether it was rotated during this time interval.

So far, deformation has been defined in terms of extension, the ratio of deformed to undeformed length, $\lambda = L/L'$. Thus when deformation do not occur, the extensions are unity and $\underline{C}^{-1} = \underline{I}$. Frequently deformation is described in terms of strain, the ratio of change in length to undeformed length

$$\epsilon = \frac{L - L'}{L'} = \lambda - 1 \quad (2.26)$$

When there is no deformation, the strains are zero. A finite strain tensor can be defined by subtracting the identity tensor from \underline{C}^{-1} thus

$$\underline{U} = \underline{C}^{-1} - \underline{I} \quad (2.27)$$

2.4 The Rate of Deformation Tensor

Along with the stress and deformation gradient tensors, the velocity gradient in any direction at a point in the fluid must be defined. Since the deformation gradient tensor

determines the relative displacement between points in a fluid element, the velocity gradient tensor determines the relative rate of displacement. The *velocity gradient tensor* represents the instantaneous rate of separation of points at present times and results from taking the limit as the past displacement is brought up to the present leading to

$$L_{ij} = \frac{\partial v_i}{\partial x_j}, i, j = 1, 2, 3 \quad (2.28)$$

In tensor notation $\underline{\underline{L}} = (\nabla \underline{v})^T$. The velocity gradient $\nabla \underline{v}$ describes the steepness of velocity variation as one moves from point to point in any direction in the flow at a given instant in time. The *rate of deformation tensor*, $\underline{\underline{2D}}$ is a symmetric tensor and is defined as

$$\underline{\underline{2D}} = (\nabla \underline{v})^T + \nabla \underline{v} \quad (2.29)$$

The *vorticity tensor*, $\underline{\underline{2W}}$ is not symmetric and is defined as

$$\underline{\underline{2W}} = (\nabla \underline{v})^T - \nabla \underline{v} \quad (2.30)$$

From the above definitions we conclude that

$$\underline{\underline{L}} = \underline{\underline{D}} + \underline{\underline{W}} = (\nabla \underline{v})^T \quad (2.31)$$

2.5 The Newtonian Fluid

In the Newtonian view “resistance” in flow depends on the “velocity by which parts of the fluid are being separated”. This “resistance” means local stress whereas “velocity by which parts of the fluid are being separated” means velocity gradient or the change of velocity with position in the fluid. The proportionality between them is the *viscosity* or “lack of slipperiness”. The rate of deformation tensor, $\underline{\underline{2D}}$ is the proper three-dimensional measure of the rate by which the parts of the fluid are being separated. Thus using $\underline{\underline{\sigma}}$ and $\underline{\underline{2D}}$ one can formulate an appropriate tensor relation between those tensors

$$\underline{\underline{\sigma}} = \eta \underline{\underline{2D}} \quad (2.32)$$

In terms of the total stress

$$\underline{\underline{T}} = -p\underline{\underline{I}} + \eta \underline{\underline{2D}} \quad (2.33)$$

In these expressions the *dilatational* term has been omitted since polymeric melts are often treated as incompressible fluids.

Although polymeric melts are generally treated as non-Newtonian liquids, many problems in polymer processing are initially solved using the Newtonian assumption, because these solutions provide simple results that help gain insight into the nature of the process as well as quick, rough, quantitative estimates. Yet, for an accurate solution in polymer processing, the non-Newtonian character of the material must be considered. To proceed, one must replace Newton’s constitutive equation with some new constitutive “law”, that is, one that is mathematically tractable and yet appropriate for the complex fluid whose flow one wishes to analyse. This new “law” must then be solved along with the momentum balance and mass balance equations. The

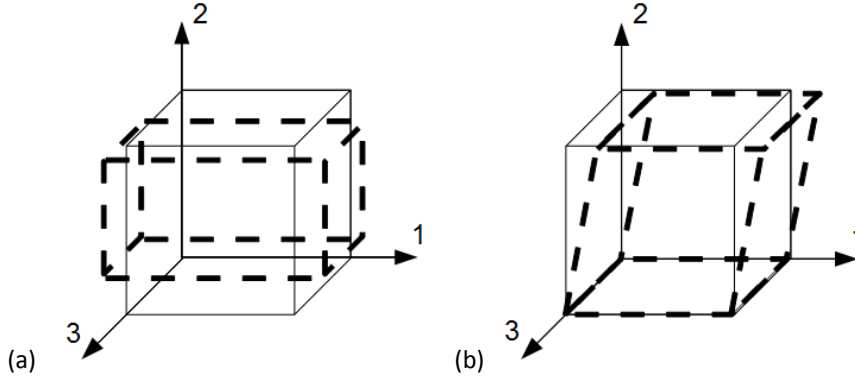


Figure 2.3: A fluid element under (a) uniaxial extension and (b) shear deformation. The uniaxial extensional rate across the “1”-direction is defined as $\dot{\epsilon} = dv_1/dx_1$ whereas the shear rate across the same direction as $\dot{\gamma} = dv_1/dx_2$.

methods required to solve such equations depend on the mathematical structure of the constitutive law needed to represent the complex fluid.

2.6 The Generalised Newtonian Fluid

The Newtonian constitutive equation is the simplest rheological equation of state that describes accurately the rheological behaviour of low molecular weight liquids and high polymers at very low shear rates of deformation. However, the viscosity can be a strong function of the rate of deformation for polymers and complex fluids.

The *general viscous fluid* model assumes that the stress depends only on the rate of deformation. Expanding the Newtonian constitutive relation in a power series and using the *Caley-Hamilton theorem* one gets

$$\underline{\underline{T}} = -p\underline{\underline{I}} + \eta_1(II_{2D}, III_{2D})2\underline{\underline{D}} + \eta_2(II_{2D}, III_{2D})(2\underline{\underline{D}})^2 \quad (2.34)$$

where η_1 and η_2 are scalar functions of the invariants of $2\underline{\underline{D}}$. This constitutive equation is also known as the *Reiner-Rivlin fluid* [15]. The Newtonian fluid is simply a special case with $\eta_1(II_{2D}, III_{2D}) = \eta$ (constant) and $\eta_2 = 0$. The second term, η_2 gives rise to normal stresses in steady shear flow, that is $N_1 = 0$ and $N_2 = \eta_2 \dot{\gamma}^2$.

These predictions are not in qualitative agreement with experimental observations. In steady simple shear flow nearly all fluids that exhibit normal stresses show a positive normal stress difference N_1 and a much smaller, typically negative second normal stress difference N_2 . Since the η_2 term gives qualitatively the wrong result, it is usually discarded. Therefore, the general viscous fluid reduces to

$$\underline{\underline{T}} = -p\underline{\underline{I}} + \eta_1(II_{2D}, III_{2D})2\underline{\underline{D}} \quad (2.35)$$

In simple shear flows, $III_{2D} = 0$, thus only the dependence of η_1 on II_{2D} is usually

kept and the generalised Newtonian fluid is further reduced to

$$\underline{\underline{T}} = -p\underline{\underline{I}} + \eta_1(II_{2D})2\underline{\underline{D}} \quad \text{or} \quad \underline{\underline{\sigma}} = 2\eta_1(II_{2D})\underline{\underline{D}} \quad (2.36)$$

2.6.1 Power Law

The most widely used form of the general viscous constitutive relation is the power law model

$$\sigma_{ij} = m_p |II_{2D}|^{(n_p - 1)/2} (2D_{ij}) \quad (2.37)$$

This model is most often applied to shearing flows. The absolute value of the second invariant of $2\underline{\underline{D}}$ becomes $|II_{2D}| = \dot{\gamma}^2$, thus for steady shear the power law gives $\sigma_{12} = \sigma_{21} = m_p \dot{\gamma}^{n_p}$ and

$$\eta_1 = m_p \dot{\gamma}^{(n_p - 1)} \quad (2.38)$$

with no other stress components. The m_p parameter usually represents a function of temperature. One obvious disadvantage of the power law is that it fails to describe the low shear rate region. Since n_p is usually less than one for most polymeric melts that show shear thinning behaviour, at low shear rate η_1 goes to infinity rather than to a constant value, η_0 .

2.6.2 Cross Model

In order to add a Newtonian plateau at low shear rates, the Cross model has been proposed

$$\frac{\eta_1 - \eta_\infty}{\eta_0 - \eta_\infty} = \frac{1}{1 + (K_c^2 |II_{2D}|)^{(1 - n_c)/2}} \quad (2.39)$$

Once $\eta_1 \gg \eta_\infty$ for the steady simple shear flow, the Cross viscosity model reduces to

$$\eta_1 = \frac{\eta_0}{1 + (K_c \dot{\gamma})^{1 - n_c}} \quad (2.40)$$

The parameter K_c depends on the critical shear stress σ^* at which η_1 transitions from the Newtonian plateau η_0 to the Power law regime.

Various other viscous models have been proposed (i.e. Yasuda, Carreau, Ellis etc.) and these are thoroughly reviewed elsewhere [15, 79].

2.6.3 Extensional Thickening Models

Viscosity measured in extension can be qualitatively different from that measured in shear. In contrast to the steady simple shear flow where $|II_{2D}| = \dot{\gamma}^2$ and $|III_{2D}| = 0$, in uniaxial extension $|II_{2D}| = 3\dot{\epsilon}^2$ and $|III_{2D}| = 2\dot{\epsilon}^3$ is nonzero. However, several models that only depend on $2\underline{\underline{D}}$ or $2\underline{\underline{W}}$ have been proposed and are thoroughly presented in the book of Macosko [15].

2.6.4 Temperature and Pressure Dependence of Viscosity

Temperature dependence of the viscosity can often be as important as its shear dependence for non-isothermal processing problems. For all liquids, the viscosity decreases with increasing temperature and decreasing pressure. A useful empirical model for both effects on the limit of low shear rate is

$$\eta_0 = K_1 \exp(b_1 T) \exp(a_1 p) \quad (2.41)$$

This equation is valid over a temperature range of about 50 °K and small pressure changes of the order of 1 kbar for polymers. Typical values of b_1 range from $-0.03 \text{ } ^\circ\text{K}^{-1}$ for polyolefins to $-0.1 \text{ } ^\circ\text{K}^{-1}$ for polystyrene and $a_1=1\text{-}4 \text{ kbar}^{-1}$ for the same materials. A relation that is valid over a wider temperature range is the *Andrade-Eyring* equation

$$\eta_0 = K_2 \exp\left\{\frac{E_a}{RT}\right\} \quad (2.42)$$

Polymer melts obey this equation at temperatures well above their glass transition. The *flow activation energy*, E_a ranges from $\approx 25 \text{ kJ/mol}$ for PE to $\approx 60 \text{ kJ/mol}$ for PS and $\approx 85 \text{ kJ/mol}$ for PC and PVC.

2.7 Characterisation of Viscoelasticity

Polymeric fluids are not Newtonian or ideal fluids. They show an intermediate behaviour between ideal solids and ideal liquids. That is, except their viscous character they also show considerable elasticity. To evaluate their elastic and viscous character one often conducts *small angle oscillatory (dynamic) shear* measurements and *shear step strain* experiments.

2.7.1 Linear Dynamic Measurements

During dynamic measurements the sample is deformed sinusoidally in shear, in an oscillatory mode, and the resulting stress is monitored as a function of time. The strain amplitude of the oscillations is kept sufficiently low so that the melt does not show a non-linear behaviour

$$\gamma = \gamma_0 \sin(\omega t) \quad (2.43)$$

The stress also oscillates sinusoidally at the same frequency but, in general, it is shifted by the *phase angle*, δ , with respect to the strain wave

$$\sigma = \sigma_0 \sin(\omega t + \delta) , \quad (2.44)$$

where ω is the rotational frequency of the applied deformation.

For Newtonian liquids $\delta = 90^\circ$. Ideal elastic solids show no phase angle hysteresis, $\delta = 0^\circ$. The data of the viscoelastic fluids are analysed by decomposing the stress wave into two waves of the same frequency, one in phase with the strain wave and one out of phase with this wave, thus,

$$\sigma = \sigma' + \sigma'' = \sigma'_0 \sin(\omega t) + \sigma''_0 \cos(\omega t) . \quad (2.45)$$

The tangent of the phase angle is defined as

$$\tan \delta = \frac{\sigma_0''}{\sigma_0'} . \quad (2.46)$$

This decomposition suggests the definition of two dynamic moduli: the in-phase *storage* or *elastic modulus*; and the out-of-phase *viscous* or *loss modulus* respectively:

$$G' = \frac{\sigma_0'}{\gamma_0} \quad (2.47)$$

$$G'' = \frac{\sigma_0''}{\gamma_0} . \quad (2.48)$$

Then the resulting stress and the tangent of the loss angle may be rewritten in terms of these two moduli:

$$\sigma = \gamma_0 [G' \sin(\omega t) + G'' \cos(\omega t)] \quad (2.49)$$

$$\tan \delta = \frac{G''}{G'} . \quad (2.50)$$

The total response of the material to this time dependent flow is described by the complex modulus, $G^* = G' + iG''$; its magnitude is:

$$|G^*| = \frac{\sigma_0}{\gamma_0} = \sqrt{G'^2 + G''^2} . \quad (2.51)$$

The energy per unit volume dissipated per cycle of the sinusoidal deformation is

$$\int_0^t \underline{\underline{\sigma}} : \underline{\underline{D}} dt = \int_0^{2\pi/\omega} \sigma \dot{\gamma} dt = \pi G'' \gamma_0^2 . \quad (2.52)$$

The shear strain rate is the derivative of strain with respect to time. For the sinusoidal deformation this becomes:

$$\dot{\gamma} = \frac{d\gamma}{dt} = \gamma_0 \omega \cos(\omega t) = \dot{\gamma}_0 \cos(\omega t) . \quad (2.53)$$

The dynamic viscosity and the elastic part of the complex viscosity are defined as:

$$\eta' = \frac{\sigma_0''}{\dot{\gamma}_0} = \frac{G''}{\omega} \quad (2.54)$$

$$\eta'' = \frac{\sigma_0'}{\dot{\gamma}_0} = \frac{G'}{\omega} , \quad (2.55)$$

while the magnitude of the complex viscosity becomes

$$|\eta^*| = \sqrt{\eta'^2 + \eta''^2} = \frac{|G^*|}{\omega} . \quad (2.56)$$

The above equations have been used for the characterisation of the viscoelastic behaviour of the materials tested in the present work at the limit of small deformations. But this characterisation is not enough, as one needs to probe also the non-linear character of the melts at larger deformation, i.e. in flow.

2.7.2 Non-linear strain dependence

The small amplitude dynamic experiments measure the small deformation behaviour of the material. As it will be extensively described below, at large deformations polymers may show non-linear behaviour (*damping* of the stresses). That is, the stresses needed for these deformation may be lower than what linearity, as measured by small amplitude dynamic experiments, would dictate.

The non-linearity of the stress - strain - rate of strain relations is usually given by the *damping function*. This will be defined in detail in Section 3.4. It suffices to state here that it describes the weakening of the resistance of the material to deformation as the deformation itself (γ in shear flow or ε in elongational flow) increases above the linearity limit.

The method to obtain information about the non-linear viscoelastic character of a material is through single step-strain and stress relaxation experiments: A shear deformation of magnitude γ_0 is applied instantaneously to the material and kept constant in time, while the stress response of the deformed material is monitored as it relaxes. The *nonlinear shear relaxation modulus* is defined as:

$$G(t, \gamma_0) \equiv \frac{\sigma_{12}(t, \gamma_0)}{\gamma_0} . \quad (2.57)$$

The ratio of the nonlinear shear relaxation modulus over $G_0(t)$ gives a measure of the deviation of the behaviour of the material from the linear:

$$h(\gamma_0) = \frac{G(t, \gamma_0)}{G_0(t)} . \quad (2.58)$$

This ratio is called *damping function* and it should be only a function of the deformation. It has values ≤ 1 where the equal sign holds for linear materials and very low values of deformation. Thus, the relaxation modulus is given by the product of the linear part, which is a function of time, $G_0(t)$, and the deformation dependent $h(\gamma)$:

$$G(t, \gamma) = h(\gamma)G_0(t) . \quad (2.59)$$

In practise, the damping function is evaluated by conducting step-strain and stress relaxation measurements at different values of strain, γ_i , and measuring the differences between the resulting curves $G(\gamma_i, t)$ and the curve at very low value of the strain γ_0 .

The same experiment may be done also in elongational flow but this is much more difficult to implement. This gives:

$$h(\varepsilon_0) = \frac{E(t, \varepsilon_0)}{E_0(t)} , \quad (2.60)$$

where E is the extensional relaxation modulus.

2.7.3 Simple shear flow

Steady state shear flow at a constant shear rate, $\dot{\gamma}_0$, is very useful experiment to gain information both on the viscous character of the fluid and on its elasticity. This flow

is usually implemented between the cone and the plate apparatus, described in the experimental section. This geometry warrants the constant shear rate everywhere in the flow field.

The general form of the stress tensor, $\underline{\underline{\sigma}}$, in such a flow is:

$$\underline{\underline{\sigma}} = \begin{pmatrix} \sigma_{11} & \sigma_{12} & 0 \\ \sigma_{21} & \sigma_{22} & 0 \\ 0 & 0 & \sigma_{33} \end{pmatrix}. \quad (2.61)$$

Since this is essentially a 2D flow with velocity in the “1” direction and velocity gradient in the “2” direction, the symmetric rate of strain tensor, $\underline{\underline{\dot{\gamma}}}$, is:

$$\underline{\underline{\dot{\gamma}}} = \begin{pmatrix} 0 & \dot{\gamma}_0 & 0 \\ \dot{\gamma}_0 & 0 & 0 \\ 0 & 0 & 0 \end{pmatrix}. \quad (2.62)$$

Thus, the shear stress $\sigma_{12} = \eta \dot{\gamma}_0$ is found by measuring the torque needed to rotate the cone. Conducting these measurements at different shear rates we can evaluate the viscosity of the fluid as a function of the shear rate.

For Newtonian fluids there is no other component of the stress tensor for this flow, except σ_{12} . For viscoelastic fluids, however the stresses σ_{11} , σ_{22} and σ_{33} are not zero. The stress differences $N_1 = \sigma_{11} - \sigma_{22}$ and $N_2 = \sigma_{22} - \sigma_{33}$ are called *primary* and *secondary normal stress differences* or *normal forces*. N_1 results in a force pushing the upper plate/cone. It is evaluated by measuring this force in experiments at different shear rates.

The existence of non-zero normal forces is a characteristic of viscoelasticity. The shape of the function $N_1(\dot{\gamma})$ is often used to test the proposed rheological equations of state.

2.8 Balance Equations in Newtonian Flow Fields

The balance equations can be formulated over a specified *macroscopic* volume, such as an extruder, or a *microscopic* volume taking the form of a differential field equation that holds at every point of the medium. In the former case, the balance holds over the *extensive* quantities of mass, momentum and energy whereas in the latter case, it holds over their *intensive* counterparts of density, specific momentum and specific energy. In the microscopic formulation the molecular nature of matter is ignored and the medium is viewed as a continuum [79].

2.8.1 Mass Balance

The *macroscopic mass balance equation* reads as

$$\frac{\partial}{\partial t} \int_V \rho dV + \int_S \rho \underline{\underline{v}} \cdot \underline{\underline{u}} dS = 0, \quad (2.63)$$

where V denotes the *control volume* and S the *control surface* of integration, \underline{u} is the unit vector normal to the surface of integration and ρ the density of the fluid. The mathematical statement of the conservation of mass in the case of any arbitrary control volume in space yields the *equation of continuity*

$$\frac{\partial \rho}{\partial t} + \nabla \cdot \rho \underline{v} = 0, \quad (2.64)$$

where ∇ is the vectorial operator known as *del* or *nabla*. This form states the mass conservation principle as measured by a stationary observer. The partial derivative $\partial/\partial t$ is evaluated at a fixed point in space and this is referred to as the *Lagrangian* point of view. It can be rewritten in terms of the substantial derivative as

$$\frac{D\rho}{Dt} = -\rho(\nabla \cdot \underline{v}), \quad (2.65)$$

where $D/Dt = \partial/\partial t + \underline{v} \cdot \nabla$. In this latter form states the conservation principle as measured (reported) by an observer who is moving with the fluid. This is referred to as the *Eulerian* point of view. In the case of incompressible fluids, the density is constant, that is it does not change with time or spatial position and therefore the equation of continuity reduces to $\nabla \cdot \underline{v} = 0$.

2.8.2 Momentum Balance

The *macroscopic linear momentum balance equation* reads as

$$\frac{\partial}{\partial t} \int_V \rho \underline{v} dV + \int_S \rho \underline{v} \underline{v} \cdot \underline{u} dS = \underline{F}_b + \underline{F}_s, \quad (2.66)$$

where \underline{F}_b are the body forces such as gravitational force and \underline{F}_s the surface forces or viscous forces that are acting on the control volume. The mathematical statement of the conservation of momentum in the case of any arbitrary control volume in space, yields the *equation of motion*

$$\rho \frac{\partial \underline{v}}{\partial t} + \rho \underline{v} \cdot \nabla \underline{v} = \nabla \cdot \underline{T} + \rho \underline{g} \quad (2.67)$$

or in terms of the substantial derivative

$$\rho \frac{D\underline{v}}{Dt} = \nabla \cdot \underline{T} + \rho \underline{g}, \quad (2.68)$$

which is recognised as Newton's Second Law. The equation of motion is very important in that it gives rise to another important equation in fluid mechanics. Substituting Newton's constitutive equation into the equation of motion, one gets the *Navier-Stokes equation*

$$\rho \frac{\partial \underline{v}}{\partial t} + \rho \underline{v} \cdot \nabla \underline{v} = -\nabla p + \eta \nabla^2 \underline{v} + \rho \underline{g} \quad (2.69)$$

in Lagrangian viewpoint, or

$$\rho \frac{D\underline{v}}{Dt} = -\nabla p + \eta \nabla^2 \underline{v} + \rho \underline{g} \quad (2.70)$$

in Eulerian viewpoint. The symbol defined as ∇^2 is called the *Laplacian*. In these forms the Navier-Stokes equation holds for Newtonian fluids and incompressible flows. Polymer processing flows are always laminar and generally creeping type flows. In the latter case, viscous forces predominate over forces of inertia and acceleration, thus the Navier-Stokes equation reduces to

$$\rho \frac{\partial \underline{v}}{\partial t} = -\nabla p + \eta \nabla^2 \underline{v} + \rho \underline{g}, \quad (2.71)$$

whereas in the former case of negligible viscosity, reduces to

$$\rho \frac{\partial \underline{v}}{\partial t} + \rho \underline{v} \cdot \nabla \underline{v} = -\nabla p + \rho \underline{g}, \quad (2.72)$$

which is the well-known *Euler equation*.

2.8.3 Energy Balance

Polymer processing operations are non-isothermal. The deforming viscous polymer melt constantly undergoes heating by internal viscous dissipation. Therefore we need to account for non-isothermal effects via appropriate equations. The *macroscopic total energy balance equation* reads as

$$\frac{dE}{dt} = \frac{\partial}{\partial t} \int_V \rho e dV + \int_S \rho e \underline{v} \cdot \underline{n} dS = \dot{Q} + \dot{W}, \quad (2.73)$$

where e is the *total specific energy* or *energy per unit mass*, \dot{Q} is the *total rate of heat* added to the control volume through the control surfaces and \dot{W} is the *total rate of work* done on the control volume through the control surfaces (including gravity). In differential form the total energy balance equation is formulated as

$$\frac{\partial e}{\partial t} + \nabla \cdot e \underline{v} + \nabla \cdot \underline{q} + \nabla \cdot \underline{T} \cdot \underline{v} - \rho \underline{g} \cdot \underline{v}, \quad (2.74)$$

where \underline{q} is the *local heat flux* and \underline{g} is the gravitational constant. It is important to notice that the macroscopic energy balance gives rise to important equations such as the *Bernoulli equation* and the *thermal energy equation* which coupled with the mass and momentum conservation relations provide the mathematical structure for the study of polymer processing flows. Solutions of such problems is complicated by the fact that viscosity also depends on temperature and thus shear heating can change the velocity profile. Then the energy and momentum equations are coupled through the temperature-dependent viscosity.

Chapter 3

Constitutive Equations for Polymer Melts

3.1 Linear Viscoelasticity

When polymeric materials are loaded in shear or extension an instantaneous deformation, as expected for a Hookean solid, is followed by a continuous, time dependent deformation or “creep”. When the load is removed, part of the deformation is recovered instantly, more is recovered with time, while a small amount is *dissipated*, in other words, not recovered at all. This time-dependent response is called *viscoelasticity*. Another common way to measure the phenomenon is by stress relaxation. When a purely viscous liquid is subject to a step increase in strain, the stress relaxes instantly to zero as soon as the strain becomes constant. An elastic solid subjected to the same deformation, would show no relaxation. However, that is not the case for polymeric liquids; in such systems the stress relaxes in an exponential fashion of the form

$$\sigma(t) = \sigma_0 \exp\left(\frac{-t}{\tau}\right), \quad (3.1)$$

where τ is commonly referred to as the *relaxation time* of the material under consideration. If we convert stress relaxation data to a relaxation modulus

$$G(t) = \frac{\sigma(t)}{\gamma} \quad (3.2)$$

all the data for small strains, typically $\gamma < \gamma_{cr} \simeq 0.5$ for polymeric liquids, fall on the same curve. This linear dependence of stress relaxation on strain is called *linear viscoelasticity*.

Another concept that is closely tied to that of elasticity, is the concept of “memory”. A material that has no memory cannot be elastic since it has no way of remembering its original shape. Hence fluids exhibiting elastic properties as well, are often referred to as *memory fluids*.

3.2 The General Linear Viscoelastic Model

In an attempt to model experiments on viscoelastic solids, Boltzmann suggested that small changes in stress equal small changes in the modulus times the strain

$$d\sigma = \gamma dG . \quad (3.3)$$

A new function, the *memory function*, can be defined as the time derivative of $G(t)$

$$\mu(t) = -\frac{dG(t)}{dt} . \quad (3.4)$$

Since the relaxation modulus decreases with time, the derivative will be negative. Thus the minus sign was added to make $\mu(t)$ a positive function. Substituting this expression for the memory function in Eq. 3.3 gives

$$d\sigma = -\mu(t)\gamma dt . \quad (3.5)$$

If the relaxation modulus and, thus, the memory function depend only on time, we can make up any larger deformation (but deformations still within the linear range of the material) by summing up all the small deformations. This can be expressed as the integral over all past time

$$\int_0^\sigma d\sigma = \sigma = - \int_{-\infty}^t \mu(t-t')\gamma(t') dt' , \quad (3.6)$$

where t' is the past time variable running from the infinite past $-\infty$ to the present time t . This summation integral over all past times till present, is commonly referred to as the *Boltzmann superposition principle*.

In an analogous way, we can write the model directly in terms of the relaxation modulus. Considering a small change in stress due to a small change in strain

$$d\sigma = G d\gamma = G \frac{d\gamma}{dt} dt = G \dot{\gamma} dt \quad (3.7)$$

and performing the integration

$$\int_0^\sigma d\sigma = \sigma = \int_{-\infty}^t G(t-t')\dot{\gamma}(t') dt' . \quad (3.8)$$

Thus, the stress is an integral over all past times of the relaxation modulus times the rate of strain. This is the form that is most frequently used because $G(t)$ can be measured directly.

The form of the measured relaxation modulus suggests an exponential decay function

$$G(t) = G_0 \exp\left(\frac{-t}{\tau}\right) , \quad (3.9)$$

where τ is the *relaxation time* of the material. Substituting this expression for the relaxation modulus into Eq. 3.8 gives the single relaxation or simple *Maxwell model*

$$\sigma = \int_{-\infty}^t G_0 \exp \left\{ \frac{-(t-t')}{\tau} \right\} \dot{\gamma}(t') dt' . \quad (3.10)$$

A single exponential term does not fit typical relaxation modulus data very well. A logical improvement on this model is to try a series of relaxation times, τ_i multiplied by the weighting constants G_i

$$G(t) = \sum_{i=1}^N G_i \exp \left(\frac{-t}{\tau_i} \right) . \quad (3.11)$$

Substituting the above series into Eq. 3.8 gives the *general linear viscoelastic model*

$$\sigma = \int_{-\infty}^t \sum_{i=1}^N G_i \exp \left\{ \frac{-(t-t')}{\tau_i} \right\} \dot{\gamma}(t') dt' . \quad (3.12)$$

Use of the extra stress tensor, $\underline{\underline{\sigma}}$ for the shear stress and the rate of deformation tensor, $2\underline{\underline{D}}$ for the rate of strain in order to accommodate various types of deformations in three dimensions, leads to

$$\underline{\underline{\sigma}} = \int_{-\infty}^t G(t-t') 2\underline{\underline{D}} dt' . \quad (3.13)$$

In the case of simple shear, there are only two components of $2\underline{\underline{D}}$, so that $2D_{12} = 2D_{21} = \dot{\gamma}$. Thus, the linear viscoelastic model does not predict normal stresses in steady shear flow, the viscosity is independent of $\dot{\gamma}$ but σ_{12} is time dependent. A fluid at rest at times $t' \leq 0$, is suddenly set into simple shear flow for $t' > 0$. The velocity gradient in such a case is simply $\dot{\gamma}$, thus,

$$\sigma_{12} = \begin{cases} \dot{\gamma} \int_0^t G(t-t') dt' & t' > 0 \\ 0 & t' \leq 0 \end{cases} .$$

The time dependent shear viscosity at the onset of simple shear flow is defined as

$$\eta_{12}^+(t) = \frac{\sigma_{12}(t)}{\dot{\gamma}} . \quad (3.14)$$

Substitution of the stress component into Eq. 3.14 gives

$$\eta_{12}^+(t) = \sum_{i=1}^N G_i \tau_i \left\{ 1 - \exp \left(\frac{-t}{\tau_i} \right) \right\} . \quad (3.15)$$

At steady state, the zero shear viscosity is defined

$$\eta_0 = \lim_{t \rightarrow \infty} \eta_{12}^+(t) = \sum_{i=1}^N G_i \tau_i . \quad (3.16)$$

3.3 The Lodge Equation for a Rubber-Like Liquid

Polymer stresses due to flow or deformation can be calculated using Eq. 2.21 if the distribution function for that particular flow or deformation can be predicted. In order to make such predictions, a molecular theory of polymer dynamics is required. Conceptually, the simplest theory is the *classical rubber elasticity theory*, which applies to rubbers made up of cross-linked polymer chains. The theory was developed by Wall, Flory and Rehner, James and Guth and Treloar in the early 1940's. Cross-link points were considered to be evenly spaced along each polymer chain. The portion of polymer between two neighbouring cross-links is called a *strand*. For any given deformation history it can be shown using Eq. 2.21 that [57, 56, 45]

$$\underline{\underline{\sigma}} = \nu k_B T \underline{\underline{C}}^{-1} = G \underline{\underline{C}}^{-1}, \quad (3.17)$$

where, $G = \nu k_B T$ is the modulus, ν , is the number of strands per unit volume and $\underline{\underline{C}}^{-1}$ is the relative Finger deformation tensor. This equation describes a purely elastic material, that is, one that dissipates no energy during or after deformation. It applies to any given volume-conserving deformation with the additional constraint of being *affine*; that is the cross-link points are convected with the macroscopic deformation.

Green and Tobolsky (1946) proposed a theory appropriate for molten polymeric liquids that was inspired from the rubber elasticity theory. This model is based on the notion that polymer chains that are not chemically cross-linked nevertheless interact with each other to form a *transient network*. These temporary cross-links or constraints are believed to be caused by *entanglements*; that is, topological constraints arising because one chain cannot pass through another. When the material is deformed, each strand is stretched *affinely* until it breaks (slips) free from its junction. After it breaks free another relaxed strand becomes entangled. However, there will be an amount of strands during deformation that survive without breaking. The contribution $d\underline{\underline{\sigma}}$ to the extra stress from those strands that meet both of these conditions leads to the constitutive equation of the form

$$\underline{\underline{\sigma}} = \int_{-\infty}^t \mu(t-t') \underline{\underline{C}}^{-1}(t', t) dt', \quad (3.18)$$

where $\mu(t-t') \equiv (G/\tau) \exp\{(t'-t)/\tau\}$ is the memory function assuming only a single relaxation process and $G = \nu k_B T$ is the *modulus of elasticity* with ν the number of strands per unit volume. The key assumptions of this temporary network model of Green and Tobolsky are :

1. The strands are Gaussian (i.e. they follow Gaussian statistics).
2. The strands deform affinely until they break.
3. The strands break with a constant probability per unit time, independent of the network deformation.
4. The strands re-form as fast as they break in configurations typical of equilibrium.

Green and Tobolsky recognised that their approach could be extended to multiple relaxation processes. The extension was carried out independently by Lodge and Yamamoto. However, Lodge gave the clearest derivation of the model with multiple relaxation modes and the constitutive equation resulting from the molecular model of Green and Tobolsky has thereby come to be named after him.

The memory function $\mu(t - t')$ can accommodate any number of *independent* relaxation processes

$$\mu(t - t') = \sum_{i=1}^N \left(\frac{G_i}{\tau_i} \right) \exp \left\{ \frac{-(t - t')}{\tau_i} \right\}. \quad (3.19)$$

With this choice for $\mu(t - t')$ the *storage*, $G'(\omega)$ and *loss moduli*, $G''(\omega)$ can be obtained through a *Fourier transform integral*

$$G'(\omega) = \omega \int_0^{\infty} G(t) \sin(\omega t) dt \quad G''(\omega) = \omega \int_0^{\infty} G(t) \cos(\omega t) dt \quad (3.20)$$

leading to the expressions

$$G'(\omega) = \sum_{i=1}^N G_i \frac{\omega^2 \tau_i^2}{1 + \omega^2 \tau_i^2} \quad \text{and} \quad G''(\omega) = \sum_{i=1}^N G_i \frac{\omega \tau_i}{1 + \omega^2 \tau_i^2}, \quad (3.21)$$

By choosing a discrete set of values for τ_i distributed over a time interval and then fitting Eqs. 3.21 to experimental data for $G'(\omega)$ and $G''(\omega)$, the weighting constants G_i can be obtained. The constitutive equation with multiple relaxation modes is the *Lodge equation* for a *rubber-like liquid*. The set of values of τ_i and G_i are referred to as the *relaxation spectrum*. In order to solve Eq. 3.18 for a particular flow history one must compute the components of the relative Finger deformation tensor, $\underline{\underline{C}}^{-1}$ and carry out the integration.

In this way, the Lodge equation predicts many of the qualitative phenomena of viscoelastic flow, including a positive first normal stress difference in shear, gradual stress relaxation after cessation of flow, and elastic recovery of strain after removal of the stress. It predicts that the time-dependent extensional viscosity, η_E^+ , rises steeply to infinity whenever the elongation rate, $\dot{\epsilon}$, exceeds $1/2\tau_1$, where τ_1 is the longest relaxation time. This prediction is accurate for some melts, namely ones with multiple long side branches. For melts composed of unbranched molecules, the rise in η_E^+ is much less dramatic.

In quantitative detail, Lodge's equation is often inaccurate. Contrary to experiment, it predicts unlimited growth in elongational viscosity whereas the data must eventually approach to a maximum value or level off. In steady shearing, it predicts that both the shear viscosity η_{12} and the first normal stress coefficient, Ψ_1 , are independent of shear rate; in experiments both decrease with increasing $\dot{\gamma}$. It also overpredicts elastic recovery. The Lodge equation, thus, overemphasises the elasticity of viscoelastic fluids.

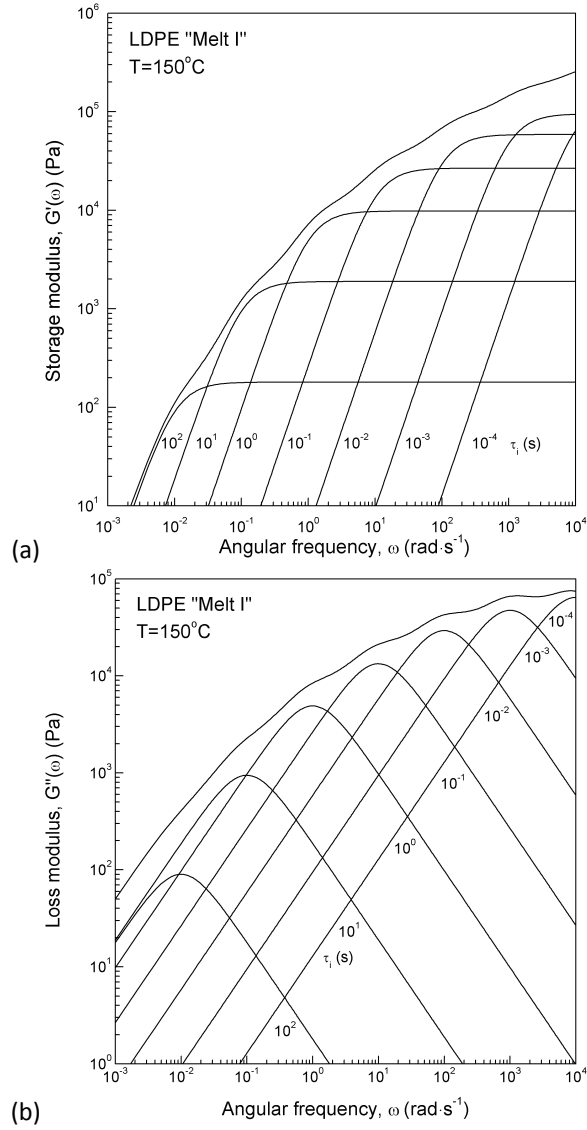


Figure 3.1: Frequency dependence of the (a) storage and (b) loss modulus of LDPE "Melt I" at constant $T=150^\circ\text{C}$ as represented by a sum of eight terms (see Table 3.1).

Table 3.1: Spectrum of relaxation modes for “Melt I”, a LDPE with LCB architecture with $M_w = 482$ kg/mol, $(M_w/M_n) = 28.1$, MFI $(190/2.16) = 1.33$ and $E_a = 54$ kJ/mol, determined at $T = 150^\circ\text{C}$ [27].

Mode Number, i	τ_i (s)	G_i (Pa)
1	10^3	$1.00 \cdot 10^0$
2	10^2	$1.80 \cdot 10^2$
3	10^1	$1.89 \cdot 10^3$
4	10^0	$9.80 \cdot 10^3$
5	10^{-1}	$2.67 \cdot 10^4$
6	10^{-2}	$5.86 \cdot 10^4$
7	10^{-3}	$9.48 \cdot 10^4$
8	10^{-4}	$1.29 \cdot 10^5$

Start-Up of Shear Flow

A simple shear flow with constant shear rate, $\dot{\gamma}$ suddenly applied at $t = 0$ and at constant volume, can be described in terms of the shear deformation $\gamma = \gamma(t', t)$ accumulated between times t' and t and the relative Finger strain tensor $\underline{\underline{C}}^{-1}(t', t)$. In steady simple shearing $\gamma(t', t) = \dot{\gamma}(t - t')$, and the Finger tensor becomes

$$\underline{\underline{C}}^{-1}(t', t) = \begin{pmatrix} 1 + \dot{\gamma}^2(t - t')^2 & \dot{\gamma}(t - t') & 0 \\ \dot{\gamma}(t - t') & 1 & 0 \\ 0 & 0 & 1 \end{pmatrix}. \quad (3.22)$$

If the sample is completely relaxed in a state of equilibrium until time $t' = 0$ and then steady shear flow begins at time $t' = 0$, the components of the Finger tensor are

$$C_{11}^{-1} = \begin{cases} 1 + \dot{\gamma}^2(t - t')^2 & t' > 0 \\ 1 + \dot{\gamma}^2(t)^2 & t' \leq 0 \end{cases}$$

$$C_{22}^{-1} = C_{33}^{-1} = \begin{cases} 1 & t' > 0 \\ 1 & t' \leq 0 \end{cases}$$

$$C_{12}^{-1} = C_{21}^{-1} = \begin{cases} \dot{\gamma}(t - t') & t' > 0 \\ \dot{\gamma}(t) & t' \leq 0 \end{cases}.$$

Note that for $t' \leq 0$ the shear rate is independent of t' since the sample is not being sheared at that portion of the time spectrum. If we define the following relations for the *shear viscosity* and *primary normal stress difference coefficient*

$$\eta_{12}^+ = \frac{\sigma_{12}}{\dot{\gamma}} \quad \Psi_1 = \frac{\sigma_{11} - \sigma_{22}}{\dot{\gamma}^2}, \quad (3.23)$$

then it is only a matter of proper integration of Eq. 3.18 to obtain the components σ_{ij} of the extra stress tensor. It is convenient, though, that the integration of the Lodge equation be performed with a single relaxation mode for the memory function, $\mu(t - t')$, and then generalise the final result for the multimode memory function. Calculating the components of the extra stress tensor, σ_{ij} , and substituting the results in Eqs. 3.23 gives

$$\eta_{12}^+(t) = \sum_{i=1}^N G_i \tau_i \left\{ 1 - \exp\left(-\frac{t}{\tau_i}\right) \right\} \quad (3.24)$$

$$\Psi_1(t) = 2 \sum_{i=1}^N G_i \tau_i^2 \left\{ 1 - \left[1 + \left(\frac{t}{\tau_i} \right) \right] \exp\left(-\frac{t}{\tau_i}\right) \right\}. \quad (3.25)$$

It follows from Figs. 3.3 that in the case of the shear viscosity, $\eta_{12}^+(t)$, only the linear viscoelastic start-up curve, and in the case of the primary normal stress coefficient $\Psi_1(t)$ only the second order start-up curve are predicted by the theory. No stress or normal stress overshoot is predicted (see Figs. 3.4). With increasing shear rate, $\dot{\gamma}$, the measured values of $\eta_{12}^+(t)$ and $\Psi_1(t)$ are increasingly lower than those computed. This is due to the shear viscosity, $\eta_{12}^+(t)$ and the primary normal stress coefficient, $\Psi_1(t)$, which are predicted by this theory to be independent of shear rate, while experiments indicate that they are decreasing functions of the rate. The strong dependence of $\eta_{12}^+(t)$ and $\Psi_1(t)$ on the shear rate indicates a change of the structure of the temporary polymer network.

Start-Up of Extensional Flow

A uniaxial elongation with constant extension rate, $\dot{\epsilon}$, suddenly applied at $t = 0$ and at constant volume can be described in terms of the stretch ratio $\lambda = \lambda(t', t)$ accumulated between times t' and t and the relative strain Finger tensor $\underline{\underline{C}}^{-1}(t', t)$. In steady uniaxial extension $\lambda(t', t) = \exp\{\dot{\epsilon}(t - t')\}$, and the Finger tensor becomes

$$\underline{\underline{C}}^{-1}(t', t) = \begin{pmatrix} \exp\{2\dot{\epsilon}(t - t')\} & 0 & 0 \\ 0 & \exp\{-\dot{\epsilon}(t - t')\} & 0 \\ 0 & 0 & \exp\{-\dot{\epsilon}(t - t')\} \end{pmatrix}. \quad (3.26)$$

Suppose the sample is completely relaxed in a state of equilibrium until time $t' = 0$, and then steady uniaxial elongation begins. The components of the Finger tensor are

$$C_{11}^{-1} = \begin{cases} \exp\{2\dot{\epsilon}(t - t')\} & t' > 0 \\ \exp\{2\dot{\epsilon}t\} & t' \leq 0 \end{cases}$$

$$C_{22}^{-1} = C_{33}^{-1} = \begin{cases} \exp\{-\dot{\epsilon}(t - t')\} & t' > 0 \\ \exp\{-\dot{\epsilon}t\} & t' \leq 0 \end{cases}$$

Note that for $t' \leq 0$ the stretch ratio $\lambda(t', t) = \exp(\dot{\epsilon}t)$, is independent of t' , since the sample is not being elongated at that portion of the time spectrum. Substituting

Table 3.2: Spectrum of relaxation modes for “Melt I”. The ten constants τ_i and G_i were determined by curve fitting the elongational data at $\dot{\epsilon}=0.001 \text{ s}^{-1}$ [43].

Mode Number, i	Set A		Set B	
	τ_i (s)	G_i (Pa)	τ_i (s)	G_i (Pa)
1	10^2	$1.903 \cdot 10^2$	10^3	$1.601 \cdot 10^{-1}$
2	10^1	$2.306 \cdot 10^3$	10^2	$1.926 \cdot 10^2$
3	10^0	$6.241 \cdot 10^3$	10^1	$1.723 \cdot 10^3$
4	10^{-1}	$3.299 \cdot 10^4$	10^0	$6.640 \cdot 10^3$
5	10^{-2}	$3.720 \cdot 10^4$	10^{-1}	$3.972 \cdot 10^4$

the Finger tensor into Eq. 3.18 and integrating, one can obtain the components σ_{ij} of the extra stress tensor in the case of extensional flow

$$\sigma_{11}(t, \dot{\epsilon}) = \sum_{i=1}^N \left\{ G_i \exp \left[\frac{-(1 - 2\dot{\epsilon}\tau_i)t}{\tau_i} \right] + \frac{G_i}{1 - 2\dot{\epsilon}\tau_i} \left[1 - \exp \left(\frac{-(1 - 2\dot{\epsilon}\tau_i)t}{\tau_i} \right) \right] \right\} \quad (3.27)$$

$$\sigma_{22}(t, \dot{\epsilon}) = \sum_{i=1}^N \left\{ G_i \exp \left[\frac{-(1 + \dot{\epsilon}\tau_i)t}{\tau_i} \right] + \frac{G_i}{1 + \dot{\epsilon}\tau_i} \left[1 - \exp \left(\frac{-(1 + \dot{\epsilon}\tau_i)t}{\tau_i} \right) \right] \right\} . \quad (3.28)$$

An *extensional viscosity* is then defined as

$$\eta_E^+(t, \dot{\epsilon}) = \frac{[\sigma_{11} - \sigma_{22}](t, \dot{\epsilon})}{\dot{\epsilon}} . \quad (3.29)$$

Note that if $\dot{\epsilon} > 1/2\tau_1$, σ_{11} diverges exponentially as time increases. If, however, $\dot{\epsilon} < 1/2\tau_1$, a steady state is reached in which

$$\sigma_{11}(\dot{\epsilon}) = \sum_{i=1}^N \frac{G_i}{1 - 2\dot{\epsilon}\tau_i} \quad (3.30)$$

$$\sigma_{22}(\dot{\epsilon}) = \sum_{i=1}^N \frac{G_i}{1 + \dot{\epsilon}\tau_i} \quad (3.31)$$

and the uniaxial extensional viscosity in this steady state is

$$\bar{\eta}_E(\dot{\epsilon}) = 3 \sum_{i=1}^N \frac{G_i \tau_i}{(1 - 2\dot{\epsilon}\tau_i)(1 + \dot{\epsilon}\tau_i)} . \quad (3.32)$$

In the limit of small extension rates, ($\dot{\epsilon} \rightarrow 0$), the *Trouton viscosity* assumes the form

$$\eta_E^+(t, \dot{\epsilon} \rightarrow 0) = 3 \sum_{i=1}^N G_i \tau_i \left\{ 1 - \exp \left(\frac{-t}{\tau_i} \right) \right\} \quad (3.33)$$

and the Trouton limit is approached for the steady state elongational viscosity

$$\bar{\eta}_E = 3 \sum_{i=1}^N G_i \tau_i \quad (3.34)$$

A comparison between the predictions of the rubber-like liquid theory of the extensional viscosity curves produced with the aid of the constants G_i and τ_i of “Set B” from Table 3.2 and the eight constants of Table 3.1 is given Fig. 3.2. It can be seen that only differences of minor importance are introduced with the change of the relaxation spectrum used to infer the prediction curves. The experimenter is free to choose an appropriate set of constants in order to fit the experimental data and make use of the theory. However, it has ever since been argued that this arbitrary choice of a discrete relaxation spectrum with multiple relaxation modes has no direct physical meaning. A quotation from Laun [27] reveals such a scepticism :

Another disadvantage of the series representation of the memory function is the fact that the relaxation strengths G_i have no direct physical meaning, because the choice of the τ_i is arbitrary. However, this representation makes it possible to describe the linear viscoelastic behaviour over a wide range of time scale by means only of a few constants.

The integration of Eq. 3.18 is simplified in all types of simple deformations examined and the contribution of each relaxation time to the material functions can easily be surveyed.

3.4 Non-Linear Viscoelasticity

The time-dependent rheological response of polymer melts in a processing flow is characterised by a dimensionless number, called the *Deborah number* defined as

$$De = \frac{\tau}{t_{exp}} = \tau\omega, \quad (3.35)$$

where τ is a characteristic relaxation time of the melt and $t_{exp} = 1/\omega$ or $t_{exp} = 1/\dot{\gamma}$ is the time scale of the processing flow. This ratio reflects the ability of the macromolecular system to flow like a *viscous fluid* when $De \ll 1$ or respond like an elastic solid able only to undergo deformation and not flow when $De \gg 1$. Between these two extremes the rheological behaviour of polymer melts is characterized as *viscoelastic*. Since both ω and $\dot{\gamma}$ represent rates of change of deformation it is not surprising that the viscosity is rate dependent and shear-thinning. The equality between the rates of shearing deformation, ω and $\dot{\gamma}$ is only valid for some types of polymer melts and it can be verified through an empirical rule called the *Cox-Merz rule*.

The time-dependent non-linear behaviour of polymer melts plays an important role in high Deborah number processes like extrusion through short dies, injection moulding, calendering, spinning and film blowing, where the material undergoes fast changes in strain by shear, elongation or a combination of both over a time scale, which is comparable to the fluid relaxation time. One of the most illustrative methods to

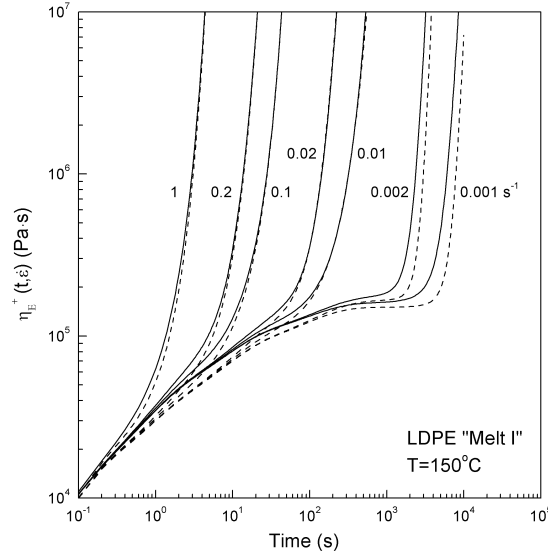


Figure 3.2: Elongational viscosity, $\eta_E^+(t, \epsilon)$ as a function of time and deformation rate, after start-up of steady uniaxial extension for the LDPE “Melt I” at $T=150^\circ\text{C}$. Solid lines are the predictions of the rubber-like liquid theory using the 8 modes of Table 3.1 while dashed lines are the predictions of the same theory using the 5 modes of “Set B” from Table 3.2.

obtain information about the nonlinear viscoelastic character of a material is through single step-strain in shear relaxation experiments. A shear deformation of magnitude γ_0 is applied to the material instantaneously and kept constant through time, while the stress response of the deformed material is monitored as it relaxes. The nonlinear shear relaxation modulus is defined as

$$G_\sigma(t, \gamma_0) \equiv \frac{\sigma_{12}(t, \gamma_0)}{\gamma_0}. \quad (3.36)$$

The principle of *time-deformation separability* suggests that the nonlinear viscoelastic response of polymeric materials should be separated in a time-dependent linear response that is governed by the memory function, $\mu(t - t')$ and a strain-dependent nonlinear response that depends only on the magnitude, γ_0 of the shear deformation imposed on the material. The *strain-dependent damping function* is defined as

$$h(\gamma_0) = \frac{G_\sigma(t, \gamma_0)}{G(t)}. \quad (3.37)$$

It reflects the deviation of the response of the shear relaxation modulus from the linear viscoelastic regime. In terms of the temporary network theory, the damping function describes the gradual dissolving of the temporary entanglements as the material is stretched to higher magnitudes of shear and is characterized by considerable *strain*

softening, that is, $h(\gamma_0)$ decreases with increasing γ_0 . On the other hand, the temporary network model and the corresponding Lodge equation suggest no strain softening, since this theory predicts that $h(\gamma_0) = 1$ for all γ_0 .

3.5 The Modified Rubber-Like Liquid Model

The constitutive relation derived for the Lodge rubber-like liquid is a valid description of polymer melt behaviour in the second order fluid limit only and it fails outside this range, i.e. at higher strains. In the context of the *modified rubber-like liquid theory* [45], this failure is attributed to the fact that temporary junction networks disentangle with increasing deformation, in contrast to the basic assumption of Lodge's theory that the deformation has no effect on the formation or dissolution of temporary network junctions. To account for the change in polymer network structure with increasing deformation a hypothesis is postulated that there are two *independent decay mechanisms* for network strands:

1. The linear viscoelastic (time-dependent) relaxation, with the probability of a network strand to survive a time difference $(t - t')$ being $\exp\{-(t - t')/\tau\}$.
2. Disentanglement due to deformation; the probability of a network strand to survive a relative deformation between times t' and t is proportional to a damping function, $h(I_{C^{-1}}(t', t), II_{C^{-1}}(t', t))$, where $I_{C^{-1}}$ and $II_{C^{-1}}$ are the first and second invariant of the relative Finger strain tensor, respectively.

Thus the total probability of a network strand to survive a time difference $(t - t')$ and a given deformation characterised by the invariants $I_{C^{-1}}$ and $II_{C^{-1}}$ is equal to the product $\exp\{-(t - t')/\tau\} \cdot h(I_{C^{-1}}, II_{C^{-1}})$. This hypothesis leads to the following constitutive equation

$$\underline{\underline{\sigma}} = \int_{-\infty}^t \mu(t - t') h(I_{C^{-1}}, II_{C^{-1}}) \underline{\underline{C}}^{-1}(t', t) dt' . \quad (3.38)$$

This modified rubber-like liquid constitutive equation is a special form of the Kaye and Bernstein-Kearsley-Zapas (K-BKZ) class of equations [45]. The function $h(I_{C^{-1}}, II_{C^{-1}})$ is a deformation-dependent damping function; it describes purely geometrical effects and it is temperature independent [27].

3.5.1 The Wagner-I Equation

The first analytical expression for the damping function was proposed by Wagner [42]

$$h(II_{C^{-1}}) = \exp\left\{-n\sqrt{II_{C^{-1}} - 3}\right\} \quad (3.39)$$

and was used to model the rheology of the LDPE "Melt I".

Shear Stress Relaxation

Using a method of *rapid strains*, i.e. stress relaxation tests with varying step height γ_0 , it is possible to determine experimentally the damping function, $h(\gamma_0)$ for a given polymeric melt. If at time $t' = 0$ a shear strain of magnitude γ_0 is applied suddenly and held constant thereafter, then $\gamma(t', t) = \gamma_0$ and the Finger tensor for this step-strain in shear becomes

$$\underline{\underline{C}}^{-1}(t', t) = \begin{pmatrix} 1 + \gamma_0^2 & \gamma_0^2 & 0 \\ \gamma_0^2 & 1 & 0 \\ 0 & 0 & 1 \end{pmatrix}, \quad (3.40)$$

while the components of the relative Finger strain tensor for this particular deformation history are

$$\begin{aligned} C_{11}^{-1} &= \begin{cases} 1 & t' > 0 \\ 1 + \gamma_0^2 & t' \leq 0 \end{cases} \\ C_{22}^{-1} = C_{33}^{-1} &= \begin{cases} 1 & t' > 0 \\ 1 & t' \leq 0 \end{cases} \\ C_{12}^{-1} = C_{21}^{-1} &= \begin{cases} 0 & t' > 0 \\ \gamma_0 & t' \leq 0 \end{cases}. \end{aligned}$$

The invariants of the Finger tensor are

$$I_{C^{-1}}(t, t') = II_{C^{-1}}(t, t') = 3 + \gamma_0^2, \quad (3.41)$$

while $III_{C^{-1}}(t, t') = 1$, due to the constant volume assumption. Wagner's damping function then takes the simple form

$$h(\gamma_0) = \exp(-n\gamma_0) \quad (3.42)$$

and it is a function of the shear deformation, γ_0 .

In this context, integration of Eq. 3.38 with respect to t' gives exact analytical expressions for the relaxation of shear stress, $\sigma_{12}(t)$ and primary normal stress difference, $N_1(t)$ as a function of time

$$\sigma_{12}(t) = \gamma_0 \exp(-n\gamma) \sum_{i=1}^N G_i \exp\left(\frac{-t}{\tau_i}\right) \quad (3.43)$$

$$N_1(t) = \gamma_0^2 \exp(-n\gamma) \sum_{i=1}^N G_i \exp\left(\frac{-t}{\tau_i}\right) \quad (3.44)$$

for a multimode relaxation spectrum. Introducing the non-linear shear relaxation moduli, $G_\sigma(t, \gamma_0)$ and $G_N(t, \gamma_0)$ defined by

$$G_\sigma(t, \gamma_0) = \frac{\sigma_{12}(t)}{\gamma_0} \quad (3.45)$$

Table 3.3: Material parameter, n of the deformation-dependent damping function for commercial polymeric melts of varying molecular architecture and molecular weight distribution at the corresponding isothermal conditions. Data from Tsenoglou [9].

Sample	M_w (kg/mol)	M_w/M_n	$T(^{\circ}\text{C})$	n
LDPE.A2	451	27.5	150	0.134
LDPE.A4	305	30.3	150	0.11
LDPE.A7	268	24.6	110, 150	0.13
LDPE.B2	143	10.2	150	0.14
LDPE.C2	69	7.6	150	0.16
LDPE IUPAC A	231	10.0	130, 150	0.18
HDPE.A	181	13.7	140, 150, 170	0.34 - 0.38
HDPE.B	118	6.1	140, 150	0.29
HDPE.C	113	11.2	150	0.28

$$G_N(t, \gamma_0) = \frac{[\sigma_{11} - \sigma_{22}](t)}{\gamma_0^2} \quad (3.46)$$

it is obvious that both shear relaxation moduli are equal

$$G_\sigma(t, \gamma_0) = G_N(t, \gamma_0) = h(\gamma_0)G(t) = \exp(-n\gamma) \sum_{i=1}^N G_i \exp\left(\frac{-t}{\tau_i}\right) \quad (3.47)$$

This result is known as the *Lodge-Meissner rule*. The time dependence of the non-linear shear relaxation moduli, $G_\sigma(t, \gamma_0)$ and $G_N(t, \gamma_0)$ is not affected by the shear strain, γ_0 providing a rational justification for the assumption of independent decay mechanisms in time and deformation for network strands as postulated in the network disentanglement hypothesis.

The way that $G_\sigma(t, \gamma_0)$ and $G_N(t, \gamma_0)$ are related proves important in testing and classifying constitutive equations. For models which are based on the Gaussian network assumption it has been proven through Eq. 3.47 that $G_\sigma(t, \gamma_0) = G_N(t, \gamma_0)$. On the other hand, it has been suggested [49] that the relation between the two moduli, when examined for a variety of constitutive models, including Lodge's rubber-like liquid model, is of the more general form

$$\frac{G_N(t, \gamma_0)}{G_\sigma(t, \gamma_0)} = \frac{\tan(A\gamma_0)}{A\gamma_0}, \quad (3.48)$$

where $0.5 > A > 0$. The partitioning of the relaxation modulus into a deformation-dependent damping function and a time-dependent part identical to the linear relaxation modulus is therefore assumed to be a simplification of a more concise relation.

The material parameter, n , of the deformation-dependent damping function has been experimentally determined for several commercial long-chain branched LDPEs

Table 3.4: Temperature dependence of the damping function for the branched LDPE “Melt I” determined from shear relaxation modulus measurements for various magnitudes of shear strain, γ_0 at the isothermal conditions listed [27].

Sample	T(°C)	120	150	210
	γ_0	$h(\gamma_0)$		
Melt I	5	0.31	0.37	0.29
	10	0.14	0.17	0.16
	15	0.066	0.093	0.090
	20	0.034	0.052	0.056

and linear HDPEs studied by Tsenoglou [9] and the results are provided in Table 3.3. These parameters were obtained by fitting Eq. 3.42 to the data of Tables C.1 and C.2 using a linear least squares routine. A comparison between the values of the parameter n corresponding to branched and linear polymeric melts of varying molecular weight distribution and polydispersity implies that the branched melts show much less damping in shear than do the linear melts. A theoretical explanation of this reduced *strain softening* of the branched melts at large magnitudes of shear strain [9] suggests that this phenomenon is the result of the complex branched topology of these melts in direct contrast to polymers that are composed of linear chains.

The temperature invariance of the damping function is demonstrated in the case of the branched LDPE “Melt I” [27]. Experimentally determined values of $h(\gamma_0)$ are provided in Table 3.4 for three different temperatures and at various magnitudes of shear strain, γ_0 . The values of $h(\gamma_0)$ are quite similar in the whole range of γ_0 and for all temperatures examined, thus demonstrating the invariance of damping in the non-linear regime of the shear relaxation modulus response. This fact implies that, similar to the linear viscoelastic response, the shift factor α_T can be used in the non-linear regime to describe the influence of the temperature on the non-linear shear behaviour of melts. Similar conclusions can be drawn out for the melts from Tsenoglou [9] (see Tables C.1 and C.2 in Appendix C).

Start-Up of Shear Flow

In a simple shear flow, at constant shear rate, $\dot{\gamma}$, suddenly applied at time $t' = 0$, the relative Finger strain tensor and the corresponding deformation history are given by Eq. 3.22, the invariants of the Finger tensor for that particular flow history take the form

$$I_{C^{-1}}(t, t') = II_{C^{-1}}(t, t') = \dot{\gamma}^2(t - t')^2 + 3, \quad (3.49)$$

while the constant volume condition, implies that $III_{C^{-1}}(t, t') = 1$. Wagner’s damping function then takes the form

$$h(\gamma_{t, t'}) = \exp(-n\gamma_{t, t'}) . \quad (3.50)$$

Analytical expressions may be derived for the shear stress growth and primary normal stress coefficient

$$\eta_{12}^+(t, \dot{\gamma}) = \sum_{i=1}^N \frac{G_i \tau_i}{(1 + n\dot{\gamma}\tau_i)^2} \left\{ 1 - [1 - n\dot{\gamma}t(1 + n\dot{\gamma}\tau_i)] \exp \left[-(1 + n\dot{\gamma}\tau_i) \left(\frac{t}{\tau_i} \right) \right] \right\} \quad (3.51)$$

$$\Psi_1(t, \dot{\gamma}) = 2 \sum_{i=1}^N \frac{G_i \tau_i^2}{(1 + n\dot{\gamma}\tau_i)^3} \left\{ 1 - \left[1 + \left(1 + n\dot{\gamma}\tau_i - \frac{n\dot{\gamma}t}{2}(1 + n\dot{\gamma}\tau_i)^2 \right) \left(\frac{t}{\tau_i} \right) \right] \exp \left[-(1 + n\dot{\gamma}\tau_i) \left(\frac{t}{\tau_i} \right) \right] \right\}. \quad (3.52)$$

A steady state shear viscosity, $\bar{\eta}_{12}(\dot{\gamma})$, and a steady state primary normal stress coefficient, $\Psi_1(\dot{\gamma})$ respectively

$$\bar{\eta}_{12}(\dot{\gamma}) = \sum_{i=1}^N \frac{G_i \tau_i}{(1 + n\dot{\gamma}\tau_i)^2} \quad (3.53)$$

$$\Psi_1(\dot{\gamma}) = 2 \sum_{i=1}^N \frac{G_i \tau_i^2}{(1 + n\dot{\gamma}\tau_i)^3} \quad (3.54)$$

are obtained for $(1 + n\dot{\gamma}\tau_i)(t/\tau_i) \gg 1$. At small shear rates this is only true for $t \gg \tau_1$, where τ_1 is the longest relaxation time of the memory function, $\mu(t - t')$, whereas at high shear rates even for $t \ll \tau_1$ a steady state is reached if $\dot{\gamma}t \gg 1/n$.

Stress- and normal stress-overshoot are predicted correctly and the predictions for both the shear viscosity and primary normal stress coefficient agree well with experimental data in the whole range of measurements. Discrepancies occur at very small shearing rates, $\dot{\gamma} < 0.1 \text{ s}^{-1}$, for both the shear viscosity and the normal stress coefficient. Additional discrepancies occur at very high shear rates, $\dot{\gamma} > 10 \text{ s}^{-1}$, in the case of primary normal stress coefficient only. Finally, for both the shear viscosity and normal stress coefficient the computed values reach a constant level for $\dot{\gamma} \geq 1 \text{ s}^{-1}$, at long times, whereas no steady state is experimentally achieved.

Start-Up of Extensional Flow

Wagner's initial proposal, in the context of the modified rubber-like liquid model [46, 44] was a single exponential approximation damping function of the form

$$h(\epsilon_{t,t'}) = \exp(-m\epsilon_{t,t'}) \quad (3.55)$$

with $m = 0.30$. According to his analysis on the LDPE "Melt I", this approximation is valid for small strains, $\epsilon < 2$. For larger strains, $\epsilon > 4$ the damping function can be approximated by

$$h(\epsilon_{t,t'}) = \frac{1}{\alpha} \exp(-2\epsilon_{t,t'}) \quad (3.56)$$

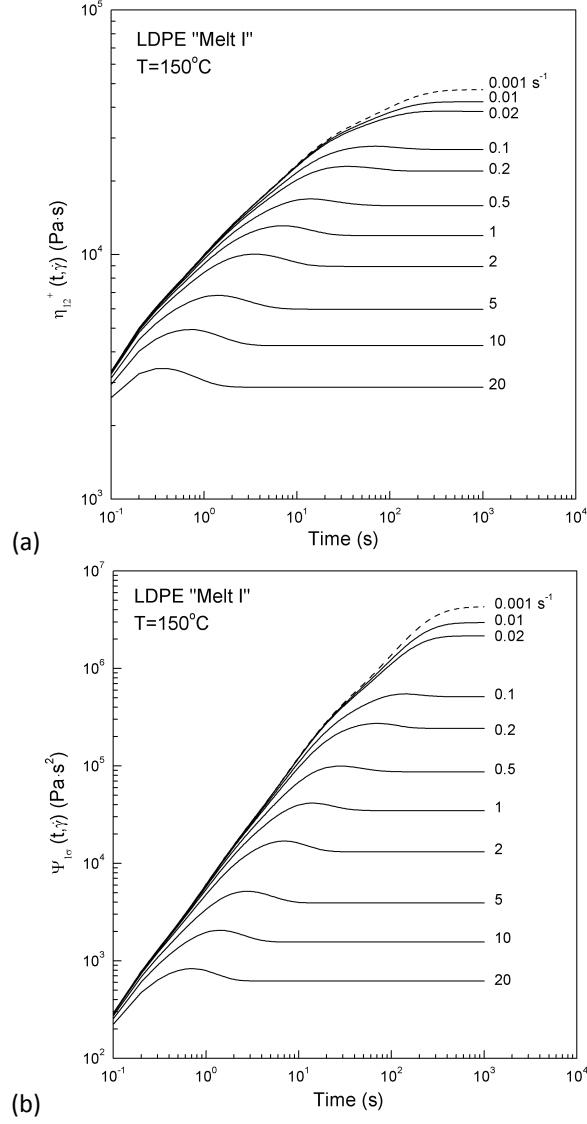


Figure 3.3: Solid lines are the predictions of the Lodge equation with Wagner's damping function using an exponent of $n = 0.14$ for the growth of the (a) shear viscosity, $\eta_{12}^{+}(t, \dot{\gamma})$ and (b) primary normal stress coefficient, $\Psi_1(t, \dot{\gamma})$ as a function of time, t and rate of shearing deformation, $\dot{\gamma}$ at the inception of steady-shearing flow. Dashed lines in both (a) and (b) correspond to the predictions of Lodge's equation in the absence of a damping function.

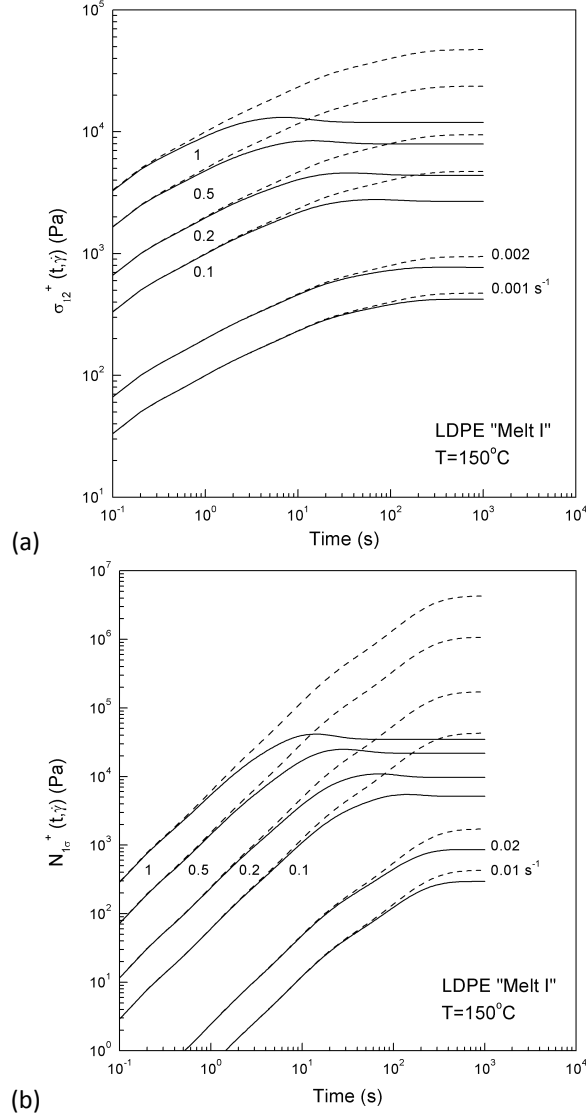


Figure 3.4: Solid lines are the predictions of the Lodge equation with Wagner's damping function using an exponent of $n=0.14$ for the (a) shear stress growth, $\sigma_{12}^+(t, \dot{\gamma})$ and (b) primary normal stress difference, $N_1(t, \dot{\gamma})$ as a function of time, t and rate of shearing deformation, $\dot{\gamma}$ at the inception of steady-shearing flow. Dashed lines in both (a) and (b) correspond to the predictions of Lodge's equation in the absence of a damping function.

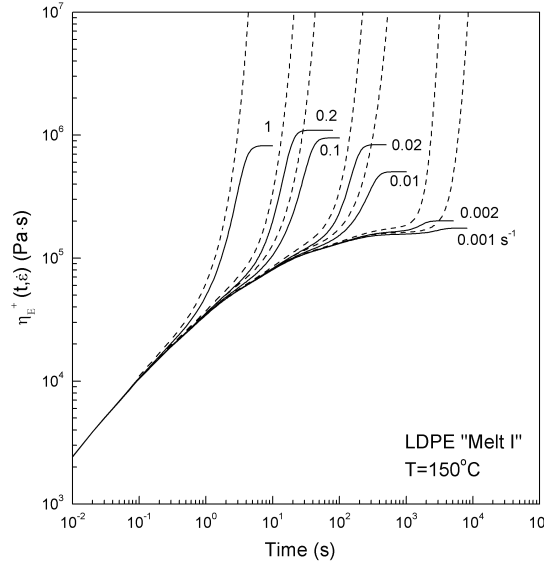


Figure 3.5: Comparison between the predictions derived from Eq. 3.18 for the Lodge rubber-like liquid (dashed lines) and the predictions corresponding to Eq. 3.38 of the modified rubber-like liquid with the damping function of Eq. 3.57 of the elongational viscosity, η_E^+ as a function of time, t and strain rate, $\dot{\epsilon}$ after the start-up of uniaxial extension with constant strain rate, $\dot{\epsilon}$ for the LDPE "Melt I" at the reference temperature of $T=150^\circ\text{C}$ [46, 44].

with $\alpha \approx 0.0025$. A combination of both limiting functions leads to

$$\frac{1}{h(\epsilon_{t,t'})} = \alpha \exp(2\epsilon_{t,t'}) + (1 - \alpha) \exp(m\epsilon_{t,t'}) . \quad (3.57)$$

The Finger strain tensor for that particular deformation history is provided by Eq. 3.26 and the corresponding tensile stress $\sigma(t, \dot{\epsilon}) = \sigma_{11}(t, \dot{\epsilon}) - \sigma_{22}(t, \dot{\epsilon})$ from

$$\sigma(t, \dot{\epsilon}) = h(t) [\exp(2\dot{\epsilon}t) - \exp(-\dot{\epsilon}t)] G(t) + \int_0^t \mu(s) h(s) [\exp(2\dot{\epsilon}s) - \exp(-\dot{\epsilon}s)] ds \quad (3.58)$$

with $s = t - t'$ and $G(t)$, the linear viscoelastic relaxation modulus. In terms of the memory function, $\mu(s)$ the 8 mode relaxation spectrum from Table 3.1 has been used and the resulting integral was solved numerically using a simple trapezoid integration routine.

Nevertheless, because of the difficulty in reaching a steady state in many shear-free flows of polymeric liquids it is not clear whether $\bar{\eta}_E$ exists for all materials and conditions. Examples of unattainability of a steady state include a LDPE melt [46, 70, 28], the commercial LDPE's Lupolen 3020D [25, 26] and Lupolen 1840D [26], the PS.290k and PS.550k polystyrene melts [54] etc. For these melts the characteristic *strain hardening* behaviour is ending at a maximum in η_E^+ , no steady state is observed even at the

lowest applied strain rates and η_E^+ is decreasing at the highest values of strain. The question remains of whether what is often considered as the beginning of the steady state is indeed so or the beginning of the rupture of the sample.

The *Considère criterion* [24] states that homogenous uniaxial elongation of a viscoelastic filament is guaranteed provided the strain is less than that at which a maximum occurs in the force versus extension curve. The value of the strain at which the force reaches a maximum is denoted as ϵ_f and occurs at a relatively early stage of the deformation. Beyond this critical value of the Hencky strain, the Considère criterion states that the material cannot be elongated homogeneously and, instead, it may undergo a *dynamic failure event*. However, even though the material is failing, numerical simulations of filament stretching rheometers show that measurements of the tensile force can still be used beyond the ϵ_f limit to accurately monitor the transient extensional viscosity of the material, under particular considerations [24].

In light of these results, a novel approach in explaining the elongational data of polymeric melts that is based on first principles [39, 9], is proposed and presented in Section 3.5.3.

3.5.2 The PSM Damping Function

Besides exponential functions, sigmoidal functions are another type of analytical expressions that have been used to describe damping functions. Papanastasiou et al. [3] proposed the PSM (Papanastasiou, Scriven, Macosco) damping function with the following form:

$$h(\gamma_0) = \frac{\alpha_p}{\alpha_p + \gamma_0^2}, \quad (3.59)$$

where α_p is a specific parameter, generally found to be smaller for linear polymers than for branched ones. This was demonstrated through the experimental investigation of Kasehagen and Macosko [36] on the rheology of commercial linear and long chain branched Polybutadienes (PB) under single step-strain in shear measurements. Their results are summarised in Table 3.5 and in the values of the parameter, α_p that best fit the results from the step-strain in shear experiments.

The long chain branched PBs were prepared by Kasehagen et al. [37] by blending a commercial long chain branched PB with a linear precursor at different proportions. This procedure resulted in PB melts of varying branching content distributed randomly in each sample [37, 36].

Both the Wagner-I equation and the PSM damping function are considered to be theoretical models of a phenomenological type. Both of these analytical expressions succeed in predicting the rheology of commercial polymer melts under various types of deformation, while no information is provided on the theoretical background for the adjustable parameters that are used to fit the experimental data.

3.5.3 The Power-Law Damping Function

Elongational flow dominates processing technologies such as melt spinning, blow moulding, sheet stretching, tube inflation, vacuum moulding, extrusion coating and foaming.

Table 3.5: Molecular characteristics for the long-chain branched PB blends studied by Kasehagen et al. [37, 36] along with the PSM parameter, α_p that best fits the data from single step-strain in shear experiments.

M_w (kg/mol)	wt(%)	η_0 (Pa · s)	B_n	α_p
137	0	12400	0	3.9
	10	28400	0.11	6.5
	26	65900	0.30	8.0
	39	340000	0.49	14.5

Essential for the success of the above applications is choosing materials with substantial elongational viscosity that shows *strain hardening*, that is, accelerated viscosity growth beyond a characteristic strain, and high *melt strength*. The latter is defined as the maximum force at which a molten thread can be drawn under standard conditions before it breaks. Imparting such properties on the polymer is most effectively accomplished by broadening the molecular weight distribution (MWD) and/or adding long chain branches. Either molecular change is manifested with an increase in the steady-state compliance, J_e^0 [30].

In the context of the temporary network model (Lodge's rubber-like liquid and its modified version), the damping function in both shear and elongational flows, $h(\gamma_{t',t})$ and $h(\epsilon_{t',t})$ respectively, is expressed in terms of the first and second invariant of the relative strain Finger tensor; that is, it describes purely geometrical effects due to the deformation of the material under consideration. More recent theories, such as the *Doi-Edwards Theory*, advance the concept of the temporary network model and its modified version by introducing such microstructural molecular mechanisms that prove to be responsible for the macroscopic rheological behaviour of polymeric fluids under general deformation.

In this modern context the damping function, h , represents the extent of destruction of the temporary polymer network due to loss of chain entanglement density and segmental orientation following a deformation. The strain invariants constitute the objective variables of h because they quantify the average extent of *chain retraction* after a sudden deformation, which is the main reason of entanglement dissolution and loss of segment orientation. This is because $\sqrt{I_{C-1}}/3$ physically signifies the average change in length of a line element in the material, averaged over all possible orientations, $\sqrt{I_{C-1}}/3 = \langle dL'/dL \rangle$. By analogy, $\sqrt{II_{C-1}}/3$ signifies the average area change on all planes in the material, $\sqrt{II_{C-1}}/3 = \langle dA'/dA \rangle$. For monodisperse polymer chains of uncomplicated linear architecture, the Doi-Edwards molecular-theory suggests that h is due only to the survival of polymer segment orientation. Then h is nearly a universal function of the strain invariants I_{C-1} (mainly) and II_{C-1} .

However, material invariance of the damping function fails in the presence of broad molecular weight distribution (MWD) and, most notably, in the presence of long chain branching. This is primarily due to the fact that stress survival after a sudden strain is

now not only due to segmental orientation but also due to some remaining segmental deformation. Therefore, the type and degree of branching as well as the branch length and relative location within the molecule (internal vs. external, i.e., crosslinked on both ends vs. tethered) improve the connectivity of the temporary polymer network, reduce entanglement destructibility upon deformation and, therefore, *smooth* the non-linear viscoelastic character of the fluid.

A form of the damping function, h , has been introduced by Tsenoglou [4, 14] in 2001; it is an attempt to merge the relative degree to which the aforementioned microstructural molecular parameters affect the macroscopic rheological behaviour of polymer melts with the simplicity and practicality of the modified rubber-like liquid constitutive equation (separable time and strain contribution) in a coherent theoretical framework. This *power-law* damping function is applicable to a range of degrees of chain branching and therefore strain hardening and stress-thinning responses. It is expressed as

$$h(\lambda) = \lambda^{-\beta}, \quad (3.60)$$

where $\lambda = \lambda(t', t)$ is the relative or *principal stretch ratio*. This is a function of the present, t and past t' time. $0 \leq \beta \leq 2$ is an adjustable parameter that depends on the *branching number*, B_n (i.e. the weight average number of branches per molecule in the melt). Increasing B_n leads to better network connectivity, improved resistance to strain-induced network destruction and, therefore, to less stress damping and smaller β values. For $\beta = 0$ there is no stress damping and one recovers Lodge's original rubber-like liquid model. On the other hand, for $\beta = 2$, there is complete damping; the elongational viscosity growth curve increases monotonically and reaches a steady state value asymptotically.

Tsenoglou et al. have generalised this theory and modelled the nonlinear viscoelasticity under a general deformation flow. The rate of strain tensor, $\underline{\underline{D}}(t', t)$ for an incompressible fluid in such a flow, is given by

$$\underline{\underline{D}}(t', t) = \begin{pmatrix} \epsilon & 0 & 0 \\ 0 & m_e \epsilon & 0 \\ 0 & 0 & -(1 + m_e) \epsilon \end{pmatrix}, \quad (3.61)$$

where $-0.5 \leq m_e \leq 1$ defines the type of extensional flow. For *uniaxial extension*, $m_e = -0.5$, for *planar extension* (pure shear), $m_e = 0$ and for *biaxial compression*, $m_e = 1$. The relative strain Finger tensor, $\underline{\underline{C}}^{-1}(t', t)$, is then given by

$$\underline{\underline{C}}^{-1}(t', t) = \begin{pmatrix} \lambda^2 & 0 & 0 \\ 0 & \lambda^{2m_e} & 0 \\ 0 & 0 & \lambda^{-2(1+m_e)} \end{pmatrix}, \quad (3.62)$$

where $\lambda = \lambda(t', t)$ is related to the *Hencky strain*, $\epsilon_H = \epsilon(t', t)$ accumulated between times t' and t , through $\lambda(t', t) = \exp \{ \dot{\epsilon}(t - t') \}$. The first and second invariant of the relative strain Finger tensor and for different types of extensional flows assume the following form

$$I_{C^{-1}}(t, t') = \lambda^2 + \lambda^{2m_e} + \lambda^{-2(1+m_e)} \quad (3.63)$$

$$II_{C^{-1}}(t, t') = \lambda^{-2} + \lambda^{-2m_e} + \lambda^{2(1+m_e)} \quad (3.64)$$

Table 3.6: Extracted β exponents for the power-law damping function, $h = \lambda_{m_e}^{-\beta}$, their dependence on extension geometry, m_e and polymer species for the eight polymers examined by Tsenoglou et al. [14].

Sample	M_w (kg/mol)	(M_w/M_n)	Extension geometry, m_e		
			$(m_e=-0.5)$	$(m_e=0)$	$(m_e=1)$
PS.50124	250	1.2	0.96		1.65
PS.606	180	2.5	0.66		1.21
IUPAC A	472	24.9	0.48	0.96	1.15
PS.I	398	2.9	0.80		1.16
LLDPE	158	12.5		1.04	1.17
HDPE.II	152	13	1.30		1.28
HDPE.S	104	5.5	0.85	0.92	0.92
PIB	120	2.2	1.17	1.49	1.33

with eigenvalues equal to the square of the principal stretch ratios. The $(I_{C-1} - II_{C-1})$ difference decreases with m_e and is a measure of the alignment strength of the flow; its relative value is often invoked as the reason of which flows of similar intensity but different geometry generate dissimilar stress response.

Both extension geometry and molecular structure affect the extent of melt strain damping. Deformations of similar magnitude but of different m_e may differ in their ability of network connectivity destruction, either through extinction of molecular associations or loss of segmental orientation. The intensity of strain hardening follows, in general, the order of *uniaxial* > *planar* > *biaxial*, while the extent of strain damping follows the reverse order, *biaxial* > *planar* > *uniaxial*. Tsenoglou et al. [14, 4] suggest the following relation between β and m_e

$$\beta \approx \beta_u \left\{ 2 - \exp \left(-\sqrt{\frac{m_e + 0.5}{0.6}} \right) \right\}, \quad (3.65)$$

where β_u is a parameter that depends on the molecular structure of the corresponding material. In their study, Tsenoglou et al. have investigated the dependence of the viscoelastic nonlinearity exponent, β , on the material character and molecular architecture, in a number of polymeric melts. The results of their investigation are summarised in Table 3.6.

Increased molecular weight polydispersity is assumed to be the cause of the lower β value for PS.606 in comparison to PS.50124. In the case of the two high-density PE's, the HDPE.S melt shows less stress damping than HDPE.II despite its narrower molecular weight polydispersity and it may therefore be suspect for the presence of some long chain branching. Molecular factors improving network connectivity and slowing chain retraction or rendering it incomplete cause β to decrease (e.g., short and, especially, long chain branching, trapped entanglements, gelation, etc.). This explains the low β value for the long-chain branched LDPE IUPAC A, when compared with its linear cousins [14].

The correlation between the parameter β and the degree of branching, B_n has also been subject to systematic experimentation by Gotsis et al. [5, 6]. Their results are summarized in Tables 3.7 - 3.8. as well as in Figs. 3.6, 3.7, 3.8, and in the following expression for the parameter β_u [14, 4]

$$\beta_u \approx 2 \exp \left(-\alpha_u \sqrt[3]{B_n} \right) . \quad (3.66)$$

Gotsis et al. [5, 6] have shown that values of the parameter $\beta_u \geq 1$ correspond to linear polymers, devoid of branching (see Tables 3.7 - 3.8). This general rule also applies in the case of the polymer melts presented in Table 3.6 with few exceptions.

The branched samples from the work of Gotsis et al. [5, 6], were obtained by two methods. Firstly, several linear polypropylene grades were used as precursors and they were modified reactively using peroxydicarbonates (PODIC's). Long chain branched samples were the products of this modification. The precursors used, as well as the modified branched samples obtained through this chemical cross-linking, are summarised in Table 3.7. The cross-linking agent, was a myristyl-peroxydicarbonate (P-26), by Akzo Nobel. Secondly, blends of the commercial linear precursor B, with a commercial branched polypropylene, PF, were prepared and the results for different amounts of PF blended with the linear sample B, are summarised in Table 3.8. The molecular weights and the degrees of branching of the modified samples and the blends, were measured using a triple sensor, high temperature SEC at Akzo Nobel Research, Arnhem, The Netherlands. The theory of Zimm and Stockmayer [8] was used to extract the branching number, B_n , from the intrinsic viscosity of the modified samples and its difference from that of the linear polymer. Further details can be found in the publications by Gotsis et al. [5, 6], in the Diploma thesis of Rob Lagendijk [60] and in the corresponding publication from Lagendijk et al. [61].

The transient extensional viscosity of the melts, was measured at a constant temperature, $T=190^\circ\text{C}$, in an RME rheometer from Rheometric Scientific. The extensional viscosity of the tested PP melts initially shows simple monotonic growth as a function of strain. However, some of the curves show an increase in their slope (as the growth of viscosity accelerates) beyond deformation of around 1.0 s.u.; this is the region of strain hardening and is considered to be a useful feature of polymers subjected in processing operations, such as film blowing, blow molding and thermoforming. The elongational viscosity of the linear PP grades, were essentially non strain hardening. Long chain branches added on these linear precursors during peroxide modification, however, increased temporary network connectivity in the melt and reduced the rate of disentanglement. Thus, the new polymers showed enhanced strain hardening of their viscosities in uniaxial elongational flow. In general, the more branches added on the chains and the longer these branches, the steeper the stress growth at strains above 1.0 s.u. The viscosity growth curve of the highly branched PF melt was also strongly strain hardening.

For the series of peroxydicarbonate modified polypropylenes (PP) tested under uniaxial elongation, with B_n values from 0 to 1, the experiments by Gotsis et al. indicate that $\alpha_u \cong 2.9$. On the other hand, when a B_n variation ($0 \leq B_n \leq 5$) is established by blending under different proportions a commercially branched PP with a linear cousin, $\alpha_u \cong 1.5$. The conclusion is that α_u is not a universal constant but

Table 3.7: Properties of commercial polypropylenes of linear molecular architecture, with initially different molecular weights modified using varying amounts (mmol/100 gr PP) of P-26 (dimyristyl peroxydicarbonate). All rheological measurements except for the melt flow index were carried out at $T=190^{\circ}\text{C}$ [5, 6].

Sample	P-26 (mmol)	M_w (Kg/mol)	(M_w/M_n)	B_n	β	MFI (230/2.16)	SHI
B	0	422	6.2	0	1	2.3	2
	1	575	7.8	0.4	0.3	1.1	8
	2	574	7.6	0.6	0.2	0.6	10.5
	3	581	8.6	0.7	0.1	0.6	28
	5	571	8.9	0.8	0	0.6	-
F93	0	333	5.8	0	1.8	6	1.25
	1	381	7.1	0.2	0.4	3.4	6
	2	413	7.8	0.4	0.25	2.5	15
	3	456	7.9	0.5	0.15	2	16
	5	458	7.7	0.6	0.2	1.8	19
F96	0	314	7	0	0.7	12.2	2
	1	363	8.1	0.1	0.5	8	4.2
	2	389	9.3	0.3	0.3	5.8	6.5
	3	407	9.2	0.5	0.15	4.2	7.5
	5	414	8.6	0.7	0.1	3.1	10

Table 3.8: Molecular data of melts of B/PF blends. The PF grade, is a commercial branched PP. All rheological measurements except for the melt flow index were carried out at $T=190^{\circ}\text{C}$ [5, 6].

PF (%)	M_w (Kg/mol)	(M_w/M_n)	B_n	β	MFI (230/2.16)	SHI
0	422	6.2	0	1	2.3	2
12.5	388	6.3	0.2	0.8	3.2	2.7
25	400	6.4	0.4	0.4	3.0	3
50	485	8	1.7	0.3	2.7	6.4
75	569	7.9	3.3	0.2	3.2	9.6
100	629	9.5	5	0.2	4.6	14.7

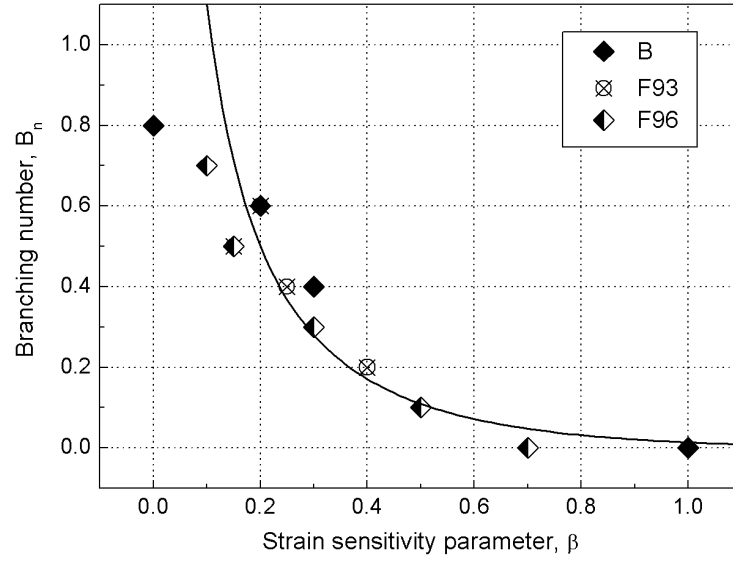


Figure 3.6: Branching number, B_n as a function of the strain sensitivity parameter, β of the power-law damping function (Eqs. 3.65-3.66) for the materials listed in Table 3.7.

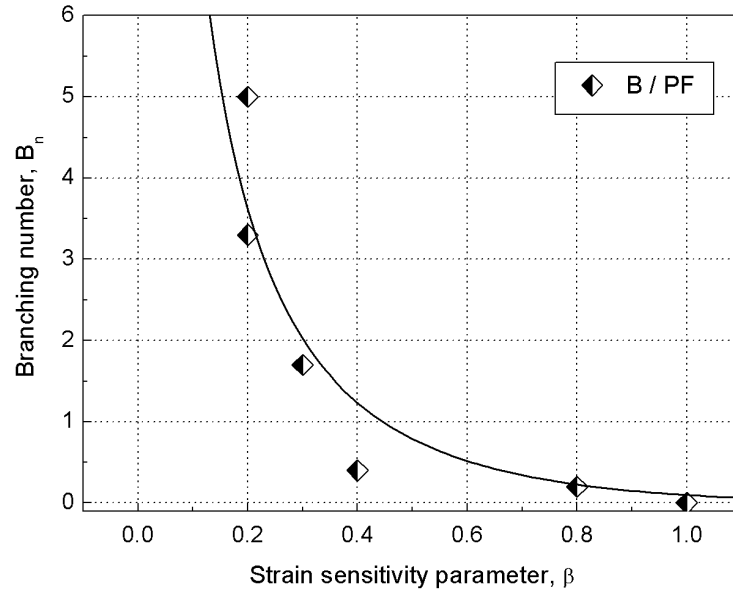


Figure 3.7: Branching number, B_n as a function of the strain sensitivity parameter, β of the power-law damping function (Eqs. 3.65-3.66) for the materials listed in Table 3.8.

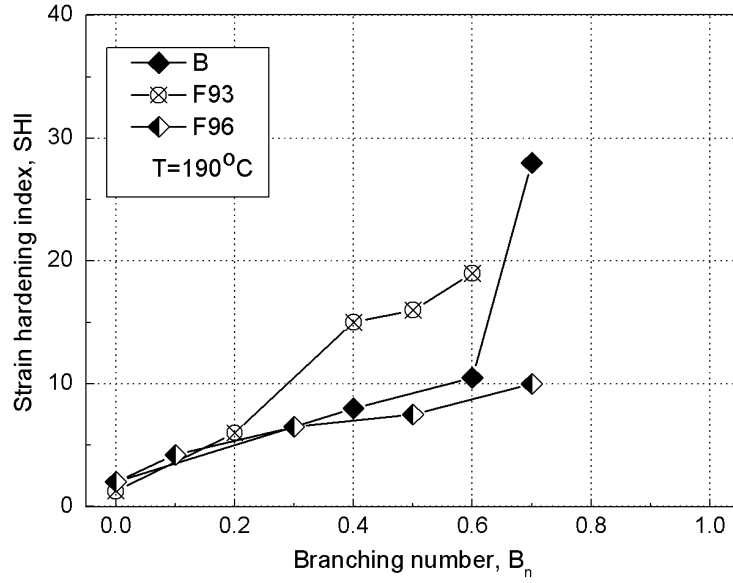


Figure 3.8: The SHI defined by Gotsis et al. [4, 5, 6] plotted against the B_n for several branched PP samples resulting from modifications of three different linear precursors (see Table 3.7) at constant $T=190^\circ\text{C}$.

depends on the MWD breadth and the details of branching. Furthermore, if one could extrapolate the data from Table 3.8, then all melts that have more than 0.8 long chain branches per molecule (in the melt), would be able to fit the original Lodge model without the need of a damping function ($\beta = 0$) and would behave as neo-Hookean solids, even at large deformations.

The *strain hardening index*, SHI of the melts has been introduced by Gotsis et al. [4, 5, 6] as a simple way to characterise the strain hardening of a melt through a comparison of the value of the elongational viscosity at two different strains: one before the point where the upward change of the slope of the viscosity growth curve takes place and one after that point. Gotsis et al. chose the strains of 0.3 and 3.0 and the ratio of the values of the elongational viscosity at these two strains is defined as the strain hardening index (SHI)

$$SHI = \frac{\sigma_E(\epsilon = 3.0)}{\sigma_E(\epsilon = 0.3)}. \quad (3.67)$$

The relation between the SHI and the B_n is shown in Fig. 3.8 for several branched PP samples resulting from modifications of three different linear precursors. Even though the modification results in approximately the same number of branches per chain on the two different precursors, F93 and F96, the effect of these branches on the strain hardening of the melts is different. The samples resulting from precursor F96 show consistently lower values of SHI than the ones resulting from F93 which has

lower molecular weight than F96. Obviously the relation between SHI and B_n is not so simple or absolute. Nor can they be generalised easily to all polymers. The degree of strain hardening of the elongational viscosity as well as various other parameters that can characterise the melt, such as the *melt strength*, MS also depend on the molecular weight and the molecular weight distribution of the modified polymer, the length of the branches, the distribution of these lengths, the tacticity of the branches and the distribution of the branches on the main chains with different lengths.

3.6 Reptative Dynamics for Entangled Polymer Melts

In non-dilute polymer solutions and melts, the polymer coils interpenetrate enough that the molecular motions of one chain are greatly slowed by the interfering effects of other chains. These interferences are attributed to intermolecular *entanglements*. Despite the complications produced by entanglements, melts and concentrated solutions are free of a couple of complications that exist in dilute solutions, namely [57]:

1. In the melt, flexible polymer chains, are *ideal*; that is, their configuration distribution is Gaussian. This is because the *excluded-volume effect* present when the chain is immersed in a small-molecule solvent is *screened* by the surrounding chains.
2. In the melt, experiments show that *hydrodynamic interaction* is also screened out so that the drag on one part of the chain does not influence the drag on a remote part of the same chain. The great complicating feature of melts is that the motion of each chain is affected by entanglements with the surrounding chains.

An illustrative representation of the effect of entanglements on the rheological behaviour of polymeric melts has been published by Onogi et al. [63] who compares the rheological behaviour between nearly monodisperse polystyrene melts of varying molecular weight. The change in the slope of the storage and loss moduli (and consequently the relaxation modulus) with varying molecular weight is characteristic of the effect of an increasing amount of entanglements (proportional to the molecular weight) on the rheological behaviour of polymers in the melt state. The plateau in the storage modulus, $G'(\omega)$ or, equivalently, in the relaxation modulus, $G(t)$ the width of which grows as the molecular weight increases, is the *entanglement plateau modulus*, G_N^0 . The molecular weight at which the plateau first appears corresponds roughly to M_C , the molecular weight at which the zero shear viscosity, η_0 begins to rise $\propto M^{3.4}$. The terminal, or longest relaxation time, τ_1 of these melts increases with molecular weight with the same power law $\propto M^{3.4}$. In the frequency range of the plateau the melt acts like a cross-linked elastic rubber because $G'(\omega)$ is nearly constant. The plateau modulus, G_N^0 , can be related to the *density of entanglements* or the *density of effective crosslinks*, ν by

$$G_N^0 = \frac{4}{5} \nu k_B T. \quad (3.68)$$

From ν and the *bulk density*, ρ of the polymer one can obtain the *molecular weight between entanglements*, M_e , from [35, 58]:

$$M_e = \frac{\rho N_A}{\nu} = \frac{4}{5} \frac{\rho N_A k_B T}{G_N^0}, \quad (3.69)$$

which is only about 0.2 to 0.5 as large as M_C .

On the other hand, if the molecules are rather short ($M < M_C$) they remain unentangled in the melt and the rheological behaviour of such melts is quantitatively and qualitatively much different than what has already been described for entangled melts of high molecular weights [57].

An explanation for the slowdown of relaxation for melts with $M > M_C$ was given by de Gennes. He considered a simpler problem, that of a single long polymer chain in a cross-linked rubber network, but since entangled chains in melts form a random mesh-like structure, the results of this analysis can qualitatively be applied to a chain moving in a mesh of other chains. The motion of an individual macromolecule across such a network structure is anisotropic since lateral displacements are restricted by the surrounding mesh. Large scale configurational rearrangements are therefore assumed to proceed mainly due to snake-like motions of the chain parallel to its own contour, as if the chain was confined in a tube-like cage. De Gennes called this motion, *reptation*. The chain changes its conformation by sliding back and forth along the tube. Those portions of the chain that escape from the ends of the tube are free to take on random orientations and the portions of the tube that are vacated are forgotten; a new conformation diffuses from the end of the chain inward at every instant of the reptation process. The longest relaxation time, $\tau_1 = \tau_d$ is predicted to be $\propto M^3$, not too different from the measured scaling law, where $\tau_1 \propto M^{3.4 \pm 0.1}$.

3.7 The Doi-Edwards Constitutive Equation

A more quantitative description of reptative dynamics for polymers, was put forward by Doi and Edwards in the form of a simple mathematical model. In this model the *contour length*, L , of the chain consisting of N_0 monomers of bond length, b each, is subdivided into N independently directed steps of *equilibrium length*, α_t ,

$$L = N\alpha_t \quad (3.70)$$

Each step consists of N_e mers, ($N_e = N_0/N$) and it is assumed to be long enough to behave as a random coil and to contribute independently to the stress. The magnitude of N is equal to the ratio of the molecular weight of the polymer to that between entanglements, $N = M/M_e$, and N_e is equal to the ratio of the molecular weight between entanglements to that of a monomer ($N_e = M_e/M_0$). Both the primitive path and the chain are assumed to be random walks with coinciding ends, that is,

$$N\alpha_t^2 = N_0 b^2 = \langle \underline{R}^2 \rangle, \quad (3.71)$$

where $\langle \underline{R}^2 \rangle$ is the mean-square end-to-end distance of the macromolecular chain. On application of an instantaneous deformation to the material, it is assumed that

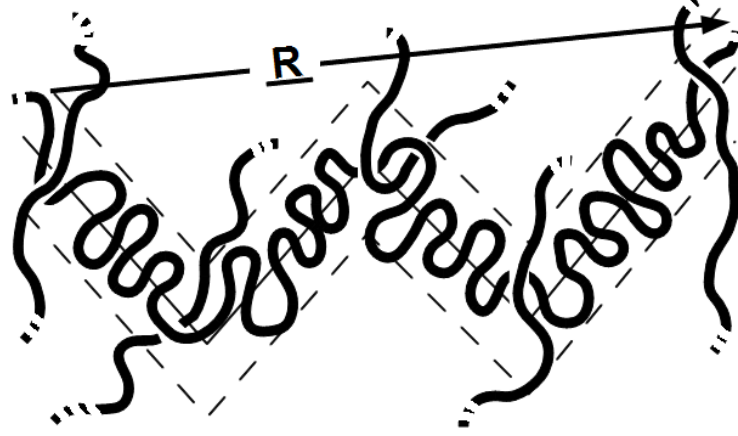


Figure 3.9: A polymer chain, its primitive path (solid line with $N=4$) and its neighbours confining it like in a tube (dashed lines). This illustration is a simplification of the physical picture since in reality more than two constraints are needed to define a primitive step. Redrawn from Tsenoglou [9].

the tube together with the chain changes shape *affinely*, that is, in accord with the macroscopic deformation. Similar behaviour is expected from permanent networks (i.e. crosslinked rubbers, gels, etc.), which means that the components of the extra stress tensor, σ_{ij} , can be obtained from the classical theory of rubber elasticity

$$\sigma_{ij} = 3\nu k_B T N \left\langle \frac{r_i r_j}{(N_e b^2)} \right\rangle, \quad (3.72)$$

which in this particular case reduces to

$$\sigma_{ij}(t=0) = 3\nu k_B T N R_{ij}(\underline{E}), \quad (3.73)$$

with $R_{ij}(\underline{E})$ is a function of the displacement gradient, \underline{E} :

$$R_{ij}(\underline{E}) = \langle (\underline{E} \cdot \underline{u})_i (\underline{E} \cdot \underline{u})_j \rangle \quad (3.74)$$

and \underline{r} is the end-to-end distance of the primitive step with initial step \underline{r}_0 stretched due to \underline{E}

$$\underline{r} = \underline{E} \cdot \underline{r}_0 = \underline{E} \cdot \alpha_t \underline{u}. \quad (3.75)$$

In these expression, the $\langle \dots \rangle$, means an average over all directions of the *unit vector*, \underline{u} , that is,

$$\langle \dots \rangle = \frac{1}{4\pi} \int_0^{2\pi} \int_0^\pi \sin \theta d\theta d\phi, \quad (3.76)$$

where the components of the unit vector, \underline{u} in the spherical coordinate system assume the form

$$\begin{bmatrix} u_1 \\ u_2 \\ u_3 \end{bmatrix} = \begin{bmatrix} \sin \theta \cos \phi \\ \sin \theta \sin \phi \\ \cos \theta \end{bmatrix}. \quad (3.77)$$

In this stage the contour length of the path has increased by a factor $\langle |\underline{E} \cdot \underline{u}| \rangle$. The disturbance to the liquid caused by the deformation relaxes in two major stages:

1. A swift motion of the chain within its distorted tube, until the primitive path of the chain equilibrates to its original length;
2. disengagement of the chain out of its original tube by reptation.

The corresponding times needed for each stage to conclude assume the following relation [39]

$$\tau_e = \frac{\tau_d}{3N}, \quad (3.78)$$

where τ_e is the *time of path equilibration* and τ_d is the *disengagement time*. The expression for the equilibration time corresponds to the *Rouse relaxation time* of the whole chain within its distorted tube, since Rouse dynamics are assumed to apply within the tube. Both these processes contribute to the decay of the initial stress. However, the nonlinear viscoelastic behaviour is explained by the molecular rearrangements taking place during the length equilibration. The lack of permanent cross-links with its neighbors obliges the polymer to snap back along its path reducing the contour length of its path from $L\langle |\underline{E} \cdot \underline{u}| \rangle$ to its equilibrium value, L . The retracting motion of the chain takes place while the surrounding tube remains affinely deformed and stops when the monomer density per unit arc length of the path is restored to its equilibrium value, N_e/α_t . This fact predetermines the size of the surviving steps, N'_e , and consequently their number, N' :

$$\frac{N'_e}{(\alpha_t \langle |\underline{E} \cdot \underline{u}| \rangle)} = \frac{N_e}{\alpha_t} \quad (3.79)$$

$$N' = \frac{N_0}{\langle N'_e \rangle} = \frac{N}{\langle |\underline{E} \cdot \underline{u}| \rangle}. \quad (3.80)$$

The resulting stress at the end of the equilibration period is calculated through Eq. 3.73 with the new values for interentanglement distance and population

$$\sigma_{ij}(t = \tau_e) = 3\nu k_B T N Q_{ij}(\underline{E}), \quad (3.81)$$

where

$$Q_{ij}(\underline{E}) = \frac{1}{\langle |\underline{E} \cdot \underline{u}| \rangle} \left\langle \frac{(\underline{E} \cdot \underline{u})_i (\underline{E} \cdot \underline{u})_j}{|\underline{E} \cdot \underline{u}|} \right\rangle \quad (3.82)$$

is commonly referred to as *Doi-Edwards universal strain tensor*. Over longer times the chain completely disengages itself from the original tube by reptation. At any time, $t > \tau_e$, the fraction of the original tube that remains unvacated is given by

$$P(t) = \sum_{i=1,3,5,\dots} \frac{8}{\pi^2 i^2} \exp\left(\frac{-i^2 t}{\tau_d}\right), \quad (3.83)$$

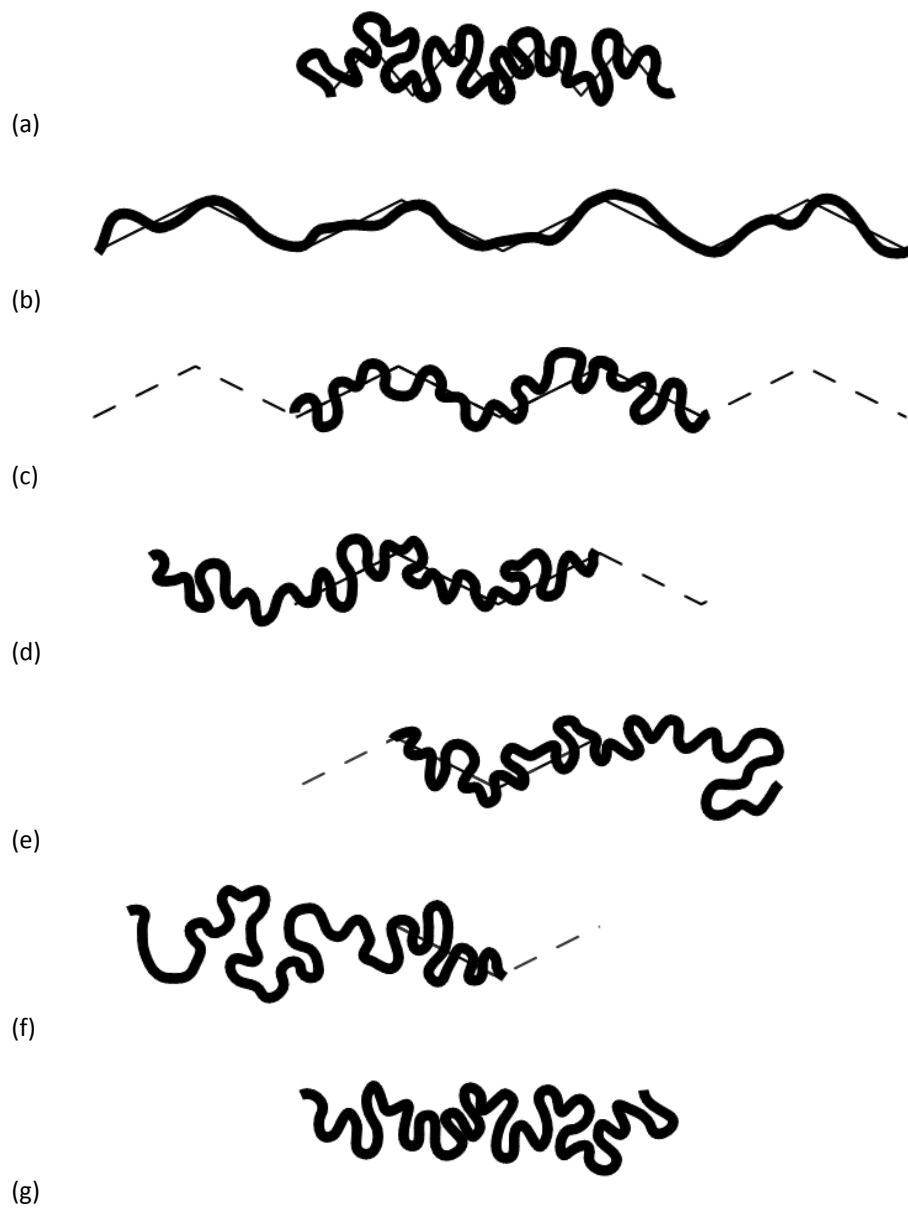


Figure 3.10: Non-equilibrium chain and path dynamics (a) before deformation, (b) after deformation, (c) after equilibration ($t = \tau_e$) with $N/N' = 2$, (d)-(f) path disengagement by reptation ($t > \tau_e$) until (g) equilibration in undistorted configuration. Dashed lines signify abandoned paths. Redrawn from Tsenoglou [9].

which corresponds to diffusion of chains out of their original tubes. The resulting stress can be calculated through

$$\sigma_{ij}(t > \tau_e) = 3\nu k_B T N Q_{ij}(\underline{E}) P(t) . \quad (3.84)$$

Therefore, the separability of the memory function into pure time and strain components finds a rational justification. The equation for stress relaxation is valid for any deformation geometry by introducing the appropriate deformation gradient tensor, \underline{E} . In a step-in shear strain experiment a factor of 15/4 is introduced in order to achieve the correct linear viscoelastic limit and a strain measure is then defined as

$$\mathfrak{S}_{DE} = \frac{15}{4} Q_{12}(\gamma_0) \quad (3.85)$$

giving the corrected expression for the relaxing stress

$$\sigma_{12}(t > \tau_e) = N G_N^0 P(t) \mathfrak{S}_{DE} \quad (3.86)$$

in which G_N^0 is the plateau modulus defined in Eq. 3.68. The strain measure, \mathfrak{S} is called the second-order orientation tensor after Larson [74]. The expression for chain diffusion, $P(t)$ (see Eq. 3.83) of the Doi-Edwards model may be translated to a multimode relaxation spectrum analogous to the classical Maxwell model through

$$G(t) = \sum_{i=1,3,5,\dots} G_i \exp\left(\frac{-t}{\tau_i}\right) , \quad (3.87)$$

where $G_i = (8G_N^0)/(\pi^2 i^2)$ and $\tau_i = (\tau_d)/(i^2)$. The storage and loss moduli are obtained through a Fourier transform integral of the linear relaxation modulus, $G(t)$ and are given by Eqs. 3.21. The damping function in step-shear stress relaxation experiments is expressed by the ratio of the strain measure, \mathfrak{S}_{DE} over the magnitude of shear strain, γ_0

$$h_{DE}(\gamma_0) = \frac{\mathfrak{S}_{DE}}{\gamma_0} = \frac{15}{4} \frac{Q_{12}(\gamma_0)}{\gamma_0} . \quad (3.88)$$

Primary and secondary normal stress differences can be calculated through

$$N_1(t, \gamma_0) = \frac{Q_{11}(\gamma_0) - Q_{22}(\gamma_0)}{Q_{12}(\gamma_0)} \sigma_{12}(t, \gamma_0) \quad (3.89)$$

$$N_2(t, \gamma_0) = \frac{Q_{22}(\gamma_0) - Q_{33}(\gamma_0)}{Q_{12}(\gamma_0)} \sigma_{12}(t, \gamma_0) . \quad (3.90)$$

3.7.1 The Independent Alignment Approximation (IAA)

In the original Doi-Edwards theory, the tube prevents lateral motion of the macromolecular chain but it does not stop the molecule from retracting along its tube contour. Since retraction does not violate the tube constraints it occurs quickly compared to reptation. The idea behind retraction is that it moves a strand from one part of

the tube to another hence the strand's orientation is determined not by the orientation of the tube it originally occupied, but by the orientation of the part of the tube into which it moves. In order to simplify the problem Doi and Edwards invoked the *Independent Alignment Approximation* which assumes that after retraction and before reptation occurs each strand is oriented independently of the others, that is, the chain contracts preserving the initial orientation as if there were no constraints due to entanglements. In this simplified context, the corresponding Doi-Edwards universal strain tensor assumes the following form

$$Q_{ij}(\underline{E}) = \frac{1}{\langle |\underline{E} \cdot \underline{u}| \rangle} \left\langle \frac{(\underline{E} \cdot \underline{u})_i (\underline{E} \cdot \underline{u})_j}{|\underline{E} \cdot \underline{u}|} \right\rangle \approx \left\langle \frac{(\underline{E} \cdot \underline{u})_i (\underline{E} \cdot \underline{u})_j}{|\underline{E} \cdot \underline{u}|^2} \right\rangle. \quad (3.91)$$

Similar to the exact expression for the orientation tensor in step-strain shear relaxation experiments, a correction factor is introduced as well, in order to achieve the correct linear viscoelastic limit. The corresponding strain measure is defined, then, as

$$\mathfrak{S}_{DE}^{IAA} = 5Q_{12}(\gamma_0). \quad (3.92)$$

The relaxing stress assumes the form

$$\sigma_{12}(t > \tau_e) = NG_N^0 P(t) \mathfrak{S}_{DE}^{IAA}, \quad (3.93)$$

where the plateau modulus, $G_N^0 = (3/5)\nu k_B T$, deviates from the exact expression by a factor of $1/5$. The associated damping function is defined as

$$h_{DE}^{IAA}(\gamma_0) = \frac{\mathfrak{S}_{DE}^{IAA}}{\gamma_0} = \frac{5Q_{12}(\gamma_0)}{\gamma_0}. \quad (3.94)$$

For uniaxial and biaxial step-strain deformations analytical expressions have been obtained by Urakawa et al. [50] both for the rigorous and the IAA versions of the theory. Yet another useful approximation for the damping function in step-strain in shear deformation has been published in the form

$$h_{DE}^{approx}(\gamma_0) \approx \frac{1}{1 + \frac{4}{15}\gamma_0^2}, \quad (3.95)$$

which seems to be helpful during calculations.

3.7.2 The History Integral

So far, the Doi-Edwards theory has been formulated mathematically for step-strain deformations, that is, rapid strains followed by stress relaxation. In this context the deformation is rapid and, thus, occurs before reptation. However, if the strain is imposed gradually, which is the usual case of inception of steady shear flow (or any other deformation such as uniaxial and biaxial extension), then reptation occurs during the deformation. Then the stress, is given by a *history integral*, analogous to the Lodge equation. This history integral is the *Doi-Edwards constitutive equation*

$$\underline{\underline{\sigma}} = \int_{-\infty}^t \mu(t-t') \underline{\underline{\mathfrak{S}}}_{DE}(t, t') dt' \quad (3.96)$$

in the case of the rigorous approach or

$$\underline{\underline{\sigma}} = \int_{-\infty}^t \mu(t-t') \underline{\underline{\mathfrak{S}}}_{DE}^{IAA}(t, t') dt' \quad (3.97)$$

if the IA approximation is invoked.

3.7.3 Predictions of Reptation Theories

At high shear rates the uniaxial extensional and shear viscosity scale as $\eta_E \propto \dot{\epsilon}^{-1}$ and $\eta_{12} \propto \dot{\gamma}^{-1.5}$ respectively. The first and second normal stress difference coefficients at high shear rates scale as $\Psi_1 \propto \dot{\gamma}^{-2}$ and $\Psi_2 \propto \dot{\gamma}^{-2.5}$ respectively. With increasing shear rate the shear stress, $\eta_{12}\dot{\gamma}$ is predicted to pass through a maximum and then decrease with further increase in $\dot{\gamma}$. Experimentally it has been reported that $\eta_{12} \propto \dot{\gamma}^{-0.82}$ and $\Psi_1 \propto \dot{\gamma}^{-1.5}$ at large $\dot{\gamma}$ [57].

The ratio between the two normal stress difference coefficients is predicted by the theory to be $\Psi_2/\Psi_1 = -0.286$ at low shear rates. This changes to $\Psi_2/\Psi_1 = -0.143$ when the IAA is dropped. The ratio is predicted to decrease towards zero as the shear rate increases. In melts of molecular weight low enough that the molecules are unentangled, both experiments and molecular dynamics simulations predict $-\Psi_2/\Psi_1 = 0.15 - 0.45$ at low shear rates [57].

further, an overshoot is predicted in the curve of the shear stress as a function of time after inception of steady shearing flow but no overshoot in the first normal stress difference. For monodisperse melts the shear stress maximum is predicted to occur at a shear strain $\dot{\gamma}t = \gamma_p \approx 2$ roughly independent of the shear rate. For low strain rates the experimental maximum is $\gamma_p \approx 2$, whereas for high strain rates it shifts to higher strains. Experiments show an overshoot in the first normal stress difference at $\gamma_p \approx 5$ for low shear rates [57].

Finally, it has been suggested that disagreements between the predictions of the Doi-Edwards theory and the experimental results may be resolved by incorporating into the theory microstructural mechanisms such as *convective constraint release* and *tube stretching*.

3.7.4 The Effect of Polydispersity on the Rheology of Entangled Melts

Most polymeric fluids that are of commercial importance are highly polydisperse (values of M_w/M_n of 2 or more); and some, such as LDPE, have long chain branching. It is important for many applications that these effects be accounted for in the constitutive equation. A simple way to account for continuous molecular weight distributions has been proposed by Tsenoglou [11, 10], des Cloizeaux [17, 18] and Tuminello [75], using a semiempirical scheme called *double reptation*. The double-reptation scheme allows accurate prediction of G' and G'' from a specified molecular weight distribution [67, 68]. The formula for a blend containing a continuous weight distribution, $W(M)$ of components is

$$\left(\frac{G_{blend}(t)}{G_N^0} \right)^{1/2} = \int_0^\infty W(M) F^{1/2}(t, M) dM, \quad (3.98)$$

where $F(t, M)$ is the relaxation function, $G(t)/G_N^0$, of a monodisperse melt with molecular weight, M and G_N^0 is the plateau modulus. The double-reptation scheme can also be applied in reverse to infer a molecular weight distribution from measurements of the linear modulus. Since the rheology of a melt is often easier to measure than its molecular weight distribution, this method of estimating molecular weight distributions from rheological data is a very useful tool.

3.7.5 The Effect of Long-Chain Branching on the Rheology of Entangled Melts

The Doi-Edwards theory attributes the nonlinearity of the stress in flexible polymers to the equilibration stage of the chain response to a sudden strain; that is, the stage when the deformed molecule restores the monomer density along its primitive path to an equilibrium value. The milder nonlinear viscoelastic behaviour observed in polymers with complex branching (see Fig. 3.17) is attributed to their molecular structure which, on a local scale, is reminiscent of a crosslinked network [9].

A polymeric liquid composed of linear chains of arc length, L , whose primitive path is formed by N steps of N_e mers each, equilibrates after the sudden imposition of a strain which stretched it $\langle |\underline{E} \cdot \underline{u}| \rangle$ times. In this system equilibration is achieved through a spontaneous unstretching motion of the free chain until its arc length returns to its initial value, L . Since the surroundings remain affinely deformed, the segmental components of the surviving path are fewer in number but larger in size,

$$\frac{(N'_{e1})_k}{(\alpha_t |\underline{E} \cdot \underline{u}|)_k} = \frac{N_e}{\alpha_t} \quad (3.99)$$

$$N'_1 = \frac{N_0}{\langle N'_e \rangle} = \frac{N}{\langle |\underline{E} \cdot \underline{u}| \rangle}, \quad (3.100)$$

where primes identify post-equilibration values, the number 1 as a subscript signifies steps on chains with at least one free end and 2 steps with both ends linked to branched points; $k = 1, 2 \dots N'_1$.

On the other hand, in the case of elastomers under strain, permanent crosslinks at the ends of the chains prevent unstretching and the monomer density per arc length remains low, as long as the strain persists. Equilibration is achieved by a modest chain rearrangement, without causing any step loss,

$$\frac{(N'_{e2})_k}{(\alpha_t |\underline{E} \cdot \underline{u}|)_k} = \frac{N_e}{\alpha_t \langle |\underline{E} \cdot \underline{u}| \rangle} \quad (3.101)$$

$$N'_2 = \frac{N_0}{\langle N'_e \rangle} = \frac{N}{\langle |\underline{E} \cdot \underline{u}| \rangle}, \quad (3.102)$$

where $k = 1, 2 \dots N'_2$.

In systems composed of branched polymers, the size of segments between successive interchain entanglements remains the same as in systems of free, linear chains of the same chemical structure and concentration. However, part of these segments

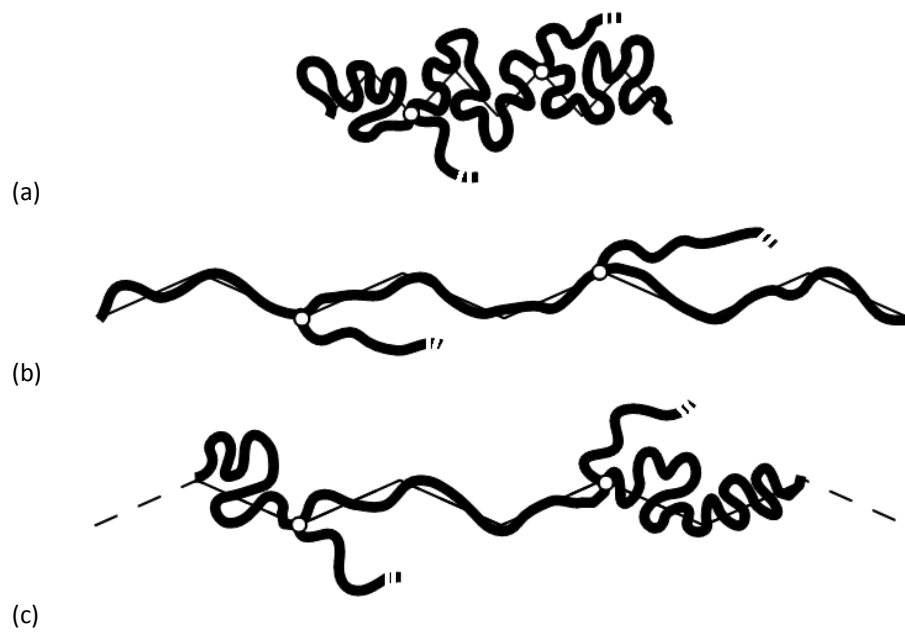


Figure 3.11: Chain and path dynamics during the length equilibration stage of a branched polymer (a) at rest, (b) just after deformation and (c) just after equilibration. Redrawn from Tsenoglou [9].

are now defined by permanent branching points instead of temporary entanglements alone. This introduces an elastomeric character to the network. External branches dangling in the periphery of randomly branched polymers equilibrate like free chains, while internal branches rearrange like elastomeric strands. The ratio between segmental populations equilibrating with both mechanisms can be approximated as a constant, independent of the intensity of the deformation but directly associated with the ratio between the number of internal and external branches in the molecule. Based on these assumptions, the average post-equilibration interentanglement distance in a system composed of randomly branched polymers, with a fraction x_n of their chain length belonging to internal branches is

$$\langle N'_e \rangle = (1 - x_n)N'_{e1} + x_n N'_{e2} = N_e [x_n + (1 - x_n) \langle |\underline{E} \cdot \underline{u}| \rangle] . \quad (3.103)$$

This weighted averaging implicitly accommodates the case of the *collapse of the network structure* for sufficiently large strains and properly bounds the stress responses of the liquid to finite values. The individual steps rearrange during deformation so that the more they point in the direction of the maximum macroscopic elongation, the bigger they are,

$$(N'_e)_k = \frac{\langle N'_e | \underline{E} \cdot \underline{u} |_k}{\langle |\underline{E} \cdot \underline{u}| \rangle} , \quad (3.104)$$

where $k = 1, 2 \dots N'$. Since the number of monomers per chain, N_0 , does not change, the number of surviving steps can also be calculated

$$N' = \frac{N_0}{\langle N'_e \rangle} = \frac{N}{[x_n + (1 - x_n) \langle |\underline{E} \cdot \underline{u}| \rangle]} . \quad (3.105)$$

The strain dependence of the stress response can now be estimated using Eq. 3.73 and the new values of the interentanglement distance and population

$$\sigma_{ij}(t > \tau_e) = 3\nu k_B T N \frac{Q_{ij}(\underline{E})}{[(1 - x_n) + \frac{x_n}{\langle |\underline{E} \cdot \underline{u}| \rangle}]^2} P(t) , \quad (3.106)$$

where $P(t)$ is the time dependent part of the stress decay. In this case it is controlled by *constraint releasing* and *path fluctuating* relaxation mechanisms [77]. For the particular case of a step in shear deformation, the strain dependent part of the relaxation modulus takes the form

$$h_{DE}(\gamma_0) = \left(\frac{15}{4} \frac{Q_{12}(\gamma_0)}{\gamma_0} \right) \left(\frac{1}{[(1 - x_n) + \frac{x_n}{\langle |\underline{E} \cdot \underline{u}| \rangle}]^2} \right) \quad (3.107)$$

The physical significance of this result is that, for branched polymers, surviving chain stretching, in addition to preservation of distorted orientations, contributes to the stress formation. Furthermore the stress is now dependent on the material microstructure, through the non-linear viscoelastic parameter, x_n , since for tree-like molecules, although not affected by the molecular size or degree of branching, x_n

Table 3.9: Physical properties of the branched LDPEs used in step-strain shear relaxation experiments. The molecular weights, polydispersity indices and experimental temperatures for these samples are listed in Table 3.3. Data from Tsenoglou [9].

Sample	M_b (kg/mol)	λ_b (10^4)	g_s	B_n	x_n	η_0 (150°C) $10^3(\text{Pa} \cdot \text{s})$
LDPE.A2	2.83	1.77	0.117	80	0.76	234.4
LDPE.A4	2.35	2.40	0.136	73	0.83	19.95
LDPE.A7	1.92	2.61	0.128	70	0.77	7.24
LDPE.B2	4.17	1.20	0.296	17	0.74	69.2
LDPE.C2	3.68	0.78	0.427	5.4	0.75	19.06
LDPE IUPAC A	4.85	1.03	0.261	24	0.65	478.6

should change with the branch point *functionality*, f , which alters the ratio between the internal and the external branches through

$$x_n \approx \frac{1}{f-1} . \quad (3.108)$$

This is the case for ideally structured tree-like macromolecules; in real systems structural imperfections and the presence of free chains decrease the elastomeric character of the network and consequently the value of the non-linear viscoelastic parameter, x_n , while persistent entanglements resisting disengagement during equilibration increase its value. The x_n values that best fit the experimental data are presented in Table 3.9. A graphical representation of these results is provided in Figs. 3.12 and 3.13. As expected for materials of the same chemical structure and composition these parameters are roughly equal in magnitude, $x_n \approx 3/4$. This value is larger than $1/2$ which is predicted by Eq. 3.108 for 3-functional branching. The conclusion based on the experimental evidence, thus, is that increasing the external branches as opposed to internal ones seems to accentuate the nonlinear strain dependence bringing it closer to the DE predictions.

The rest of the physical parameters listed in Table 3.9, as well as those listed in Table 3.3, were inferred from experimental characterisation of the samples through a combination of *Gel Permeation Chromatography*, (*GPC*), along with *intrinsic viscosity* measurements [9]. The *molecular size ratio*, g_s , was used along with Eq. 2.15 to evaluate the branching content of the samples. The rest of the physical parameters of Table 3.9 were evaluated using analytical expressions listed in Section 2.1.4.

3.7.6 The Effect of Strain-Induced Crystallisation on the Rheology of Entangled Melts

Representative examples of a series of step-strain shear relaxation measurements on commercial polyethylenes are reproduced from the work of Tsenoglou [9]. Extensive details on the experimental procedure are also provided in that work. Physical properties of the materials are given in Table 3.10.

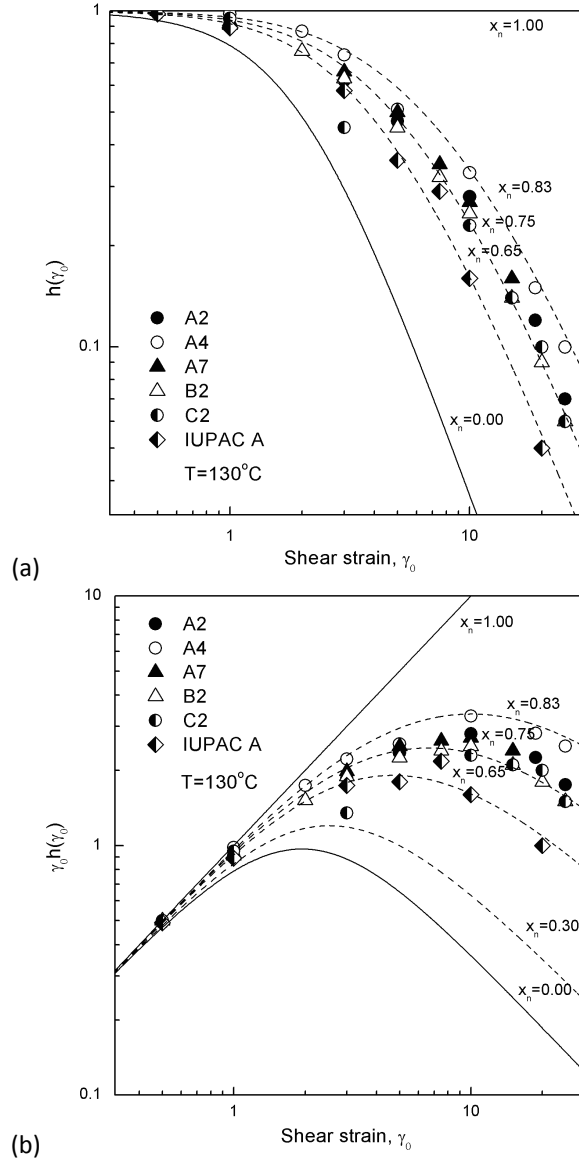


Figure 3.12: Dependence of (a) the strain component of the relaxation function (eq. 3.107) and (b) the strain component of the stress (eq. 3.106) on the shear deformation for the branched LDPEs listed in Table 3.9. Solid lines with $x_n = 0$ correspond to the DE theory while for $x_n = 1$ there is no damping. Replotted from Tsenoglou [9].

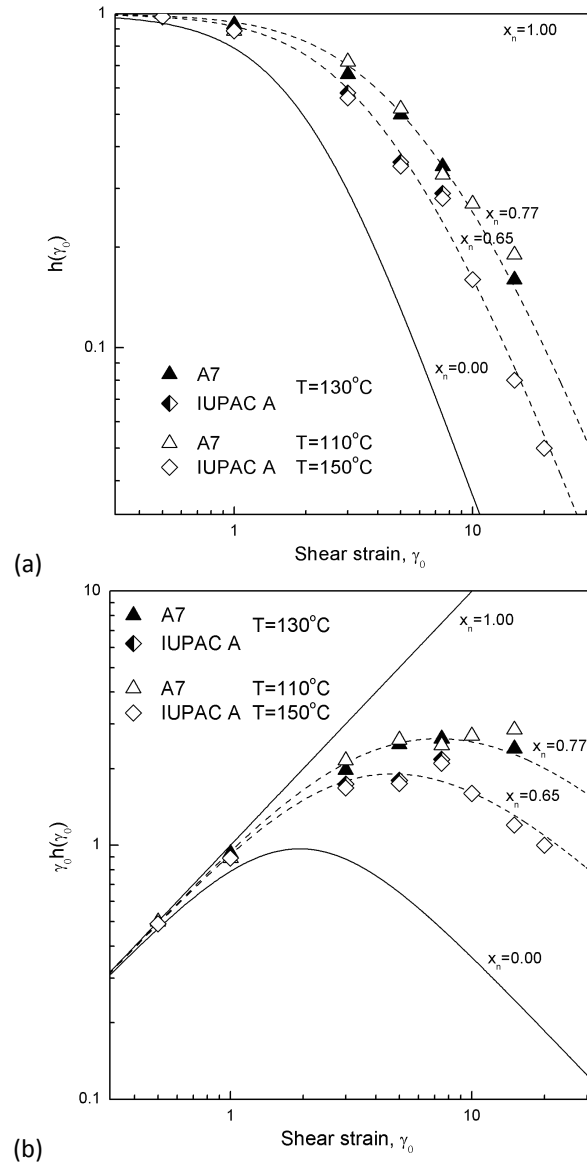


Figure 3.13: Same as Fig. 3.12 but for the branched LDPEs A7 and IUPAC A, demonstrating the temperature invariance of the damping function. Data from Tsenoglou [9].

Table 3.10: Physical properties of three commercial HDPE's and a Linear LDPE used in step-strain shear relaxation experiments. The Melt Flow Index (MFI), provided for the HDPE's, is an inverse measure of their average molecular weight. Data from Tsenoglou [9].

Sample	M_w (Kg/mol)	(M_w/M_n)	MFI (190/2.16)	Density, ρ (25°C) (gr/cm ³)	$T(^{\circ}\text{C})$
HDPE.A	181	13.7	0.03	0.952	140,150,170
HDPE.B	118	6.1	0.25	0.955	140,150
HDPE.C	113	11.2	0.80	0.964	140
LLDPE			0.15	0.920	150

The strain-time superposition assumption has been verified for these polyethylenes. The non-linear strain dependence of the stress (proportional to $\gamma h(\gamma)$ from eq. 3.86 and 3.88) for the HDPEs is illustrated in Figs. 3.14, 3.15, 3.16 and 3.17. Initially, the viscoelastic nonlinearity closely follows the Doi-Edwards theory predictions, i.e. the curve with $x_n = 0$ (eq. 3.107). Then, at around $\gamma_0 = 1.5$, the stress becomes strain insensitive, as if it hesitates to follow the simple Doi-Edwards curve ($x_n = 0$) or a rubber-like curve (no damping, or $x_n = 1$). For flows at lower temperatures the stress starts increasing again at higher strains. This particular behaviour is expected for polymers that show strain induced crystallisation [51, 2]. At higher temperatures the deviation from the lower curve is less, as strain induced crystallisation occurs later, if at all.

The strain induced crystallisation contributes to an improvement of the connectivity of the network since newly formed nuclei act as additional chain junctions. This network strengthening mechanism competes with the disentanglement process during the length equilibration in the tube and includes in some persistent segmental stretching and orientation. As a result, the value of x_n of the polymer increases. At larger strains and lower temperatures, the crystal nuclei acting as additional chain junctions are now created at a rate which overcompensates the loss of entanglements due to chain equilibration, resulting in a net strengthening of the network formation and a recurrent rubber-like behaviour without damping.

The effect of varying the average molecular weight for the HDPEs examined is illustrated in Fig. 3.16. Under moderate deformations the two polymers with the highest melt index (MFI) (i.e. HDPE.B and HDPE.C) and, therefore, the lowest average molecular size show an identical strain dependence and a slightly milder nonlinearity than HDPE.A. On the other hand, under larger strains, a recurrence of the rubber-like behaviour is stronger for the samples with the lowest MFI (i.e. HDPE.A and HDPE.B); this means that the extent of the shear induced crystallisation is larger in systems with higher molecular weight.

The comparison of linear and branched chains is presented in Fig. 3.17. The figure shows the HDPE.C as above (linear chain), a LLDPE (short branches) and the LDPE.B (extensive long chain branching). The linear low density material has a molecular architecture which is an intermediate between the other two polymers. It can be easily seen in Fig. 3.17 that the long chain branched polymer follows eq. 3.107 with $x_n = 0.8$ for all

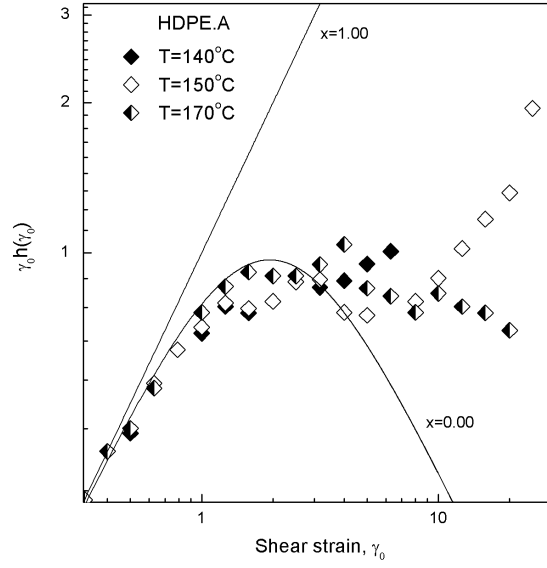


Figure 3.14: Dependence of the strain component of the stress, $\gamma_0 h(\gamma_0)$, on the shear deformation for HDPE.A at several isothermal conditions. The line with $x_n = 0$ is the simple DE prediction while for $x_n = 1$ there is no damping. Replotted from Tsenoglou [9].

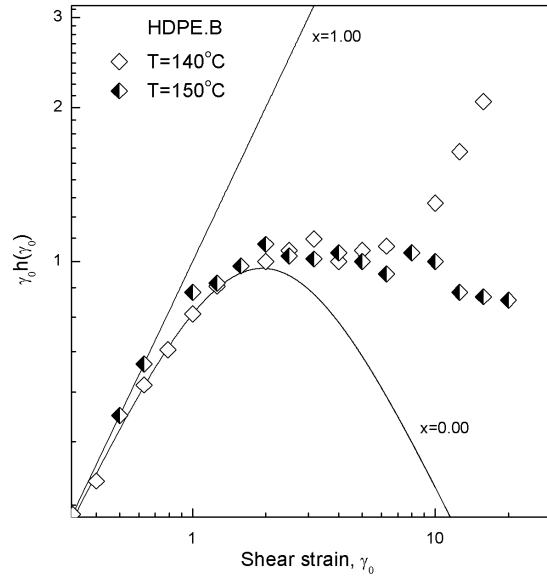


Figure 3.15: Dependence of the strain component of the stress, $\gamma_0 h(\gamma_0)$, on the shear deformation for HDPE.B at several isothermal conditions. Replotted from Tsenoglou [9].

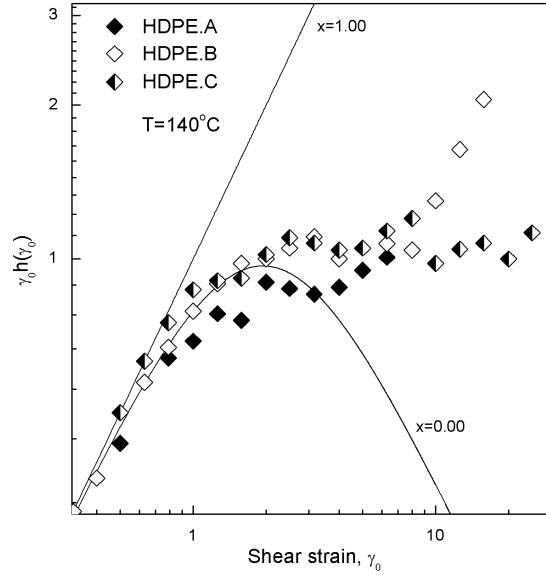


Figure 3.16: Dependence of the strain component of the stress, $\gamma_0 h(\gamma_0)$, on the shear deformation for the three HDPE's examined at $T=140^\circ\text{C}$. Replotted from Tsenoglou [9].

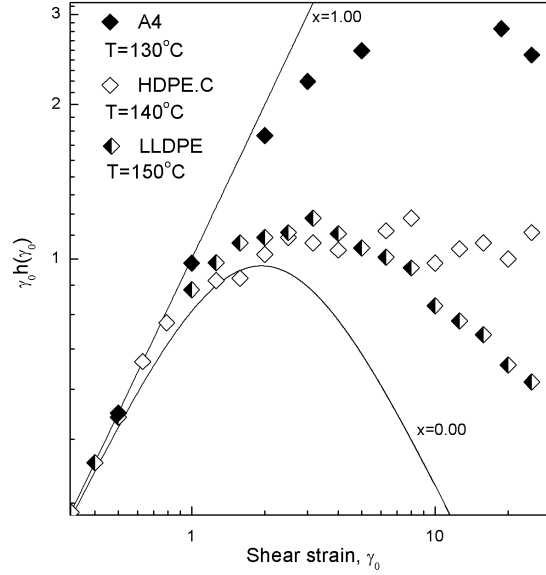


Figure 3.17: Dependence of the strain component of the stress, $\gamma_0 h(\gamma_0)$, on the shear deformation for the branched LDPE.B, the HDPE.C and the linear LDPE at the corresponding isothermal conditions. Replotted from Tsenoglou [9].

strains. The linear polymer with the short chains also follows eq. 3.107 with $x_n = 0.2$ for all strains. The linear HDPE shows the behaviour described above. Therefore, it seems that only linear chains can undergo strain induced crystallisation in shear flow under these conditions. This happens at high strains and depends on the temperature in the flow. The presence of branches on the main chain makes strain induced crystallisation in shear flow much more difficult.

3.8 Maxwell-Type Differential Constitutive Equations

The concept of linear viscoelasticity can also be written in a differential form

$$\sigma + \tau \frac{d\sigma}{dt} = \eta \dot{\gamma}, \quad (3.109)$$

where $\eta = G_0\tau$. This is known as the *Maxwell model* and it is equivalent to Eq. 3.10. It is often represented as a series combination of *springs* (elastic elements) and *dash-pots* (viscous elements). Most of, if not all of the constitutive equations that exist in differential form have their basis on the Maxwell model.

3.8.1 The Upper-Convected Maxwell Differential Equation

A simple way to combine time-dependent phenomena and rheological nonlinearity is to incorporate nonlinearity into the Maxwell model. This can be done by replacing the *substantial time derivative* in the model with the *upper-convected time derivative* of $\underline{\underline{\sigma}}$, that is,

$$\underline{\underline{\sigma}} + \tau \frac{\nabla}{\nabla} \underline{\underline{\sigma}} = 2\eta_0 \underline{\underline{D}}, \quad (3.110)$$

where

$$\eta_0 = G_0\tau \quad (3.111)$$

and

$$\frac{\nabla}{\nabla} \underline{\underline{\sigma}} \equiv \frac{\partial}{\partial t} \underline{\underline{\sigma}} + \underline{\underline{v}} \cdot \nabla \underline{\underline{\sigma}} - (\nabla \underline{\underline{v}})^T \cdot \underline{\underline{\sigma}} - \underline{\underline{\sigma}} \cdot \nabla \underline{\underline{v}}. \quad (3.112)$$

The upper-convected time derivative is a time derivative in a special coordinate system whose base coordinate vectors stretch and rotate with material lines. With this definition stresses are produced only when material elements are deformed; mere rotation produces no stress. For small strain amplitudes the nonlinear terms disappear and the upper-convected time derivative reduces to the substantial time derivative. On the other hand, at steady flow steady and small strain rates $\underline{\underline{\sigma}}$ is negligible and Newtonian behaviour is recovered. The upper-convected Maxwell equation is the differential equivalent to the Lodge integral equation and, in an analogous way to the latter, it can be extended to include multiple relaxation modes. The predictions of the UCM equation are the same as those obtained when one uses the integral version.

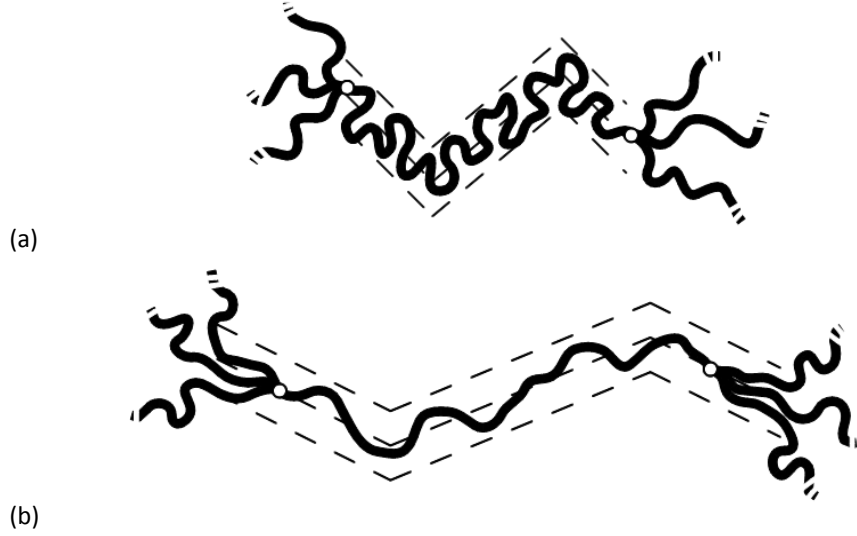


Figure 3.18: The structure of a Pom-Pom polymer with a backbone within its confining tube and $2q_x$ dangling arms, with $q_x=3$ arms attached on each side of the pom-pom. The polymer is depicted in (a) undeformed configuration; and (b) deformed configuration with arm withdrawal into the stretched tube.

3.8.2 The eXtended Pom-Pom Model

The K-BKZ and other integral constitutive equations can be regarded as generalisations of the Lodge integral equation. The UCM equation can also be generalised to obtain more realistic predictions of nonlinear phenomena [15]. A more recent proposal [76] is the *XPP model*, which is based on the molecular background of the original *Pom-Pom model* introduced by McLeish and Larson [72, 47].

The Pom-Pom model uses on the concept shown in Fig. 3.18. The branched polymer is approximated by the molecular structure shown in this figure. The reptation idea of De Gennes and Doi, Edwards are used to find the deformation dynamics of such a molecule constrained in a tube. The viscoelastic stress in the XPP model is given by

$$\underline{\underline{\dot{\sigma}}}_i + \tau(\underline{\underline{\sigma}}_i)^{-1} \underline{\underline{\sigma}}_i = 2G_i \underline{\underline{D}}, \quad (3.113)$$

where

$$\tau(\underline{\underline{\sigma}}_i)^{-1} = \frac{1}{\tau_{0b,i}} \left[\frac{\alpha_{x,i}}{G_i} \underline{\underline{\sigma}}_i + f(\underline{\underline{\sigma}}_i)^{-1} \underline{\underline{I}} + G_i [f(\underline{\underline{\sigma}}_i)^{-1} - 1] \underline{\underline{\sigma}}_i^{-1} \right] \quad (3.114)$$

is the *relaxation time tensor* and

$$\frac{1}{\tau_{0b,i}} f(\underline{\underline{\sigma}}_i)^{-1} = \frac{2 \exp \{ \nu_{x,i} (\Lambda - 1) \}}{\tau_{0s,i}} \left(1 - \frac{1}{\Lambda} \right) + \frac{1}{\tau_{0b,i} \Lambda^2} \left(1 - \frac{\alpha_{x,i} \underline{\underline{I}} \cdot \underline{\underline{\sigma}}_i}{3G_i^2} \right) \quad (3.115)$$

is an *extra function*. Within this set of equations, the basic features of the XPP model are illustrated, that is the *backbone tube stretch*

$$\Lambda = \sqrt{1 + \frac{I_{\underline{\sigma}_i}}{3G_i}} \quad (3.116)$$

defined as the length of the backbone tube divided by its length at equilibrium and the corresponding *backbone stretch relaxation times*

$$\frac{\tau_{s,i}}{\tau_{0s,i}} = \exp \{ -\nu_{x,i}(\Lambda - 1) \} . \quad (3.117)$$

The subscript i indicates the i^{th} relaxation mode. G_i is the corresponding relaxation modulus, $\tau_{0b,i}$ are the sets of *backbone orientation relaxation times* taken as the mode relaxation times in the relaxation spectrum obtained from linear rheology. Also $I_{\underline{\sigma}_i} = \text{tr}(\underline{\sigma}_i)$ and $I_{\underline{\sigma}_i \cdot \underline{\sigma}_i} = \text{tr}(\underline{\sigma}_i \cdot \underline{\sigma}_i)$. The parameter $\nu_{x,i} = 2/q_{x,i}$ is related to the *number of arms*, $q_{x,i}$ attached at the end of a backbone chain. The scalar parameter, $\alpha_{x,i}$ is an *anisotropy parameter*. Finally, the net deviatoric stress is given by $\underline{\underline{\sigma}} = \sum_i \underline{\sigma}_i$.

The physical process that follows the deformation of the pom-pom molecule is based on molecular arguments introduced in the DE theory with the complication of the pom-poms at the end of the backbone chain (Fig. 3.18). The backbone stretch relaxation times, $\tau_{0s,i}$, correspond to the time scale for retraction of the pom-pom molecules following a deformation of given magnitude, that is, the time scale needed for the stretched contour lengths of the pom-poms to contract to their equilibrium length. This is a fast process compared to the backbone orientation relaxation times, $\tau_{0b,i}$, which correspond to the time scale needed for the relaxation of the orientational anisotropy that occurred in the melt after the end of the equilibration period.

Start-Up of Uniaxial Extension

In the case of start-up of steady uniaxial extensional flow the upper-convected time derivative of the stress tensor reduces to

$$\underline{\underline{\dot{\sigma}}} = \begin{pmatrix} \dot{\sigma}_{11} & 0 & 0 \\ 0 & \dot{\sigma}_{22} & 0 \\ 0 & 0 & \dot{\sigma}_{33} \end{pmatrix} - \begin{pmatrix} 2\sigma_{11}\dot{\epsilon} & 0 & 0 \\ 0 & -\sigma_{22}\dot{\epsilon} & 0 \\ 0 & 0 & -\sigma_{33}\dot{\epsilon} \end{pmatrix} , \quad (3.118)$$

while the rate of deformation tensor for this type of flow is

$$2\underline{\underline{D}} = \begin{pmatrix} 2\dot{\epsilon} & 0 & 0 \\ 0 & -\dot{\epsilon} & 0 \\ 0 & 0 & -\dot{\epsilon} \end{pmatrix} \quad (3.119)$$

Substituting the above expressions into the constitutive relation Eq. 3.113 provides a system of three distinct ordinary differential equations of the first order that can be solved numerically in order to provide the values of stress components with respect

to time. The appropriate initial conditions for the system of differential equations is $\sigma_{11} = \sigma_{22} = \sigma_{33} = 0$ at $t = 0$. If a multiple mode relaxation spectrum is used instead, the stresses must be computed for each mode separately and finally added together in order to provide the net deviatoric stress. The uniaxial extensional viscosity is then computed from Eq. 3.29.

3.8.3 The Rolie-Poly Constitutive Equation for Linear Polymer Melts

A simple constitutive equation in differential form, also based on the reptation idea of de Gennes, has been proposed by Likhtman and Graham [7, 62]. Its aim is to describe the rheology observed in monodisperse linear polymeric materials. Its theoretical basis is literally that of the tube model of Doi and Edwards. The main mechanism of stress relaxation in the linear regime is assumed to be reptation. In non-linear flows or large step strain experiments the mechanism of *convective constraint release*, CCR, which was introduced by Marrucci [21], plays an important role in stress relaxation. The Rolie-Poly constitutive equation has the form

$$\frac{\nabla \underline{\underline{\sigma}}_i}{\tau_{d,i}} = -\frac{1}{\tau_{d,i}}(\underline{\underline{\sigma}}_i - \underline{\underline{I}}) - \frac{2(1 - \sqrt{\frac{3}{tr \underline{\underline{\sigma}}_i}})}{\tau_{r,i}} \left\{ \underline{\underline{\sigma}}_i + \beta_{rp} \left(\frac{tr \underline{\underline{\sigma}}_i}{3} \right)^{\delta_{rp}} (\underline{\underline{\sigma}}_i - \underline{\underline{I}}) \right\}, \quad (3.120)$$

where $\tau_{d,i}$ and $\tau_{r,i}$ are the *reptation* and *Rouse relaxation times*, respectively, of the i^{th} relaxation mode; β_{rp} is the CCR coefficient; and δ_{rp} is a fitting parameter. It has to be emphasised that the stretch becomes unbounded in this model, that is, finite extensibility of the chains is not accounted for.

In the case of the start-up of steady uniaxial extensional flow the upper-convected time derivative of the stress tensor reduces to that of Eq. 3.118. The stress tensor is found by solving Eq. 3.120 using this terms. The appropriate initial conditions for the differential equations ($\sigma_{11} = \sigma_{22} = \sigma_{33} = 0$ at $t = 0$) lead to singularities due to the $tr \underline{\underline{\sigma}}_i$ parameter being in the denominator below the square root. This is easily bypassed by setting the initial conditions for the stress components to a very small number. The uniaxial extensional viscosity is then computed from Eq. 3.29.

Chapter 4

Experimental

4.1 Introduction

Rheological measurements were conducted in order to investigate differences between commercial resins of branched and linear architecture, with respect to their physical and mechanical response. Two samples were used, a tubular reactor produced LDPE, consisting of long-chain branched macromolecules, and a linear HDPE-hexene copolymer. Both polymers contained antioxidants and were provided by Eni S.p.A. Their physical properties and molecular characteristics are provided in Table 4.1. The rheological response of these melts was investigated in terms of shearing and extensional flows. Regarding shear flow, *dynamic mechanical analysis (DMA)* and *single step-strain* measurements were conducted, whereas the shear-free flow response was investigated through *uniaxial extensional* deformation.

4.2 Shear Flows

In general, shearing flows are imposed through simple geometries. A review of the basic geometries used to impose shearing flows is given in textbooks, such as the books of Macosko [15], Larson [57], Bird et al. [55] etc. Depending on the geometry used, either *drag* or *pressure flow* is imposed. For the samples used in the experimental section of the current thesis, only drag flows were investigated. The Ares-II[®] rheometer from Rheometric Scientific (TA Instruments) with a resolution of 2 - 2000 mNm was used for all shearing flows and for both samples.

Samples were prepared by compression moulding of polymer pellets between flat steel plates at a temperature not exceeding 180°C. Sample thickness was controlled by using thin flat window frame moulds of uniform gage, sandwiched between the flat steel panels. A thin sheet of PTFE oil was spread over the inner surface of the panels and the moulds in order to facilitate the removal of the solid plastic sample after it had cooled down. The total time of heating did not exceed 5 - 8 min to prevent thermal degradation of the polymer. The maximum pressure applied during heating did not exceed 10 MPa. The cooling procedure at room temperature took less than 20 - 30

min. Finally, circular samples of 25 mm in diameter and thicknesses in the range of 0.5 - 1.0 mm were cut from the solid by means of sharp scissors.

4.2.1 Cone and plate geometry

A *cone and plate* geometry was used for the single step-strain measurements. A single plate diameter of 25.0 mm was used with a cone angle of 0.1 radians. The invariance of the rheological response with respect to different plate diameters and cone angles has been investigated by Tsenoglou and his results were presented in the previous chapter. Besides the small cone angle assumption, *edge effects* were also considered. Extra care was taken in order to clean the excess of liquid around the cone and plate in order to avoid a *drowned edge* and to maintain the *spherical edge surface* assumption throughout the measurements. Thus, in terms of edge effects, the results are assumed to be valid.

Various magnitudes of shear strain in the range of 0.01 - 2.0 s.u. were imposed to the samples and the resulting stress growth and relaxation was recorded with respect to time. The maximum strain imposed was limited by the resolution of the rheometer. Consecutive measurements were conducted with a 2-3 min break between each imposed strain magnitude, in order for the sample to relax and discard remaining stresses and, therefore, to maintain the single step-strain assumption. In terms of the rheological formalism, the shear strain imposed is given by

$$\gamma_0 = \frac{\phi}{\beta_c}, \quad (4.1)$$

where ϕ is the angle of rotation of the plate with respect to the stationary cone, and β_c is the cone angle. The shear stress is then given by

$$\sigma_{12} = \frac{3M_t}{2\pi R_p^3}, \quad (4.2)$$

where M_t is the resulting torque and R_p is the plate radius.

4.2.2 Parallel disk geometry

A *parallel disk* geometry was used for the dynamic mechanical analysis. A disk diameter of 25 mm was used with a gap between plates not exceeding a maximum of 1.0 - 1.5 mm. Extra care was taken in order to avoid the drowned edge effect and maintain the spherical surface assumption at the edge. The linear viscoelastic regime (LVE) was determined by means of a *strain sweep* at a constant rotational frequency of 1.0 rad/s. A fresh sample was used for each isothermal condition in order to prevent the melt from thermal and/or oxidative degradation due to excessive periods of heating.

The results of the strain sweep are provided in Fig. 4.1 for both samples. From these figures the LVE limit for both melts was determined to be ≈ 0.05 - 0.1 s.u. Notice that the difference between the two melts is that at the same rotational frequency the LDPE shows a liquid-like behaviour ($G' < G''$), whereas the HDPE shows a solid-like

Table 4.1: Physical properties and molecular characteristics of the commercial resins investigated. The g'_s value for the LDPE FF20 sample was provided by the supplier. The g_s value is estimated from Eq. 2.12 and the branching content from Eqs. 2.13 or 2.14.

	LDPE Riblene FF20	HDPE Eraclene FA506
MFI (2.16/190) (gr/10 min)	0.8	-
MFI (5/190) (gr/10 min)	-	0.6
MFI (21.6/190) (gr/10 min)	-	15
Density (25°C)(gr/cm ³)	0.921	0.939
Melting Point (°C)	112	129
M_n (kg/mol)	13.4	12.3
M_w (kg/mol)	160.3	196.6
M_z (kg/mol)	841.1	1536.0
M_w/M_n	12.0	16.0
g'_s	0.612	-
g_s	0.612	-
B_n	8.8	-

behaviour ($G' > G''$). The shear rate is determined by

$$\dot{\gamma} = \frac{\omega R_p}{h_p}, \quad (4.3)$$

where R_p is the plate radius, ω is the rotational frequency and h_p is the gap between the parallel plates. Then the resulting shear stress at the edge of the plate is considered homogenous and equal to

$$\sigma_{12} = \frac{M_t}{2\pi R_p^3} \left[3 + \frac{d \ln M_t}{d \ln \dot{\gamma}} \right], \quad (4.4)$$

where M_t is the resulting torque. The simplification of $d \ln M_t / d \ln \dot{\gamma} = 1$ is only valid for Newtonian liquids. The frequencies examined span from 0.1 s^{-1} to 100 s^{-1} and for both samples the isothermal test temperatures were 120°C - 190°C for the LDPE and 150°C - 200°C for the HDPE.

4.3 Extensional Flow

Shear-free flow was examined for both resins through uniaxial extensional measurements. An RME[®] elongational rheometer from Rheometrics with a resolution of 1 - 2000 mN and an accuracy of $\approx 1 \text{ mN}$ was used to conduct the experiments [66, 29]. Samples from both resins were prepared with the same procedure followed for the shearing experiments. The solid plastic was cut into rectangular bars of approximate dimensions $60 \times 10 \times 1.5 \text{ mm}$ ($L \times W \times H$) with a sharp knife. The test conditions were isothermal at 150°C for the LDPE and at 170°C for the HDPE.

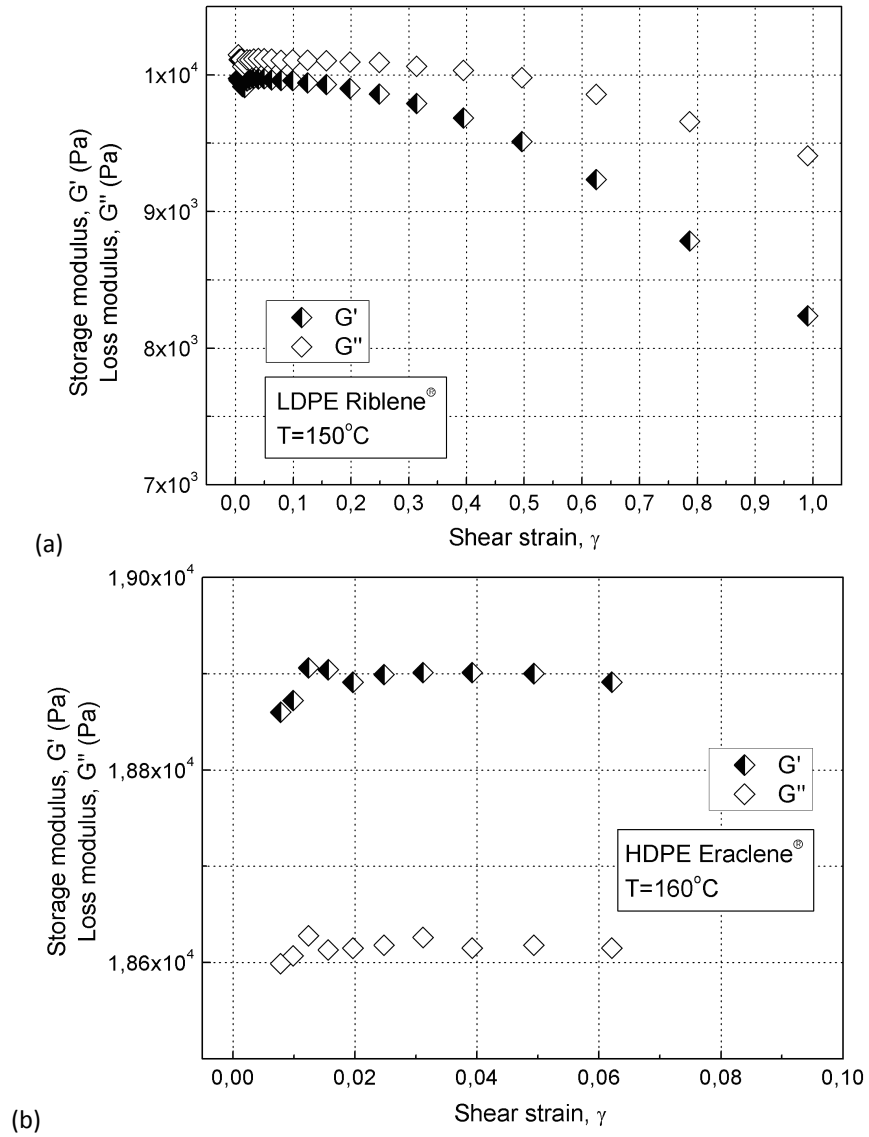


Figure 4.1: Strain sweep with a parallel disk geometry for (a) LDPE at $T=150^{\circ}\text{C}$, $d=25$ mm, $h=1.43$ mm and (b) HDPE at $T=160^{\circ}\text{C}$, $d=25$ mm, $h=1.482$ mm.

After calibrating the force transducer with a single weight of 200 g (as suggested by the manufacturer) an isothermal condition had to be maintained inside the chamber. The rectangular bars were placed on the lower belts and left there for not more than 5 min in order for the stresses inside the material to relax completely. It is important to notice that the sample should relax on the lower belts only. Otherwise if one lowers the upper belts then the sample gets confined between the belts and thermal expansion during melting results in a distorted sample. Yet another important detail that should be noticed is that the rheometer bank vertical position should be checked in order to avoid sliding of the melted samples and thus distortion of the uniformity of the rectangular geometry of the sample. Cylindrical metal pins were also used, as suggested, on both edges of the sample in order to prevent excessive squeezing of the samples.

After relaxation and when thermal expansion of the samples had ended, the upper belts were lowered and the actual measurement took place. A constant distance between the clamps of 50 mm was used and a value of 5 mm for the tongue length. The distance between the clamps is important because it defines the speed with which the clamps rotate, thus controlling the actual strain rate.

During experimentation it was observed that the LDPE samples did not deform enough up to the end of each measurement. This fact was carefully examined and the conclusion was that the LDPE samples adhered too well at the tongues of the belts so that the belts themselves were glued together by the sample and were prevented to complete their rotation and stretch the sample all the way to the set deformation. A thin sheet of wax thus was spread on the lower belts before each measurement in order to prevent stick. This resulted in uniform extension of the samples until break without introducing any slip, as it is found in the process below for the evaluation of the true strain rate.

In order to establish the deviations from the nominal strain rate [65] for every deformation rate, a video camera was used to record the deforming sample until break. Then a series of snapshots at regular time intervals were obtained from the video for each sample and the width of the sample was recorded during elongation. Three measurements of the width were performed at each snapshot, one at each edge and one at the middle, thus the mean value of the sample width was constantly recorded. An example of a series of pictures taken for this particular reason during elongation is shown in Fig. 4.3 for the LDPE resin at 150°C with nominal strain rate of 2.0 s^{-1} and true strain rate of 1.61 s^{-1} .

The basic equations of uniaxial extensional flow of rectangular bars at constant elongation rate read as [66, 29]

$$L(t) = L_0 \exp(\dot{\epsilon}t) \quad (4.5)$$

$$W(t) = W_0 \exp\left(-\frac{\dot{\epsilon}t}{2}\right) \quad (4.6)$$

$$H(t) = H_0 \exp\left(-\frac{\dot{\epsilon}t}{2}\right), \quad (4.7)$$

where $\dot{\epsilon}$ is the strain rate and t is the time. Assuming the stretch of the sample in terms

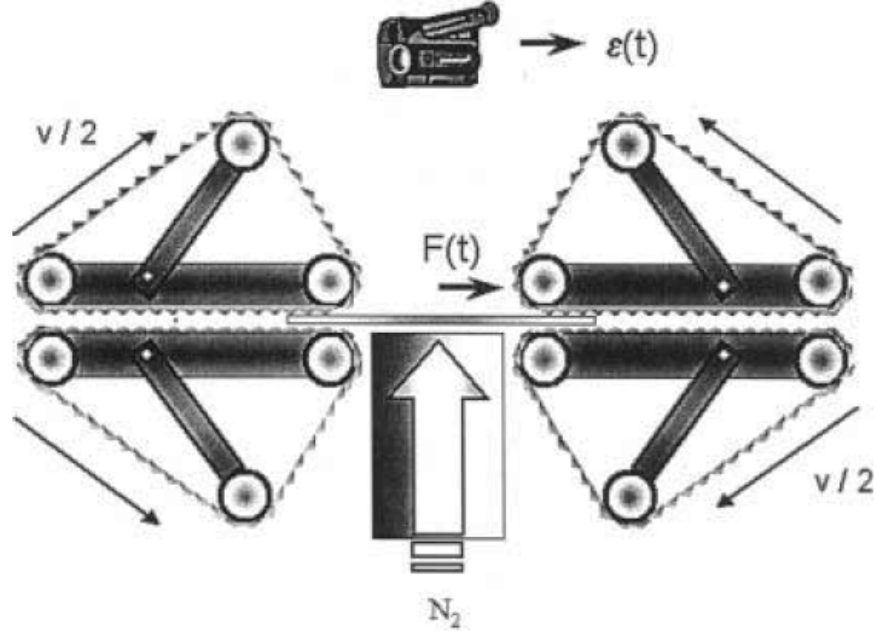


Figure 4.2: Schematic representation of the RME setup for uniaxial extensional measurements of polymer melts. The values of L_0 along with the set strain rate, $\dot{\epsilon}$ are used in order to set the speed of the belts, $v = (\dot{\epsilon}L_0/2) = \text{const}$ [65].

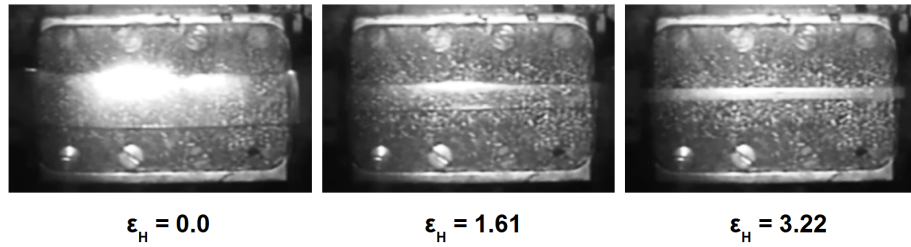


Figure 4.3: A series of snapshots taken at the corresponding Hencky strains during uniaxial elongation of the LDPE Riblene melt at $T=150^\circ\text{C}$ with true strain rate of 1.61 s^{-1} .

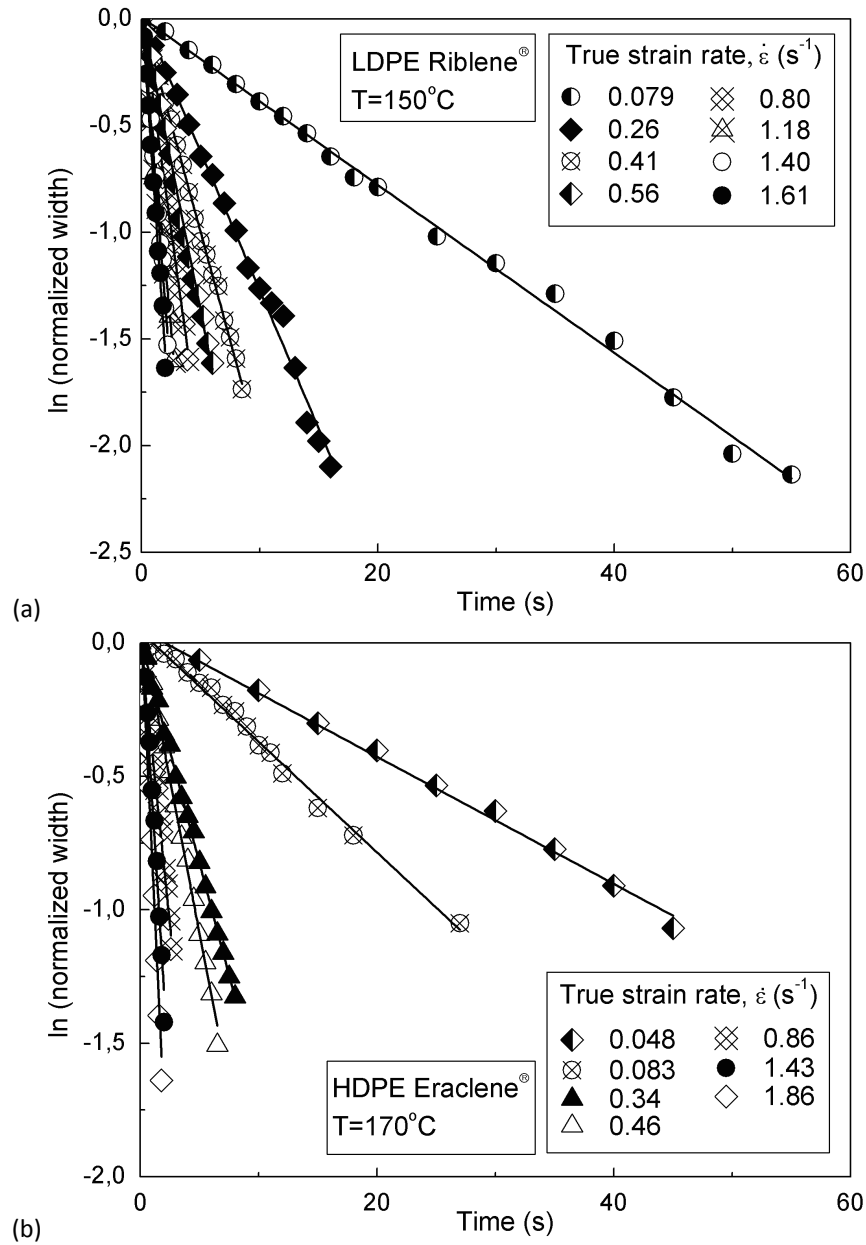


Figure 4.4: The true strain rates obtained during uniaxial extension of (a) the LDPE and (b) HDPE samples at the corresponding isothermal conditions.

of its initial and final length, then the *principal stretch ratio* is defined as

$$\lambda = \frac{L_f}{L_0} \quad (4.8)$$

and the strain measure is defined as the natural logarithm of the principal stretch ratio

$$\epsilon_H = \int_{L_0}^{L_f} \frac{dL}{L} = \ln\left(\frac{L_f}{L_0}\right) = \ln \lambda. \quad (4.9)$$

This is called the Hencky strain and is equal to

$$\epsilon_H = \dot{\epsilon} t. \quad (4.10)$$

For a uniaxial extensional deformation at constant strain rate the dimensions of the sample change proportionally. Thus, a uniform extension along the principal axis of deformation results in a uniform reduction of the sample width and height. From the change in width during elongation and through a combination of Eqs. 4.9 and 4.10 one obtains the true strain rate from the slope of the linear fitting of the natural logarithm of the normalized width against time [65, 29]. This is demonstrated in Fig. 4.4 for both resins. For all samples tested the fit of the straight lines are good ($r^2 > 0.993$ always) indicating that no slippage occurs during elongation. The deviations from the nominal strain rate are given in Table 4.2. These are in good agreement with published values obtained under different test conditions [65].

While the force during elongation is constantly measured, the resulting stress in the sample is computed from

$$\sigma(t) = \frac{F(t)}{A(t)} = \frac{F(t)}{A_0 \exp(-\dot{\epsilon} t)}. \quad (4.11)$$

The elongational viscosity, then, is given by

$$\eta_E(t) = \frac{\sigma(t)}{\dot{\epsilon}}. \quad (4.12)$$

An important correction to the results comes from the change in density, ρ , or equivalently the specific volume, v_s , of the samples resulting from the melting [66, 29]. The change in the initial dimensions of the samples due to thermal expansion has also to be accounted for in the calculations of the stress and the viscosity. These corrections are calculated from

$$A_0 = H_0 W_0 \left[\frac{v_s(T)}{v_{s,0}} \right]^{2/3} = H_0 W_0 \left[\frac{\rho_0}{\rho(T)} \right]^{2/3} \quad (4.13)$$

where v_s designates the specific volume of the fluid. The density of LDPE at 150°C was determined to be 0.782 gr/cm³ and that of HDPE at 170°C to be 0.772 gr/cm³ [55]. The corrected dimensions of all samples tested were used for the calculations.

A less important correction comes from the inclusion of the sample surface tension in the calculation of the elongational stress [66, 71]. It is assumed that a small portion

Table 4.2: Set strain rate and true strain rate determined for the LDPE and HDPE resins in uniaxial extensional flow.

	LDPE Riblene FF20	HDPE Eraclene FA506
Set strain rate (s^{-1})	True strain rate (s^{-1})	
0.05		0.048
0.1	0.081	0.083
0.3	0.26	
0.4		0.34
0.5	0.41	0.46
0.7	0.56	
1.0	0.80	0.86
1.5	1.18	1.43
1.7	1.40	
2.0	1.61	1.86

of the force required to extend the sample is used for the increase of the surface of the sample due to the surface tension and must be subtracted from the recorded stress. For PEs in the current thesis, a surface tension of 0.025 N/m [48] is considered reasonable. After calculating the resulting stress, the relative error introduced for not including this correction is always $\leq 1.0\%$. Thus this correction was deemed insignificant and was not included in the results.

Chapter 5

Results

The results from shear and extensional flows for the examined resins are presented in detail in the present chapter. The results from the dynamic mechanical analysis are of primary concern and are presented first, as they form the basis for the impending analysis of all the data gathered. A series of step-strain in shear and uniaxial elongational measurements then follow to complete the experimental investigation.

5.1 Dynamic Measurements

The results of the dynamic mechanical analysis for both resins are provided in Figs. 5.1 and 5.2. The *time - temperature superposition principle* was applied to both materials with a reference temperature of 150°C for the LDPE and 170°C for the HDPE. What this principle states, is that the resulting storage and loss moduli at every temperature can be shifted horizontally and vertically with respect to a given temperature in order to produce a *master curve* at that reference temperature. The resulting master curves are provided in Fig. 5.3 for the LDPE and Fig. 5.4 for the HDPE.

In order for the superpositions to be successful it is often preferred to evaluate the shift factors from the corresponding dynamic viscosity curves, $\eta^*(\omega)$, rather than the moduli. The complex viscosity curve at each temperature is computed from the storage and loss moduli using Eqs. 3.21 and Eqs. 2.54, 2.55 along with Eq. 2.56. The results of these calculations are shown in Fig. 5.5 and 5.6 for the LDPE and the HDPE respectively. The lines in these figures are fits of the Cross viscosity model from Eq. 2.40. The values of the zero shear viscosities, η_0^* and the two parameter of the Cross model for the polymers at each temperature are provided in Table 5.1.

When the viscosity curves are shifted horizontally and vertically the resulting viscosity master curves are shown in Fig. 5.7 and 5.8. The amount of horizontal shifting for each temperature is the *time shift factor*, α_T at that temperature. The amount of the vertical shift, β_T , corresponds to changes in the density of the material:

$$\alpha_T \beta_T = \frac{\eta_0^*(T)}{\eta_0^*(T_0)} \quad \beta_T = \frac{\rho T}{\rho_0 T_0} \quad (5.1)$$

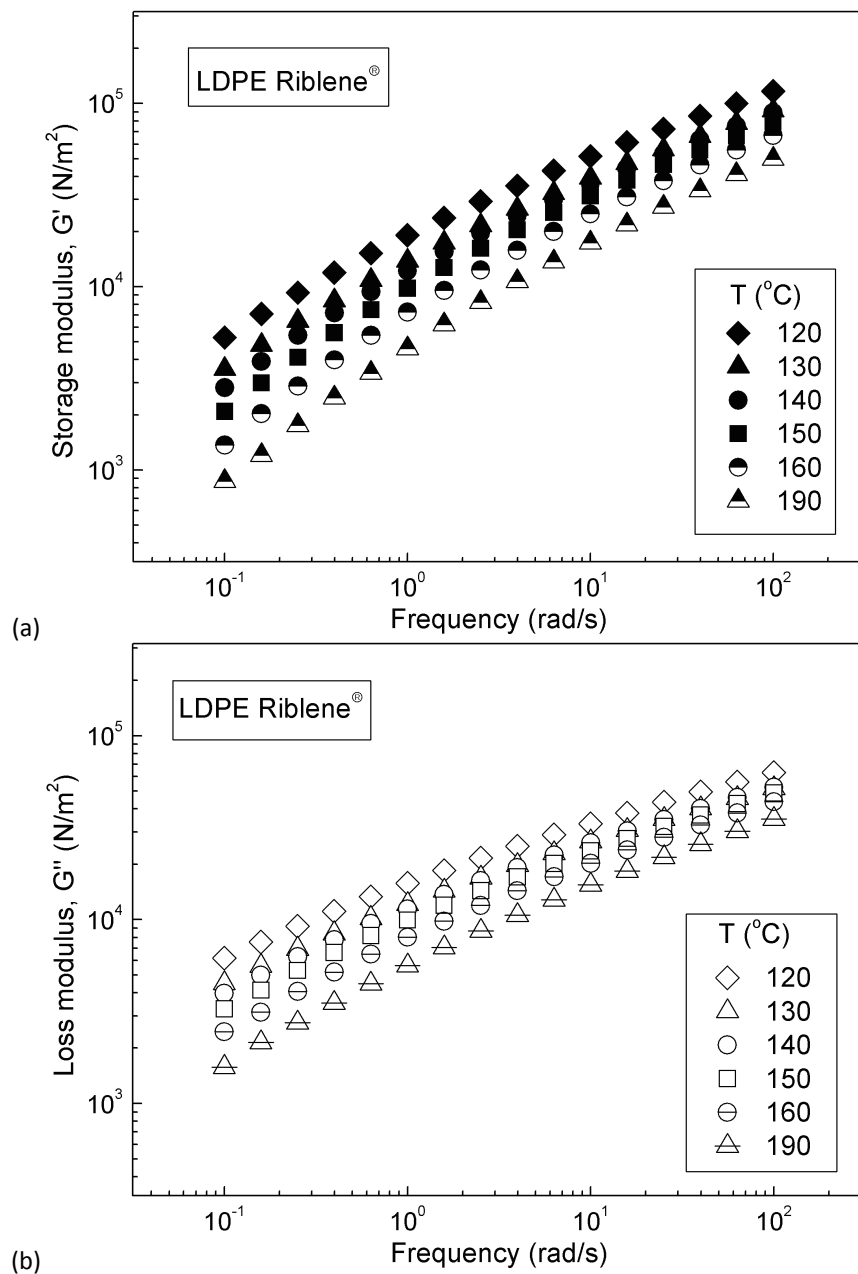


Figure 5.1: (a) Storage, G' , and (b) loss, G'' , moduli measured at dynamic mechanical analysis of the LDPE Riblene melt at a wide range of isothermal conditions.

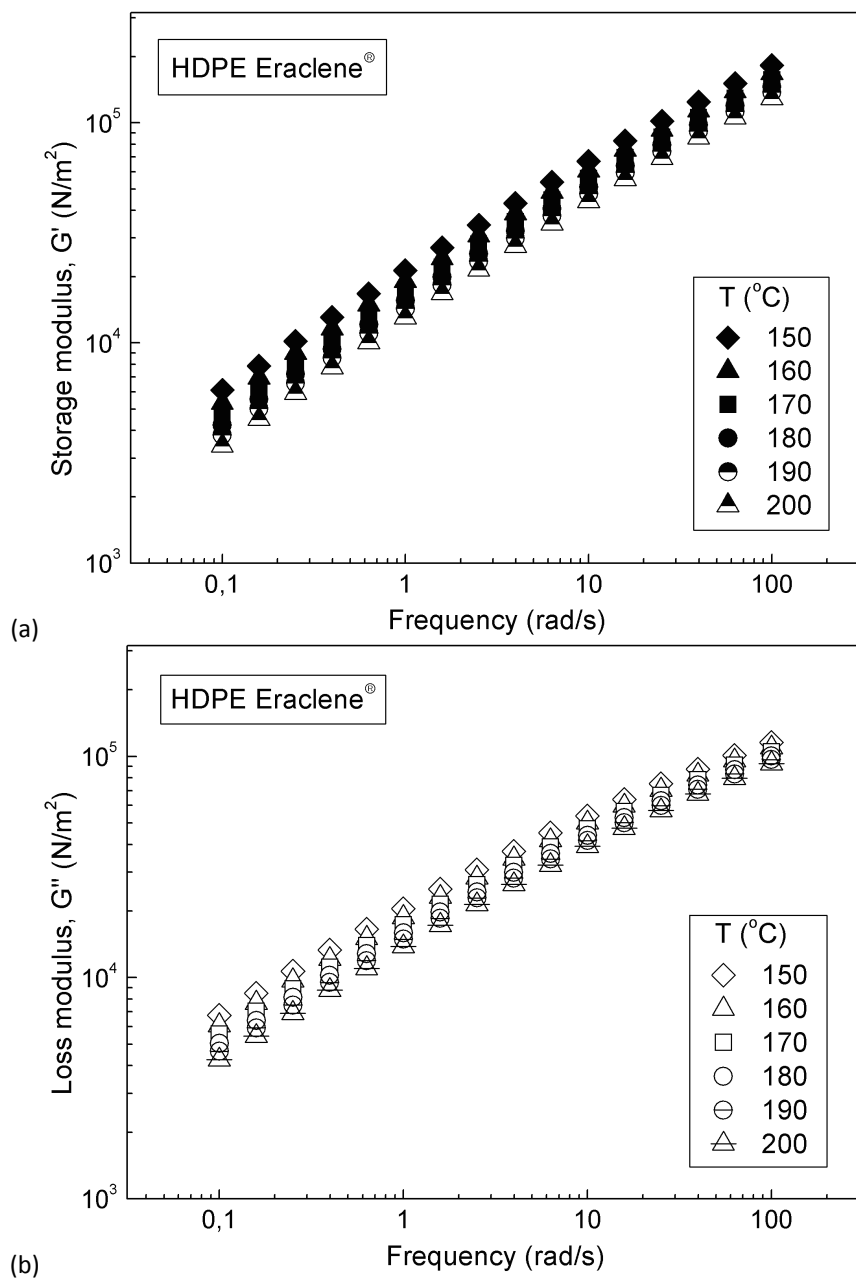


Figure 5.2: (a) Storage, G' , and (b) loss, G'' , moduli measured at dynamic mechanical analysis of the HDPE Eraclene melt at a wide range of isothermal conditions.

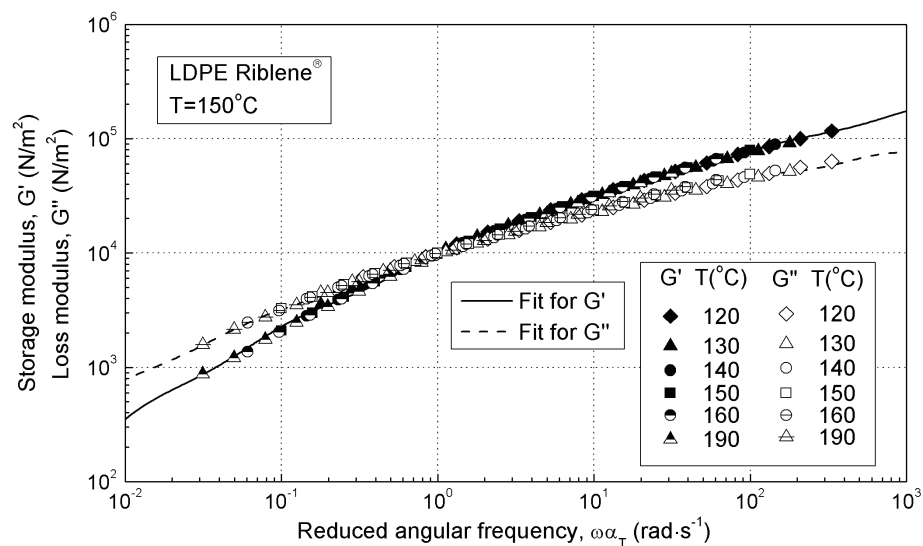


Figure 5.3: Storage and loss moduli for the LDPE Riblene melt taken at several isothermal conditions, superimposed at $T=150^{\circ}\text{C}$.

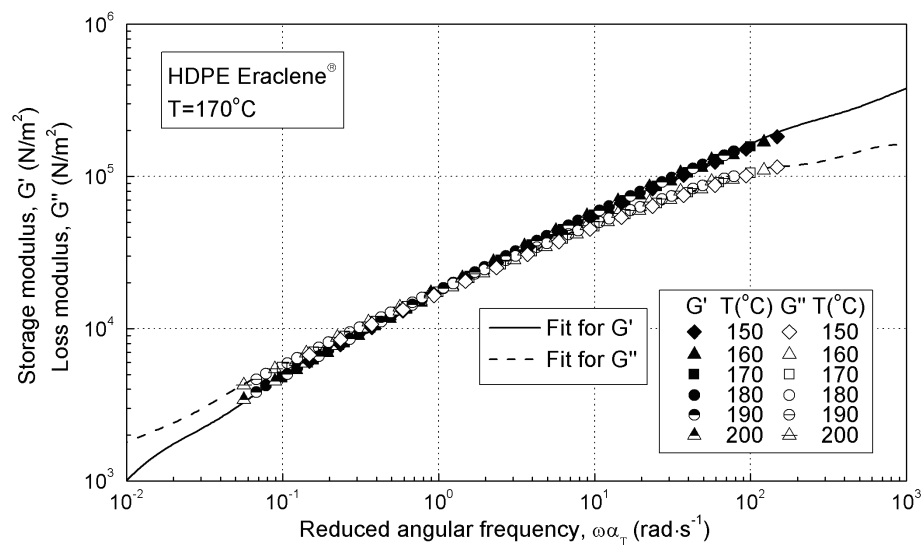


Figure 5.4: Storage and loss moduli for the HDPE Eraclene melt taken at several isothermal conditions, superimposed at $T=170^{\circ}\text{C}$.

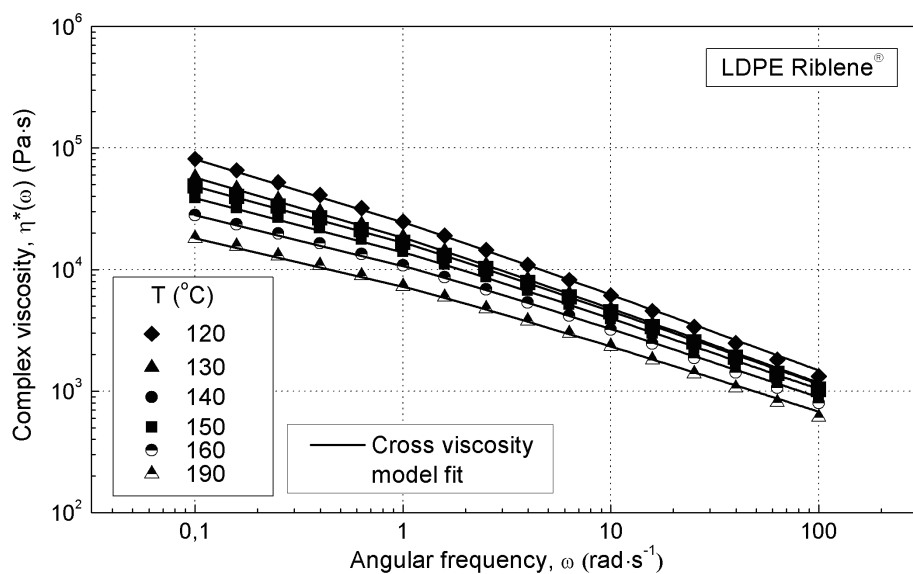


Figure 5.5: Complex shear viscosity for the LDPE Riblene melt at several isothermal conditions. Lines are fits of the Cross viscosity model (Eq. 2.40) at the corresponding temperatures.

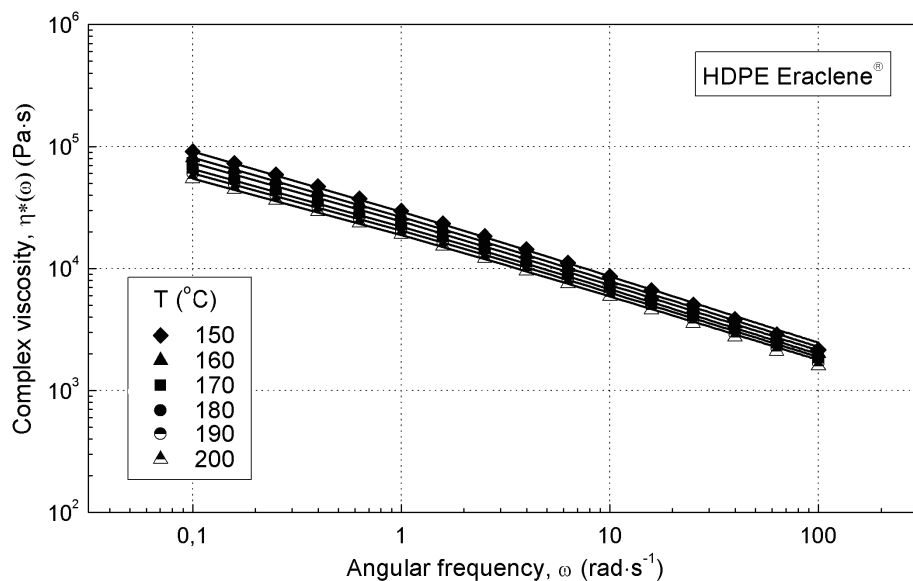


Figure 5.6: Complex shear viscosity for the HDPE Eraclene melt at several isothermal conditions. Lines are fits of the Cross viscosity model (Eq. 2.40) at the corresponding temperatures.

Table 5.1: Cross viscosity model parameters for the LDPE and HDPE at various isothermal conditions.

LDPE Riblene FF20				HDPE Eraclene FA506			
T (°C)	η_0 (Pa · s)	K_c	n_c	T (°C)	η_0 (Pa · s)	K_c	n_c
120	272052	38.9	0.37	150	479939	153.1	0.45
130	172967	31.2	0.38	160	427459	143.9	0.45
140	128149	22.5	0.39	170	377281	138.3	0.46
150	98396	20.9	0.41	180	327755	131.1	0.46
160	66147	17.2	0.42	190	294080	128.3	0.47
190	42488	17.3	0.45	200	259917	124.1	0.47

Table 5.2: Time shift factors, α_T for both resins with respect to the reference temperature at various isothermal conditions.

LDPE Riblene FF20 T=150°C		HDPE Eraclene FA506 T=170°C	
T(°C)	α_T	T(°C)	α_T
120	3.3221	150	1.4831
130	1.7852	160	1.2164
140	1.4514	170	1.0000
150	1.0000	180	0.7843
160	0.6084	190	0.6803
190	0.3137	200	0.5638

where T_0 is the reference temperature and ρ is the density of the material at temperature T . The values of the shift factors are shown in Table 5.2. These master curves (Figs. 5.7 and 5.8) show that the complex viscosity curves are smooth and continuous for both melts. The time shift factors evaluated in this manner are applied to the storage and loss moduli to produce the master curves in Fig. 5.3 and 5.4.

The magnitude of the zero shear viscosity, as well as the values of the dynamic moduli at a given frequency decrease as the temperature increases. The reduction is reflected to the change of the time shift factor, $\alpha_T(T)$, with temperature. This function should have the form of an Arrhenius relation:

$$\alpha_T(T) = \exp \left[\frac{E_a}{R} \left(\frac{1}{T} - \frac{1}{T_0} \right) \right], \quad (5.2)$$

where T_0 is the reference temperature, E_a is the flow activation energy and R is the *universal gas constant*. Thus, by plotting $\ln \alpha_T$ vs. $1/T$ one should get a straight line, the slope of which gives the flow activation energy at the reference temperature (Fig. 5.9). For the LDPE melt it was found that $E_a = 50.4 \pm 3.4$ kJ/mol for $T_0 = 150$ °C, while for HDPE $E_a = 32.5 \pm 0.8$ kJ/mol for $T_0 = 170$ °C.

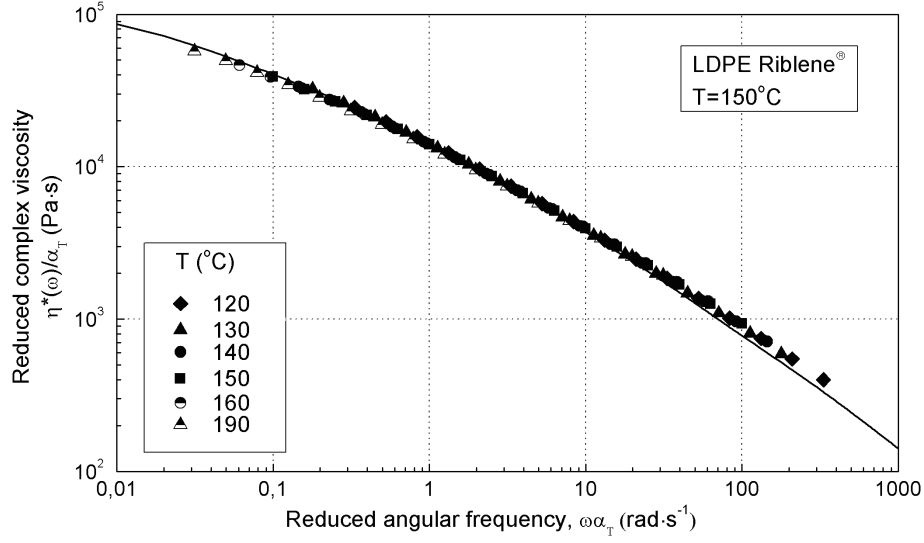


Figure 5.7: Steady state shear viscosity for the LDPE Riblene melt at several isothermal conditions, superimposed at $T=150^\circ\text{C}$. Solid line is the prediction of the shear thinning response (see Eq. 3.53) according to the modified rubber-like liquid theory with $n=0.25$.

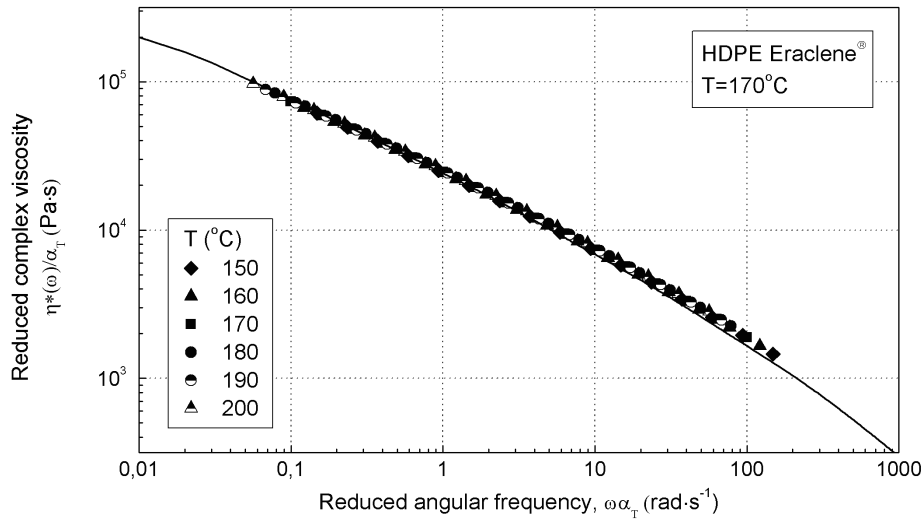


Figure 5.8: Steady state shear viscosity for the HDPE Eraclene melt at several isothermal conditions, superimposed at $T=170^\circ\text{C}$. Solid line is the prediction of the shear thinning response (see Eq. 3.53) according to the modified rubber-like liquid theory with $n=0.28$.

Table 5.3: Relaxation spectra for the LDPE and HDPE melts at the reference temperature.

Mode Number, i	LDPE Riblene FF20 $T=150^{\circ}\text{C}$		HDPE Eraclene FA506 $T=170^{\circ}\text{C}$	
	τ_i (s)	G_i (Pa)	τ_i (s)	G_i (Pa)
1	10^2	$6.45 \cdot 10^2$	10^2	$1.90 \cdot 10^3$
2	10^1	$3.00 \cdot 10^3$	10^1	$5.68 \cdot 10^3$
3	10^0	$12.87 \cdot 10^3$	10^0	$2.02 \cdot 10^4$
4	10^{-1}	$3.00 \cdot 10^4$	10^{-1}	$5.77 \cdot 10^4$
5	10^{-2}	$5.98 \cdot 10^4$	10^{-2}	$1.50 \cdot 10^5$
6	10^{-3}	$1.37 \cdot 10^5$	10^{-3}	$2.90 \cdot 10^5$

The master curves were fitted by a 6-mode discrete Maxwell relaxation spectrum (Eqs. 3.21). The resulting curve seems to describe well the rheological behaviour of the melts with respect to the frequency of the shear deformation. The fitting procedure gave a set of relaxation times, τ_i , along with the corresponding moduli, G_i . These are provided in Table 5.3. The fit of the Maxwell model is also shown as a continuous line in Fig. 5.3 for the LDPE and Fig. 5.4 for the HDPE melt.

Steady state viscosity, $\eta(\dot{\gamma})$ measurements were not conducted for our polymers. Instead, the Cox-Merz rule was employed to estimate $\eta(\dot{\gamma})$ from the dynamic viscosity at $\dot{\gamma} = \omega$:

$$|\eta^*(\omega) = \eta(\dot{\gamma})|_{\dot{\gamma}=\omega} \quad (5.3)$$

In order to account for the shear thinning in the steady state shear viscosity curves, the temporary network model theory and the Wagner-I single exponential damping function was used. An exponent $n = 0.25$ was found to be adequate to fit the steady state curve of the LDPE at 150°C using Eq. 3.53. This fit is seen in Fig. 5.7. Additionally, an exponent $n = 0.28$ was found to fit the steady state viscosity data for the HDPE at 170°C . This fit is seen in Fig. 5.8.

Another interesting feature of the dynamic data is the characteristic *crossover frequency*, ω_{cr} . At low frequencies the storage modulus, $G'(\omega)$, has lower values than the loss modulus, $G''(\omega)$. However, the slope of the curve of the former is 2, while the slope of the latter is 1. Thus, at $\omega = \omega_{cr}$ the storage modulus crosses over the loss modulus. This characteristic frequency is related to the characteristic *relaxation time* for the polymer, $\tau_{cr} = 1/\omega_{cr}$ and it is an intrinsic property of the material. The crossover frequencies and the corresponding relaxation times at each temperature are provided in Table 5.4.

It has to be emphasised that longer τ_{cr} (lower ω_{cr}) indicates higher elasticity and, indirectly, higher levels of long chain branching [4]. For the melts under consideration it should be pointed out that the higher the temperature the more viscous or liquid-like the polymer melt becomes, thus decreasing the critical relaxation time, τ_{cr} .

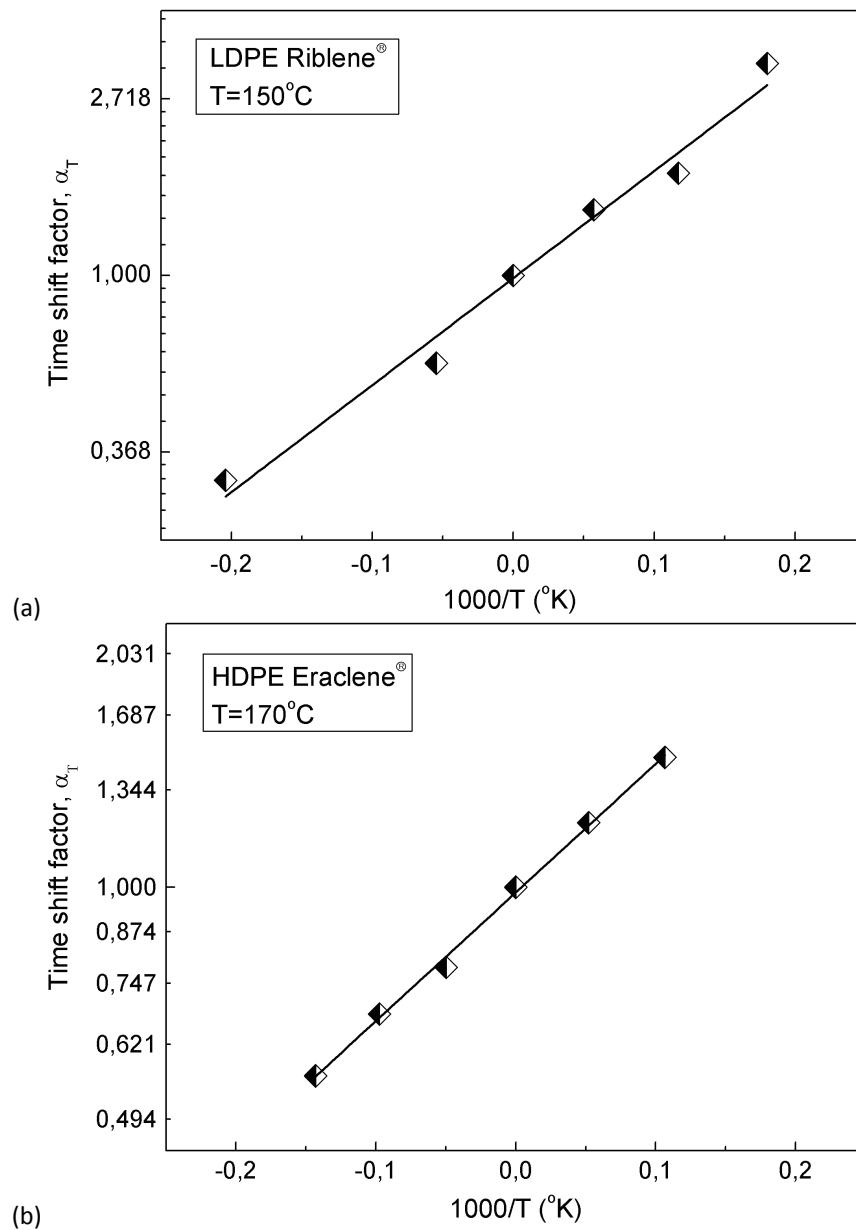


Figure 5.9: Linear least squares fit of the linearized version of Eq. 5.2 for (a) LDPE Riblene at T=150°C and (b) HDPE Eraclene at T=170°C.

Table 5.4: Crossover frequencies and corresponding relaxation times for both resins at various isothermal conditions.

LDPE Riblene FF20			HDPE Eraclene FA506		
T (°C)	$\omega_{cr}=1/\tau_{cr}$ (rad/s)	$\tau_{cr}=1/\omega_{cr}$ (s)	T (°C)	$\omega_{cr}=1/\tau_{cr}$ (rad/s)	$\tau_{cr}=1/\omega_{cr}$ (s)
120	0.24	4.17	150	0.64	1.56
130	0.40	2.50	160	1.00	1.00
140	0.69	1.45	170	1.27	0.79
150	1.07	0.93	180	1.59	0.63
160	1.95	0.51	190	2.00	0.50
190	3.65	0.27	200	3.99	0.25

Table 5.5: Damping function values for the LDPE Riblene melt at corresponding magnitudes of shear strain.

LDPE Riblene FF20 T=150°C							
Strain	0.01	0.05	0.1	0.2	0.5	1.0	2.0
$h(\gamma_0)$	1.00	1.00	1.00	1.00	0.99	0.91	0.71

5.2 Step-Strain Tests

The results for the LDPE Riblene melt of the step-strain in shear experiments at $T=150^\circ\text{C}$ are shown in Fig. 5.10, along with the vertical shift (superposition). Values of the vertical shift at the corresponding magnitudes of shear strain are given in Table 5.5 and the resulting Wagner-I single exponential damping function is given in Fig. 5.11. The exponent from the linear fit of the single exponential was found to be $n = 0.23$ somewhat lower than the value of $n = 0.25$ found from the dynamic viscosity data at the same temperature.

5.3 Uniaxial Elongation

Both polymers were measured in uniaxial extensional flow at the same reference temperature as the shear flows to facilitate the direct comparison between the rheological responses of the melts in different flows. The growth of the extensional viscosity is usually shown in log-log plots as a function on time. It can also be shown in a semi log plot as a function of strain. The power-law damping function (Eq. 3.60) was used to model both melts in extensional flow. The results along with the predictions of the modified rubber-like liquid theory are shown in Figs. 5.12 and 5.13 for the LDPE and Figs. 5.14 and 5.15 for the HDPE both in log-log and semi-log plots.

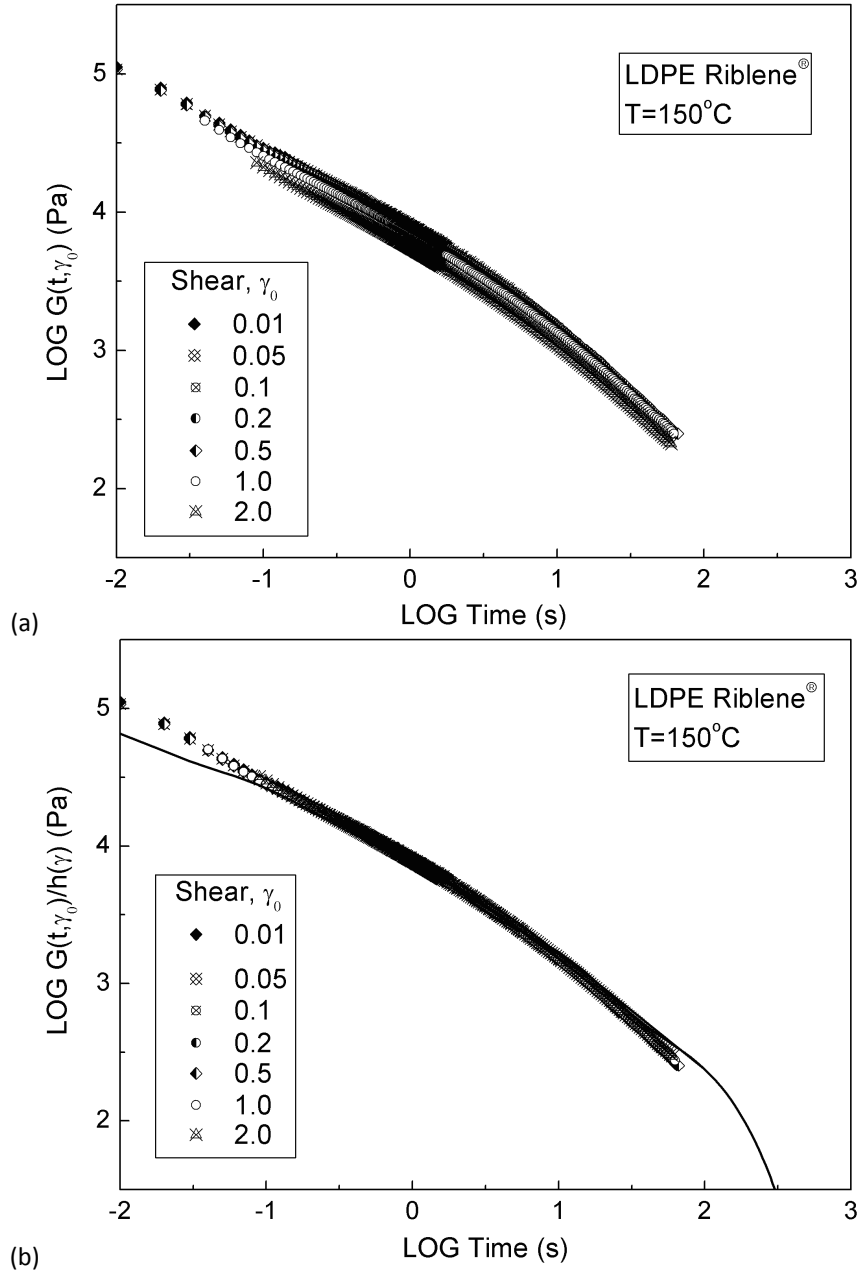


Figure 5.10: Results in (a) from the step-strain experiment for the LDPE Riblene and (b) superimposed data for the same melt. The solid line in (b) is the linear relaxation modulus, $G(t)$ of the 6-mode Maxwell spectrum (see Table 5.3).

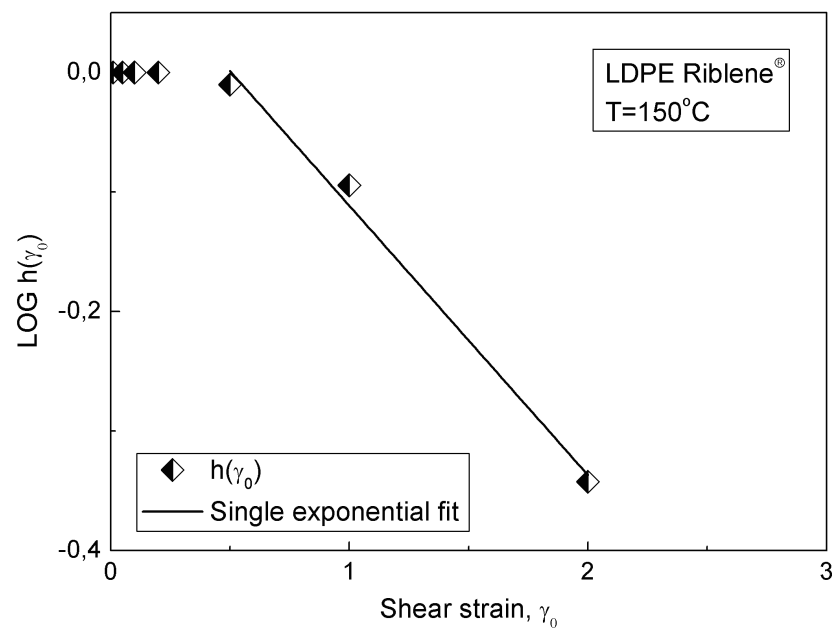


Figure 5.11: Damping function for the LDPE Riblene melt in a log-linear plot. Solid line is the single exponential damping function, with $n=0.23$.

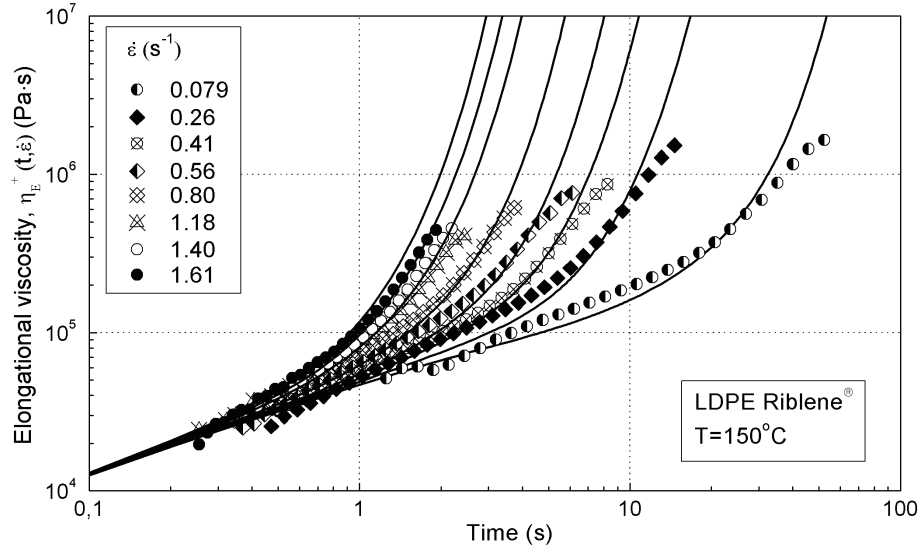


Figure 5.12: Transient uniaxial extensional viscosity as a function of time for the LDPE Riblene melt at $T=150^\circ\text{C}$ and for various strain rates (as indicated in the legend). Lines are fits of the modified rubber-like liquid theory with the power-law damping function (see Eqs. 3.65 and 3.66) and $\beta=0.25$.

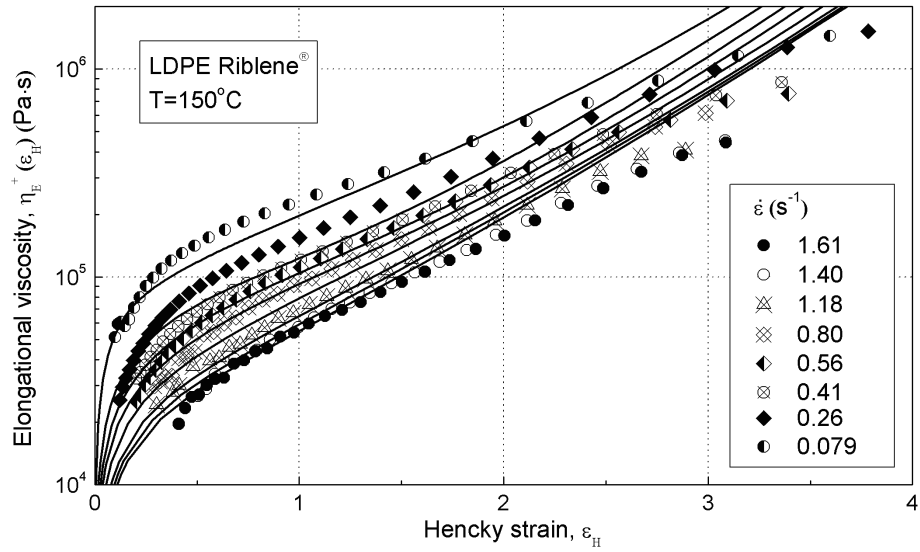


Figure 5.13: Same as in Fig. 5.12 but with respect to the Hencky strain.

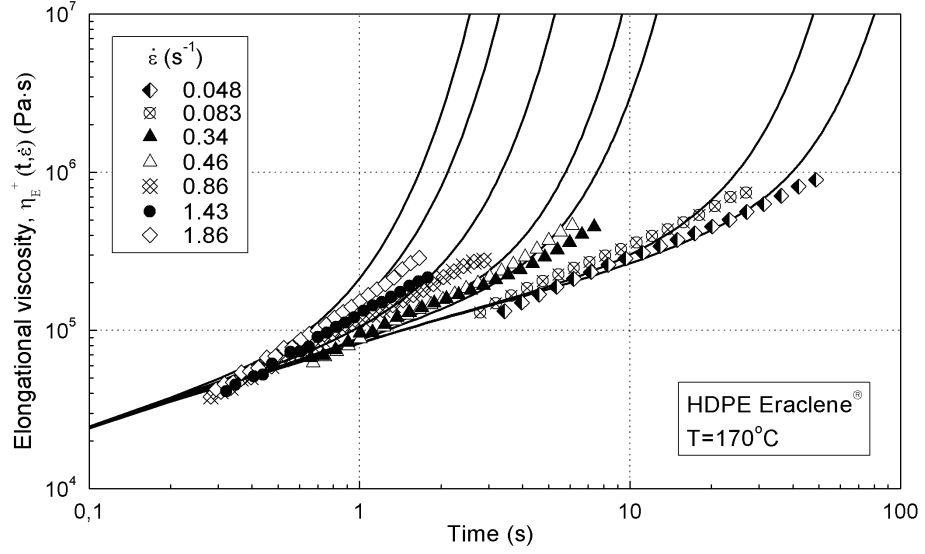


Figure 5.14: Transient uniaxial extensional viscosity as a function of time for the HDPE Eraclene melt at $T=170^\circ\text{C}$ and for various strain rates (as indicated in the legend). Lines are fits of the modified rubber-like liquid theory with the power-law damping function (see Eqs. 3.65 and 3.66) and $\beta=0.40$.

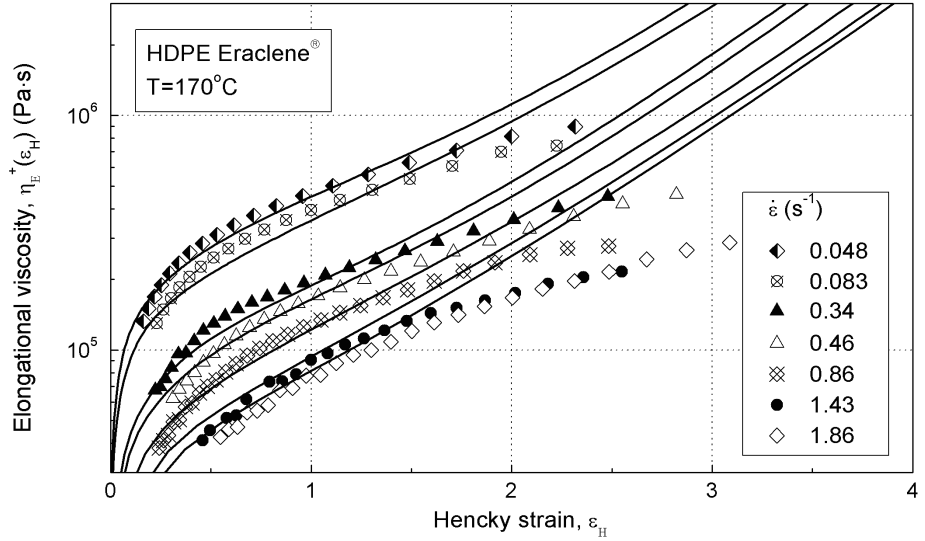


Figure 5.15: Same as in Fig. 5.14 but with respect to the Hencky strain.

It can be seen in these figures that the LDPE shows strong strain hardening in its elongational viscosity. The HDPE shows much less strain hardening. This is, of course, due to the extended branching structure of LDPE. The small strain hardening of the basically linear HDPE can be due to its broad molecular weight distribution and to some small degree of branching that was not reported by the manufacturer. The *strain hardening index*, *SHI* of the Riblene melt was determined from the uniaxial extensional viscosity curve at $\dot{\epsilon}=0.081 \text{ s}^{-1}$ and was found to be ≈ 10.2 , whereas for HDPE this could not be calculated since for $\dot{\epsilon} \leq 1$ the sample broke shortly before reaching $\epsilon_H=3$.

The damping function in extensional flow was determined graphically from these experiments by recording the deviation of the experimental data from Lodge's rubber-like liquid theory predictions (using the 6-mode relaxation spectrum defined from shear experiments) for every strain rate at regular time intervals. The results are provided in Fig. 5.16 for both melts. The lines in the graphs were determined through a linear least squares fitting of the damping function values obtained from the experiment. The power-law exponent was determined to be $\beta=0.25$ for the LDPE and $\beta=0.40$ for the HDPE.

Besides Lodge's rubber-like liquid with a damping function, the XPP model was also tested against the data. The 6-mode Maxwell relaxation spectrum derived from the LVE analysis was used to model the backbone orientation relaxation times, $\tau_{0b,i}$. The additional sets of stretch relaxation times, $\tau_{0s,i}$ and the rest of the nonlinear parameters of the model were obtained by trial and error fitting of the experimental data in uniaxial flow. The parameters thus found to best fit the data are provided in Tables 5.6 and 5.7 for the LDPE and HDPE melts respectively. The corresponding plots are given in Figs. 5.17-5.18 for the LDPE and Figs. 5.19-5.20 for the HDPE.

Some explanatory details regarding the manual fitting of the various parameters of the XPP model are provided here. In the case of a branched molecule, going from the free ends inwards an increasing number of arms is attached to every backbone of the representative pom-pom. The relaxation time of a backbone segment is determined by its distance to the nearest free end, which can be released from its tube constraint by retraction. Towards the middle of a complex molecule the relaxation time increases exponentially. Thus, the $q_{x,i}$ parameters and the orientation relaxation times of the backbone, $\tau_{0b,i}$, increase towards the centre of the molecule. The stretch relaxation times are physically bounded in the region $\tau_{0b,i-1} < \tau_{0s,i} \leq \tau_{0b,i}$. To evaluate the anisotropy parameter $\alpha_{x,i}$ it is advised to use second normal stress difference or second planar viscosity data. In the absence of such data the value for the parameter $\alpha_{x,i}$ could be chosen as $0.1/q_{x,i}$, since the number of arms attached to the branch points increase while going towards the centre of the molecule and, thus, $\alpha_{x,i}$ decreases.

The Rolie-Poly constitutive equation was used to model the rheology of the HDPE Eracene melt. The reptation and Rouse relaxation times that have been used were those computed for the XPP model and are provided in Table 5.7. The fit of the model is given in Figs. 5.21 and 5.22. The predictions of the Rolie-Poly constitutive equation are obtained in units of the relaxation moduli, G_i for each mode of the corresponding strain rate. The predicted viscosity growth curves have to be multiplied by the corresponding moduli of the Maxwell spectrum before computing the values of the uniaxial extensional viscosity. The CCR coefficient, β_{rp} has been found to have no implication on the predictions of the uniaxial extensional viscosity whether it was set to zero or

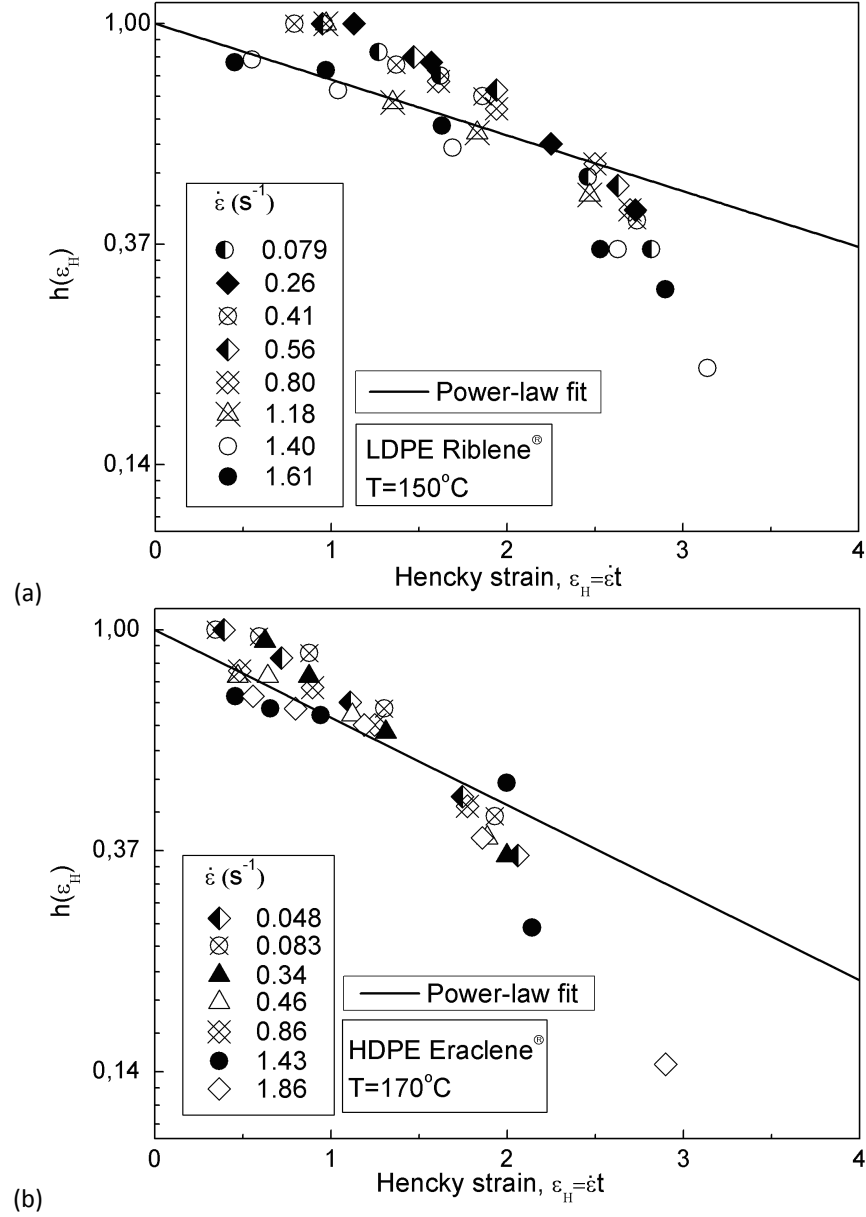


Figure 5.16: Damping function in extensional flow for (a) LDPE Riblene and (b) HDPE Eraclene melts at the corresponding temperatures. The power-law exponent assumes a value of $\beta=0.25$ for LDPE while for HDPE $\beta=0.40$.

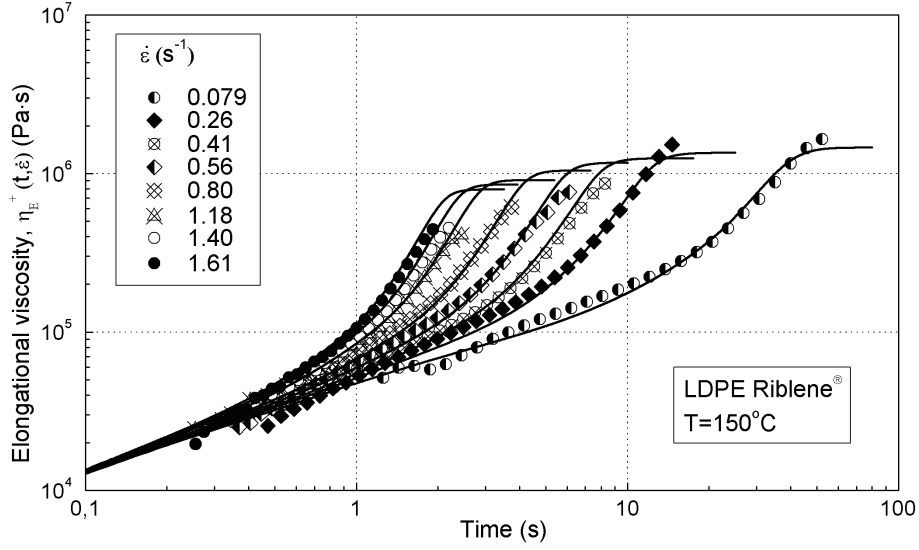


Figure 5.17: Transient uniaxial extensional viscosity as a function of time for the LDPE Riblene melt at $T=150^\circ\text{C}$ and for various strain rates (as indicated in the legend). Lines are fits of the XPP model with parameters given in Table 5.6.

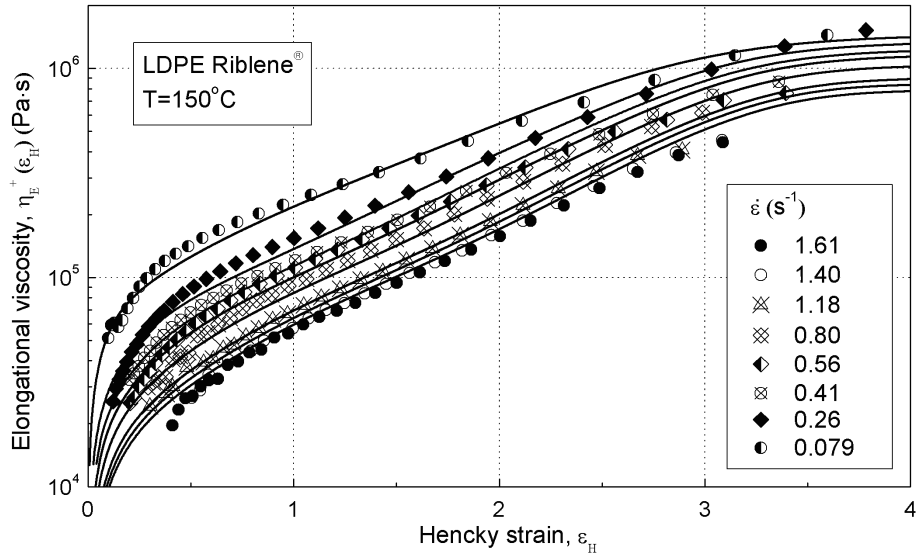


Figure 5.18: Same as in Fig. 5.17 but with respect to the Hencky strain.

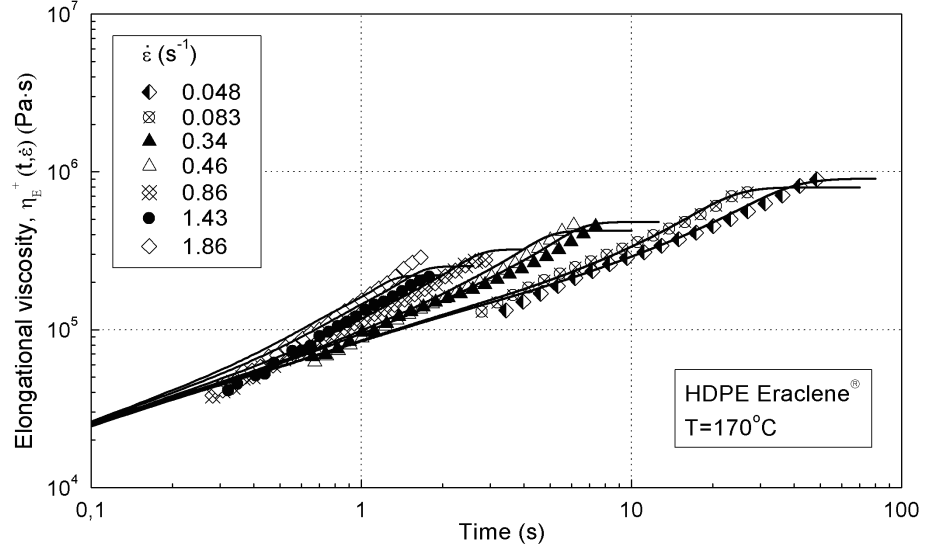


Figure 5.19: Transient uniaxial extensional viscosity as a function of time for the HDPE Eraclene melt at $T=170^\circ\text{C}$ and for various strain rates (as indicated in the legend). Lines are fits of the XPP model with parameters given in Table 5.7.

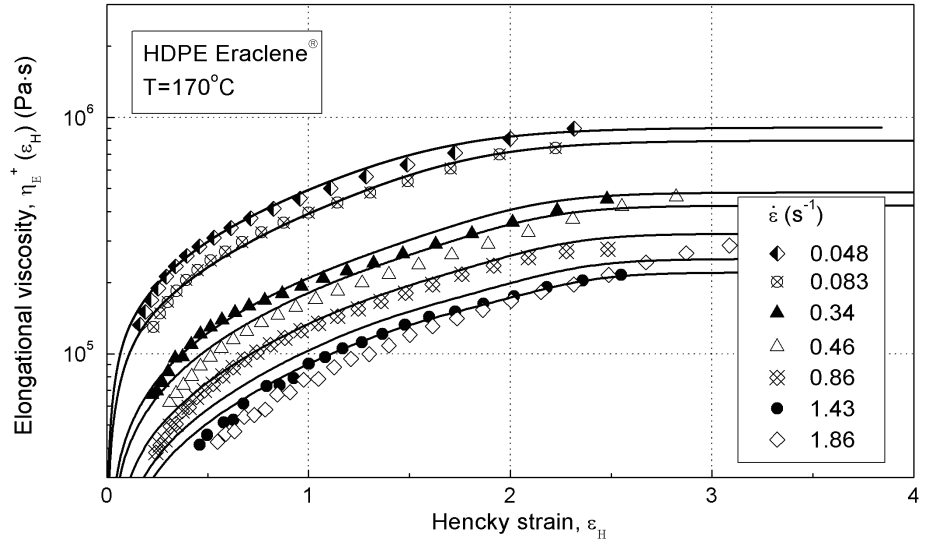


Figure 5.20: Same as in Fig. 5.19 but with respect to the Hencky strain.

Table 5.6: XPP parameters for fitting the LDPE Riblene melt, $T=150^{\circ}\text{C}$, $M_w=160.3$ (kg/mol), ($M_w/M_n=12$, $E_a=50.4$ (kJ/mol))

Maxwell parameters				XPP model			
i	$\tau_{0b,i}$ (s)	G_i (Pa)	$q_{x,i}$	$\tau_{0s,i}$ (s)	$\tau_{0b,i}/\tau_{0s,i}$	$\alpha_{x,i}$	$\nu_{x,i}$
1	0.001	137370	1	0.0002	5	0.1	2
2	0.01	59813	1	0.0025	4	0.1	2
3	0.1	30000	2	0.03	3.33	0.05	1
4	1	12869	2	0.53	1.9	0.05	1
5	10	3000	6	7.3	1.4	0.016	0.33
6	100	645	6	74.1	1.35	0.016	0.33

Table 5.7: XPP parameters for fitting the HDPE Eraclene melt, $T=170^{\circ}\text{C}$, $M_w=196.6$ (kg/mol), ($M_w/M_n=16$, $E_a=32.5$ (kJ/mol))

Maxwell parameters				XPP model			
i	$\tau_{0b,i}$ (s)	G_i (Pa)	$q_{x,i}$	$\tau_{0s,i}$ (s)	$\tau_{0b,i}/\tau_{0s,i}$	$\alpha_{x,i}$	$\nu_{x,i}$
1	0.001	290000	1	0.0002	5	0.1	2
2	0.01	150000	1	0.002	5	0.1	2
3	0.1	57721	1	0.025	4	0.1	2
4	1	20178	1	0.33	3	0.1	2
5	10	5683	1	3.6	2.8	0.1	2
6	100	1900	2	41.7	2.4	0.05	1

anywhere between 0 and 1. The value of the parameter δ_{rp} was always set to -0.5. In addition, a change of the δ_{rp} parameter from -0.5 to 0 was found to have no implications on the predictions of the uniaxial extensional viscosity.

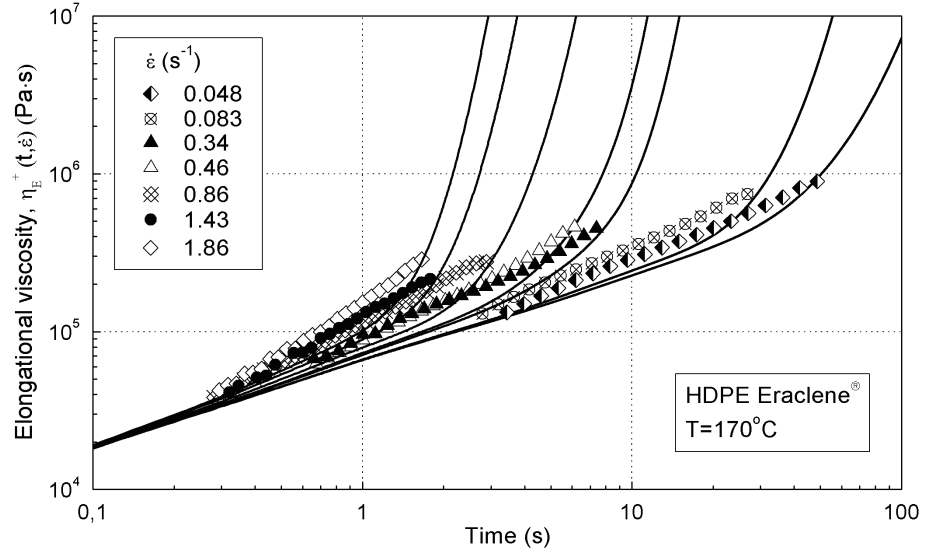


Figure 5.21: Transient uniaxial extensional viscosity as a function of time for the HDPE Eraclene melt at $T=170^\circ\text{C}$ and for various strain rates (as indicated in the legend). Lines are fits of the Rolie-Poly constitutive equation with the Maxwell spectrum of Table 5.7.

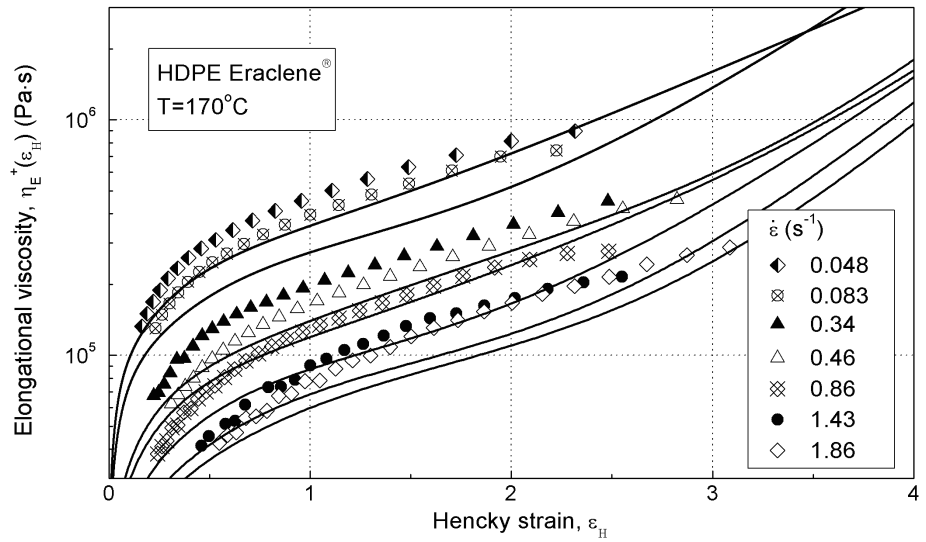


Figure 5.22: Same as in Fig. 5.21 but with respect to the Hencky strain.

Chapter 6

Discussion

6.1 The Relaxation Spectrum

Strain damping does not occur in the small angle oscillatory shear measurements, as they are performed within the linear viscoelastic regime (LVE). Thus, the dynamic mechanical analysis provides information purely on the linear viscoelastic response of the melt. A relaxation spectrum with 6 Maxwell elements (G_i, τ_i) was determined for each melt. A limited number of modes was decided in order to facilitate the calculations and to reduce computational time. The zero shear viscosity evaluated from these relaxation spectra

$$\eta_0 = \sum_{i=1}^6 \tau_i G_i \quad (6.1)$$

was estimated to be $\approx 1,1 \cdot 10^5$ (Pa·s) in the case of the LDPE Riblene and $\approx 2,7 \cdot 10^5$ (Pa·s) in the case of the HDPE Eraclene melt. These predictions deviate from the values estimated using the empirical Cross viscosity model (see Table 5.1) at the same temperature for each sample by 12.9% and 27.2% respectively. These deviations may be due to the limited number of relaxation modes used to describe the linear viscoelastic behaviour of the melts or the empirical nature of Cross's model. Adding more modes may provide a better estimate of the value of the zero shear viscosity. However, even the addition of more modes may not improve the results because rheological data at low enough frequencies were not obtained and the curvature of the viscosity curve at the onset of the Newtonian plateau was not determined experimentally with accuracy.

An *average relaxation or disengagement time* may be calculated for the two melts through

$$\tau_0 = \frac{\sum_{i=1}^6 G_i \tau_i^2}{\sum_{i=1}^6 G_i \tau_i} . \quad (6.2)$$

This averaged relaxation time corresponds roughly to the longest relaxation time for reptation of the chains out of their confining tubes. For the Riblene melt this was found to be $\tau_0=60.9$ s, lower than $\tau_0=71.3$ s for the Eraclene melt.

6.2 Thermorheological Complexity of Commercial PEs

Useful information about the microstructure of the polymeric melts can be derived from dynamic mechanical analysis data. The shape of the curve of the loss angle, $\delta = \arctan(G''/G')$ as a function of the reduced angular frequency, and the relative values at low and high frequencies provide information about the polydispersity and the existence of long chain branching in the melts [4].

The curves of δ vs. $\omega\alpha_T$ are shown in Fig. 6.1 for both the LDPE and HDPE melts. When the polydispersity of the polymer increases, the loss angle at low frequencies lies relatively low (lower than 90°). Thus, the values of δ at low frequencies for both melts in Fig. 6.1 indicate relatively high polydispersity in the molecular weight distribution of the two polymers, with HDPE being more polydisperse.

The shape of the curve in Fig. 6.1 (whether it is concave or convex and whether inflection points exist) can give some information on the structure of the macromolecular chains. The concave shape of the curve of LDPE is characteristic of a highly branched polymer. This plateau appearing at moderate frequencies indicates the formation of a *physical gel*. The relaxation behaviour of this physical gel is bounded by two characteristic relaxation times (the two inflection points that define the limits of the plateau) corresponding to the crossover to different relaxation mechanisms. This probably has to do with the non-permanent nature of the gel formed, which is essentially based on the entanglements involving the branches [4]. On the other hand, the curve of the HDPE is mostly convex. This is an indication of linear chains. The inflection point at $\omega\alpha_T \approx 0.2$ rad/s, however, may indicate that there are also a few long chain branches in this polymer. A wider frequency range at the corresponding temperatures could provide a clearer view of the behaviour of the polymers and clearer indications for their polydispersity and molecular structure.

Polymers with complicated molecular structure, such as long chain branching, are not thermorheologically simple materials. Thus, the time-temperature superposition of their dynamic moduli curves may not be very successful. The degree to which superposition is successful is rarely judged on the basis of an objective criterion [32]. Wood-Adams and Costeux [52] proposed the use of linear scales to detect the *thermorheological complexity* of polymer melts. Such plots are provided in Fig. 6.2 for the two polymers. The horizontal shift factors for these plots were the zero shear viscosity at each temperature evaluated from the complex viscosity data fitted to the Cross viscosity model.

Wood-Adams and Costeux showed that for a linear polymer the corresponding curves should superpose exactly. This is obviously not the case for the LDPE melt. The curves corresponding to 130°C and 190°C deviate significantly from the rest with increasing frequency. In the case of the HDPE melt, the curve corresponding to 150°C also deviates from the rest, although not in such an extreme manner as in the case of the LDPE melt. However, this is the case of thermorheological complexity and as mentioned in Wood-Adams and Costeux [52] it is indicative of the presence of long-chain branching in the melt. On the other hand, short-chain branching (SCB) has been experimentally verified not to alter the behaviour of the loss angle against frequency [53].

Another simple and direct technique for detecting complexity is the use of van

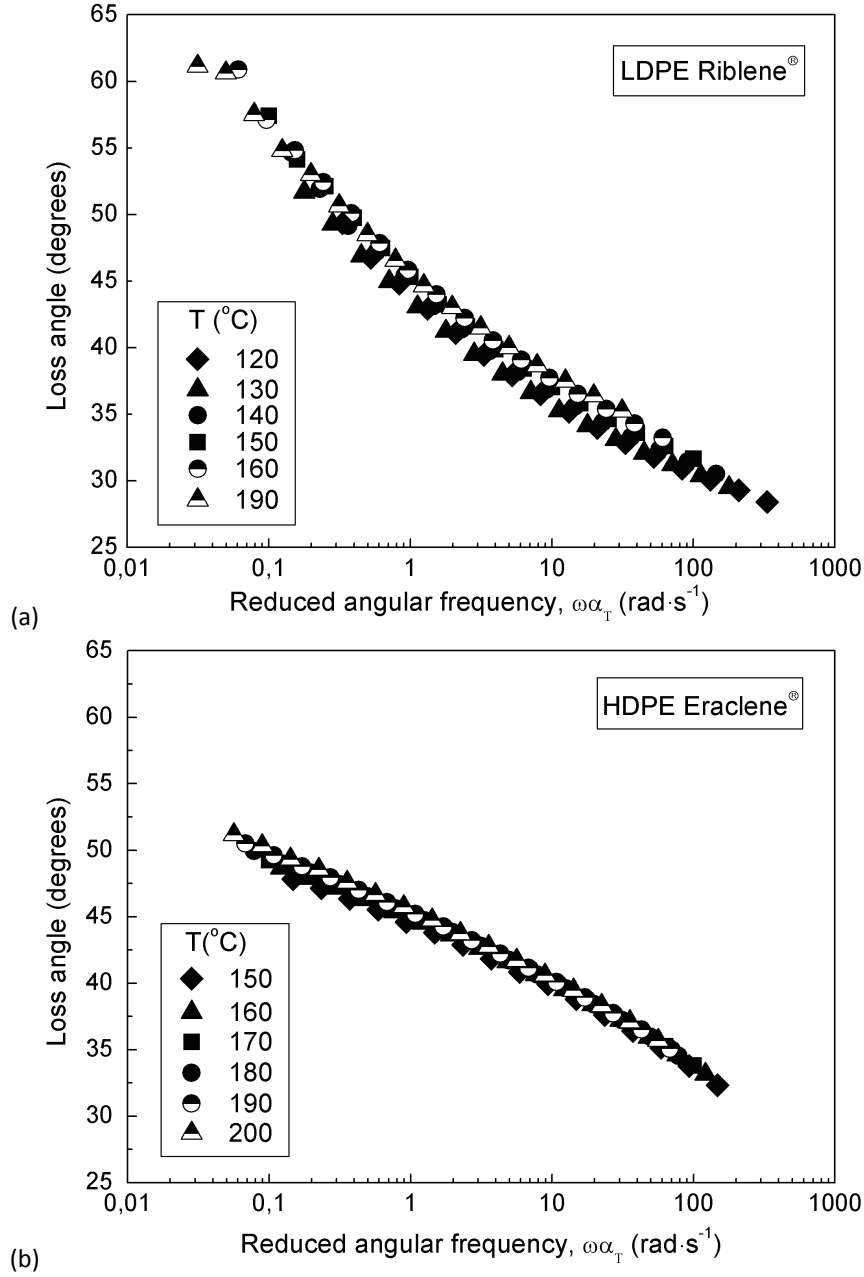


Figure 6.1: Superimposed plots of the loss angle, $\delta=\arctan(G''/G')$ for the (a) LDPE Riblene and (b) HDPE Eraclene against the reduced angular frequency.

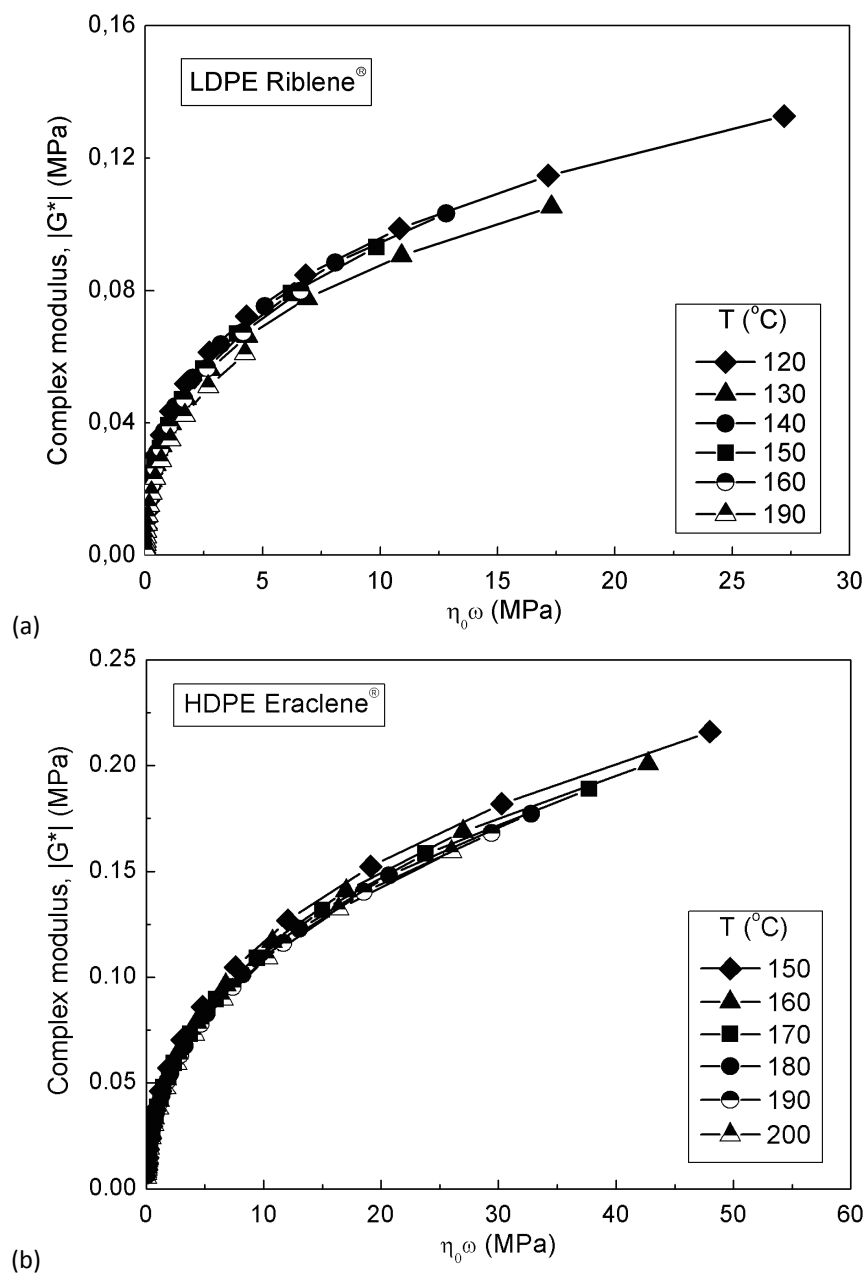


Figure 6.2: Demonstration of the complex thermorheological behaviour of the (a) LDPE Riblene and (b) HDPE Eraclene melts.

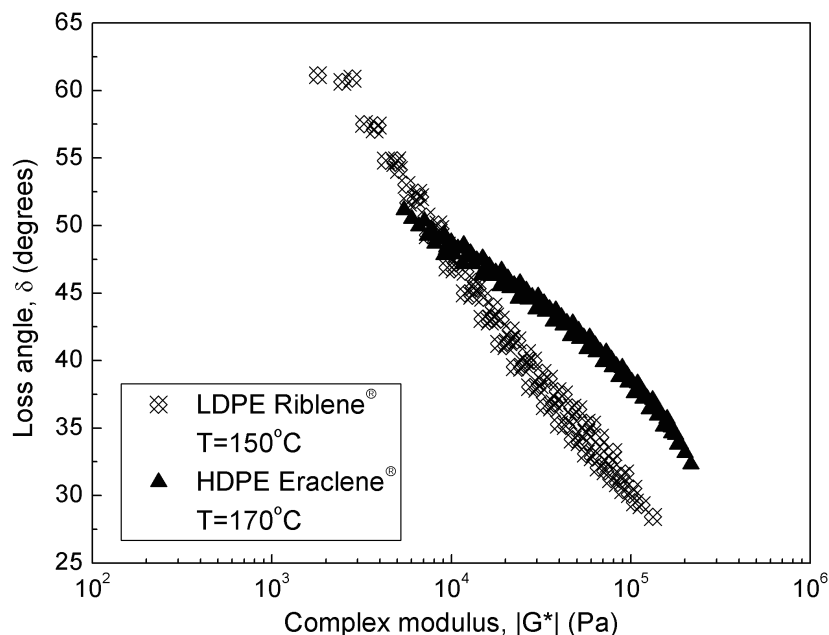


Figure 6.3: Van Gorp-Palmen plot for the two PE resins examined at the corresponding isothermal conditions.

Gorp-Palmen plots [73]. These are parametric graphs that show the loss angle, $\delta(\omega)$ plotted against the magnitude of the complex modulus, $|G^*(\omega)|$, with frequency as the parameter. The resulting curves, thus, show the relative elasticity of the material normalised by its modulus at a wide frequency range. This plot is provided for both resins in Fig. 6.3.

If the frequency range examined is wide enough, the curve decreases with $|G^*(\omega)|$, reaches a minimum at a value of $|G^*(\omega)|$ that is approximately equal to G_N^0 , and then increases again. In the case of the HDPE Eraclene the van Gorp-Palmen plot shows the typical behaviour of a linear HDPE with increased polydispersity [64], whereas the LDPE Riblene melt shows the curve of a long-chain branched polymer [19, 20]. However, the frequency range of the experimental investigation has to be much wider for a meaningful comparison with published data and to extract safe conclusions about the molecular nature of the melts. To conclude, within the limits of the current experimental investigation, the technique proposed by Wood-Adams and Costeux is the most distinctive when it comes to the molecular architecture of the melts.

The presence of LCB in commercial linear polymers such as the HDPE melt examined in this work, is not surprising. Vega et al. [31] have also reported a lot of commercial metallocene-catalysed HDPE-hexene copolymers containing or suspected to contain long chain branches. The flow activation energy of the HDPE Eraclene agrees well with the values of these copolymers with comparable molecular weight and poly-

dispersity. Further, the increased flow activation energy calculated for the LDPE Riblene agrees with what should expect from the increased polydispersity and long chain branching content of the polymer.

6.3 The Damping Function

The “memory loss” that is related to large strains was quantified for both resins through the exponential damping function, $h(\gamma_0) = \exp(-n\gamma_0)$ for shear deformation and $h(\epsilon_H) = \exp(-m\epsilon_H)$ for extensional flow. The latter is equivalent to the form proposed by Tsenoglou, $h(\lambda) = \lambda^{-\beta}$ for $m = \beta$.

The two adjustable parameters, n and m (or β) were evaluated using three different methods :

1. From step-strain experiments in shear.
2. From the complex viscosity master curves evaluated from small angle oscillatory shear measurements.
3. From uniaxial extensional flow measurements using the method proposed by Wagner [44].

These parameters may differ in their values at different types of flow (shear or elongational). According to the temporary network model this is attributed to the relative amount of permanent network destruction achieved for the same deformation under different flows.

6.3.1 Damping Function from Shear Flow Measurements

The experimentally determined values of the damping function for the LDPE Riblene evaluated from single step-strain in shear measurements are provided in Table 5.5. A graphical representation of the data along with the corresponding fit of the single exponential damping function is given in Fig. 5.11. A value of $n = 0.23$ for this exponential form was found to fit the data at higher strains, while $n = 0.25$ was the value that best fits the complex viscosity master curve at the same temperature, according to the predictions of the temporary network model (using Eq. 3.53 and shown graphically in Fig. 5.7). These values seem close to each other, given the uncertainties inherent in the curve fitting procedures. The small difference is probably due to the estimation of the exponent from the step-strain measurements, which were limited to relatively low strains (≤ 2 s.u.). On the other hand, the single exponential damping function in shear is valid up to ≈ 10 s.u. thus a better estimate of the exponent should be obtained if higher strain magnitudes were included. It should be noticed that such a problem was not encountered during the evaluation of the damping function exponent from the uniaxial elongational experiments for both resins since the single exponential damping function in the latter case is considered to be valid up to ≈ 2 s.u. while the total elongation achieved was always more than that.

A comparison between the values of the exponent of Wagner’s damping function obtained for the LCB and linear PEs from Tsenoglou (see Table 3.3) and those obtained

for the two commercial polymers that were examined in this work verifies the general expectation that LCB polymers show much less damping in shear than do melts composed of mostly linear chains. The corresponding values of the exponential damping function of the LCB melts remain lower than those obtained for linear polymers. The value of $n = 0.25$ for the LDPE Riblene melt is much higher than the values tabulated in Table 3.3 for LCB melts, while it is still lower than the lowest value of $n = 0.28$ obtained for the commercial HDPEs (from the same work). On the other hand the $n = 0.28$ value obtained for the HDPE Eraclene melt lies within the region of values obtained for the commercial HDPEs.

6.3.2 Damping Function from Extensional Flow Measurements

The results for the damping function of the LDPE Riblene and HDPE Eraclene melts are provided in Tables C.3 and C.4 of Appendix C, respectively, and graphically in Fig. 5.16. The power-law exponent of $h(\lambda)$ was determined to be $\beta=0.25$ for the LDPE and $\beta=0.40$ for the HDPE melt.

A comparison between β for the HDPE Eraclene melt and the values obtained for the melts of Table 3.6 reveals that linear polymer melts, such as the *PS.50124*, *PS.606*, *PS.I* and *HDPE.S*, have values of β in the range 0.66 - 0.96, whereas for the HDPE Eraclene it is lower, $\beta=0.40$, even lower than the *IUPAC.A* melt, which is a highly branched LDPE. In general, linear polymer melts with low polydispersity should have $\beta \geq 1$ in uniaxial extension. These melts seem to break the rule because of the increased molecular weight polydispersity or the possible presence of sparse long-chain branching.

A comparison between the power-law and Wagner's damping function in elongation reveals major differences between the two. Wagner's model includes the parameter, α in the damping function (see Eqs. 3.56 and 3.57) and provides a different fit to the data. Wagner's damping function is not followed by an microstructural explanation of the adjustable parameters, m and α and is considered to be a phenomenological description of the rheological behaviour of the melt. The power-law damping function is also an empirical model but the values of β have been related with the long chain structure (B_n) through the studies of Gotsis et al. [14, 5, 6]. Furthermore the incorporation of the parameter α into Wagner's single exponential approximation predetermines that a steady state is reached (see Fig. 3.5), while the unattainability of a steady state has been observed for several melts. The difference between the two damping functions in elongation is clear and the power-law provides an advantageous starting point for describing rheological data in the context of rubber-like liquid theories and their extensions.

The uniaxial extensional data were finally used to test the predicting capabilities of the Doi-Edwards constitutive equation, as well as the modified version of the theory that has been proposed by Tsengoglou for commercial long-chain branched polyethylenes. The Doi-Edwards universal orientation tensor in the case of uniaxial extension has been provided in analytical form by [50, 22, 39]

$$f(\lambda) = \left(\frac{15}{8} \right) \frac{(2\lambda^3 + 1)}{(\lambda^3 - 1)} \left(\frac{1}{1 + A(\lambda)} \right) \left(1 - \left(\frac{4\lambda^3 - 1}{2\lambda^3 + 1} \right) A(\lambda) \right), \quad (6.3)$$

where

$$A(\lambda) = \frac{\sinh^{-1} \sqrt{\lambda^3 - 1}}{\sqrt{\lambda^3(\lambda^3 - 1)}} \quad (6.4)$$

and $\lambda = \exp \epsilon_H$. In the case of the modified version the above relations translate to

$$\underline{\underline{\sigma}} = \int_{-\infty}^t \mu(t - t') f(\lambda) \left(\frac{1}{[(1 - x_n) + \frac{x_n}{\langle \underline{\underline{E}} \cdot \underline{\underline{u}} \rangle}]^2} \right) dt' , \quad (6.5)$$

where

$$\langle \underline{\underline{E}} \cdot \underline{\underline{u}} \rangle = \frac{1}{2} \lambda (1 + A(\lambda)) . \quad (6.6)$$

These forms correspond to the rigorous approach, whereas the IAA is also provided in analytical form [50, 22, 39] and an analogous procedure is then followed if one wants to use the modified version instead. The tensile stress in the rigorous approach is evaluated from

$$\sigma_T = \sigma_{11}(t, \dot{\epsilon}) - \sigma_{22}(t, \dot{\epsilon}) = G(t) f(t) + \int_0^t \mu(s) f(s) ds \quad (6.7)$$

with $s = t - t'$. The integral may be solved numerically using a simple trapezoid integration routine and the corresponding viscosity growth values are computed for each strain rate by dividing the resulting tensile stress values with the corresponding strain rate.

The predictions of the theory with respect to the damping function in uniaxial elongation assume the form

$$h_{DE}(\epsilon_H) = f(\lambda) \left(\frac{\lambda}{\lambda^3 - 1} \right) , \quad (6.8)$$

whereas for the modified version this result translates to

$$h_{DE}(\epsilon_H) = f(\lambda) \left(\frac{\lambda}{\lambda^3 - 1} \right) \left(\frac{1}{[(1 - x_n) + \frac{x_n}{\langle \underline{\underline{E}} \cdot \underline{\underline{u}} \rangle}]^2} \right) . \quad (6.9)$$

The predictions of both the DE model and the modified version are provided for both melts in Fig. 6.4. The corresponding predictions for the tensile viscosity growth are provided in Fig. 6.5, 6.6, 6.7 and 6.8 with respect to time and Hencky strain.

Regarding the interpretation of the experimental results under the Doi and Edwards theoretical scheme, it should be mentioned that the milder nonlinear behaviour of the LDPE Riblene melt (see Fig. 6.4-(a)) is attributed to the presence of long chain branches in the melt. On the other hand, if milder nonlinear behaviour is seen for HDPE melts, it is usually attributed to the strain induced crystallisation of the melt in the elongational flow that enhances the melt strength and increases its elasticity [2]. The milder nonlinear behaviour of the HDPE-hexene copolymer studied in this work (see Fig. 6.4-(b)), however, cannot be attributed to crystallisation. Orientation of the coiled macromolecules for this type of melt is rather hindered due to the presence of

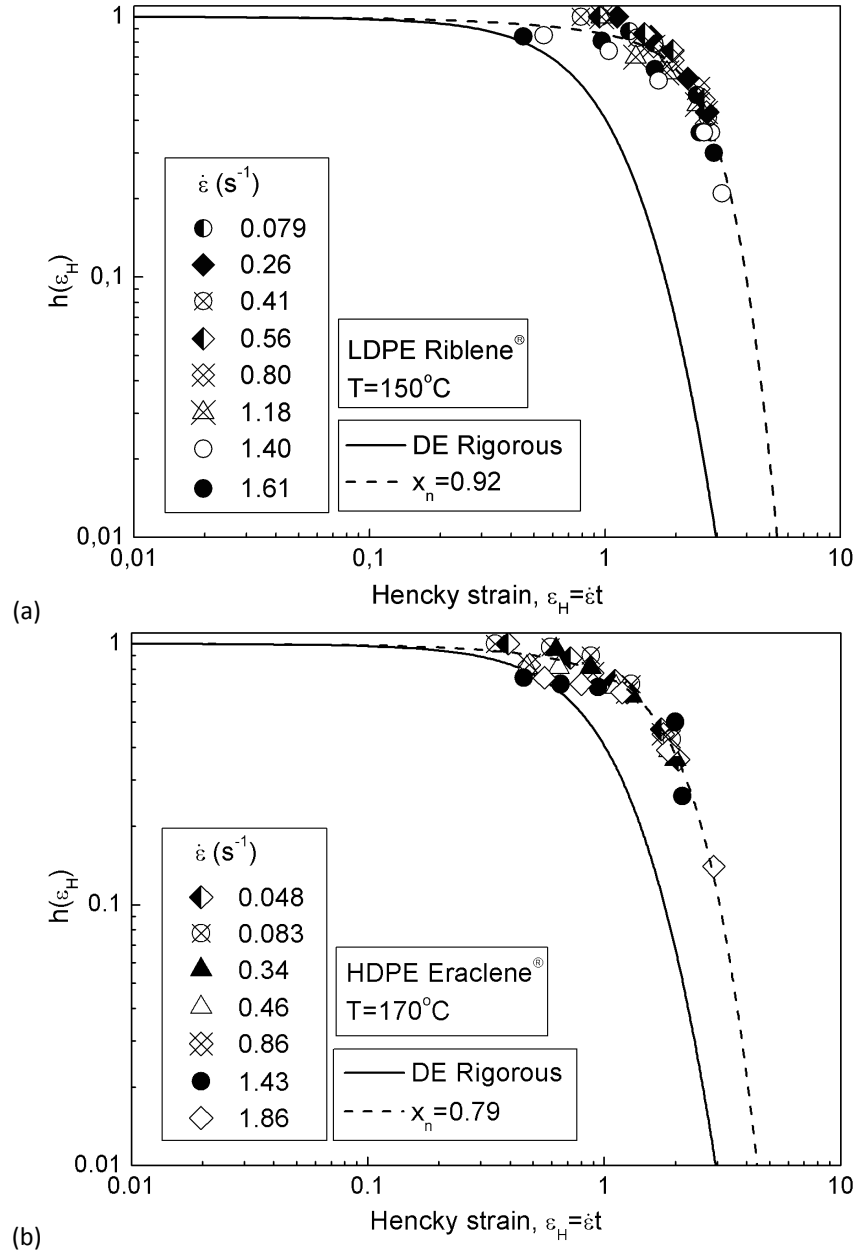


Figure 6.4: Damping function in extensional flow for (a) LDPE Riblene and (b) HDPE Eraclene melts at the corresponding temperatures. The nonlinear viscoelastic parameter in the case of the long-chain branched LDPE assumes a value of $x_n = 0.92$ whereas in the case of the HDPE-hexene copolymer a value of $x_n = 0.79$.

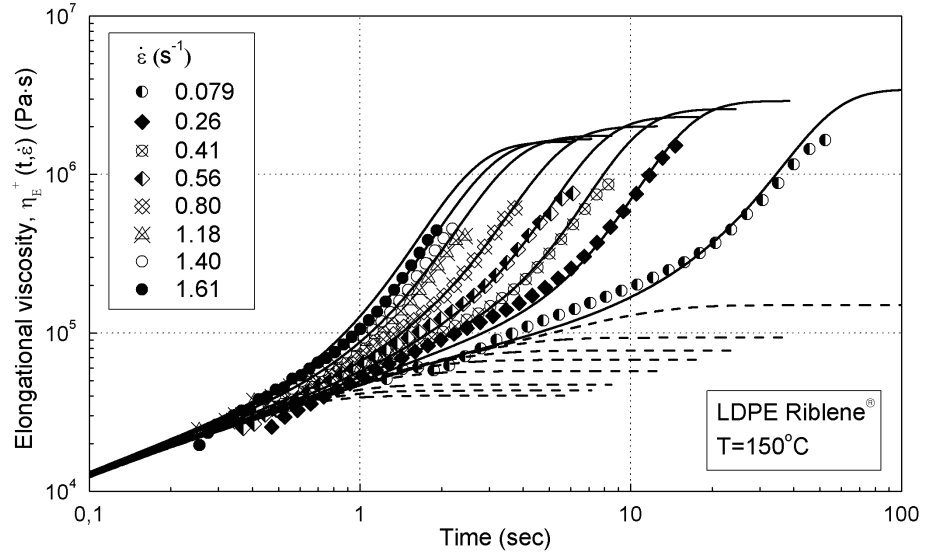


Figure 6.5: Predictions of the Doi-Edwards model (dashed lines) and the modified Doi-Edwards model (solid lines with $x_n = 0.92$) for the uniaxial extensional viscosity of the LDPE Riblene melt at $T=150^\circ\text{C}$ with respect to time.

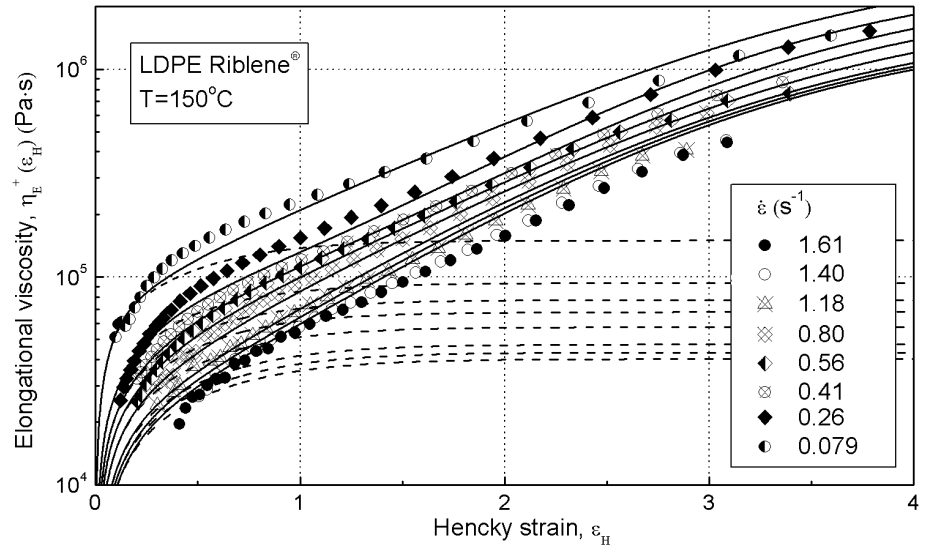


Figure 6.6: Same as in Fig. 6.5 but with respect to Hencky strain.

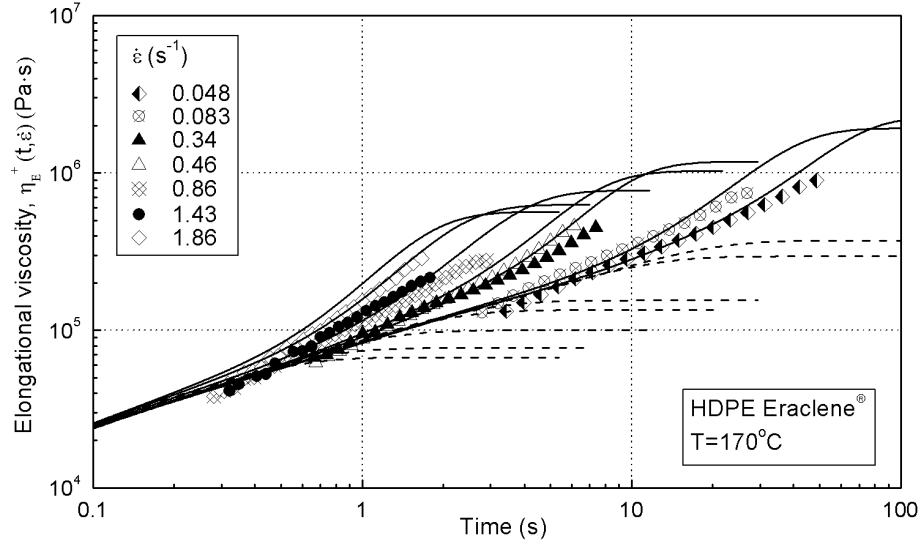


Figure 6.7: Predictions of the Doi-Edwards model (dashed lines) and the modified Doi-Edwards model (solid lines with $x_n = 0.79$) for the uniaxial extensional viscosity of the HDPE Eraclene melt at $T=170^\circ\text{C}$ with respect to time.

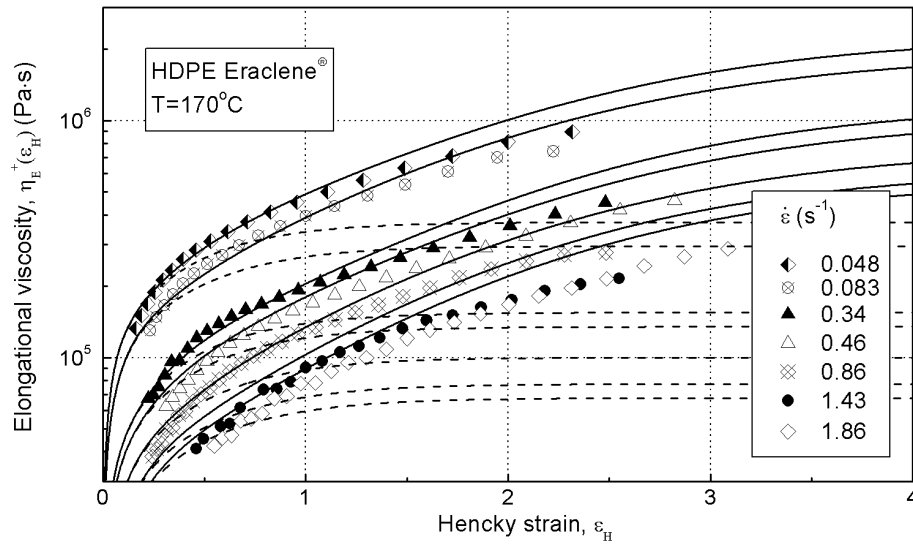


Figure 6.8: Same as in Fig. 6.7 but with respect to Hencky strain.

the hexene sidearms on the backbone of the linear chain. The milder nonlinear behaviour should rather be attributed to the presence of some long chain branching and to the increased polydispersity of the melt. It seems, thus, reasonable to apply the modified version of the Doi-Edwards theory to the experimental results of this melt and obtain a value of the nonlinear viscoelastic parameter, $x_n = 0.79$.

6.4 LCB and Rheology

Various methods of detecting LCB content in commercial polymer melts have been suggested in Section 6.2. In addition, the determination of the branching content using rheological data only, is also suggested in the foregoing sections.

6.4.1 Estimating B_n from Rheological Data

Estimation of the branching content, B_n of the LDPE Riblene melt, within the theoretical context of the power-law damping function, is not possible as the parameter a_{ul} is not known. However, rheological models such as the “pom-pom” model may be able to achieve this goal. The eXtended Pom-Pom (XPP) model was used to fit the uniaxial extensional data of the commercial LDPE Riblene and HDPE Eraclene melts. The fit of the model is provided in Figs. 5.17-5.18 for the LDPE and Figs. 5.19-5.20 for the HDPE. The fitting parameters are given in Tables 5.6 and 5.7 respectively. The number of dangling arms, $q_{x,i}$ at the periphery of the pom-pom molecule provide an indirect measure of branching in the melt. In the case of the LDPE, depending on how one places the arms in each mode, a branching content of $10 \leq B_n \leq 12$ is assigned on average in every molecule in the melt. These values correlate well with the estimated value of 8.8 from Table 4.1. Besides, the B_n estimate from the GPC measurements may also be subject to small variations depending on how one correlates the value of the g_s parameter with the value of the g'_s through Eq. 2.12.

Further, fitting the uniaxial extensional data of the HDPE melt with the XPP model reveals the presence of some long chain branching in this melt because the $q_{x,6}$ parameter of the model (see Table 5.7) is $\neq 1$. However, it is not possible for the model to estimate LCB content with $B_n \leq 2$ and a good estimate of the LCB content of the HDPE melt is not possible.

The influence of the anisotropy parameter, α_x on the predictions of the XPP model where investigated by Verbeeten et al. [76]. It was found that the influence of α_x on the viscosity, η , is rather small. The parameter α_x mostly influences the second normal stress coefficient, Ψ_2 : $\alpha_x = 0 \Rightarrow \Psi_2 = 0$. Furthermore, the parameter α_x has almost no influence on the first planar viscosity, but a significant influence on the second planar viscosity. In the absence of normal stress difference or planar viscosity data, the value of the parameter, α_x was set to the default value, $0.1/q_{x,i}$. One can avoid the use of this parameter in the expense of not predicting a second normal stress coefficient, Ψ_2 . Furthermore, as it has already been mentioned, the influence of this parameter in the predictions of the model is rather small, thus, the calculations of Tables 5.6 and 5.7 are considered to be valid.

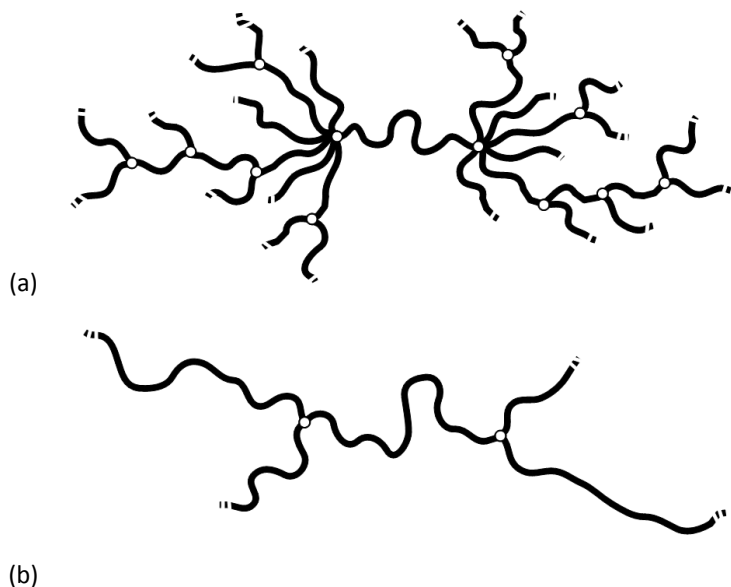


Figure 6.9: Demonstration of one possible distribution of the dangling arms on the periphery of the pom-pom molecule for the (a) LDPE Riblene with $B_n = 12$ and (b) HDPE Eraclene with $B_n = 2$.

6.4.2 Correlation between B_n and x_n

In a recent publication, Tsenoglou et al. [13, 12] suggested that the nonlinear viscoelastic parameter, x_n , in eq. 3.107 of the modified DE theory (which is actually a measure of the internal branching of the melt) should correlate with the branching content of the melt. Thus, merging the available data for commercial LDPEs from Tsenoglou with those reported from Kasehagen in Table 3.5 for commercial PBs of varied branching content, one ends up with a plot that shows a pattern relating the amount of internal branching and the actual branching content (measured independently, i.e. from GPC) shown in Fig. 6.10. This pattern spans the range of branching from as low as 0.1 to as high as 80 branches on average per molecule.

In addition, all the available rheological data of the modified LCB PPs (see Tables 3.7 and 3.8) may be translated (with a grain of salt) into the nonlinear viscoelastic parameter, x_n . This is mostly because the power-law damping function is of an exponential form, whereas the modified DE damping function is of a sigmoidal form. This in turn gives accurate results when $\beta \leq 0.5$ but may result in small errors (of the order of not more than 20%) when $\beta \geq 0.5$. The result is shown in Fig. 6.11.

The values of the nonlinear viscoelastic parameter, x_n that correspond to each sample of those in Figs. 6.10 and 6.11 are provided in Tables 3.9, 6.2 and 6.3. A comparison between all samples is made in Fig. 6.12 by adjoining the data from Figs. 6.10 and 6.11. It is obvious from this plot that in the case of the PP samples the x_n parameter changes in a very abrupt way with the branching content and saturates at

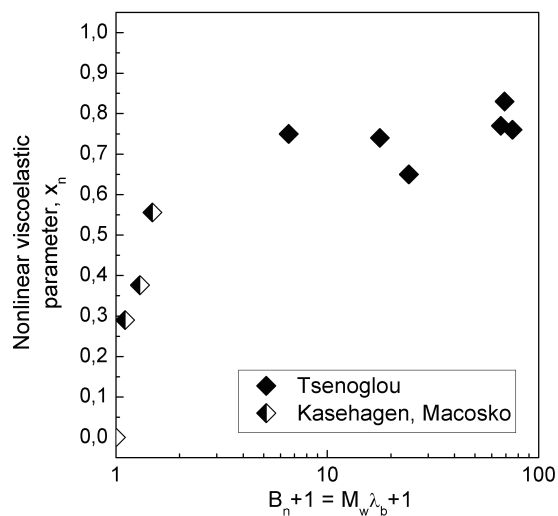


Figure 6.10: The nonlinear viscoelastic parameter, x_n as a function of the branching number, B_n for selected commercial LDPE and PB melts of varying branching content. Tsenoglou's parameter, x_n represents the amount of internal branches in the polymeric structure. It is inferred from rheological data only.

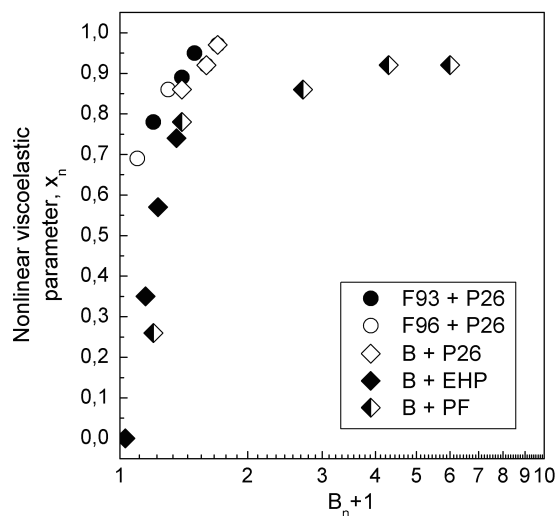


Figure 6.11: The nonlinear viscoelastic parameter, x_n as a function of the branching number, B_n for commercial LCB PPs including those of Table 6.1.

Table 6.1: Molecular data for melts of B/EHP blends from Lagendijk et al. [61]. The commercial linear precursor B was modified using varying amounts (mmol/100 gr PP) of EHP peroxydicarbonate.

Sample	EHP (mmol)	M_w (Kg/mol)	(M_w/M_n)	B_n	β
B	0	410	5.5	0	1.1
	0.5	400	5.7	0.03	0.95
	1	410	6.6	0.15	0.75
	2	460	6.8	0.23	0.6
	3	485	6.8	0.36	0.45

Table 6.2: PB samples from Kasehagen et al. and the corresponding x_n values for each sample.

Sample	B_n	α_p	x_n
PB	0	3.9	0
	0.11	6.5	0.29
	0.30	8.0	0.38
	0.49	14.5	0.56

Table 6.3: PP samples from Gotsis et al. and the corresponding x_n values for each sample.

Sample	B_n	β	x_n	Sample	B_n	β	x_n
B+P26	0	1.0	≈ 0	F93+P26	0	1.8	-
	0.4	0.3	0.86		0.2	0.4	0.78
	0.6	0.2	0.92		0.4	0.25	0.89
	0.7	0.1	0.97		0.5	0.15	0.95
	0.8	0.0	-		0.6	0.20	0.92
B+EHP	0	1.1	≈ 0	F96+P26	0	0.7	-
	0.03	0.95	≈ 0		0.1	0.5	0.69
	0.15	0.75	0.35		0.3	0.3	0.86
	0.23	0.6	0.57		0.5	0.15	0.95
	0.36	0.45	0.74		0.7	0.1	0.97
B+PF	0	1.0	≈ 0				
	0.2	0.8	0.26				
	0.4	0.4	0.78				
	1.7	0.3	0.86				
	3.3	0.2	0.92				
	5.0	0.2	0.92				

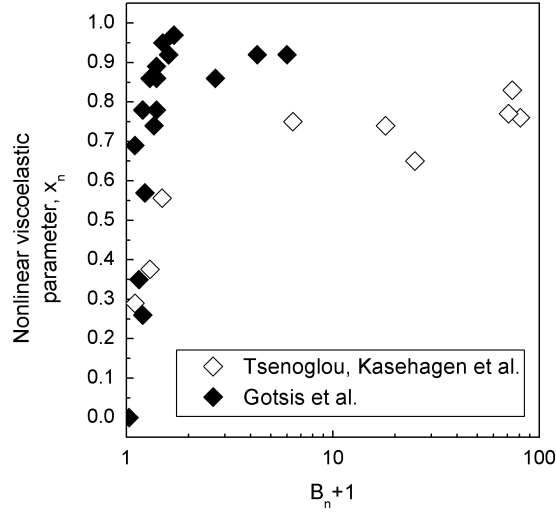


Figure 6.12: The nonlinear viscoelastic parameter, x_n as a function of the branching number, B_n for the melts of Figs. 6.10 and 6.11.

$B_n \leq 10$. On the other hand, in the case of the PB and LDPE samples, the form of $x_n(B_n)$ is more gradual at $B_n \leq 10$ and saturates at lower values of x_n for $B_n > 10$. It is not clear though, if this difference is due to the type of flow, the type of the polymer, the branching architecture or the experimental method that was used in order to produce the branching structure etc.

6.4.3 Correlation Between x_n and the Branching Structure

A *dendrimer* is a repetitively branched compound. A tree-like polymer is a type of dendrimer. A *Cayley tree* or *Bethe lattice* is a special type of a regular dendrimer (see Fig. 6.13). For such a polymer we can define the *number of segments*, sgm in each generation of the tree and the total number of segments in the tree (from the core to generation g_n). The following expression may be derived using the sum of a geometric series

$$sgm(g_n) = f \left(\frac{1 - (f - 1)^{g_n}}{2 - f} \right), \quad (6.10)$$

which is valid for $g_n \geq 1$, while $sgm(g_n)=0$ for $g_n=0$. The total number of branching points, B_n per branched molecule (assuming that all branching points have the same constant functionality) is

$$B_n(g_n) = 1 + f \left(\frac{1 - (f - 1)^{g_n - 1}}{2 - f} \right), \quad (6.11)$$

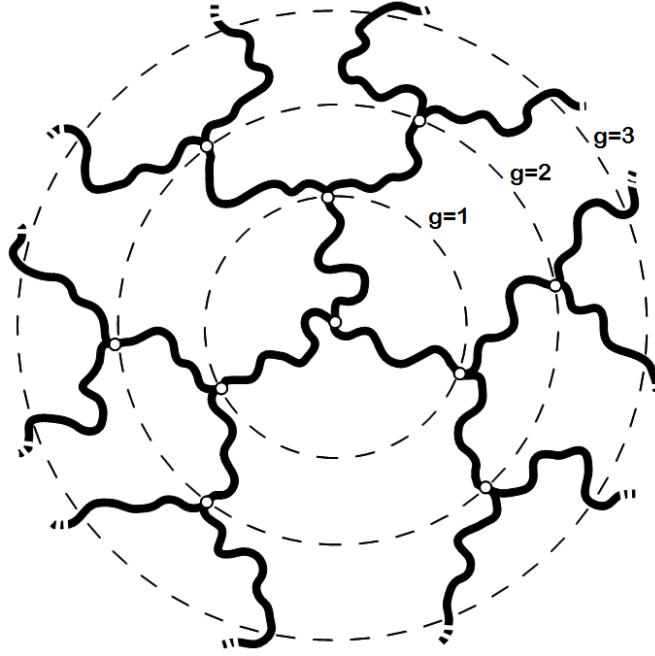


Figure 6.13: A Cayley-tree or Bethe lattice of constant branch point functionality, $f = 3$ and generation, $g_n=3$. The nonlinear viscoelastic parameter for this structure is $1/2$ while for commercial PEs it is lower ($\approx 3/4$).

Table 6.4: Calculated parameter values of the Cayley-tree model for the commercial LDPE samples from Tsenoglou. The last column is the relative error between the x_n value calculated from the model and the actual value (see Table 3.9) inferred from the experiment.

Sample	B_n	functionality, f (from Eq. 3.108)	$\text{sgm}(g_n)$	g_n	x_n	% difference from experiment
LDPE.A2	80	2.3	106.3	9.9	0.74	2.6
LDPE.A4	73	2.2	88.95	11.9	0.81	2.4
LDPE.A7	70	2.3	91.9	9.8	0.75	2.6
LDPE.B2	17	2.35	24	5.05	0.67	9.5
LDPE.C2	5.4	2.33	8.2	2.7	0.54	28
LDPE IUPAC A	24	2.54	37.9	5.11	0.61	6.1

Table 6.5: Calculated parameter values of the Cayley-tree model for the commercial LDPE samples from Tsenoglou. The last column is the relative error between the x_n value calculated from the model and the actual value (see Table 3.9) inferred from the experiment.

Sample	B_n	functionality, f (from Eq. 6.14)	$sgm(g_n)$	g_n	x_n	% difference from experiment
LDPE.A2	80	2.3	103.9	10.5	0.76	0
LDPE.A4	73	2.2	86.7	12.9	0.83	0
LDPE.A7	70	2.3	89.6	10.4	0.77	0
LDPE.B2	17	2.2	21.6	5.8	0.74	0
LDPE.C2	5.4	1.9	5.9	3.5	0.75	0
LDPE IUPAC A	24	2.4	35.4	5.5	0.65	0

which is valid for $g_n \geq 1$, while $sgm = 0$ for $g_n=0$. Multiplying both sides of Eq. 6.11 by $(f - 1)$ and performing the appropriate calculations, it may easily be shown that

$$B_n = \frac{sgm(g_n) - 1}{f - 1} . \quad (6.12)$$

The fraction of chains corresponding to internal segments equals

$$x_n = 1 - \frac{f(f - 1)^{g_n - 1}}{sgm(g_n)} . \quad (6.13)$$

Making use of Eqs. 6.10, 6.11, 6.12 and 6.13, one may show that

$$x_n = \frac{1 - \frac{1}{B_n}}{(f - 1) + \frac{1}{B_n}} \quad \text{or} \quad f = \left(1 + \frac{1}{x_n}\right) \left(1 - \frac{1}{B_n}\right) , \quad (6.14)$$

from which Eq. 3.108 naturally arises as an approximation.

The predictions of this model provide an illustrative way to compare between long chain branched melts of varying branching content. The results are provided in Table 6.4.

The approximate expression Eq. 3.108 is a good approximation for large branching numbers ($B_n \geq 10$), while it fails for smaller branching numbers, ($B_n < 10$). This can be seen from the relative error introduced when comparing the experimentally determined value of the x_n parameter with the value calculated through the model for the sample LDPE.C2. The relative error introduced for this sample is $\approx 28\%$. However, if Eq. 6.14 is used instead of Eq. 3.108, then, for all samples of Table 6.4, one calculates instead the values of Table 6.5. A perfect reproducibility of the experimentally determined values of the nonlinear viscoelastic parameter, x_n , is achieved.

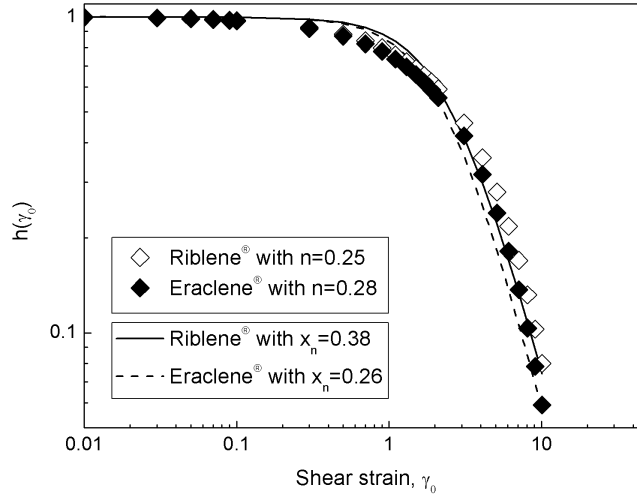


Figure 6.14: The single exponential damping function in shear for both LDPE and HDPE melts (symbols) and the modified Doi-Edwards damping function in shear (lines) for the same melts.

6.4.4 Correlation Between the Values of x_n Determined from Shear and Uniaxial Extensional Measurements

It has been suggested that the experimentally determined nonlinear viscoelastic parameter, x_n , is a measure of internal branching for commercial polymer melts. In fact, it is an exact measure of the ratio of internal (segments with both ends attached to a branch point) to external segments (segments with one free end). The correspondence between the experimentally determined values of the parameter, x_n and those predicted by the model has been demonstrated for the commercial LDPE samples from Tsenoglou (see Table 6.5).

While the parameter x_n is a measure of internal branching, it must have the same value irrespective of the deformation type. However, in the case of the LDPE Riblene melt, it was found that $x_n=0.92$ in uniaxial extensional measurements, while $x_n \approx 0.38$ in shear flow (see Fig. 6.14). In the case of the HDPE Eraclene melt, a value of $x_n=0.79$ best fits the uniaxial data, while $x_n \approx 0.26$ is the estimated value that best fits the shear data. This difference has to be resolved and a good starting point is to examine the thermodynamics of deformation within the context of the Doi-Edwards theory and its modified version.

The *free energy function* within the theoretical framework of the Doi-Edwards theory and for an arbitrary deformation type is given by [23]

$$A(\underline{E}) = \langle \ln |\underline{E} \cdot \underline{u}| \rangle. \quad (6.15)$$

In the case of a step-strain in shear deformation (assuming that the IAA is invoked in

order to derive the results) the above expression translates to

$$A(\gamma_0) = \frac{1}{2} \int_0^1 \ln \left(\frac{1 + \gamma_0^2 x^2 + \sqrt{x^4(\gamma_0^4 + 4\gamma_0^2) - 2\gamma_0^2 x^2 + 1}}{2} \right) dx, \quad (6.16)$$

while an analytical expression corresponds to the uniaxial extensional deformation (again within the IAA of the theory)

$$A(\lambda) = \ln \lambda + \frac{\arctan \sqrt{\lambda^3 - 1}}{\sqrt{\lambda^3 - 1}} - 1. \quad (6.17)$$

Both expressions provide a dimensionless measure of the free energy change per strain unit. A plot of both functions is provided in Fig. 6.15.

The predictions of the Doi and Edwards theory in shear and uniaxial extension are provided graphically in Fig. 6.16-(a) (within the IAA approximation in order to compare with Eqs. 6.16 and 6.17). These predictions are then plotted against the free energy change (that is needed in order to achieve a certain magnitude of strain) using the data from Fig. 6.15. The result is provided in Fig. 6.16-(b). The plot shows that the “memory loss” or the relative amount of permanent network destruction is related to the free energy change of the melt. The free energy change with a minus sign corresponds to the work done by the system (the rheometer in that case) in order to deform (shear or elongate) the melt. Thus Fig. 6.16-(b) shows that within the Doi and Edwards theory the “memory loss” or the relative amount of permanent network destruction is independent of the type of deformation (shear deformation or uniaxial extension). Consequently, the difference in the free energy change between a shear and a uniaxial extensional deformation (see Fig. 6.15) is attributed to the different amount of permanent network destruction achieved between different types of deformation. This characteristic behaviour is also predicted by the modified version of the theory with the incorporation of the nonlinear viscoelastic parameter, x_n . The predictions of the theory under different types of deformation are the same as long as x_n is the same for these different types of deformation (see Fig. 6.17).

On the other hand, the predictions of the modified temporary network model for the LDPE Riblene melt in shear and uniaxial extension are the same. This theory suggests that the “memory loss” or the relative amount of permanent network destruction is the same both in shear and uniaxial extension (since for the LDPE Riblene, $n = \beta = 0.25$) in contrast to the predictions of the Doi Edwards model.

Judging from the experimental results for the LDPE Riblene melt and assuming that within experimental error there is a difference between the predicted values of the x_n parameter in uniaxial extension and shear deformation, one unavoidably reaches to the conclusion that the Doi Edwards theory is an over-simplification of reality. The Doi Edwards theory assumption that the extra free energy (or work done by the system) needed to perform 1 s.u. in uniaxial extension, rather than 1 s.u. in shear deformation is wholly attributed to the amount of permanent network destruction seems to contradict the experimental evidence.

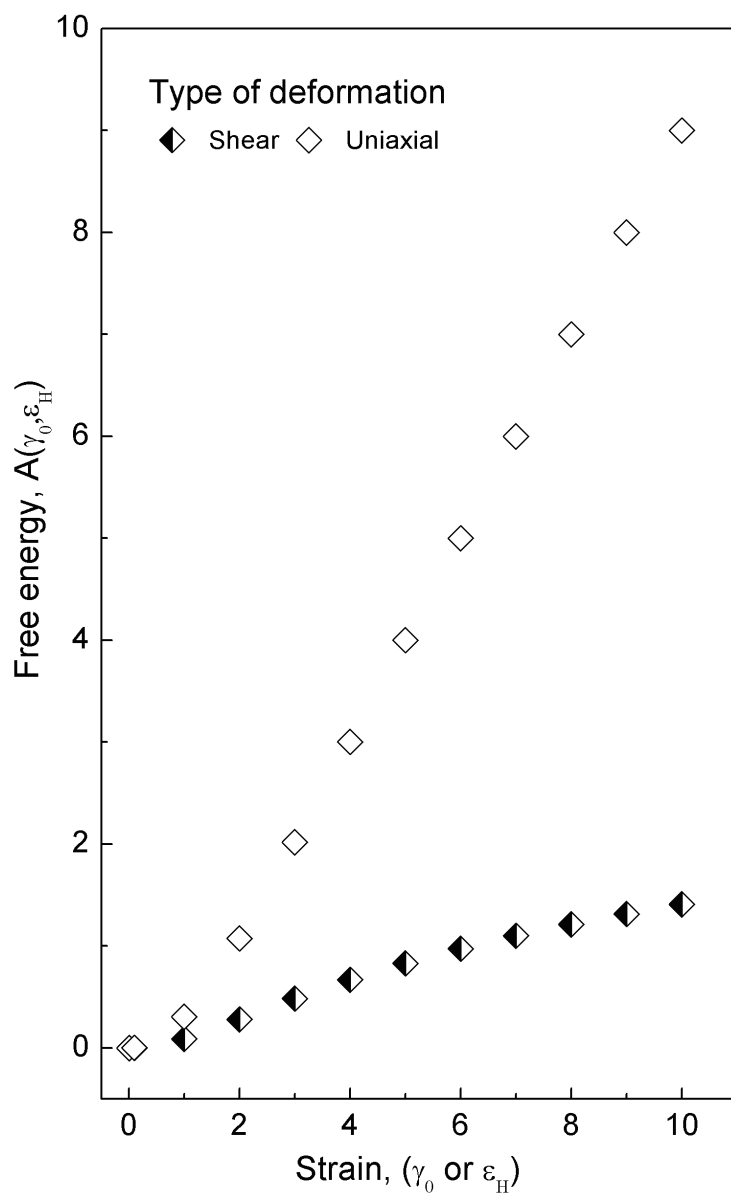


Figure 6.15: The free energy function, $A(\underline{E})$ in the Doi-Edwards theory for a step-strain in shear and a uniaxial elongational deformation.

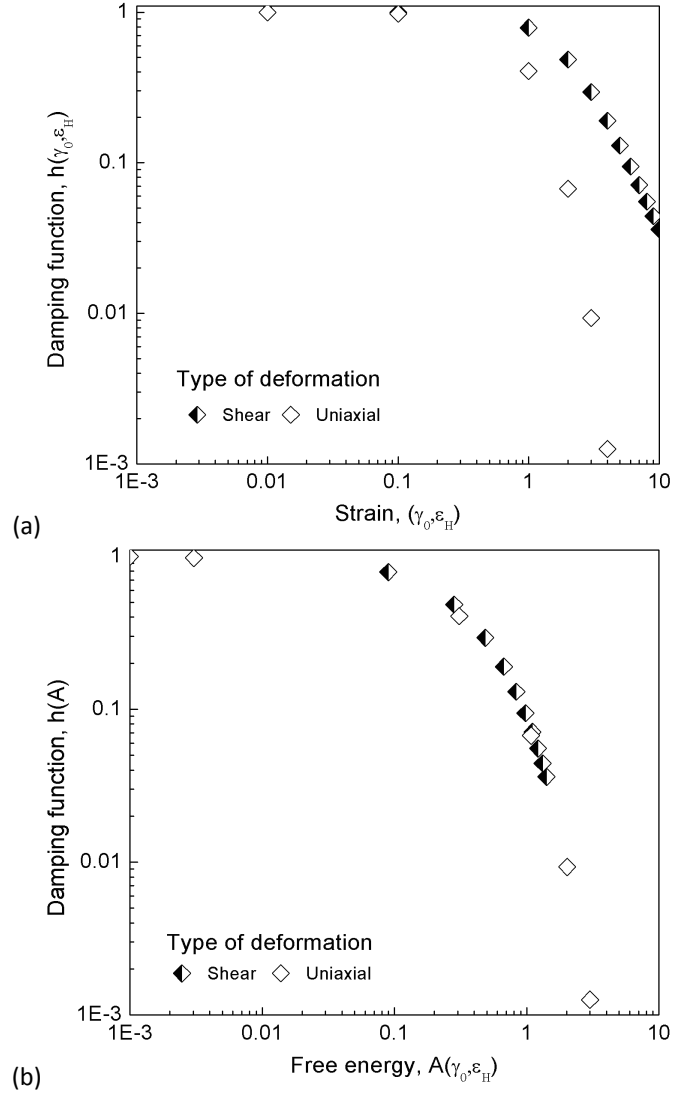


Figure 6.16: The predictions of the DE theory for the damping function, h_{DE} in shear and elongation, (a) with respect to the strain unit of elongation (γ_0 or ϵ_H), and (b) with respect to the change in the free energy, $A(\underline{E})$.

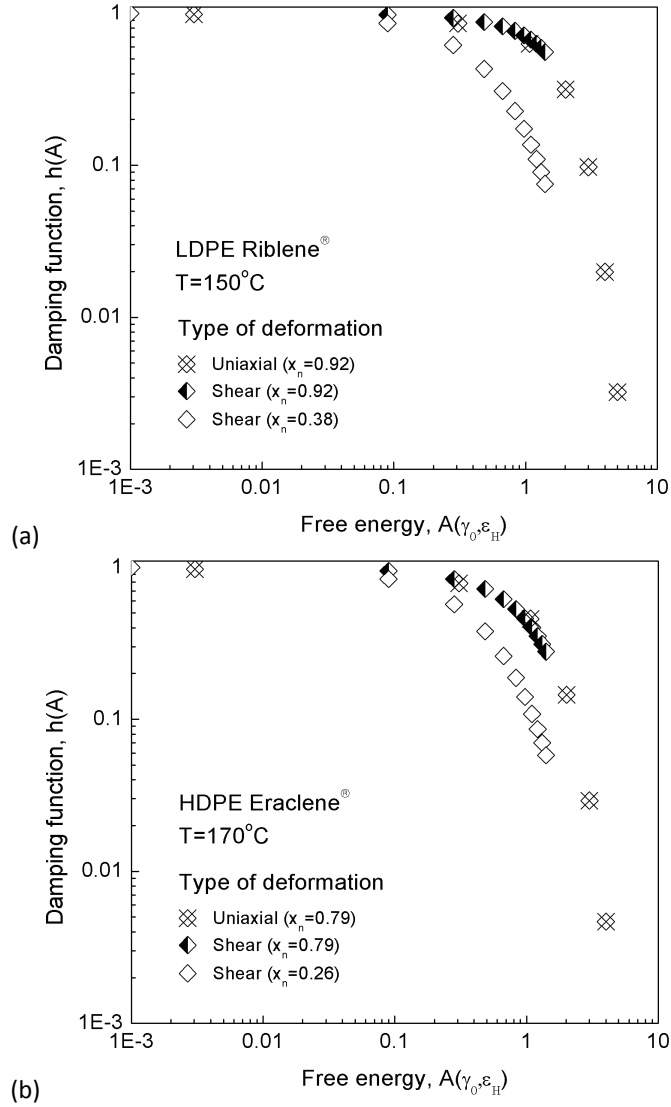


Figure 6.17: Predictions of the modified Doi and Edwards model for the (a) LDPE Riblene melt under shear deformation with $x_n \approx 0.38$ and uniaxial extension with $x_n=0.92$ and (b) HDPE Eraclene melt under shear deformation with $x_n \approx 0.26$ and uniaxial extension with $x_n = 0.79$. Plots of hypothetical $x_n = 0.92$ and $x_n = 0.79$ in shear deformation for both melts are also included in order to demonstrate the predictive behaviour of the theory.

Chapter 7

Conclusions and Recommendations

7.1 Conclusions

- It was verified through comparison of experimental data with the predictions of the Doi-Edwards theory that commercial long chain branched polyolefins undergo considerable but limited strain softening when subjected to a single step-strain in shear deformation at large magnitudes of shear strain. In addition, these melts undergo significant strain hardening when subjected to uniaxial extensional deformation. Both these effects are mainly attributed to the presence of long chain branching in the melt. Other parameters such as increased polydispersity are assumed to play a complementary role in this behaviour. Both these effects (reduced strain softening in shear and strong strain hardening in elongation) do not hold, in general, for linear melts, such as HDPEs. However, one may find several reports that show linear melts with a small amount of strain softening in shear or strain hardening behaviour in uniaxial elongation. In these cases, these effects have their cause either to strain induced crystallisation at large magnitudes of strain or the presence of small amounts of long chain branching. The latter is suspected in certain types of commercial nominally linear polyolefin melts, i.e. higher α -olefin copolymers. Other parameters, such as increased polydispersity are assumed to play a complementary role in this behaviour, as well.
- Several types of commercial polymer melts have been studied in this work. The rheological behaviour of these melts was initially modelled by making use of the modified rubber-like liquid theory. The results, based on experimental evidence showed that the single exponential term of Wagner's damping function in shear, takes much lower values in the case of long chain branched polyolefins than for commercial linear melts. The presence of significant amounts of long chain branching is assumed to be the cause for these lesser values, while in-

creased polydispersity is not excluded from playing a complementary role in this behaviour.

When commercial melts were examined by the same procedure under uniaxial extension, the result was that the single exponential term of Wagner's damping function, again takes lower values for long chain branched melts than for linear melts. This is mostly attributed to the presence of long chain branching while increased polydispersity is a complementary factor.

The values of the parameters of Wagner's damping function does not lead to insight about the physical causes of this behaviour. The single exponential term in both cases (shear and elongation) does not provide quantitative details of the molecular structure of the melts. On the other hand, a more recent proposal by Tsenoglou et al. introduced a power-law damping function that provides a unified description in all shear-free flows under a simple analytical expression. The power-law exponent has a physical basis and it interlinks the experimentally determined values of its exponent with the branching content of the melts under investigation. However, recent studies by Gotsis et al. have lead to the conclusion that the power-law damping function in its present form is far too simple to describe the complex behaviour of commercial polyolefin melts. The power-law damping function does not account for parameters such as polydispersity and the details of the branching architecture, i.e., the molecular weight distribution and the length of the branches that have been found by Gotsis et al. to add significantly to the rheological behaviour of polymer melts. Thus it has not been possible to use the power-law damping function in order to make predictions about the branching content of commercial melts from rheological data only.

- In addition to the temporary network model, more advanced molecular theories such as the Doi and Edwards model have been used to describe the rheological behaviour of commercial melts. While the Doi and Edwards model has a physical basis it was found to be incapable of explaining the rheological behaviour of commercial long chain branched polyolefins. A modification of the theory was proposed by Tsenoglou with the incorporation of a nonlinear viscoelastic parameter into the constitutive equation. The nonlinear viscoelastic parameter corresponds to the amount of internal branching in the melt and, thus, provides a rational explanation of the strain softening of these melts observed at large magnitudes of shear strain. The modified version of the theory accounts for all types of deformation and provides a unified description of the rheological behaviour of polymer melts.
- Two more constitutive equations (in differential form) have been used in order to gain insight in the physics of the rheological behaviour of commercial polyolefin melts. The eXtended Pom-Pom model (an extension of the original Pom-Pom model) and the Rolie-Poly constitutive equation (a simplified version of a more complete model) are both relative recent proposals. The former essentially applies to all types of polymer melts (whether linear or long chain branched) while the later applies only to melts that are comprised of macromolecular chains of linear architecture.

- All of the aforementioned models were used in order to simulate the rheological behaviour of two commercial melts, the HDPE Eraclene and the LDPE Riblene. Both of these melts are polydisperse, the former being a hexene-copolymer, while the latter having a branching content of ≈ 8.8 branching units per backbone chain. Both of these melts were tested in dynamic shear analysis and uniaxial extensional deformation. The LDPE was also subjected to a single step-strain in shear experiment.
- The thermorheological complexity of both melts was experimentally verified. A plot of the loss angle against the rotational frequency of deformation revealed a typical behaviour in the case of the LDPE sample, while, in the case of the HDPE sample, it indicated the possibility of the presence of small amounts of long chain branching. This latter assumption was verified by making use of the technique proposed by Wood-Adams and Cousteaux. The corresponding plot for the HDPE sample indicated the presence of small amounts of long chain branching in the melt. Finally, the Van-Gurp Palmen plots for both melts proved not to be quite helpful. The resulting curves could not be satisfactorily compared to published data, since the frequency range of examination was too narrow, and the resulting curves were only half that of the complete picture that would allow meaningful comparisons with published data.
- Application of the modified rubber-like liquid theory into the experimental results for both melts did not reveal anything unexpected. Wagner's single exponential term, determined from the corresponding master curves of the steady state shear viscosity, was found to be 0.25 in shear for the LDPE, slightly lower than the 0.28 value that was attained for the HDPE. However, the single exponential term fitted to the data from the step-strain in shear for the LDPE gave a slightly lower value ≈ 0.23 . This small difference may be attributed to the relatively low maximum strain attained (2 s.u. due to experimental restrictions) that hampers the accurate determination of the slope of the damping function.
- The power-law damping function was used in order to simulate the uniaxial extensional rheology of the melts. The power-law exponent for the LDPE in this case assumes a value of 0.25, while that for HDPE a value of 0.40. It is generally assumed that linear melts should have a power-law exponent ≥ 1 . For the commercial Eraclene melt this was not the case. Numerous commercial linear melts, however, were found in the literature to have values of β much lower than 1. This is mostly attributed to the presence of long chain branching and to the increased polydispersity of the melt. The absolute branching content of the LDPE could not be evaluated from the elongational data since the power-law damping function is far too simple to make such predictions.
- In terms of the Doi and Edwards theory it was found that both melts deviate from the predictions of the theory in shear as well as in uniaxial extension. In the case of the HDPE this deviation was attributed mainly to the presence of small amounts of long chain branching and to a lesser extent to the increased polydispersity of this commercial melt. The formation of crystal nuclei was cancelled out since this HDPE-hexene copolymer is assumed to have many small

arms on the backbone of the main chain preventing any alignment of neighbouring chains during strain. In the case of the LDPE, the reduced strain softening in shear was attributed to the presence of long chain branching and to a lesser extent to the increased polydispersity of the molecular weight. These were considered to be the main reasons for the considerable strain hardening observed during uniaxial elongation.

- The modified version of the Doi and Edwards theory was tested against the experimental data for the LDPE Riblene as well as the HDPE Eraclene. It was not possible to attain the same value of the nonlinear viscoelastic parameter from shear and elongational data. In the case of the LDPE Riblene it was found that $x_n \approx 0.92$ in uniaxial elongation while $x_n \approx 0.38$ in shear deformation. In the case of the HDPE Eraclene it was found that $x_n \approx 0.79$ in uniaxial elongation, while $x_n \approx 0.26$ in shear deformation. A rough thermodynamic analysis of the experimental data for the LDPE and HDPE samples revealed rather that the present formulation of the Doi and Edwards model is far too simple to account for complex molecular structures.
- A more detailed modification of the Doi and Edwards model (the eXtended Pom-Pom model) proved capable of predicting the branching content of the LDPE melt. The result for the XPP model was a branching content $10 \leq B_n \leq 12$ not too far from the tabulated value of 8.8 (determined from GPC). The XPP model was also able to detect the presence of long chain branching in the HDPE sample. However, due to the very low branching content of this polymer ($B_n < 1$), an exact amount of branching was not determined.
- The competent predictions of the Rolie-Poly constitutive equation in the case of the HDPE sample during uniaxial elongation were not followed by an analogous physical explanation of the adjustable parameter, δ_{rp} . The indications of this model are that the CCR mechanism should be accounted for in the description of the rheological behaviour of linear melts. Application of Marrucci's nonlinear dumbbell model into the steady state shear viscosity data of the HDPE Eraclene melt rather suggests that the CCR parameter (analogous to the β_{rp} parameter of the Rolie-Poly constitutive equation) should be set to 0.6.

7.2 Recommendations

The present research has left a number of open questions and possibilities that merit further investigation :

- The present analytical formulation of the power-law exponent based damping function is far too simple and, consequently, this damping function is incapable of predicting the absolute LCB content and the details of polymer melts. This is demonstrated by the presence of the adjustable parameter, α_u in the equation relating β with B_n (eq. 3.66). Parameters such as the molecular weight polydispersity, distribution and the lengths of the branches (in LCB melts) should be

included in order to reduce (if possible) the significance of the adjustable parameter, α_u .

- The modified version of the Doi and Edwards theory was incapable of giving the same value for the nonlinear viscoelastic parameter in shear and uniaxial elongation (in the case of the LDPE Riblene). This suggests that the modification proposed by Tsenoglou indicates that the Doi and Edwards theory is far too simple to describe the rheological behaviour of commercial polydisperse melts. Important parameters at large deformations or fast flows, such as strain dependent drag forces during deformation of the sample at large deformations, or even molecular mechanisms, such as the CCR relaxation introduced in the Rolie-Poly constitutive equation, are not included in the constitutive scheme. Including such parameters into the constitutive equation is expected to solve the discrepancy and provide the value of x_n in any type of deformation. Further experimental investigation on long chain branched polyolefins of well-control branching content and branching architecture should lead to new modifications and improvement in the quantitative predictions of the theory.
- The degree to which the predictions of the XPP model are valid, regarding the exact determination of the branching content of polymer melts, should be verified under similar experimentation on well characterised polymer melts with controlled branching architecture and LCB content.

Bibliography

- [1] Kaye A., R.F.T. Stepto, W.J. Work, J.V. Aleman, and A.Ya. Malkin. Definition of terms relating to the non-ultimate mechanical properties of polymers. *Pure and Appl. Chem.*, 70(3):701–754, 1998.
- [2] Peterlin A. Crystallization from a strained melt or solution. *Polym. Eng. and Sci.*, 16(3):126–137, 1976.
- [3] Papanastasiou A.C., L.E. Scriven, and C.W. Macosko. An integral constitutive equation for mixed flows : Viscoelastic characterization. *J. of Rheol.*, 27:387–410, 1983.
- [4] Gotsis A.D. *Applied Polymer Rheology : Polymeric Fluids with Industrial Applications*, chapter 3. Branched Polyolefines, pages 59–112. John Wiley and Sons, Inc., 2012.
- [5] Gotsis A.D., B.L.F. Zeevenhoven, and A.H. Hogt. The effect of long-chain branching on the processability of polypropylene in thermoforming. *Polym. Eng. and Sci.*, 44(5):973–982, 2004.
- [6] Gotsis A.D., B.L.F. Zeevenhoven, and C.J. Tsenoglou. Effect of long branches on the rheology of polypropylene. *J. of Rheol.*, 48(4):895–914, 2004.
- [7] Likhtman A.E. and R.S. Graham. Simple constitutive equation for linear polymer melts derived from molecular theory : Rolie-poly equation. *J. of Non-Newt. Fluid Mech.*, 114:1–12, 2003.
- [8] Zimm B.H. and W.H. Stockmayer. The dimensions of chain molecules containing branches and rings. *J. of Rheol.*, 17(12):1301–1314, 1949.
- [9] Tsenoglou C.J. *Nonlinear Viscoelasticity of Polymer Melts and Molecular Constitutive Theories*. PhD thesis, Department of Chemical Engineering, Northwestern University, Evanston, Illinois, August 1985.
- [10] Tsenoglou C.J. Viscoelasticity of binary homopolymer blends. *ACS Polym. Preprints*, 28:185–186, 1987.
- [11] Tsenoglou C.J. Molecular weight polydispersity effects on the viscoelasticity of entangled linear polymers. *Macromolecules*, 24:1762–1767, 1991.

- [12] Tsenoglou C.J., I.S. Stratigakis, and A.D. Gotsis. Nonlinear viscoelasticity of commercial low density polyethylenes : Relaxation experiments and constitutive modeling of the effect of long-chain branching in the presence of entanglements. In *HSR14 Book of Abstracts*, page 24, July 2014.
- [13] Tsenoglou C.J., I.S. Stratigakis, and A.D. Gotsis. Nonlinear viscoelasticity of commercial low density polyethylenes : The effect of long-chain branching in the presence of entanglements. In *AERC 2014 Book of Abstracts*, page 27. European Society of Rheology, April 2014.
- [14] Tsenoglou C.J., E. Voyiatzis, and A.D. Gotsis. Simple constitutive modelling of non-linear viscoelasticity under general extension. *J. of Non-Newt. Fluid Mech.*, 138:33–43, 2006.
- [15] Macosko C.W. *Rheology : Principles, Measurements and Applications*. Wiley-VCH, 1994.
- [16] Lecacheux D., J. Lessec, and C. Quivoron. High-temperature coupling of high-speed gpc with continuous viscometry. i. long chain branching in polyethylene. *J. of Appl. Polym. Sci.*, 27:4867–4877, 1982.
- [17] Cloizeaux des J. Double reptation vs simple reptation in polymer melts. *J. Europhys. Lett.*, 5:437–442, 1988.
- [18] Cloizeaux des J. Double reptation vs simple reptation in polymer melts. *J. Europhys. Lett.*, 6:475, 1988.
- [19] Lohse D.J., S.T. Milner, L.J. Fetters, M. Xenidou, N. Hadjichristidis, R.A. Mendelson, C.A. Garcia-Franco, and M.K. Lyon. Well-defined model long chain branched polyethylene. 2. melt rheological behaviour. *Macromolecules*, 35:3066–3075, 2002.
- [20] Stadler F.J., J. Kaschta, and H. Munstedt. Thermorheological behaviour of various long chain branched polyethylenes. *Macromolecules*, 41:1328–1333, 2008.
- [21] Marrucci G. Dynamics of entanglements : A nonlinear model consistent with the cox-merz rule. *J. of Non-Newt. Fluid Mech.*, 62:279–289, 1996.
- [22] Marrucci G. and B. de Cindio. The stress relaxation of molten pmma at large deformations and it's theoretical interpretation. *Rheol. Acta*, 19:68–75, 1980.
- [23] Marrucci G. and N. Grizzuti. The free energy function of the doi-edwards theory : Analysis of the instabilities in stress relaxation. *J. of Rheol.*, 27:433–450, 1983.
- [24] McKinley G.H. and O. Hassager. The considère condition and rapid stretching of linear and branched polymer melts. *J. of Rheol.*, 43:1195–1212, 1999.
- [25] Bastian H. *Nonlinear Viscoelasticity of Linear and Long-Chain Branched Polymer Melts in Shear and Extensional Flows*. PhD thesis, Institute of Plastics Technology IKT, University of Stuttgart, Germany, June 2001.

- [26] Rasmussen H.K., J.K. Nielsen, A. Bach, and O. Hassager. Viscosity overshoot in the start-up of uniaxial elongation of low density polyethylene melts. *J. of Rheol.*, 49:369–381, 2005.
- [27] Laun H.M. Description of the non-linear shear behaviour of a ldpe melt by means of an experimentally determined strain dependent memory function. *Rheol. Acta*, 17(1):1–15, 1978.
- [28] Meissner J. Experimental aspects in polymer melt elongational rheometry. *Chem. Eng. Commun.*, 33:159–180, 1985.
- [29] Meissner J. and J. Hostettler. A new elongational rheometer for polymer melts and other highly viscoelastic liquids. *Rheol. Acta*, 33:1–21, 1994.
- [30] Ferry J.D. *Viscoelastic Properties of Polymers*. John Wiley and Sons, 3 edition, 1980.
- [31] Vega J.F., A. Santamaria, A.M. Escalona, and P. Lafuente. Small amplitude oscillatory shear flow measurements as a tool to detect very low amounts of long chain branching in polyethylenes. *Macromolecules*, 31:3639–3647, 1998.
- [32] Dealy J.M. and D. Plazek. Time-temperature superposition : A user's guide. *Rheol. Bull.*, 78(2):16–29, 2009.
- [33] Dealy J.M. and J. Wang. *Melt Rheology and It's Applications in the Plastics Industry*. Springer, 3 edition, 2013.
- [34] Kulin L.I., N.L. Meijerink, and P. Starck. Long and short chain branching frequency in low density polyethylene LDPE. *Pure and Appl. Chem.*, 40(9):1403–1415, 1988.
- [35] Fetters L.J., D.J.Lohse, D. Richter, T.A. Witten, and A.Zirkel. Connection between polymer molecular weight, density, chain dimensions and melt viscoelastic properties. *Macromolecules*, 27(17):4639–4647, 1994.
- [36] Kasehagen L.J. and C.W. Macosko. Nonlinear shear and extensional rheology of long-chain branched polybutadiene. *J. of Rheol.*, 42:1303–1327, 1998.
- [37] Kasehagen L.J., C.W. Macosko, D. Trowbridge, and F. Magnus. Rheology of long-chain randomly branched polybutadiene. *J. of Rheol.*, 40:689–709, 1996.
- [38] Doi M. *Introduction to Polymer Physics*. OUP, 1996.
- [39] Doi M. and S.F. Edwards. *The Theory of Polymer Dynamics*. OUP, 1986.
- [40] Gahleitner M. Melt rheology of polyolefines. *Prog. Polym. Sci.*, 26:895–944, 2001.
- [41] Rubinstein M. and R.H.Colby. *Polymer Physics*. OUP, 2003.
- [42] Wagner M.H. Analysis of stress-growth data for simple extension of a low density branched polyethylene melt. *Rheol. Acta*, 15(2):133–135, 1976.

- [43] Wagner M.H. Analysis of time-dependent non-linear stress growth data for shear and elongational flow of a low density branched polyethylene melt. *Rheol. Acta*, 15(2):136–142, 1976.
- [44] Wagner M.H. A constitutive analysis of uniaxial elongational flow data of a low density polyethylene melt. *J. of Non-Newt. Fluid Mech.*, 4:39–55, 1978.
- [45] Wagner M.H. and J. Meissner. Network disentanglement and time-dependent flow behaviour of polymer melts. *Makromol. Chem.*, 181:1533–1550, 1980.
- [46] Wagner M.H., T. Raible, and J. Meissner. Tensile stress overshoot in uniaxial extension of a LDPE melt. *Rheol. Acta*, 18:427–428, 1979.
- [47] Inkson N.J., T.C.B. McLeish, O.G. Harlen, and D.J. Groves. Predicting low density polyethylene melt rheology in elongation and shear flows with “pom-pom” constitutive equations. *J. of Rheol.*, 43:873–896, 1999.
- [48] Demarquette N.R., F.T. daSilva, S.D. Brandi, and D. Gouvea. Surface tension of polyethylene used in thermal coating. *Polym. Eng. and Sci.*, 40(7):1663–1671, 2000.
- [49] Hassanger O. and S. Pedersen. Relations between shear and normal stresses in a step-shear experiment. *J. of Non-Newt. Fluid Mech.*, 4:261–268, 1978.
- [50] Urakawa O., M. Takahashi, T. Masuda, and N.G. Ebrahimi. Damping functions and chain relaxation in uniaxial and biaxial extensions : Comparison with the doiedwards theory. *Macromolecules*, 28:7196–7201, 1995.
- [51] Andersen P.G. and S.H. Carr. Crystal nucleation in sheared polymer melts. *Polym. Eng. and Sci.*, 18(3):215–221, 1978.
- [52] Wood-Adams P.M. and S. Costeux. Thermorheological behaviour of polyethylene : Effects of microstructure and long chain branching. *Macromolecules*, 34:6281–6290, 2001.
- [53] Wood-Adams P.M., J.M.Dealy, A.W. deGroot, and O.D. Redwine. Effect of molecular structure on the linear viscoelastic behaviour of polyethylene. *Macromolecules*, 33:7489–7499, 2000.
- [54] Huang Q. *Molecular Rheology of Complex Fluids*. PhD thesis, Department of Chemical and Biochemical Engineering, Technical University of Denmark, Denmark, January 2013.
- [55] Bird R.B., R.C. Armstrong, and O. Hassanger. *Dynamics of Polymeric Liquids*, volume 1. Fluid Mechanics. John Wiley and Sons, 2 edition, 1987.
- [56] Larson R.G. *Constitutive Equations for Polymer Melts and Solutions*. AT&T Bell Labs and Butterworth, 1988.
- [57] Larson R.G. *The Structure and Rheology of Complex Fluids*. OUP, 1999.

- [58] Larson R.G., T. Sridhar, L.G. Leal, G.H. McKinley, A.E. Likhtman, and T.C.B. McLeish. Definitions of entanglement spacing and time constants in the tube model. *J. of Rheol.*, 47:809–818, 2003.
- [59] Tanner R.I. and K. Walters. *Rheology : An Historical Perspective*. Elsevier, 1998.
- [60] Lagendijk R.P. Modification of pp with peroxydicarbonates to improve it's melt strength. Master's thesis, Department of Chemical Engineering, Delft University of Technology, Delft, The Netherlands, 1999.
- [61] Lagendijk R.P., A.H. Hogt, A. Buijtenhuijs, and A.D. Gotsis. Peroxydicarbonate modification of polypropylene and extensional flow properties. *Polymer*, 42:10035–10043, 2001.
- [62] Graham R.S., A.E. Likhtman, T.C.B. McLeish, and S.T. Milner. Microscopic theory of linear, entangled polymer chains under rapid deformation including chain stretch and convective constraint release. *J. of Rheol.*, 47:1171–1200, 2003.
- [63] Onogi S., T. Masuda, and K. Kitagawa. Rheological properties of anionic polystyrenes. i. dynamic viscoelasticity of narrow distribution polystyrenes. *Macromolecules*, 3(2):109–116, 1970.
- [64] Trinkle S. and C. Friedrich. Van gurg-palmen plot : A way to characterize polydispersity of linear polymers. *Rheol. Acta*, 40:322–328, 2001.
- [65] Schulze J.S. et al. A comparison of extensional viscosity measurements from various rheometers. *Rheol. Acta*, 40:457–466, 2001.
- [66] Rheometric Scientific. *Polymer Melt Elongational Rheometer, RME : Instrument Manual*, revision a edition, August 1995.
- [67] Wasserman S.H. and W.W. Graessley. Effects of polydispersity on linear viscoelasticity in entangled polymer melts. *J. of Rheol.*, 36:543–572, 1992.
- [68] Wasserman S.H. and W.W. Graessley. Prediction of linear viscoelastic response for entangled polyolefin melts from molecular weight distribution. *Polym. Eng. and Sci.*, 36(6):852–861, 1996.
- [69] Hama T., K. Yamaguchi, and T. Suzuki. Long chain branching and solution properties of low density polyethylene. *Makromol. Chem.*, 155:283–298, 1972.
- [70] Raible T., A. Demarmels, and J. Meissner. Stress and recovery maxima in ldpe melt elongation. *Polym. Bull.*, 1:397–402, 1979.
- [71] Schweizer T. The uniaxial elongational rheometer rme : Six years of experience. *Rheol. Acta*, 39:428–443, 2000.
- [72] McLeish T.C.B. and R.G. Larson. Molecular constitutive equations for a class of branched polymers : The pom-pom polymer. *J. of Rheol.*, 42:81–110, 1998.

- [73] Gorp van M. and J. Palmen. Time-temperature superposition for polymeric blends. *Rheol. Bull.*, 67(1):5–8, 1998.
- [74] Garrido V.H.R. and M.H. Wagner. The damping function in rheology. *Rheol. Acta*, 48:245–284, 2009.
- [75] Tuminello W.H. Molecular weight and molecular weight distribution from dynamic measurements of polymer melts. *Polym. Eng. Sci.*, 26:1339–1347, 1986.
- [76] Verbeeten W.M.H., G.W.M. Peters, and F.P.T. Baaijens. Differential constitutive equations for polymer melts : The extended pom-pom model. *J. of Rheol.*, 45:823–843, 2001.
- [77] Graessley W.W. *Advances in Polymer Science*, volume 47. Synthesis and Degradation Rheology and Extrusion, chapter 4. Entangled Linear, Branched and Network Polymer Systems - Molecular Theories, pages 67–117. Springer Berlin Heidelberg, 1982.
- [78] Graessley W.W. *Polymeric Liquids and Networks : Structure and Properties*. Garland Science, New York, 2004.
- [79] Tadmor Z. and C.G. Gogos. *Principles of Polymer Processing*. John Wiley and Sons, 2 edition, 2006.

Appendix A

Fourier Transform Integrals

The single mode relaxation modulus, $G(t)$ is given by

$$G(t) = G_0 \exp(-t/\tau_0) , \quad (\text{A.1})$$

where G_0 is the plateau modulus and τ_0 is the characteristic relaxation time of the material under consideration. If more than a single mode is used, instead then one gets a summation over all N modes, that is,

$$G(t) = \sum_{i=1}^N G_i \exp(-t/\tau_i) , \quad (\text{A.2})$$

where G_i are modulus constants and τ_i are the corresponding relaxation times obtained from experiment. If one wishes to express these relations in terms of the frequency of observation, ω instead of time, t then one has to use a *Fourier transform integral*, that is,

$$G'(\omega) = G_{eq} + \omega \int_0^{\infty} [G(t) - G_{eq}] \sin(\omega t) dt \quad (\text{A.3})$$

$$G''(\omega) = \omega \int_0^{\infty} [G(t) - G_{eq}] \cos(\omega t) dt , \quad (\text{A.4})$$

where $G'(\omega)$ and $G''(\omega)$ are the storage and loss moduli respectively and G_{eq} is the *equilibration modulus* obtained after a step-strain experiment which is a non-zero constant for solids at low frequencies (or equivalently at long times) but is zero in the case of liquids. In the case of a polymer melt Eqs. A.3 and A.4 reduce to

$$G'(\omega) = \omega \int_0^{\infty} G(t) \sin(\omega t) dt \quad (\text{A.5})$$

$$G''(\omega) = \omega \int_0^{\infty} G(t) \cos(\omega t) dt . \quad (\text{A.6})$$

Substituting Eq.A.1 into these last two expressions, one gets

$$G'(\omega) = \frac{\omega G_0}{\tau_0} \int_0^{\infty} \exp(-t/\tau_0) \sin(\omega t) dt \quad (\text{A.7})$$

$$G''(\omega) = \frac{\omega G_0}{\tau_0} \int_0^{\infty} \exp(-t/\tau_0) \cos(\omega t) dt . \quad (\text{A.8})$$

Introducing the transformation $1/\tau_0 = a$ and $\omega = b$, the corresponding integrals assume the standard form

$$\int_0^{\infty} \exp(-ax) \sin(bx) = \frac{b}{a^2 + b^2} \quad (\text{A.9})$$

$$\int_0^{\infty} \exp(-ax) \cos(bx) = \frac{a}{a^2 + b^2} , \quad (\text{A.10})$$

with solutions tabulated in tables with special forms of integrals of the above kind. Then the storage and loss moduli are obtained

$$G'(\omega) = G_0 \frac{\omega^2 \tau_0^2}{1 + \omega^2 \tau_0^2} \quad (\text{A.11})$$

$$G''(\omega) = G_0 \frac{\omega \tau_0}{1 + \omega^2 \tau_0^2} . \quad (\text{A.12})$$

The generalization for the multimode relaxation modulus, is given in the form of a summation over all N modes in Eqs. 3.21.

Appendix B

The Doi-Edwards Universal Orientation Tensor

The *Doi-Edwards universal orientation tensor* has been formulated mathematically through the following expression

$$Q_{12}(\underline{E}) = \frac{1}{\langle |\underline{E} \cdot \underline{u}| \rangle} \left\langle \frac{(\underline{E} \cdot \underline{u})_1 (\underline{E} \cdot \underline{u})_2}{|\underline{E} \cdot \underline{u}|} \right\rangle \quad (\text{B.1})$$

in the case of a step-in shear strain deformation. The corresponding *deformation gradient tensor* is

$$\underline{E} = \begin{bmatrix} 1 & \gamma_0 & 0 \\ 0 & 1 & 0 \\ 0 & 0 & 1 \end{bmatrix}, \quad (\text{B.2})$$

where γ_0 is the shear strain. The associated *unit vector*, \underline{u} in the spherical coordinate system, is

$$\underline{u} = \begin{bmatrix} \sin \theta \cos \phi \\ \sin \theta \sin \phi \\ \cos \theta \end{bmatrix} \quad (\text{B.3})$$

and the $\langle \dots \rangle$, means an average over all directions of this unit vector

$$\langle \dots \rangle = \frac{1}{4\pi} \int_0^{2\pi} \int_0^\pi \sin \theta d\theta d\phi \quad (\text{B.4})$$

The dot product of the deformation gradient tensor with the unit vector produces a new vector (i.e. a transformed unit vector due to the imposed deformation gradient) and the $|\dots|$ means the magnitude of this new vector after it has been transformed. Then Eq. B.1 for a step-shear strain flow is

$$Q_{12} = \frac{1}{\left\langle \sqrt{1 + 2\gamma_0 u_1 u_2 + \gamma_0^2 u_2^2} \right\rangle} \left\langle \frac{(u_1 + \gamma_0 u_2) u_2}{\sqrt{1 + 2\gamma_0 u_1 u_2 + \gamma_0^2 u_2^2}} \right\rangle, \quad (\text{B.5})$$

where u_1, u_2 and u_3 are the components of the unit vector. Two double integrals rise from this analysis, namely,

$$\alpha(\gamma_0) = \left\langle \sqrt{1 + 2\gamma_0 u_1 u_2 + \gamma_0^2 u_2^2} \right\rangle \quad (\text{B.6})$$

$$= \frac{1}{4\pi} \int_0^\pi \sin \theta d\theta \int_0^{2\pi} d\phi \sqrt{1 + 2\gamma_0 \sin^2 \theta \sin \phi \cos \phi + \gamma_0^2 \sin^2 \theta \sin^2 \phi} \quad (\text{B.7})$$

$$= \int_0^1 dx \quad (\text{B.8})$$

$$\int_0^1 dy \sqrt{1 + \frac{1}{2}\gamma_0^2(1-x^2) + \gamma_0(1-x^2) \sin(4\pi y) - \frac{1}{2}\gamma_0^2(1-x^2) \cos(4\pi y)}, \quad (\text{B.9})$$

for which the variable transformation $x = \cos \theta$ and $y = \phi/2\pi$ has been introduced. Then

$$Q_{12} = \frac{1}{\alpha(\gamma_0)} \frac{1}{2} \int_0^1 dx \quad (\text{B.10})$$

$$\int_0^1 dy \frac{(1-x^2) \sin(4\pi y) + \gamma_0(1-x^2) - \gamma_0(1-x^2) \cos(4\pi y)}{\sqrt{1 + \frac{1}{2}\gamma_0^2(1-x^2) + \gamma_0(1-x^2) \sin(4\pi y) - \frac{1}{2}\gamma_0^2(1-x^2) \cos(4\pi y)}}. \quad (\text{B.11})$$

These integrals can easily be solved numerically using a simple trapezoidal integration routine by first integrating the inner integral and then integrating the outer integral. An analogous procedure is followed for the IAA integral. Sample values of the orientation tensor, Q_{12} in shear with an accuracy of up to five decimal points for both the exact and the IAA versions are provided in Table B.1 along with the corresponding values obtained for the damping functions, $h(\gamma_0)_{DE}$ and $h(\gamma_0)_{DE}^{IAA}$ (using Eqs. 3.88 and 3.94) respectively. The associated plot is also provided in Fig. B.1.

Table B.1: Values of the Doi-Edwards orientation tensor, Q_{12} in shear with an accuracy of five decimal digits and the corresponding damping functions, $h(\gamma_0)$ for both the exact and the IAA versions.

Shear magnitude γ_0	Q_{12} (exact DE)	$h(\gamma_0)_{DE}$	Q_{12} (IAA)	$h(\gamma_0)_{DE}^{IAA}$
0.1	0.02659	0.99725	0.01995	0.99765
0.3	0.07806	0.97575	0.05874	0.97903
0.5	0.12472	0.93542	0.09439	0.94391
0.7	0.16442	0.88081	0.12541	0.89581
0.9	0.19614	0.81723	0.15102	0.839
1	0.20897	0.78365	0.16173	0.80865
1.5	0.24682	0.61704	0.19621	0.65403
2	0.25376	0.4758	0.20689	0.51723
2.5	0.24526	0.36789	0.20433	0.40867
3	0.2306	0.28825	0.1956	0.32599
5	0.1708	0.1281	0.1517	0.1517
7	0.13082	0.07008	0.11914	0.0851
9	0.10501	0.04375	0.09717	0.05398
12	0.08056	0.02518	0.07571	0.03155
15	0.06517	0.01629	0.06188	0.02063
20	0.04933	0.00925	0.04736	0.01184
30	0.03312	0.00414	0.03218	0.00536
35	0.02843	0.00305	0.02773	0.00396

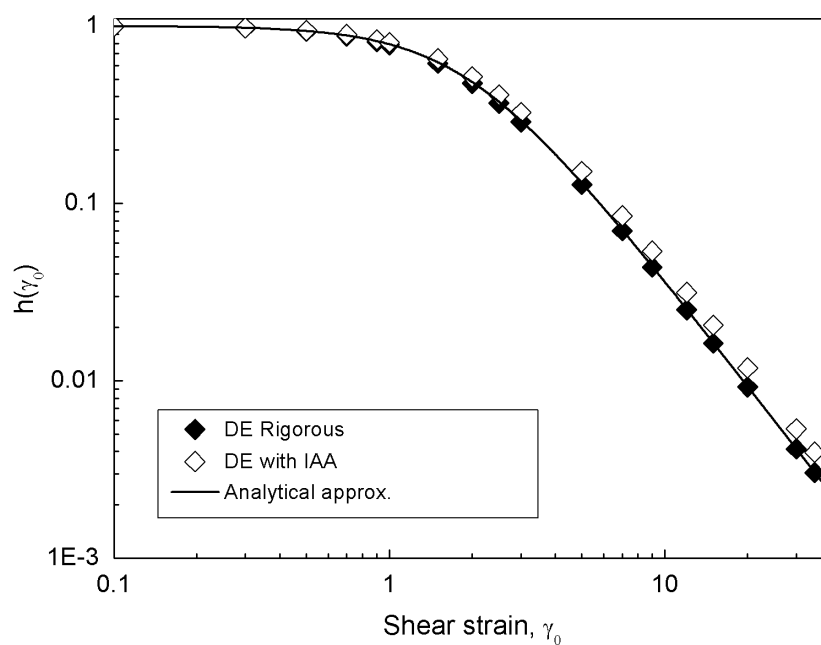


Figure B.1: A log-log plot of the Doi-Edwards damping function, $h(\gamma_0)$, in shear for both the exact and the IAA version. A plot of the analytical approximation (see Eq. 3.95) is also included for comparison.

Appendix C

Tables

The present section contains tables of the values of the damping function, $h(\gamma_0)$ calculated from the experimental data of step-strain in shear experiments for the commercial long-chain branched LDPE's and commercial HDPE's examined by Tsenoglou [9]. Tables of the damping function, $h(\epsilon_H)$ calculated from the experimental data of uniaxial extensional measurements for the commercial LDPE Riblene and Eraclene melts are also included.

Table C.1: Values of $h(\gamma_0)$ as a function of shear strain for the commercial long-chain branched LDPE's examined by Tsenoglou [9].

	A2	A4	A7	B2	C2	IUPAC A	A7	IUPAC A
Strain	130	130	130	130	130	130	110	150
0.25	1.00	1.00	1.00	1.00	1.00	1.00	1.00	1.00
0.50	0.98	1.00	1.00	1.00	1.00	0.98	1.00	0.98
1.00	0.91	0.98	0.93	0.91	0.95	0.89	0.89	0.89
2.00		0.87		0.76				
3.00	0.62	0.74	0.66	0.63	0.45	0.58	0.72	0.56
5.00	0.47	0.51	0.50	0.45		0.36	0.52	0.35
7.50			0.35	0.32		0.29	0.33	0.28
10.00	0.28	0.33	0.27	0.25	0.23	0.16	0.27	0.16
15.00	0.14		0.16	0.14	0.14		0.19	0.08
18.75	0.12	0.15						
20.00				0.09	0.10	0.05		0.05
25.00	0.07	0.10		0.06	0.06			

Table C.2: Values of $h(\gamma_0)$ as a function of shear strain for the commercial linear HDPE's examined by Tsenoglou [9]. The last column contains values of the damping function for a commercial LLDPE from the same work [9].

	A		A	B		C	LLDPE
Strain	140	150	170	140	150	140	150
0.25	1.00	1.00		1.00		1.00	
0.32	0.95	0.95	1.00	1.00			1.00
0.40			1.00	0.93			1.00
0.50	0.87		0.89		1.00	1.00	0.98
0.63		0.87	0.85	0.91	1.00	1.00	
0.79	0.81	0.81		0.85		0.95	
1.00	0.69	0.71	0.76	0.79	0.87	0.87	0.87
1.26	0.62	0.63	0.68	0.71	0.72	0.72	0.78
1.58	0.48	0.49	0.58	0.62	0.62	0.58	0.68
2.00	0.45	0.40	0.45	0.50	0.54	0.51	0.55
2.50	0.35	0.35	0.36	0.42	0.41	0.44	0.45
3.16	0.27	0.28	0.30	0.35	0.32	0.34	0.38
4.00	0.22	0.19	0.26	0.25	0.26	0.26	0.28
5.00	0.19	0.15	0.17	0.21	0.20	0.21	0.21
6.30	0.16	0.13	0.13	0.17	0.15	0.18	0.16
8.00		0.10	0.095	0.13	0.13	0.15	0.12
10.00		0.089	0.083	0.13	0.10	0.098	0.081
12.60		0.081	0.062	0.13	0.069	0.083	0.060
15.80		0.074	0.048	0.13	0.054	0.068	0.045
20.00		0.066	0.035		0.042	0.050	0.031
25.00		0.078				0.045	0.023

Table C.3: Values of $h(\epsilon_H)$ as a function of the Hencky strain (for each individual strain rate) for the commercial long-chain branched LDPE Riblene melt at $T=150^\circ\text{C}$.

Strain rate $\dot{\epsilon} \text{ (s}^{-1}\text{)}$	Hencky strain ϵ_H	$h(\epsilon_H)$
0.081	0.96	1.00
	1.27	0.88
	1.62	0.79
	2.46	0.50
	2.82	0.36
0.26	1.13	1.00
	1.57	0.84
	2.25	0.58
	2.73	0.43
0.41	0.79	1.00
	1.37	0.83
	1.86	0.72
	2.74	0.41
0.56	0.95	1.00
	1.47	0.86
	1.94	0.74
	2.63	0.48
0.80	1.61	0.77
	1.94	0.68
	2.50	0.53
	2.70	0.43
1.18	0.97	1.00
	1.35	0.70
	1.83	0.61
	2.47	0.46
1.40	0.55	0.85
	1.04	0.74
	1.69	0.57
	2.63	0.36
	3.14	0.21
1.61	0.45	0.84
	0.97	0.81
	1.63	0.63
	2.53	0.36
	2.90	0.30

Table C.4: Values of $h(\epsilon_H)$ as a function of the Hencky strain (for each individual strain rate) for the commercial linear HDPE Eralene melt at $T=170^\circ\text{C}$.

Strain rate $\dot{\epsilon} \text{ (s}^{-1}\text{)}$	Hencky strain ϵ_H	$h(\epsilon_H)$
0.048	0.39	1.00
	0.72	0.88
	1.11	0.72
	1.75	0.47
	2.06	0.36
0.083	0.35	1.00
	0.59	0.97
	0.88	0.90
	1.30	0.70
	1.93	0.43
0.34	0.63	0.95
	0.87	0.81
	1.31	0.63
	2.00	0.36
0.46	0.47	0.81
	0.64	0.81
	1.12	0.68
	1.89	0.39
0.86	0.48	0.83
	0.90	0.77
	1.25	0.65
	1.77	0.45
1.43	0.46	0.74
	0.66	0.70
	0.94	0.68
	2.00	0.50
	2.14	0.26
1.86	0.56	0.74
	0.80	0.70
	1.19	0.65
	1.86	0.39
	2.90	0.14

Appendix D

Graphs from the Theoretical Section

The present section contains all the plots related to the experimental investigation of the rheological properties of commercial long-chain branched LDPE's in terms of single step-strain in shear experiments. The molecular characteristics of these melts are presented in Tables [3.3](#) and [3.9](#). From Tsenoglou's PhD Dissertation [\[9\]](#).

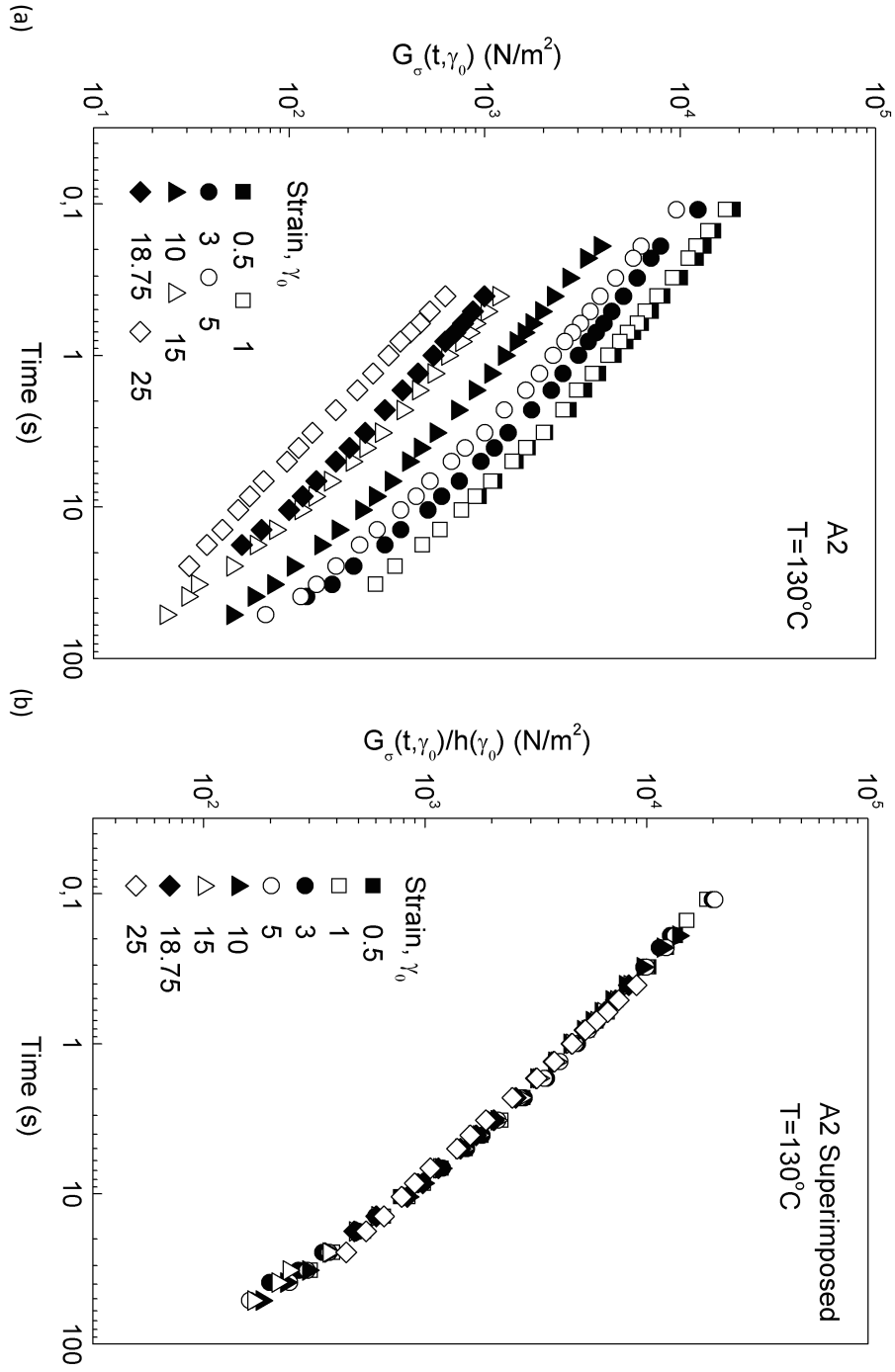


Figure D.1: Relaxation modulus of commercial long-chain branched LDPE A2 at $T = 130^\circ\text{C}$ in (a) and (b) superimposed plot with values of $h(\gamma_0)$ as in Table C.1.

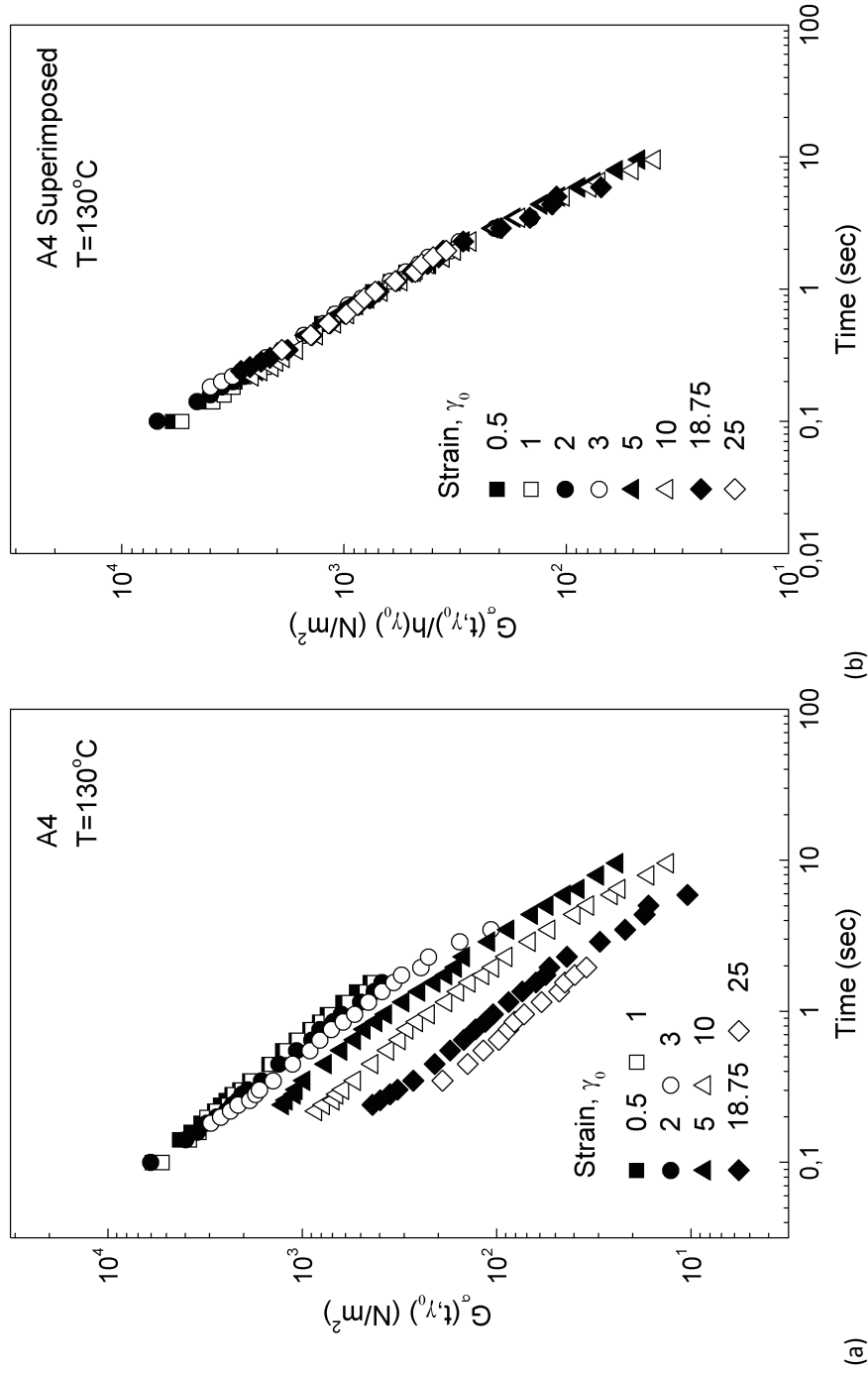


Figure D.2: Relaxation modulus of commercial long-chain branched LDPE A4 at $T = 130^\circ\text{C}$ in (a) and (b) superimposed plot with values of $h(\gamma_0)$ as in Table C.1.

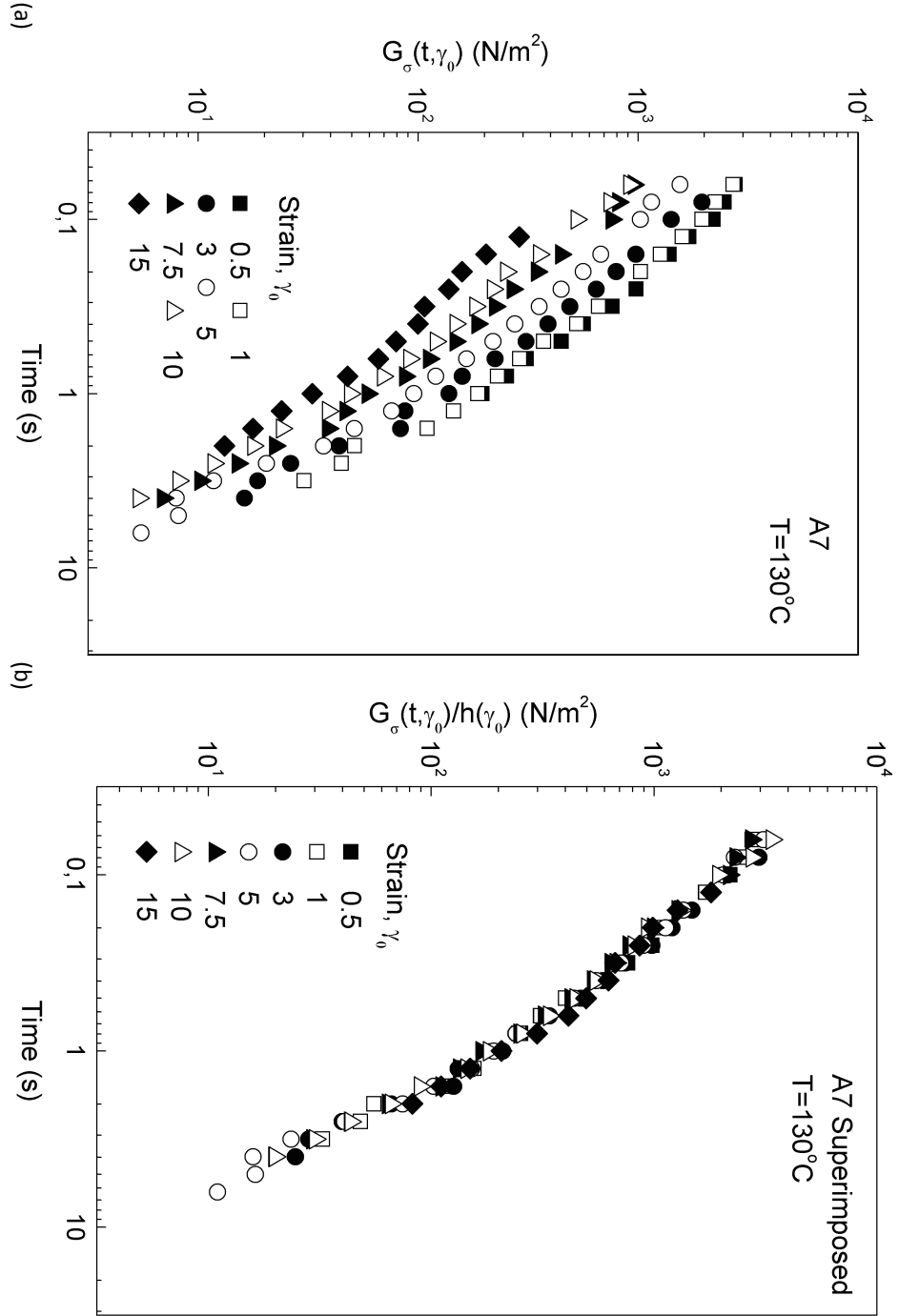


Figure D.3: Relaxation modulus of commercial long-chain branched LDPE A7 at $T = 130^\circ\text{C}$ in (a) and (b) superimposed plot with values of $h(\gamma_0)$ as in Table C.1.

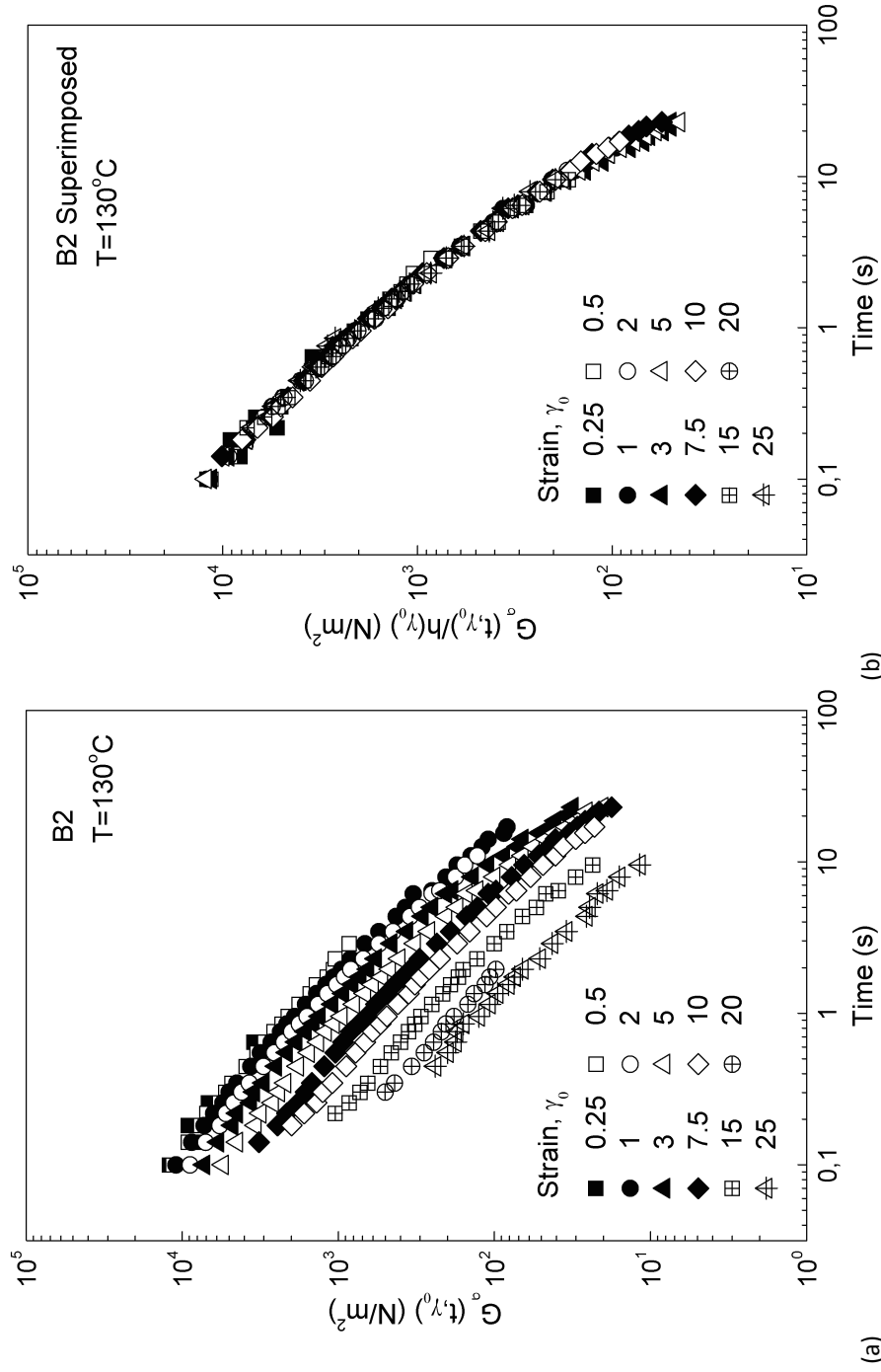


Figure D.4: Relaxation modulus of commercial long-chain branched LDPE B2 at $T = 130^\circ\text{C}$ in (a) and (b) superimposed plot with values of $h(\gamma_0)$ as in Table C.1.

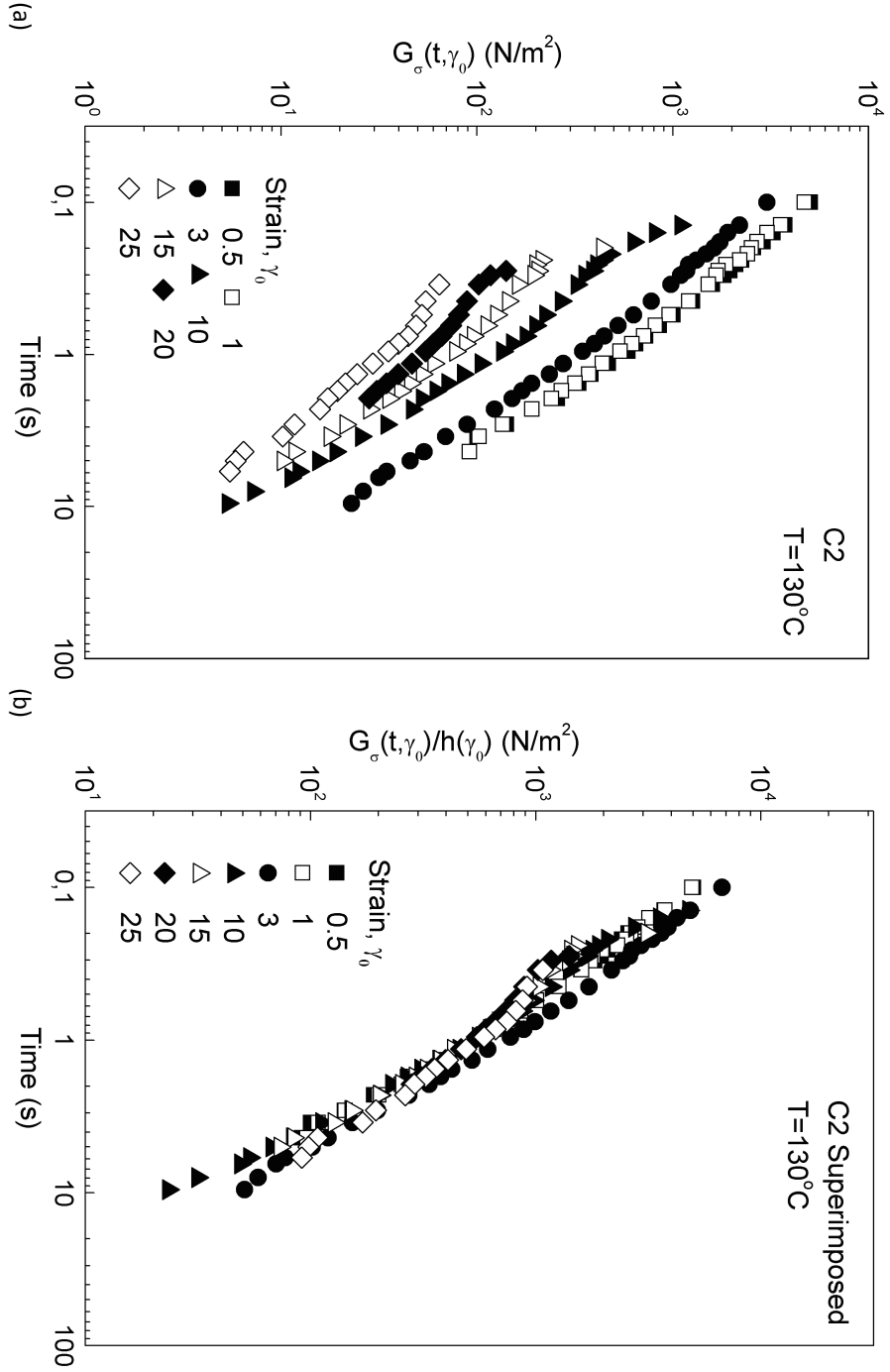


Figure D.5: Relaxation modulus of commercial long-chain branched LDPE C2 at $T = 130^\circ\text{C}$ in (a) and (b) superimposed plot with values of $h(\gamma_0)$ as in Table C.1.

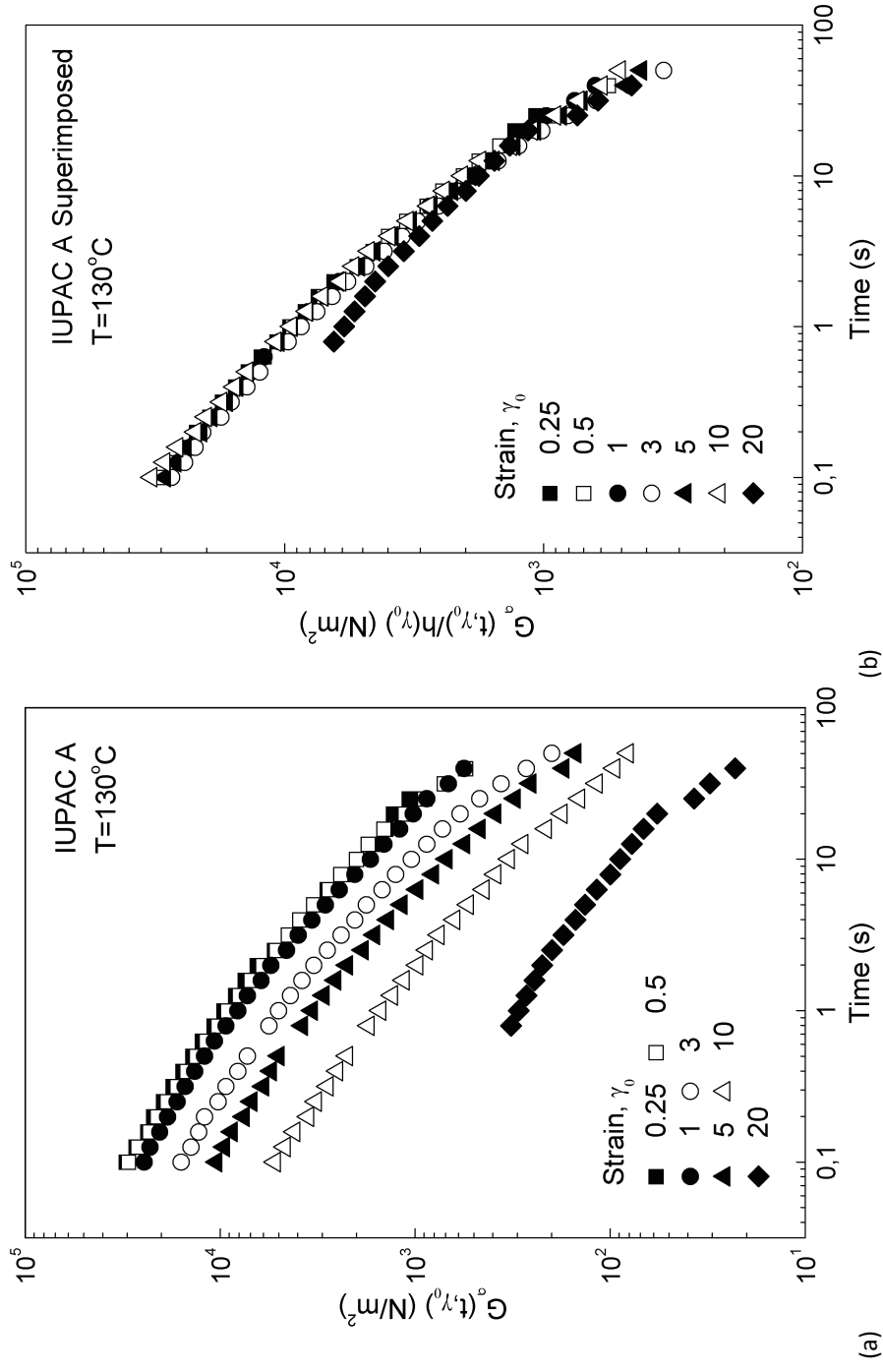


Figure D.6: Relaxation modulus of commercial long-chain branched IUPAC A at $T = 130^\circ\text{C}$ in (a) and (b) superimposed plot with values of $h(\gamma_0)$ as in Table C.1.

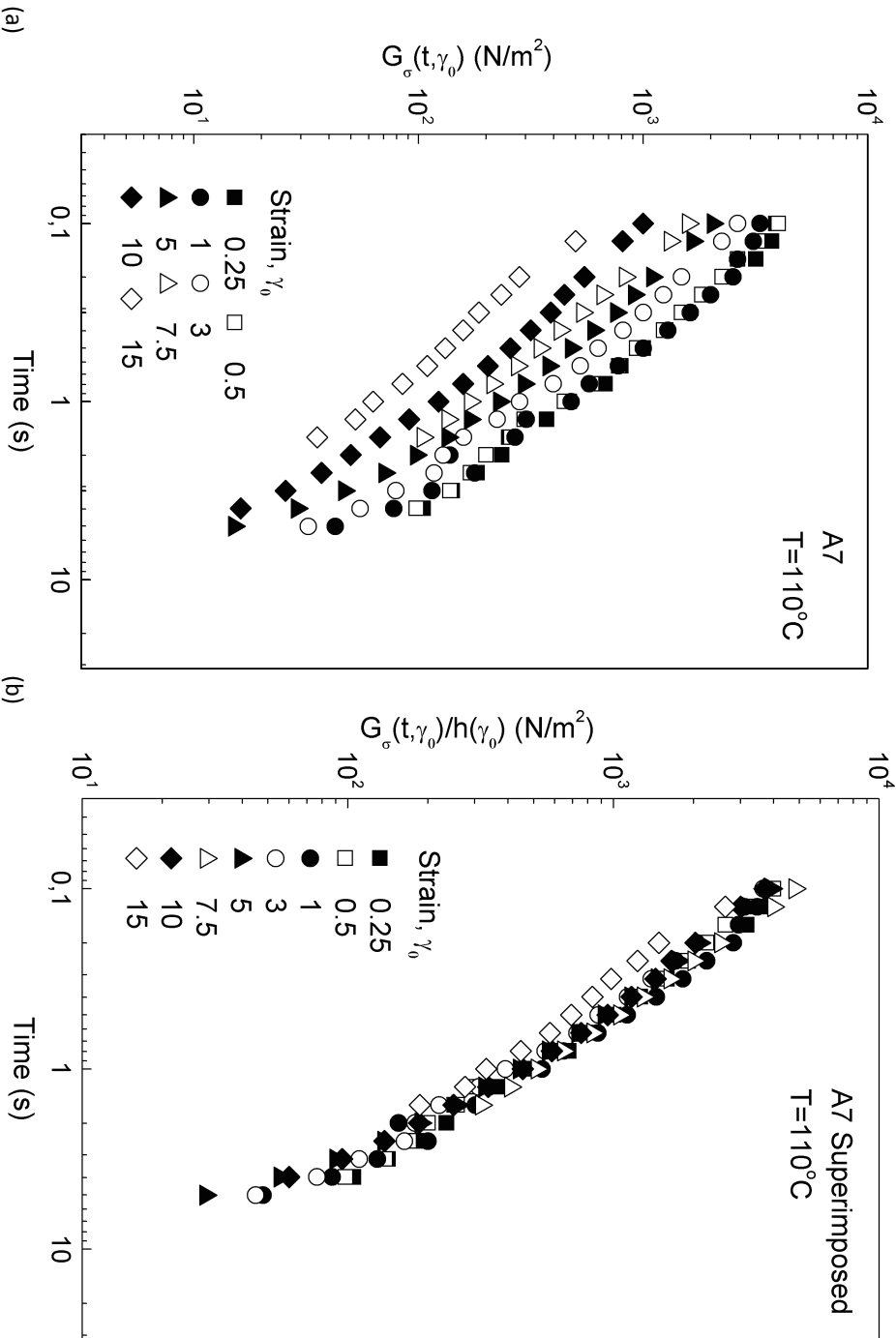


Figure D.7: Relaxation modulus of commercial long-chain branched LDPE A7 at $T = 110^\circ\text{C}$ in (a) and (b) superimposed plot with values of $h(\gamma_0)$ as in Table C.1.

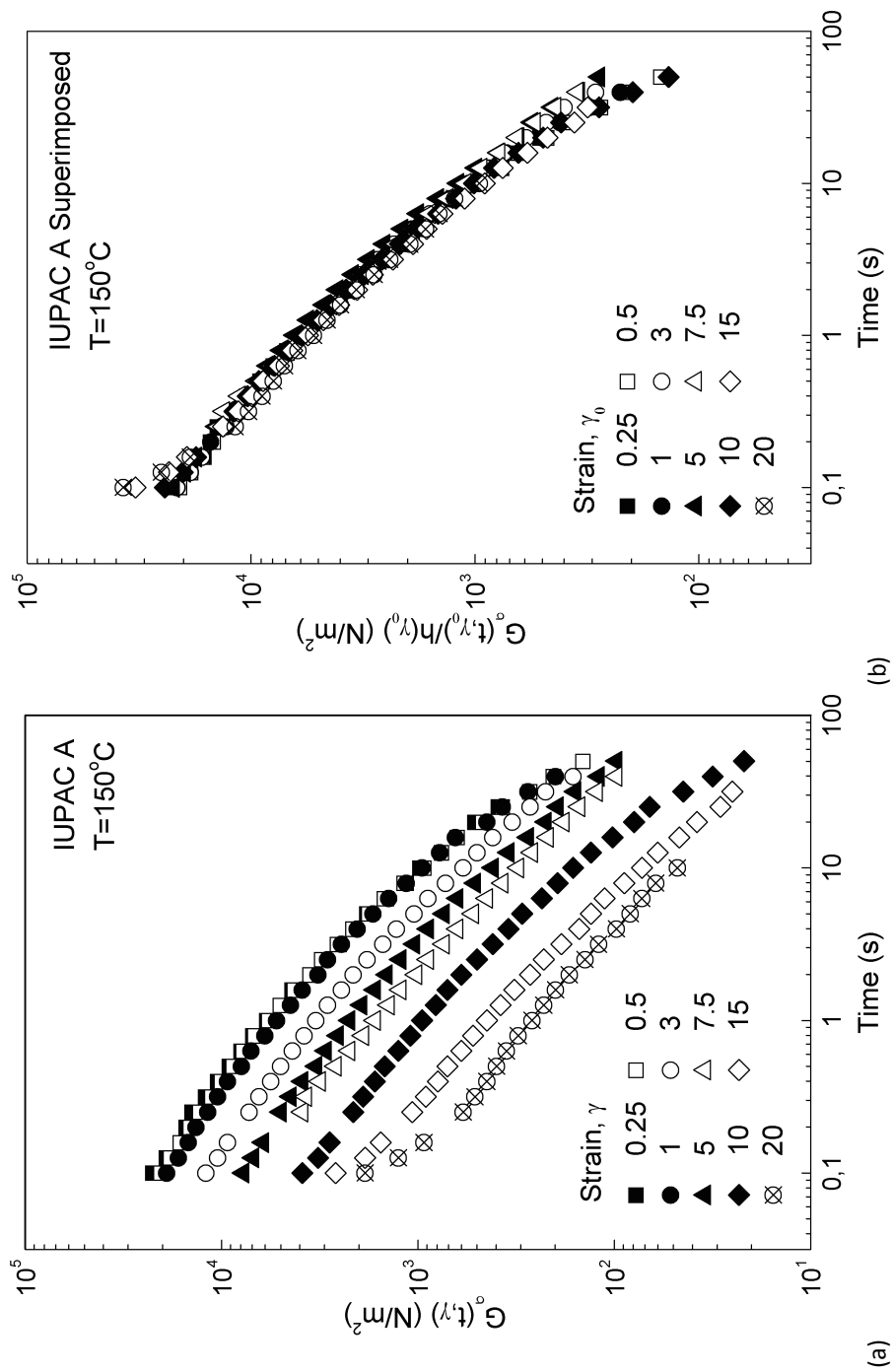


Figure D.8: Relaxation modulus of commercial long-chain branched IUPAC A at $T = 150^\circ\text{C}$ in (a) and (b) superimposed plot with values of $h(\gamma_0)$ as in Table C.1.

List of Tables

1	Τιμές της παραμέτρου n της απλής εκθετικής συνάρτησης απόσβεσης του Wagner για εμπορικά τυχαία διακλαδωμένα και γραμμικής αρχιτεκτονικής πολυαιθυλένια. Τα δείγματα χαρακτηρίζονται από ποικιλία μοριακών βαρών και πολυδιασποράς.	12
2	Τιμές της παραμέτρου β της συνάρτησης απόσβεσης Τσενόγλου για πολυολεφίνες διαφορετικής χημικής σύστασης, μοριακού βάρους και πολυδιασποράς που υποβλήθηκαν σε διαφορετικές πειραματικές μετρήσεις εφελκυσμού.	13
3	Μοριακά χαρακτηριστικά εμπορικών πολυπροπυλενίων με τυχαία κατανομή μακρινών διακλαδώσεων που παρασκευάστηκαν από το αντίστοιχο γραμμικό πολυμερές προσθέτοντας στο τελευταίο διαφορετικά ποσοστά διασταυρωτή, P-26 και τιμές της παραμέτρου β και του δείκτη εργοσκήρυνσης, SHI, όπως προσδιορίστηκαν από μετρήσεις μονοαξονικού εφελκυσμού σε θερμοκρασία $T=190^{\circ}\text{C}$	14
4	Μοριακά χαρακτηριστικά γραμμικού και μιγμάτων γραμμικού και εμπορικού διακλαδισμένου πολυπροπυλενίου σε διαφορετικές αναλογίες. Η παράμετρος β και ο δείκτης σκλήρυνσης, SHI, προσδιορίστηκαν για κάθε δείγμα από πειραματικές μετρήσεις ροής εφελκυσμού σε θερμοκρασία $T = 190^{\circ}\text{C}$	14
5	Φυσικές ιδιότητες των πολυαιθυλενίων του Τσενόγλου (βλ. και Πίν. 1).	17
6	Μοριακά χαρακτηριστικά των εμπορικών δειγμάτων Riblene και Eracene που εξετάστηκαν πειραματικά σε διάτμηση και εφελκυσμό.	21
1.1	Some synthetic olefinic polymers, their monomers and their structural units.	40
3.1	Spectrum of relaxation modes for “Melt I”, a LDPE with LCB architecture with $M_w = 482 \text{ kg/mol}$, $(M_w/M_n) = 28.1$, MFI $(190/2.16) = 1.33$ and $E_a = 54 \text{ kJ/mol}$, determined at $T = 150^{\circ}\text{C}$ [27].	65
3.2	Spectrum of relaxation modes for “Melt I”. The ten constants τ_i and G_i were determined by curve fitting the elongational data at $\dot{\epsilon}=0.001 \text{ s}^{-1}$ [43].	67

3.3	Material parameter, n of the deformation-dependent damping function for commercial polymeric melts of varying molecular architecture and molecular weight distribution at the corresponding isothermal conditions. Data from Tsenoglou [9].	72
3.4	Temperature dependence of the damping function for the branched LDPE "Melt I" determined from shear relaxation modulus measurements for various magnitudes of shear strain, γ_0 at the isothermal conditions listed [27].	73
3.5	Molecular characteristics for the long-chain branched PB blends studied by Kasehagen et al. [37, 36] along with the PSM parameter, α_p that best fits the data from single step-strain in shear experiments.	79
3.6	Extracted β exponents for the power-law damping function, $h = \lambda_{m_e}^{-\beta}$, their dependence on extension geometry, m_e and polymer species for the eight polymers examined by Tsenoglou et al. [14].	81
3.7	Properties of commercial polypropylenes of linear molecular architecture, with initially different molecular weights modified using varying amounts (mmol/100 gr PP) of P-26 (dimyristyl peroxydicarbonate). All rheological measurements except for the melt flow index were carried out at $T=190^\circ\text{C}$ [5, 6].	83
3.8	Molecular data of melts of B/PF blends. The PF grade, is a commercial branched PP. All rheological measurements except for the melt flow index were carried out at $T=190^\circ\text{C}$ [5, 6].	83
3.9	Physical properties of the branched LDPEs used in step-strain shear relaxation experiments. The molecular weights, polydispersity indices and experimental temperatures for these samples are listed in Table 3.3. Data from Tsenoglou [9].	97
3.10	Physical properties of three commercial HDPE's and a Linear LDPE used in step-strain shear relaxation experiments. The Melt Flow Index (MFI), provided for the HDPE's, is an inverse measure of their average molecular weight. Data from Tsenoglou [9].	100
4.1	Physical properties and molecular characteristics of the commercial resins investigated. The g'_s value for the LDPE FF20 sample was provided by the supplier. The g_s value is estimated from Eq. 2.12 and the branching content from Eqs. 2.13 or 2.14.	109
4.2	Set strain rate and true strain rate determined for the LDPE and HDPE resins in uniaxial extensional flow.	115
5.1	Cross viscosity model parameters for the LDPE and HDPE at various isothermal conditions.	122
5.2	Time shift factors, α_T for both resins with respect to the reference temperature at various isothermal conditions.	122
5.3	Relaxation spectra for the LDPE and HDPE melts at the reference temperature.	124
5.4	Crossover frequencies and corresponding relaxation times for both resins at various isothermal conditions.	126

5.5	Damping function values for the LDPE Riblene melt at corresponding magnitudes of shear strain.	126
5.6	XPP parameters for fitting the LDPE Riblene melt, $T=150^{\circ}\text{C}$, $M_w=160.3$ (kg/mol), $(M_w/M_n)=12$, $E_a=50.4$ (kJ/mol)	135
5.7	XPP parameters for fitting the HDPE Eraclene melt, $T=170^{\circ}\text{C}$, $M_w=196.6$ (kg/mol), $M_w/M_n=16$, $E_a=32.5$ (kJ/mol)	135
6.1	Molecular data for melts of B/EHP blends from Lagendijk et al. [61]. The commercial linear precursor B was modified using varying amounts (mmol/100 gr PP) of EHP peroxydicarbonate.	151
6.2	PB samples from Kasehagen et al. and the corresponding x_n values for each sample.	151
6.3	PP samples from Gotsis et al. and the corresponding x_n values for each sample.	151
6.4	Calculated parameter values of the Cayley-tree model for the commercial LDPE samples from Tsenoglou. The last column is the relative error between the x_n value calculated from the model and the actual value (see Table 3.9) inferred from the experiment.	153
6.5	Calculated parameter values of the Cayley-tree model for the commercial LDPE samples from Tsenoglou. The last column is the relative error between the x_n value calculated from the model and the actual value (see Table 3.9) inferred from the experiment.	154
B.1	Values of the Doi-Edwards orientation tensor, Q_{12} in shear with an accuracy of five decimal digits and the corresponding damping functions, $h(\gamma_0)$ for both the exact and the IAA versions.	177
C.1	Values of $h(\gamma_0)$ as a function of shear strain for the commercial long-chain branched LDPE's examined by Tsenoglou [9].	180
C.2	Values of $h(\gamma_0)$ as a function of shear strain for the commercial linear HDPE's examined by Tsenoglou [9]. The last column contains values of the damping function for a commercial LLDPE from the same work [9].	181
C.3	Values of $h(\epsilon_H)$ as a function of the Hencky strain (for each individual strain rate) for the commercial long-chain branched LDPE Riblene melt at $T=150^{\circ}\text{C}$	182
C.4	Values of $h(\epsilon_H)$ as a function of the Hencky strain (for each individual strain rate) for the commercial linear HDPE Eraclene melt at $T=170^{\circ}\text{C}$	183

List of Figures

1	Από αριστερά προς τα δεξιά : Γραμμικό Πολυαιθυλένιο Υψηλής Πυκνότητας (HDPE), γραμμικό Πολυαιθυλένιο Χαμηλής Πυκνότητας με κοντές διακλαδώσεις (LLDPE) και Πολυαιθυλένιο Χαμηλής Πυκνότητας με μακριές διακλαδώσεις στον κορμό και στους κλάδους (LDPE).	8
2	Ποσοστό διακλάδωσης, B_n , ως συνάρτηση της παραμέτρου β για τα δείγματα του Πίνακα 3	15
3	Ποσοστό διακλάδωσης, B_n ως συνάρτηση της παραμέτρου β για τα δείγματα του Πίνακα 4	15
4	Μεταβολή του δείκτη σκλήρυνσης, SHI ως συνάρτηση του ποσοστού διακλαδώσεων, B_n για τα δείγματα του Πίνακα 3.	16
5	Εξάρτηση της παραμέτρου x_n της τροποποιημένης συνάρτησης απόσβεσης των Doi-Edwards από το μέγεθος διατμητικής παραμόρφωσης για τα δείγματα του Πίνακα 5.	18
6	Εξάρτηση της παραμέτρου x_n της τροποποιημένης συνάρτησης απόσβεσης των Doi-Edwards από το ποσοστό διακλαδώσεων, B_n για τα δείγματα του Πίνακα 5 και τα τροποποιημένα με τυχαία κατανομή μακρών διακλαδώσεων εμπορικά πολυβουταδιένια των Kasehagen και Macosko (βλ. Πίνακα 3.5 και 6.2).	18
7	Εξάρτηση της παραμέτρου x_n της τροποποιημένης συνάρτησης απόσβεσης των Doi-Edwards από το ποσοστό διακλαδώσεων, B_n για τα δείγματα των Πινάκων 3, 4 και 6.1.	19
8	Εξάρτηση της παραμέτρου x_n της τροποποιημένης συνάρτησης απόσβεσης των Doi-Edwards από το ποσοστό διακλαδώσεων, B_n για όλα τα δείγματα των Σχ. 6 και 7.	19
9	Θερμορεολογική πολυπλοκότητα στα δείγματα (a) Riblene® και (b) Eraclene® με βάση την τεχνική των Wood-Adams και Costeux.	24
10	Θερμο-ρεολογική πολυπλοκότητα στα δείγματα Riblene® και Eraclene® με βάση την τεχνική των VanGurp και Palmen.	25
2.1	A self-avoiding random walk consisting of 10000 steps in (a) three dimensions and (b) its projection in two dimensions.	44
2.2	A fluid element (a) before and (b) after a general three-dimensional deformation seen from a Lagrangian point of view (see Eq.2.22).	48

2.3	A fluid element under (a) uniaxial extension and (b) shear deformation. The uniaxial extensional rate across the "1"-direction is defined as $\dot{\epsilon} = dv_1/dx_1$ whereas the shear rate across the same direction as $\dot{\gamma} = dv_1/dx_2$.	51
3.1	Frequency dependence of the (a) storage and (b) loss modulus of LDPE "Melt I" at constant $T=150^\circ\text{C}$ as represented by a sum of eight terms (see Table 3.1).	64
3.2	Elongational viscosity, $\eta_E^+(t, \dot{\epsilon})$ as a function of time and deformation rate, after start-up of steady uniaxial extension for the LDPE "Melt I" at $T=150^\circ\text{C}$. Solid lines are the predictions of the rubber-like liquid theory using the 8 modes of Table 3.1 while dashed lines are the predictions of the same theory using the 5 modes of "Set B" from Table 3.2.	69
3.3	Solid lines are the predictions of the Lodge equation with Wagner's damping function using an exponent of $n = 0.14$ for the growth of the (a) shear viscosity, $\eta_{12}^+(t, \dot{\gamma})$ and (b) primary normal stress coefficient, $\Psi_1(t, \dot{\gamma})$ as a function of time, t and rate of shearing deformation, $\dot{\gamma}$ at the inception of steady-shearing flow. Dashed lines in both (a) and (b) correspond to the predictions of Lodge's equation in the absence of a damping function.	75
3.4	Solid lines are the predictions of the Lodge equation with Wagner's damping function using an exponent of $n=0.14$ for the (a) shear stress growth, $\sigma_{12}^+(t, \dot{\gamma})$ and (b) primary normal stress difference, $N_1(t, \dot{\gamma})$ as a function of time, t and rate of shearing deformation, $\dot{\gamma}$ at the inception of steady-shearing flow. Dashed lines in both (a) and (b) correspond to the predictions of Lodge's equation in the absence of a damping function.	76
3.5	Comparison between the predictions derived from Eq. 3.18 for the Lodge rubber-like liquid (dashed lines) and the predictions corresponding to Eq. 3.38 of the modified rubber-like liquid with the damping function of Eq. 3.57 (solid lines) of the elongational viscosity, η_E^+ as a function of time, t and strain rate, $\dot{\epsilon}$ after the start-up of uniaxial extension with constant strain rate, $\dot{\epsilon}$ for the LDPE "Melt I" at the reference temperature of $T=150^\circ\text{C}$ [46, 44].	77
3.6	Branching number, B_n as a function of the strain sensitivity parameter, β of the power-law damping function (Eqs. 3.65-3.66) for the materials listed in Table 3.7.	84
3.7	Branching number, B_n as a function of the strain sensitivity parameter, β of the power-law damping function (Eqs. 3.65-3.66) for the materials listed in Table 3.8.	84
3.8	The SHI defined by Gotsis et al. [4, 5, 6] plotted against the B_n for several branched PP samples resulting from modifications of three different linear precursors (see Table 3.7) at constant $T=190^\circ\text{C}$.	85

3.9	A polymer chain, its primitive path (solid line with $N=4$) and its neighbours confining it like in a tube (dashed lines). This illustration is a simplification of the physical picture since in reality more than two constraints are needed to define a primitive step. Redrawn from Tsenoglou [9].	88
3.10	Non-equilibrium chain and path dynamics (a) before deformation, (b) after deformation, (c) after equilibration ($t = \tau_e$) with $N/N' = 2$, (d)-(f) path disengagement by reptation ($t > \tau_e$) until (g) equilibration in undistorted configuration. Dashed lines signify abandoned paths. Redrawn from Tsenoglou [9].	90
3.11	Chain and path dynamics during the length equilibration stage of a branched polymer (a) at rest, (b) just after deformation and (c) just after equilibration. Redrawn from Tsenoglou [9].	95
3.12	Dependence of (a) the strain component of the relaxation function (eq. 3.107) and (b) the strain component of the stress (eq. 3.106) on the shear deformation for the branched LDPEs listed in Table 3.9. Solid lines with $x_n = 0$ correspond to the DE theory while for $x_n = 1$ there is no damping. Replotted from Tsenoglou [9].	98
3.13	Same as Fig. 3.12 but for the branched LDPEs A7 and IUPAC A, demonstrating the temperature invariance of the damping function. Data from Tsenoglou [9].	99
3.14	Dependence of the strain component of the stress, $\gamma_0 h(\gamma_0)$, on the shear deformation for HDPE.A at several isothermal conditions. The line with $x_n = 0$ is the simple DE prediction while for $x_n = 1$ there is no damping. Replotted from Tsenoglou [9].	101
3.15	Dependence of the strain component of the stress, $\gamma_0 h(\gamma_0)$, on the shear deformation for HDPE.B at several isothermal conditions. Replotted from Tsenoglou [9].	101
3.16	Dependence of the strain component of the stress, $\gamma_0 h(\gamma_0)$, on the shear deformation for the three HDPE's examined at $T=140^\circ\text{C}$. Replotted from Tsenoglou [9].	102
3.17	Dependence of the strain component of the stress, $\gamma_0 h(\gamma_0)$, on the shear deformation for the branched LDPE.B, the HDPE.C and the linear LDPE at the corresponding isothermal conditions. Replotted from Tsenoglou [9].	102
3.18	The structure of a Pom-Pom polymer with a backbone within its confining tube and $2q_x$ dangling arms, with $q_x=3$ arms attached on each side of the pom-pom. The polymer is depicted in (a) undeformed configuration; and (b) deformed configuration with arm withdrawal into the stretched tube.	104
4.1	Strain sweep with a parallel disk geometry for (a) LDPE at $T=150^\circ\text{C}$, $d=25$ mm, $h=1.43$ mm and (b) HDPE at $T=160^\circ\text{C}$, $d=25$ mm, $h=1.482$ mm.	110

4.2	Schematic representation of the RME setup for uniaxial extensional measurements of polymer melts. The values of L_0 along with the set strain rate, $\dot{\epsilon}$ are used in order to set the speed of the belts, $v = (\dot{\epsilon}L_0/2) = \text{const}$ [65].	112
4.3	A series of snapshots taken at the corresponding Hencky strains during uniaxial elongation of the LDPE Riblene melt at $T=150^\circ\text{C}$ with true strain rate of 1.61 s^{-1}	112
4.4	The true strain rates obtained during uniaxial extension of (a) the LDPE and (b) HDPE samples at the corresponding isothermal conditions. . .	113
5.1	(a) Storage, G' , and (b) loss, G'' , moduli measured at dynamic mechanical analysis of the LDPE Riblene melt at a wide range of isothermal conditions.	118
5.2	(a) Storage, G' , and (b) loss, G'' , moduli measured at dynamic mechanical analysis of the HDPE Eraclene melt at a wide range of isothermal conditions.	119
5.3	Storage and loss moduli for the LDPE Riblene melt taken at several isothermal conditions, superimposed at $T=150^\circ\text{C}$	120
5.4	Storage and loss moduli for the HDPE Eraclene melt taken at several isothermal conditions, superimposed at $T=170^\circ\text{C}$	120
5.5	Complex shear viscosity for the LDPE Riblene melt at several isothermal conditions. Lines are fits of the Cross viscosity model (Eq. 2.40) at the corresponding temperatures.	121
5.6	Complex shear viscosity for the HDPE Eraclene melt at several isothermal conditions. Lines are fits of the Cross viscosity model (Eq. 2.40) at the corresponding temperatures.	121
5.7	Steady state shear viscosity for the LDPE Riblene melt at several isothermal conditions, superimposed at $T=150^\circ\text{C}$. Solid line is the prediction of the shear thinning response (see Eq. 3.53) according to the modified rubber-like liquid theory with $n=0.25$	123
5.8	Steady state shear viscosity for the HDPE Eraclene melt at several isothermal conditions, superimposed at $T=170^\circ\text{C}$. Solid line is the prediction of the shear thinning response (see Eq. 3.53) according to the modified rubber-like liquid theory with $n=0.28$	123
5.9	Linear least squares fit of the linearized version of Eq. 5.2 for (a) LDPE Riblene at $T=150^\circ\text{C}$ and (b) HDPE Eraclene at $T=170^\circ\text{C}$	125
5.10	Results in (a) from the step-strain experiment for the LDPE Riblene and (b) superimposed data for the same melt. The solid line in (b) is the linear relaxation modulus, $G(t)$ of the 6-mode Maxwell spectrum (see Table 5.3).	127
5.11	Damping function for the LDPE Riblene melt in a log-linear plot. Solid line is the single exponential damping function, with $n=0.23$	128

5.12	Transient uniaxial extensional viscosity as a function of time for the LDPE Riblene melt at $T=150^{\circ}\text{C}$ and for various strain rates (as indicated in the legend). Lines are fits of the modified rubber-like liquid theory with the power-law damping function (see Eqs. 3.65 and 3.66) and $\beta=0.25$	129
5.13	Same as in Fig. 5.12 but with respect to the Hencky strain.	129
5.14	Transient uniaxial extensional viscosity as a function of time for the HDPE Eraclene melt at $T=170^{\circ}\text{C}$ and for various strain rates (as indicated in the legend). Lines are fits of the modified rubber-like liquid theory with the power-law damping function (see Eqs. 3.65 and 3.66) and $\beta=0.40$	130
5.15	Same as in Fig. 5.14 but with respect to the Hencky strain.	130
5.16	Damping function in extensional flow for (a) LDPE Riblene and (b) HDPE Eraclene melts at the corresponding temperatures. The power-law exponent assumes a value of $\beta=0.25$ for LDPE while for HDPE $\beta=0.40$	132
5.17	Transient uniaxial extensional viscosity as a function of time for the LDPE Riblene melt at $T=150^{\circ}\text{C}$ and for various strain rates (as indicated in the legend). Lines are fits of the XPP model with parameters given in Table 5.6.	133
5.18	Same as in Fig. 5.17 but with respect to the Hencky strain.	133
5.19	Transient uniaxial extensional viscosity as a function of time for the HDPE Eraclene melt at $T=170^{\circ}\text{C}$ and for various strain rates (as indicated in the legend). Lines are fits of the XPP model with parameters given in Table 5.7.	134
5.20	Same as in Fig. 5.19 but with respect to the Hencky strain.	134
5.21	Transient uniaxial extensional viscosity as a function of time for the HDPE Eraclene melt at $T=170^{\circ}\text{C}$ and for various strain rates (as indicated in the legend). Lines are fits of the Rolie-Poly constitutive equation with the Maxwell spectrum of Table 5.7.	136
5.22	Same as in Fig. 5.21 but with respect to the Hencky strain.	136
6.1	Superimposed plots of the loss angle, $\delta=\arctan(G''/G')$ for the (a) LDPE Riblene and (b) HDPE Eraclene against the reduced angular frequency.	139
6.2	Demonstration of the complex thermorheological behaviour of the (a) LDPE Riblene and (b) HDPE Eraclene melts.	140
6.3	Van Gurp-Palmen plot for the two PE resins examined at the corresponding isothermal conditions.	141
6.4	Damping function in extensional flow for (a) LDPE Riblene and (b) HDPE Eraclene melts at the corresponding temperatures. The nonlinear viscoelastic parameter in the case of the long-chain branched LDPE assumes a value of $x_n = 0.92$ whereas in the case of the HDPE-hexene copolymer a value of $x_n = 0.79$	145
6.5	Predictions of the Doi-Edwards model (dashed lines) and the modified Doi-Edwards model (solid lines with $x_n = 0.92$) for the uniaxial extensional viscosity of the LDPE Riblene melt at $T=150^{\circ}\text{C}$ with respect to time.	146

6.6	Same as in Fig. 6.5 but with respect to Hencky strain.	146
6.7	Predictions of the Doi-Edwards model (dashed lines) and the modified Doi-Edwards model (solid lines with $x_n = 0.79$) for the uniaxial extensional viscosity of the HDPE Ercelene melt at $T=170^\circ\text{C}$ with respect to time.	147
6.8	Same as in Fig. 6.7 but with respect to Hencky strain.	147
6.9	Demonstration of one possible distribution of the dangling arms on the periphery of the pom-pom molecule for the (a) LDPE Riblene with $B_n = 12$ and (b) HDPE Ercelene with $B_n = 2$	149
6.10	The nonlinear viscoelastic parameter, x_n as a function of the branching number, B_n for selected commercial LDPE and PB melts of varying branching content. Tsengoglou's parameter, x_n represents the amount of internal branches in the polymeric structure. It is inferred from rheological data only.	150
6.11	The nonlinear viscoelastic parameter, x_n as a function of the branching number, B_n for commercial LCB PPs including those of Table 6.1.	150
6.12	The nonlinear viscoelastic parameter, x_n as a function of the branching number, B_n for the melts of Figs. 6.10 and 6.11.	152
6.13	A Cayley-tree or Bethe lattice of constant branch point functionality, $f = 3$ and generation, $g_n=3$. The nonlinear viscoelastic parameter for this structure is $1/2$ while for commercial PEs it is lower ($\approx 3/4$).	153
6.14	The single exponential damping function in shear for both LDPE and HDPE melts (symbols) and the modified Doi-Edwards damping function in shear (lines) for the same melts.	155
6.15	The free energy function, $A(\underline{E})$ in the Doi-Edwards theory for a step-strain in shear and a uniaxial elongational deformation.	157
6.16	The predictions of the DE theory for the damping function, h_{DE} in shear and elongation, (a) with respect to the strain unit of elongation (γ_0 or ϵ_H), and (b) with respect to the change in the free energy, $A(\underline{E})$	158
6.17	Predictions of the modified Doi and Edwards model for the (a) LDPE Riblene melt under shear deformation with $x_n \approx 0.38$ and uniaxial extension with $x_n=0.92$ and (b) HDPE Ercelene melt under shear deformation with $x_n \approx 0.26$ and uniaxial extension with $x_n = 0.79$. Plots of hypothetical $x_n = 0.92$ and $x_n = 0.79$ in shear deformation for both melts are also included in order to demonstrate the predictive behaviour of the theory.	159
B.1	A log-log plot of the Doi-Edwards damping function, $h(\gamma_0)$, in shear for both the exact and the IAA version. A plot of the analytical approximation (see Eq. 3.95) is also included for comparison.	178
D.1	Relaxation modulus of commercial long-chain branched LDPE A2 at $T = 130^\circ\text{C}$ in (a) and (b) superimposed plot with values of $h(\gamma_0)$ as in Table C.1.	186

D.2	Relaxation modulus of commercial long-chain branched LDPE A4 at $T = 130^{\circ}\text{C}$ in (a) and (b) superimposed plot with values of $h(\gamma_0)$ as in Table C.1.	187
D.3	Relaxation modulus of commercial long-chain branched LDPE A7 at $T = 130^{\circ}\text{C}$ in (a) and (b) superimposed plot with values of $h(\gamma_0)$ as in Table C.1.	188
D.4	Relaxation modulus of commercial long-chain branched LDPE B2 at $T = 130^{\circ}\text{C}$ in (a) and (b) superimposed plot with values of $h(\gamma_0)$ as in Table C.1.	189
D.5	Relaxation modulus of commercial long-chain branched LDPE C2 at $T = 130^{\circ}\text{C}$ in (a) and (b) superimposed plot with values of $h(\gamma_0)$ as in Table C.1.	190
D.6	Relaxation modulus of commercial long-chain branched IUPAC A at $T = 130^{\circ}\text{C}$ in (a) and (b) superimposed plot with values of $h(\gamma_0)$ as in Table C.1.	191
D.7	Relaxation modulus of commercial long-chain branched LDPE A7 at $T = 110^{\circ}\text{C}$ in (a) and (b) superimposed plot with values of $h(\gamma_0)$ as in Table C.1.	192
D.8	Relaxation modulus of commercial long-chain branched IUPAC A at $T = 150^{\circ}\text{C}$ in (a) and (b) superimposed plot with values of $h(\gamma_0)$ as in Table C.1.	193

Curriculum Vitae

Ioannis S. Stratigakis

istratigakis@isc.tuc.gr

Born on 20 November 1982 in Thessaloniki, Greece

- **July 2014**

Participant in the 7th *International Meeting of the Hellenic Society of Rheology* with a poster entitled “*Rheology of Commercial Polyolefines : Relating the Viscoelastic Behaviour to Microstructure*” as the main author and as a co-author in the publication entitled “*Nonlinear Viscoelasticity of Commercial Low Density Polyethylenes : Relaxation Experiments and Constitutive Modeling of the Effect of Long Chain Branching in the Presence of Entanglements*” with Dr. Chris Tsenoglou and Prof. Alexandros D. Gotsis.

- **April 2014**

Co-author in the publication entitled “*Nonlinear Viscoelasticity of Commercial Low Density Polyethylenes : The Effect of Long Chain Branching in the Presence of Entanglements*” with Dr. Chris Tsenoglou and Prof. Alexandros D. Gotsis for the 9th *Annual European Rheology Conference*.

- **March 2014**

Enrolled in the Research Programm *COVISCO-THALES* with a Postgraduate Scholarship for the accomplishment of the Master Thesis entitled “*Rheology of Commercial Polyolefins : Relating the Viscoelastic Behaviour to Microstructure*” under the supervision of Prof. Alexandros D. Gotsis.

- **November 2012**

Diploma from the Univeristy of Crete in Heraklion in the field of *Material's Science and Technology* with a certified grade 6.59/10.

- **September 2012**

Enrolled for the Master Thesis programm of the *Department of Sciences* in the field of *Mechanics and Technology of Materials and Constructions* at the Technical University of Crete.